



MACQUARIE
University
SYDNEY • AUSTRALIA

***Functional properties, neurochemistry
and connectivity of medullary neural
networks that control breathing and
circulation***

Sheng Le (MBBS)

Faculty of Medicine and Health Sciences

Macquarie University

A thesis submitted to Macquarie University in fulfilment of the requirement for
the degree of Doctor of Philosophy

Principal Supervisor: **Dr Simon McMullan**

Associate Supervisor: **Dr Anita Turner**

Table of Contents

Abstract	i
Declaration of originality	iii
Declaration of contribution	iv
Publications	v
Publications arising from this thesis	v
Publications during the period of candidature	v
In preparation	v
Communications	v
Awards arising during the period of candidature	vii
Acknowledgements	viii
List of Figures	ix
List of Tables	x
Abbreviations	xi
1. Introduction	1
Single cell approaches to bridge functional properties and neurochemical profiles	3
Respiratory networks	4
Chemical markers for respiratory function	6
Cardiovascular networks	12
Interaction of the respiratory and cardiovascular networks	13
Respiratory-sympathetic coupling under normal conditions	15
Pathological implications of respiratory-sympathetic coupling in the control of blood pressure	16
Site of respiratory-sympathetic coupling	18
Sources of respiratory input to RVLM presympathetic neurons	19
Genetically restricted trans-synaptic tracing	25

The field of connectomics in neuroscience-----	28 -
Aims of this thesis -----	30 -
2. Recording, labelling and transfection of single neurons in deep brain structures --	33 -
Abstract -----	34 -
Introduction -----	35 -
Methods -----	38 -
General Preparation -----	38 -
Histology -----	40 -
Recording parameters -----	41 -
Plasmid preparation -----	44 -
Avoidance of inadvertent neuronal labelling-----	44 -
Results -----	45 -
Dye-labelling in vitro -----	45 -
Single-cell transfection in vitro-----	49 -
Establishing cell contact in blind recordings-----	50 -
Single-cell transfection in vivo -----	55 -
Discussion -----	58 -
3. Somatostatin 2a receptors are not expressed on functionally identified respiratory neurons in the ventral respiratory column of the rat-----	63 -
Abstract -----	64 -
Introduction -----	65 -
Methods -----	68 -
Electrophysiology experiments-----	68 -
Perfusion and tissue collection -----	71 -
Histology, in situ hybridization and immunohistochemistry -----	71 -
Microscopy and analysis -----	76 -
Definition of VLM respiratory compartments -----	76 -
Results -----	79 -
General pattern of sst _{2a} immunoreactivity -----	79 -
sst _{2a} immunoreactive neurons are present in the RVLM C1 region but not Bötzing Complex -----	80 -
sst _{2a} immunoreactive neurons in the preBötzing Complex are either NK1R- or TH-immunoreactive ----	82 -
sst _{2a} immunoreactivity on functionally identified respiratory neurons -----	84 -
Discussion -----	90 -
Somatic expression of sst _{2a} receptor is absent in the Bötzing Complex-----	90 -

sst _{2a} is associated with preBötzinger Complex NK1R neurons but not widely expressed on functionally identified neurons-----	91 -
Technical considerations -----	91 -
Functional implications-----	93 -
4. The connectome of rostral ventrolateral medulla C1 neurons -----	96 -
Abstract-----	97 -
Introduction-----	98 -
Methods-----	102 -
Vector preparation -----	102 -
Vector injections -----	102 -
Perfusion and tissue collection -----	103 -
Histology, in situ hybridization and immunohistochemistry -----	104 -
Imaging -----	107 -
Data analysis-----	107 -
Results-----	113 -
Starter neurons are located within the rostral RVLM and are immunoreactive to tyrosine hydroxylase. -	113 -
The majority of inputs to the RVLM C1 neurons arise from the medulla -----	116 -
Input neurons from the RVLM, the BötC, and the preBötC-----	118 -
Input neurons from other medullary nuclei-----	121 -
Input neurons from the supramedullary regions -----	124 -
Discussion -----	126 -
Inputs from respiratory related nuclei -----	126 -
Inputs from cardiovascular related nuclei -----	131 -
Inputs from other nuclei -----	133 -
Technical consideration-----	134 -
Summary and future direction -----	136 -
5. General discussion -----	138 -
Chapters 2&3-----	139 -
Chapter 4 -----	140 -
Final thoughts -----	142 -
References-----	144 -
Appendices-----	189 -

Abstract

The autonomic nervous system governs basic homeostatic functions such as regulating cardiac output, blood pressure, body temperature, and the generation of respiratory rhythm. Although traditionally conceptualised as independent entities, the neural networks that underlie respiratory rhythm and vasomotor tone are intimately connected, with each component influencing the activity of the other. This respiratory-sympathetic coupling contributes to cardiac sinus arrhythmia and underlies the strong respiratory modulation of vasomotor sympathetic nerve activity, which may play an important role in initiation and development of neurogenic hypertension. The experiments described in this thesis explore the neurochemical profiles, functional properties, and circuit architecture of medullary neurons that control breathing and circulation.

Genetically modifying a single functionally identified neuron in an intact neural network would provide the ultimate way to bridge neuronal circuit structure and function. The work described in Chapter 2 of this thesis describes a novel method that combines extracellular recording with the labelling of neurons recorded in the ventral lateral medulla with either dyes or plasmid DNA, permitting conventional cell labelling or gene delivery. We demonstrate that our approach has several advantages over traditional single-cell labelling approaches, and therefore provides a useful tool for correlation of functional properties of single neurons with their neurochemical phenotypes that can also be used for targeted single cell gene delivery under blind recording conditions.

We then apply this technique to address a controversial topic in the field of respiratory neuroscience; the neurochemical signature of the neurons responsible for generating respiratory rhythm. Previous investigations have suggested that the neuropeptide somatostatin plays a critical role in respiratory rhythmogenesis and is a marker for excitatory respiratory interneurons in the pre-Bötzinger complex (preBötC). Somatostatin receptor type 2a (sst_{2a}) has been postulated as a mediator of such effects, and has also been proposed as a marker for respiratory neurons. In Chapter 3 we systematically examine the expression pattern of sst_{2a} with regards to the functionally distinguished subcomponents of the ventral respiratory column. We further examine the feasibility of sst_{2a} as a reliable marker of respiratory function at the single cell level.

In Chapter 4 we examine the anatomical substrate responsible for linking the respiratory and sympathetic circuits using a modified trans-synaptic tracing tool. We first extensively map sources of monosynaptic drive to putative sympathetic premotor neurons in the rostral ventrolateral medulla (RVLM) using a genetically restricted rabies variant, that is selectively directed towards RVLM neurons that express the Phox2b transcription factor. We identify likely sources of inputs within brainstem compartments with proven roles in generation of respiratory rhythm and phase transition in normotensive animals.

The data from this thesis extends our knowledge of respiratory neuroanatomy and provides important clues to the organisation of the circuits that underlie respiratory-sympathetic coupling.

Declaration of originality

I acknowledge that the work conducted in this thesis entitled “Functional properties, neurochemistry and connectivity of medullary neural networks that control breathing and circulation” has not been submitted for a degree nor has it been submitted as part of the requirements for a degree to any other university or institution other than Macquarie University. All work in this thesis was conducted in the Faculty of Medicine and Health Science under the direct supervision of Dr Simon McMullan and co-supervision of Dr Anita Turner. Parts of this text have been published, details of which can be found on page v.

I declare that the contents of this thesis represent the original experimental and written work of the candidate except where due acknowledgements are made. All research presented in this thesis were conducted with the consent of Macquarie University Ethics Committees (Animal Research Authority No.: 2012/030, 2013/022, 2014/028).

Sheng Le

Declaration of contribution

Chapter 2: Dr Simon McMullan, Dr Anita Turner and the candidate performed the *in vivo* electrophysiological experiments. Dr Bowen Dempsey performed the *in vitro* electrophysiological experiments. Dr Bowen Dempsey and the candidate performed the histological processing and imaging. Analysis was primarily performed by Dr Simon McMullan. All authors contributed to the manuscript.

Chapter 3: Dr Simon McMullan, Dr Anita Turner and the candidate performed the single cell labelling experiments. The candidate performed all immunohistochemistry and imaging. Dr Lindsay Parker synthesized the ISH probe. The analysis was primarily performed by the candidate. The candidate was the major contributor to the manuscript.

Chapter 4: Dr Simon McMullan and the candidate performed the vector injections. The candidate performed all histological processing and imaging. Dr Simon McMullan developed the image processing work flow. Data analysis was performed by the candidate. The candidate was the major contributor to the manuscript.

Publications

Publications arising from this thesis

Le, S., Turner, A. J., Parker, L. M., Burke, P. G., Kumar, N. N., Goodchild, A. K., & McMullan, S. (2016). Somatostatin 2a receptors are not expressed on functionally identified respiratory neurons in the ventral respiratory column of the rat. *J Comp Neurol*, 524(7), 1384-1398. doi:10.1002/cne.23912

Dempsey, B., Turner, A. J., **Le, S.**, Sun, Q. J., Bou Farah, L., Allen, A. M., Goodchild, A. K., McMullan, S. (2015). Recording, labeling, and transfection of single neurons in deep brain structures. *Physiol Rep*, 3(1), e12246. doi: 10.14814/phy2.12246

Publications during the period of candidature

Bou Farah, L., Bowman, B. R., Bokinieć, P., Karim, S., **Le, S.**, Goodchild, A. K., & McMullan, S. (2016). Somatostatin in the rat rostral ventrolateral medulla: Origins and mechanism of action. *J Comp Neurol*, 524(2), 323-342. doi: 10.1002/cne.23846

In preparation

Menuet, C., **Le, S.**, Dempsey, B., Connelly, A. A., Kamar, J., Jancovski, N., Bassi, J. K., Hammond, A., Fong, A.Y., Goodchild, A. K., McMullan, S., Allen, A. M. Excessive respiratory modulation of blood pressure triggers hypertension.

Dempsey, B., **Le, S.**, Turner, A., Ramadas, R., Bjaalie, J.G., L., Menuet, C., Neve, R., Allen, A. M., Goodchild, A. K., McMullan, S. The mesoscale connectome of sympathetic premotor neurons of the rat rostral ventrolateral medulla

Parker, L., Wearne, T., **Le, S.**, Hardwick, K., Kumar, N., McMullan, S., Goodchild, A. Are neurochemically distinct neurons in the ventrolateral medulla activated by two acute physiological stressors?

Communications

Le S, Turner A, McMullan S (2013) Somatostatin 2a receptors (sst_{2a}) are not expressed in functionally identified respiratory neurons. Poster presentation at the Macquarie University Biofocus Research Conference, Sydney, Australia.

Dempsey B, Turner A, Bou Farah L, **Le S** and McMullan S (2013). A novel technique that combines single cell electroporation with extracellular recordings *in vitro* and *in vivo*. Poster presentation at the 8th Congress of the International Society for Autonomic Neuroscience (ISAN) and the 15th Meeting of the European Federation of Autonomic Societies (EFAS), Giessen, Germany.

Dempsey B, Turner A, Bou Farah L, **Le S** and McMullan S (2013). A novel technique that combines single cell electroporation with extracellular recordings *in vitro* and *in vivo*. Poster presentation at the Central Cardiovascular and Respiratory Control: Future Directions, Sydney, Australia.

Le S, Turner A, McMullan S (2014) Somatostatin type 2a receptors (sst_{2a}) are not expressed on respiratory neurons in the ventral respiratory column (VRC). Oral presentation at the Central Cardiorespiratory Control: Future Directions conference, Melbourne, Australia

Le S, Dempsey B, Turner A, Qi-Jian S, Bou Farah L, Allen AM, Goodchild AK, McMullan S (2014). Recording and transfection of single neurons in deep brain structures. Oral presentation (presented by Dr Anita Turner) at the 13th Oxford Breathing meeting, Sydney, Australia.

Le S, Turner A, Parker L, Burke P, Kumar N, Goodchild A & McMullan S. (2014) Somatostatin 2a receptors are not expressed on functionally identified respiratory neurons in the ventral respiratory column. Oral presentation (presented by Dr McMullan) at the 13th Oxford Breathing meeting, Sydney, Australia.

Dempsey B, Turner A, **Le S**, Allen AM, Goodchild AK, McMullan S (2015). The connectome of rostral ventrolateral medulla sympathetic premotor neurons. Oral presentation at the meeting of the International Society for Autonomic Neuroscience (ISAN) in conjunction with the American Autonomic Society (AAS), the European Federation of Autonomic Societies (EFAS) and the Japanese Society for Neurovegetative Research (JNSR), Stresa, Italy.

Dempsey B, Turner A, **Le S**, Allen AM, Goodchild AK, McMullan S (2015). The connectome of rostral ventrolateral medulla sympathetic premotor neurons. Oral presentation at the Central Cardiovascular and Respiratory Control: Future Directions conference, Sydney, Australia.

Le S, Turner A, Parker L, Burke P, Kumar N, Goodchild A & McMullan S. (2015) Somatostatin 2a receptors are not expressed on functionally identified respiratory neurons in the ventral respiratory column. Poster presentation at the 6th FAONS Congress and 11th Biennial Conference of CNS, WuZhen, China.

Le S, Turner A, Parker L, Burke P, Kumar N, Goodchild A & McMullan S. (2015) Somatostatin 2a receptors are not expressed on functionally identified respiratory neurons in the ventral respiratory column. Poster presentation at the 25th ISN-APSN Joint Biennial Meeting in conjunction with the Australasian Society for Neuroscience (ANS), Cairns, Australia.

Le S, Dempsey B, Turner A, Allen A, Goodchild A, & McMullan S. (2016) The connectome of rostral ventrolateral medulla C1 neurons. Poster presentation at the Experimental biology conference, San Diego, USA.

Awards arising during the period of candidature

2014 – Macquarie University, Australian School of Advanced Medicine - The HDR Director's Data Club Prize

2014 – Central Cardiovascular & Respiratory Control: Future Direction Conference Committee
– Most Innovative Student Presentation

2015 – Skipper Foundation – Skipper Postgraduate Travel Award

Acknowledgements

I would never been able to finish this thesis without the tremendous support and help from my supervisors, colleagues, friends, and my family.

Foremost, a gazillion thanks to my mentor, Dr Simon McMullan. Simon, I consider myself extremely fortunate to have had the opportunity to learn and develop as a researcher under your supervision. Not only for the scientific knowledge and experimental techniques I learnt from you, but also for your wisdom and attitudes to life that inspire me.

Special thanks to my co-supervisor Dr Anita Turner, for teaching me all the cool experimental techniques, keeping my spirits up by your contagiously positive attitude and boosting my cerebral activities with all kinds of delicious cakes from time to time. Many thanks to Lama, Bowen, and Erin for helping me out in experiments and keeping me accompanied along the way.

To the Goodchild team, Ann, Phil, Sarah, Belinda and Lindsay, you guys have been great sources of help and support. Thank you for generously sharing your expertise and experiences to guide me through the journey, and special thanks to Phil for the hundreds of cups of coffee to pull me through the writing phase.

I'm grateful to the funding bodies that have supported me through my study. In particular, Macquarie University Research Excellence Scholarships, the Faculty Top-ups, and the Skipper Foundation Travel Awards.

Last but not least, to my family: my parents, Jie Yu and Liping Le, my wife, Yajie Ren, and my little sunshine, Annabel, you guys are everything to me. I couldn't thank you enough for all the love and support.

List of Figures

Figure 1.1 Respiratory modulation of sympathetic nerve activities (SNA).....	- 15 -
Figure 1.2 Inputs to the RVLM.....	- 24 -
Figure 1.3 Monosynaptic tracing with glycoprotein-deleted EnvA-pseudotyped rabies (SADΔG(EnvA)).	- 28 -
Figure 2.1 Illustration of workflow used for constant-current electroporation in vitro.....	- 46 -
Figure 2.2 Extracellular recording and constant-current electroporation of a spontaneously active neuron in an acute brain slice.	- 48 -
Figure 2.3 Circuit configuration used for recording and constant-voltage electroporation.	- 49 -
Figure 2.4 Single-cell microstimulation of a medullary respiratory neuron in vivo.	- 52 -
Figure 2.5 Examples of non-respiratory A. and respiratory B. - D. neurons recorded in extracellular mode in the ventrolateral medulla and labelled with neurobiotin by constant-voltage electroporation in vivo.	- 54 -
Figure 2.6 Transfection of ventrolateral brainstem neurons following intracellular penetration in vivo.....	- 57 -
Figure 3.1 Electrophysiological recording and labelling of brainstem respiratory neuron.	- 70 -
Figure 3.2 sst2a - immunoreactive cells are distributed along the ventrolateral medulla....	- 79 -
Figure 3.3 sst2a expression is colocalized with markers of cardiovascular but not respiratory function in the RVLM/BötC.....	- 81 -
Figure 3.4 sst2a immunoreactivity in the preBötC is partially colocalized with NK1R and TH.	- 83 -
Figure 3.5 Functional classifications and anatomical locations of recovered respiratory neurons.	- 86 -
Figure 3.6 Medullary respiratory neurons do not express sst2a.	- 89 -
Figure 4.1 Anchoring workflow.	- 109 -
Figure 4.2 Distribution and phenotype of starter neurons.	- 114 -
Figure 4.3 Starter and input neurons occasionally extended into the retrotrapezoid nucleus (RTN).	- 115 -
Figure 4.4 Distribution of monosynaptic input neurons.	- 117 -
Figure 4.5 Neurochemical phenotypes of input neurons in the BötC & preBötC.	- 121 -
Figure 4.6 Medullary input neurons to RVLM C1 neurons.....	- 123 -
Figure 4.7 Supramedullary input neurons to RVLM C1 neurons.....	- 125 -

List of Tables

Table 1.1 Inputs to the RVLM.....	- 22 -
Table 3.1 Antibodies.....	- 73 -
Table 4.1 Antibodies.....	- 105 -
Table 4.2 Input neurons segregated by brain structures in Waxholm rat brain atlas.....	- 118 -

Abbreviations

A5	A5 noradrenaline cells
AmbC	nucleus ambiguus, compact part
AmbSC	nucleus ambiguus, subcompact part
BötC	Bötzinger complex
C1	catecholaminergic
CCHS	congenital central hypoventilation syndrome
CeA	central nucleus of the amygdala
CIH	chronic intermittent hypoxia
CNS	central nervous system
CPA	caudal pressor area
CTB	cholera toxin subunit B
CVLM	caudal ventrolateral medulla
cVRG	caudal ventral respiratory group
DMH	dorsomedial hypothalamic nucleus
GABA	Gamma-Aminobutyric acid
Glyt2	glycine transporter 2
IML	intermediolateral cell column
IO	inferior olive
KF	Kölliker-Fuse nucleus

LC	locus coeruleus
LHA	lateral hypothalamic nucleus
LPBN	lateral parabrachial nucleus
LTF	lateral tegmental field
MnPo	median preoptic nucleus
NK1R	neurokinin 1 receptors
NTS	nucleus of the solitary tract
OSA	obstructive sleep apnea
PAG	periaqueductal gray
PBS	phosphate buffered saline
PFA	paraformaldehyde
pFRG	parafacial respiratory group
PNA	phrenic nerve activities
preBötC	preBötzinger complex
PRG	pontine respiratory group
PVN	paraventricular nucleus of the hypothalamus
RTN	retrotrapezoid nucleus
RVLM	rostral ventrolateral medulla
RVMM	rostral ventromedial medulla
rVRG	rostral ventral respiratory group
SCE	single cell electroporation

scp	superior cerebellar peduncle
SD	Sprague Dawley rats
SHR	spontaneous hypertensive rats
SIDS	sudden infant death syndrome
SNA	sympathetic nerve activity
SO	superior olive
SPN	sympathetic preganglionic neurons
SST	somatostatin
sst _{2a}	somatostatin receptor 2a
TMR	tetramethylrhodamine
TTC	C-fragment of tetanus toxin
V	motor trigeminal nucleus
Vglut2	type 2 vesicular glutamate transporter
VII	facial nucleus
VL pons	ventrolateral pons
VRC	ventral respiratory column
WKY	Wistar-Kyoto rats

1.

Introduction

There is little doubt that the human brain is the most complex biological structure in the known universe. The idea of the brain as the control centre for the body was first advocated by Hippocrates and further promoted by the Greek physician Galen more than 2000 years ago. Phrenologists in the early 19th century believed that the human mind is composed of multiple, distinct, innate faculties that correspond to separate “organs” in the brain. Despite being discredited as a science in the mid-19th century, phrenology ironically fostered the right notion of varying brain functions associated with different brain regions.

The modern conception of the brain was largely based on the ground-breaking neuroanatomical work by Santiago Ramón y Cajal (Lopez-Munoz *et al.*, 2006). From brain tissue stained by the Golgi technique, Cajal illustrated the delicate structure of brain cells via his legendary medical artistic skills. His work demonstrated that individual cellular elements, coined “neurons” by Waldeyer (Fishman, 1994), act as the basic building blocks for the nervous system. More importantly, he defined “the law of dynamic polarization”, which described the unidirectional flow of information between neuronal connections. His discoveries set the organizational and functional principles of modern neuroscience.

In contrast to our achievements in understanding the physiological mechanisms that dictate the function of other organs, our understanding of how interconnected circuits of neurons work together to generate co-ordinated output remains for the most-part immature. Unlike well-established structural and cellular motifs seen in other organs, the problems associated with visualising and mapping the connectivity of brain circuits, and in aligning function with circuit structure, have posed significant challenges to the field of neuroscience.

Multiple overlapping parameters are used by neuroscientists to classify neurons, including anatomical location, dendritic and somatic morphology, axonal projection, electrophysiological properties, gene expression pattern, neurochemical profiles and physiological functions. Categorizing neurons using a unique combination of the aforementioned parameters has proved

foundational for the description and investigation of neural circuits and has framed the way that neuroscientists think about the brain (Migliore & Shepherd, 2005; Callaway, 2008). The emergence of new technologies, and the subsequent field of connectomics, will provide a new perspective for investigators to differentiate distinct groups of neurons (Carandini, 2012; Denk *et al.*, 2012; Mitra, 2014).

Evolutionarily conserved neural circuits with accessible and measurable nerve outputs provide good models for the investigation of general principles of neurobiology. The brainstem, the phylogenetically oldest brain structure (Reiner, 1990), hosts neural networks that govern basic physiological functions, such as regulation of blood pressure, cardiac output, body temperature and generation of respiratory rhythm. Cardiovascular and respiratory parameters (such as blood pressure, heart rate, sympathetic nerve activities (SNA), respiratory rate, tidal volumes and phrenic nerve activities, etc.) are measurable and quantifiable in various animal models. Understanding the neural control of blood pressure and breathing may help us to generate theories that apply not only to autonomic neuroscience but also to other disciplines of neuroscience.

Single cell approaches to bridge functional properties and neurochemical profiles

It is widely believed that the organization of neuronal connections underlie the fundamental determinant of brain function. However, a number of studies have demonstrated the functional importance of single neurons. For example, stimulation of single neurons can trigger network synchronization in the hippocampus *in vitro* (Miles & Wong, 1983), change global brain activity state *in vivo* (Li *et al.*, 2009), or evoke observable motor and behavioural changes (Brecht *et al.*, 2004; Houweling & Brecht, 2008). Presumably, these phenomenal effects rely on the complicated connections converging on or diverging from specific single neurons.

Recent developments in optogenetics, molecular biology and virus-based circuit tracing have provided incentives for genetically manipulating single neurons with characterised electrophysiological properties. Such approaches provide new perspectives for understanding the functions and genetics of neurons in general. A few methods have been developed to deposit nucleotides into target cells; such as using a low-resistance recording pipette (Rancz *et al.*, 2011), single cell electroporation (SCE) (Haas *et al.*, 2001; Rae & Levis, 2002), or the combination of conventional electrophysiological recording and SCE (Rathenberg *et al.*, 2003; Bestman *et al.*, 2006b; Oyama *et al.*, 2013). SCE has been proven to be most effective and suitable for gene delivery *in vivo* (Kitamura *et al.*, 2008b). However, as the reported success rates of SCE are closely related to the position of the recording pipette, applications of this technique are largely limited to preparations in which cells can be visualized. As such, the efficacy of applying these methods to genetically manipulate respiratory and cardiovascular neurons located deep in the brainstem, has remained untested.

Conventional techniques to label recorded neurons with dyes, such as intracellular recording and labelling (Horikawa & Armstrong, 1988) and juxtacellular iontophoresis (Pinault, 1996) are common methods used by neurobiologists to correlate functional properties and neurochemical profiles at the single neuron level. However, the incompatibility of gene delivery, and the painstaking learning curve of these techniques limit the application, especially for inexperienced researchers. Therefore, an easy-to-apply, optical-guidance-free, gene-delivery-compatible, single cell recording and labelling technique is desirable to study cardiovascular and respiratory neurons *in vivo*.

Respiratory networks

Eupneic respiratory activity requires sequentially coordinated contraction of respiratory muscles. It is generally accepted that the key elements for respiratory rhythm generation reside

in the medullary ventral respiratory column (VRC), which is comprised of spatially and functionally interconnected neural circuits that lie bilaterally in the ventral medulla (see review Alheid & McCrimmon, 2008; Smith *et al.*, 2012, 2013). In addition, nuclei in the pons are essential for shaping respiratory motor output into a three-phased eupneic pattern, as transection at pontine medullary junction abolished the post-inspiratory phase (Smith *et al.*, 2007; Dutschmann & Dick, 2012). The rostral half of the VRC contains circuits that are thought to be responsible for rhythmogenesis, and the caudal half transmits and modulates respiratory motor output. Respiratory neurons can be broadly classified as inspiratory, expiratory or phase-spanning neurons according to the temporal relationship between their peak activities and the respiratory cycle (Smith *et al.*, 1990; Johnson *et al.*, 1994; Bianchi *et al.*, 1995; Sun *et al.*, 1998; Smith *et al.*, 2009). Inspiratory and expiratory neurons can be further classified into augmenting, flat, or decrementing subtypes based on their firing patterns (Ezure *et al.*, 1988; Sun *et al.*, 1998; Lindsey *et al.*, 2012; Richter & Smith, 2014).

Prominence of particular types of respiratory neurons is used to divide the VRC into subregions. The rostral VRC contains at least three functionally distinguishable subregions: the retrotrapezoid nucleus (RTN)/parafacial respiratory group (pFRG), Bötzing complex (BötC), and preBötzing complex (preBötC). The caudal half of the VRC is subclassified into rostral ventral respiratory group (rVRG) and caudal ventral respiratory group (cVRG) based on the prominence of inspiratory neurons in the rVRG (Dobbins & Feldman, 1994; Iscoe, 1998) and expiratory neurons in the cVRG (Ezure *et al.*, 2003b) (Figure 1.2 A)

The pontine respiratory nuclei forms rich reciprocal connections with all VRC subnuclei (Bianchi *et al.*, 1995; Alheid *et al.*, 2004; Chamberlin, 2004) and receives various visceral sensory inputs relayed from the NTS (Ricardo & Koh, 1978; Herbert *et al.*, 1990). Lesion of the pontine respiratory neurons leads to a prolonged inspiratory phase, characterised by abolished post-inspiratory activity and laryngeal adduction (Dutschmann & Herbert, 2006),

suggesting a critical role for the pons in shaping respiratory motor patterns, especially in coordinating the transition from inspiration to expiration (Smith *et al.*, 2007; Bautista & Dutschmann, 2014; Dutschmann *et al.*, 2014). More recent studies demonstrate the pontine respiratory neurons contribute to the generation of cardiac vagal tone and are largely responsible for respiratory sinus arrhythmia (Baekey *et al.*, 2008; Farmer *et al.*, 2016).

Chemical and genetic markers for respiratory function

Numerous chemical markers and neurodevelopmental transcription factors have been proposed to distinguish neurons in the RTN/pFRG, BötC, and the preBötC (Figure 1.2 A').

The RTN and pFRG refer to very similar anatomical regions along the ventral surface of the brainstem just beneath the facial nucleus and extending caudally to the rostral ventrolateral medulla. The RTN has been identified as a source of efferent projections to the dorsal and ventral respiratory groups and was postulated to be the site of putative central chemoreceptors (Smith *et al.*, 1989; Li *et al.*, 1999; Mulkey *et al.*, 2004; Guyenet *et al.*, 2010). In contrast, the pFRG was identified as a region where pre-inspiratory (pre-I) neurons were recorded in neonatal rats (Onimaru & Homma, 1987). These neurons have been proposed as an inspiratory oscillator that is coupled with the preBötC (Onimaru & Homma, 2003; Feldman & Del Negro, 2006; Onimaru *et al.*, 2006), an expiratory rhythm generator or precursor cells of central chemoreceptor neurons seen in the RTN of the adult rat (Feldman & Del Negro, 2006; Janczewski & Feldman, 2006). The persisting difficulty in identifying pre-I neurons in the adult make it controversial to integrate the pFRG into adult respiratory circuits. A recent study supporting an active role of the RTN/pFRG in driving active expiration in adult rats (Huckstepp *et al.*, 2015), as well as a dynamic interaction between the RTN/pFRG and the preBötC, has been suggested to drive respiratory activities under different physiological conditions and at different developmental stages (Huckstepp *et al.*, 2016).

Transcription factor Phox2b (Stornetta *et al.*, 2006) and neurokinin 1 receptors (NK1R) (Nattie & Li, 2002) have been proposed as chemical markers of RTN glutamatergic neurons. Lesion of NK1R positive RTN neurons (with Substance P-conjugated saporin) results in an attenuation of the central response to carbon dioxide (CO₂) (Nattie & Li, 2002). Knock-out of the Phox2b gene leads to an absence of Phox2b-expressing neurons in the parafacial region, lack of respiratory response to CO₂, and fatal central apnea in mice (Dubreuil *et al.*, 2008). Furthermore, selectively activating the Phox2b RTN neurons produced a powerful activation of breathing without affecting cardiovascular function (Abbott *et al.*, 2009a; Burke *et al.*, 2015), suggesting that Phox2b RTN neurons function as central respiratory chemoreceptors. In humans, mutations in Phox2b have been associated with conditions such sudden infant death syndrome (SIDS) and congenital central hypoventilation syndrome (CCHS) (Amiel *et al.*, 2003; Weese-Mayer *et al.*, 2008; Amiel *et al.*, 2009). Evidence from animal models suggests that the potentially fatal incidences of sleep apnea seen in these conditions are largely due to failure in recruiting RTN neurons that detect changes of CO₂ in the blood (Ramanantsoa *et al.*, 2011). The alkaline-activated TASK-2 potassium channels and the proton-activated receptor GPR4 are found to be selectively expressed in Phox2b-expressing RTN neurons and are the essential molecular components for central respiratory chemosensitivity (Gestreau *et al.*, 2010; Wang *et al.*, 2013; Kumar *et al.*, 2015).

In addition to Phox2b, proneural transcription factor *Math 1* (also known as *Atoh1*) has been shown to be critical for the development of the Phox2b/NK1R expressing neurons in the RTN/pFRG, as *Math 1* null mice do not survive due to a central respiratory failure (Rose *et al.*, 2009). Furthermore, genetically inactivating *Math 1* in Phox2b expressing RTN neurons or inactivating Phox2b in *Math 1* expressing RTN neurons in transgenic mice eliminates central CO₂ chemosensitivity (Ruffault *et al.*, 2015), suggesting a critical role of both Phox2b and *Math 1* in governing the development of RTN neurons.

The neuropeptide galanin is co-expressed on ~50% of Phox2b-expressing RTN neurons (Stornetta *et al.*, 2009), and these galanin-expressing neurons are selectively activated by hypercapnia, but not hypoxia (Spirovski *et al.*, 2012). A recent study proposed that a subset of RTN/pFRG neurons expressing bombesin-like neuropeptide or gastrin-releasing peptide comprise the core circuits in control of sighing (Li *et al.*, 2016).

The BötC contains a collection of expiratory neurons that lie in a region ventral to the compact formation of nucleus ambiguus, dorsal to the RVLM pre-sympathetic neurons, and extending ~600µm caudally from the caudal pole of the facial nucleus in rats (Kanjhan *et al.*, 1995). BötC expiratory neurons send monosynaptic inhibitory projections throughout the VRC, targeting both inspiratory and expiratory bulbospinal neurons in cats (Jiang & Lipski, 1990) and in rats (Tian *et al.*, 1999). Bulbospinal BötC neurons also provide direct inhibitory inputs to phrenic motor neurons located in the C4-C5 segments of the spinal cord (Tian *et al.*, 1998). It has been proposed that the inhibitory circuitries in the BötC play a critical role in generating eupneic respiratory rhythms (Smith *et al.*, 2007; Richter & Smith, 2014).

Glycine is the classic chemical marker for the BötC, as it is the major neurotransmitter used by the BötC expiratory augmenting and decrementing neurons in rats (Schreihofer *et al.*, 1999; Ezure *et al.*, 2003a). However, GABA also has been detected in NTS projecting and spinally projecting BötC neurons in cats (Livingston & Berger, 1989; Song *et al.*, 2000). Bilateral microinjection of inhibitory peptides somatostatin or substance P into the BötC, evokes an apneustic response characterized by a prolonged inspiratory period (Burke *et al.*, 2010), and caused bradypnea by increasing expiratory duration respectively. The identity of cellular targets in both cases remains unexamined.

The preBötC is enriched with inspiratory propriobulbar neurons, and is thought to be the kernel for rhythmogenesis (Smith *et al.*, 1991; Monnier *et al.*, 2003). The inspiratory preBötC neurons can be further classified into subtypes based on their decrementing or incrementing firing

pattern and membrane properties (Rekling *et al.*, 1996; Gray *et al.*, 1999; Richter & Spyer, 2001). A subpopulation of preBötC inspiratory neurons characterized to burst intrinsically depending on either the Ca^{2+} -activated non-specific current or the persistent Na^+ current (Thoby-Brisson & Ramirez, 2001; Del Negro *et al.*, 2002a), is thought to be the pacemaker in generating respiratory rhythm. However, the expression of these currents is found ubiquitously on preBötC neurons (Del Negro *et al.*, 2005; Pace *et al.*, 2007a), and rhythmic activities persist after blockade of the conductance of putative pacemaker preBötC neurons (Pace *et al.*, 2007b; Montandon & Horner, 2013), suggesting that pacemaker properties are not necessary for respiratory rhythmogenesis (reviewed by Feldman *et al.*, 2013; Feldman & Kam, 2014).

Surprisingly, after almost thirty years of research, the mechanism of rhythmogenesis in the preBötC remains unknown (Feldman *et al.*, 2013). Both excitatory and inhibitory neurons are intermingled in the preBötC (Stornetta *et al.*, 2003a; Winter *et al.*, 2009; Koizumi *et al.*, 2013), but their roles in the generation of respiratory drive are extremely contentious. There is little doubt that excitatory preBötC neurons are the critical component in rhythm generation (Gray *et al.*, 2010; Koizumi *et al.*, 2013), as glutamatergic transmission is an obligatory component of rhythmogenesis (Funk *et al.*, 1993; Wallen-Mackenzie *et al.*, 2006). On the other hand the role of inhibitory neurons in the generation of inspiratory bursts is unclear. One school of thought suggests that inhibitory preBötC neurons modulate the inspiratory pattern and mediate reflex or volitional apnea, as pharmacological blockade of GABAergic and glycinergic transmission in the preBötC and BötC does not affect normal respiratory rhythm (Janczewski *et al.*, 2013). But the other suggests that inhibitory transmission represents a critical component of the preBötC microcircuit that ultimately generates respiratory drive (Richter & Smith, 2014; Abdala *et al.*, 2015; Marchenko *et al.*, 2016). Although the mechanism of respiratory rhythm generation is certainly a hot topic in the field, a comprehensive review of such is beyond the scope of this

thesis, interested readers are directed to the latest reviews (Feldman & Kam, 2014; Richter & Smith, 2014).

Many chemical markers have been proposed to distinguish the preBötC from adjacent regions. NK1R and μ -opioid receptors are found to be expressed on a similar population of neurons clustered in the region of the preBötC (Gray *et al.*, 1999; Gray *et al.*, 2001), and a subpopulation of NK1R positive preBötC neurons are found to express type 2 vesicular glutamate transporter (VGlut2) (Wang *et al.*, 2001; Guyenet *et al.*, 2002). Somatostatin peptide (SST) and somatostatin receptor 2a (sst_{2a}) are also found to be localized in the preBötC (Stornetta *et al.*, 2003a; Llona *et al.*, 2004; Gray *et al.*, 2010). The glycoprotein reelin (Tan *et al.*, 2012), as well as tyrosine kinase B (Thoby-Brisson *et al.*, 2003) are also proposed to be useful markers to define the preBötC.

Transcription factor Dbx1 has been found to determine the fate of glutamatergic interneurons in the preBötC (Bouvier *et al.*, 2010; Gray *et al.*, 2010), and most Dbx1 expressing preBötC neurons have a pre-inspiratory firing pattern and lack dendritic spines (Picardo *et al.*, 2013). Selective ablation of Dbx1 preBötC neurons irreversibly compromises the respiratory motor output and eventually leads to loss of rhythmic activities *in vitro* (Wang & Hayes, 2014). The preBötC Dbx1 derived neurons have been subsequently proposed to represent the core respiratory rhythmogenic circuits (Ruangkittisakul *et al.*, 2014).

Accessing and manipulating distinct populations of neurons expressing particular receptors, neurotransmitters, or transcription factors in the preBötC has proven a useful approach to dissect the neural circuitries responsible for respiratory rhythm genesis. For example, targeted ablation of NK1R positive preBötC neurons by substance P conjugated saporin induces an irreversible ataxic breathing pattern *in vivo* (Gray *et al.*, 2001; Wang *et al.*, 2002); pharmacogenetically silencing somatostatinergic neurons with an allatostatin ligand induced apnea *in vivo* (Tan *et al.*, 2008); photoactivation of the glycinergic preBötC neurons stops breathing, but

photoinhibition of the same population of neurons does not affect the respiratory rhythm (Sherman, Worrell, Cui, & Feldman, 2015), and acute photoinhibition of glutamatergic, Dbx1 expressing or somatostatin expressing preBötC neurons reduce the inspiratory frequency in a laser power dependent manner, suggesting these phenotypically defined neurons share a neuronal voltage dependent frequency control mechanism in respiratory rhythm generation (Koizumi *et al.*, 2016b). It is worth noting that the functional significance of some proposed markers themselves are unclear. For example, genetic deletion of SST (Low *et al.*, 2001), somatostatin receptors (Allen *et al.*, 2003; Qiu *et al.*, 2008; Rajput *et al.*, 2011), substance P and neurokinin A (Berner *et al.*, 2007; Shvarev *et al.*, 2010) produce only mild respiratory disturbances, and selective elimination of glutamatergic drive from SST-synthesizing neurons evokes no respiratory phenotype (Tupal *et al.*, 2014).

In fact, bridging functional properties with neurochemical phenotypes remains a major challenge in many fields of neuroscience, including the autonomic domain. Neurons with similar functional properties may express diverse neurochemical markers; conversely, neurons that share a common neurochemical phenotype may be functionally diverse (Luo *et al.*, 2008). The relationship between function and neurochemical content is loose in respiratory neurons; for example: bulbospinal, augmenting inspiratory neurons in the VRC are mostly glutamatergic (Stornetta, Sevigny *et al.* 2003), but propriobulbar, augmenting inspiratory neurons have been reported to be GABAergic (Okazaki, Takeda *et al.* 2001). Even within the same region, neurons with similar discharge patterns can have different neurochemical profiles. Expiratory decrementing neurons in the BötC have been reported to be glycinergic (Ezure, Tanaka *et al.* 2003) or GABAergic (Okazaki, Takeda *et al.* 2001), but both glycine and GABA are widely expressed in other functional classes of neuron in the medulla and throughout the brain. The link between neuronal respiratory activities and proposed chemical markers is often inadequately addressed. For example, the widely adopted preBötC ‘marker’ NK1R is only

found on one third of electrophysiologically identified pre-inspiratory preBötC neurons (Guyenet and Wang 2001) and, although a role for SST-expressing glutamatergic neurons in rhythm genesis is suggested by loss of function (Tan *et al.*, 2008) and recent optogenetic experiments (Cui *et al.*; Cui *et al.*, 2016; Koizumi *et al.*, 2016a); surveys for somatostatinergic preBötC respiratory neurons have thus far been fruitless (Stornetta, Rosin et al. 2003). We attempt to address this in Chapter 3.

Cardiovascular networks

The neural circuits that control cardiovascular function are predominantly located in the ventral medulla (comprehensively reviewed by Dampney, 1994; Guyenet, 2006). A comprehensive review of the central control of blood pressure is out of the scope of this thesis. In brief, the contractility of vascular smooth muscle regulates blood pressure and flow in response to neuronal and hormonal signals. The neuronal signals come from sympathetic ganglionic neurons (subpopulations of which also innervate other viscera, the kidney and sino-atrial node). The ganglionic neurons are catecholaminergic neurons that receive monosynaptic inputs from cholinergic sympathetic preganglionic neurons (SPN) located in the thoracic spinal cord. Although the SPN serve as an important relay for efferent sympathetic signals, sympathetic vasomotor tone is primarily generated and maintained by supraspinal circuits, as it is completely abolished by transection of the cervical spinal cord (Alexander, 1946).

As described by the seminal work of Strack *et al.* (1989), there are five supraspinal neuron groups that provide direct input to the SPN. These are the paraventricular nucleus of the hypothalamus (PVN), the region of the A5 cell group, the caudal raphe group, the rostral ventromedial medulla (RVMM) and the rostral ventrolateral medulla (RVLM). Although all are important in regulating blood pressure, the RVLM emerged as the kernel in generating and maintaining sympathetic vasomotor tone as its electrolytic destruction or chemical suppression

(Guertzenstein & Silver, 1974; Dampney & Moon, 1980; Willette *et al.*, 1983) dramatically decreases blood pressure and SNA to the level seen in animals which have received a transection at the medulla-spinal cord junction (Alexander, 1946). Subsequent works have established the pivotal role of the RVLM in tonic and phasic regulation of cardiovascular function (Dampney *et al.*, 1982; Ross *et al.*, 1984; Dampney *et al.*, 2002; Goodchild & Moon, 2009).

Interaction of the respiratory and cardiovascular networks

The respiratory and cardiovascular systems work harmoniously to deliver oxygenated blood to all organs, to eliminate CO₂ from the body and to maintain homeostasis. Despite the obvious differences in the structure and organization of the peripheral respiratory and cardiovascular systems in vertebrates, the neural networks that coordinate these two systems are highly conserved throughout evolution (reviewed by Taylor *et al.*, 1999). Neurons that are essential for the generation of respiratory rhythm and neurons that are responsible for generating baseline SNA form two overlapping columns in the ventral medulla (Guyenet, 2006; Alheid & McCrimmon, 2008). Although traditionally treated as independent entities, the activities of the cardiovascular and respiratory neural networks are intimately interwoven (Feldman & Ellenberger, 1988; Habler *et al.*, 1994; Taylor *et al.*, 1999; Dick *et al.*, 2014).

Respiratory rhythms influence heart rate (respiratory sinus arrhythmia), blood pressure (Traube-Hering waves) (reviewed by Billman, 2011; Dick *et al.*, 2014), and modulate basal SNA (Malpas, 1998) via both central and peripheral pathways. On the other hand, cardiovascular modulation of respiration is less obvious, but the temporal coherence of the cardiac and respiratory rhythms have been observed in humans, rats, rabbits, and guinea pigs (Galletly & Larsen, 1997; Larsen & Galletly, 1999; Tzeng *et al.*, 2003; Friedman *et al.*, 2012). Input from baroreceptors influences inspiratory timing in anaesthetised rats (Tzeng *et al.*, 2007), and baroreceptor stimulation evokes subtle decreases in respiratory frequency by increasing the

expiratory period and its variability (McMullan & Pilowsky, 2010). It has been suggested that baroreceptor inputs activate expiratory and post-inspiratory neurons, thus delaying the onset of inspiration (Dick & Morris, 2004; Dick *et al.*, 2005; Baekey *et al.*, 2010). We focus on respiratory effects on the cardiovascular system, in particular, the respiratory related oscillation seen in the SNA, referred to as “respiratory-sympathetic coupling” hereafter in this thesis.

Rhythmical changes of arterial blood pressure were observed more than two hundred and fifty years ago (for review see De Burgh Daly, 2011). A form of large sweeping waves in the arterial blood pressure trace was described by Traube in curarized dogs under asphyxia condition in 1865, Hering later postulated a central respiratory origin of these waves, which came to be known as Traube-Hering waves (Halliburton, 1919). It was speculated that such low-frequency fluctuation of blood pressure may result from oscillations in sympathetic outflow (Karemaker, 1999). Early work from Adrian *et al.* (1932) demonstrated the presence of burst discharge in SNA in phase with phrenic nerve activity (PNA) (Figure 1.1), and reported that the maximum discharge coincided with inspiration (for reviews see Habler *et al.*, 1994; Malpas, 1998).

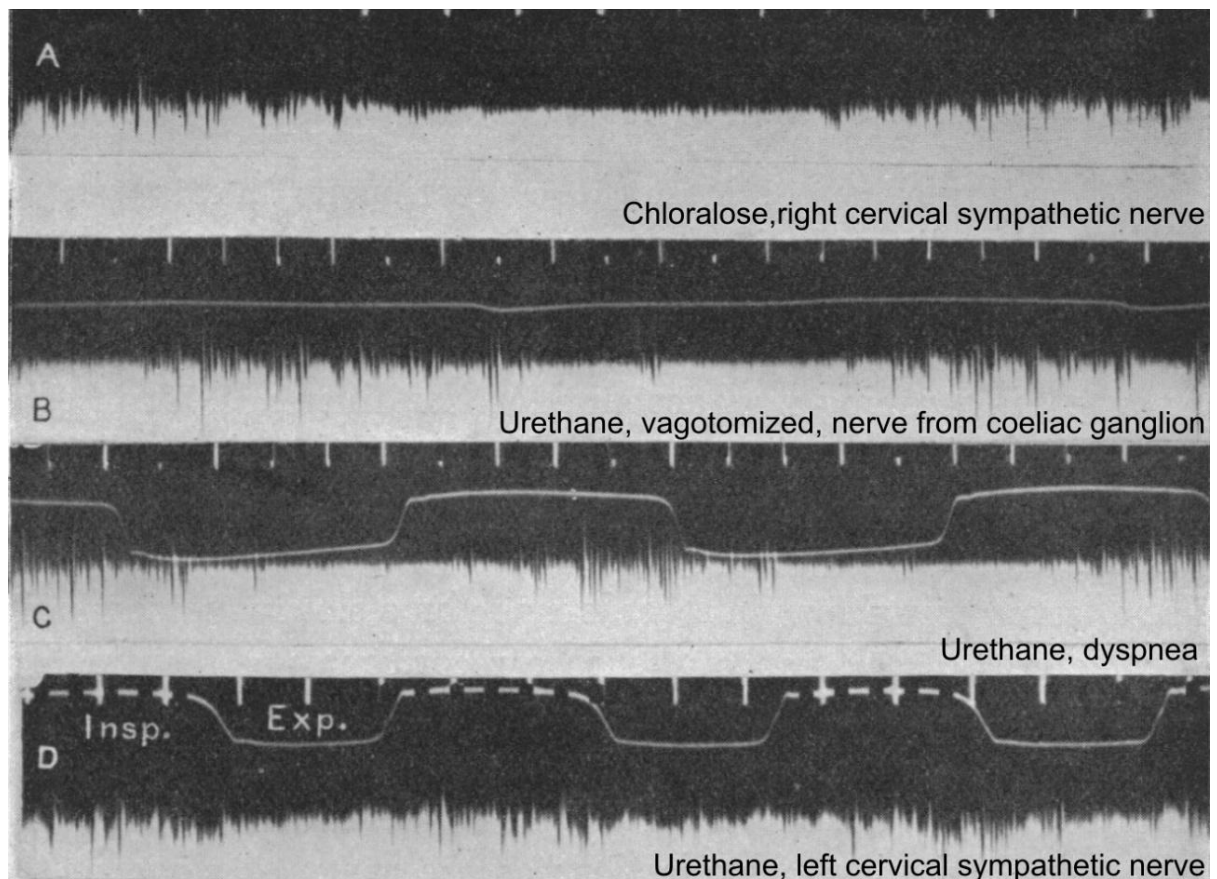


Figure 1.1 Respiratory modulation of sympathetic nerve activities (SNA). A - D, SNA recorded from different nerves in rabbits under different anaesthetic condition. Black trace representing SNA, white trace representing spontaneous respiratory movement, adapted from Adrian et al (1932).

This finding has been replicated in both human and animal models, including rats and cats under different experimental conditions (Bainton *et al.*, 1985; Eckberg *et al.*, 1985; McAllen, 1987; Haselton & Guyenet, 1989a; Czyzyk-Krzeska & Trzebski, 1990; Dempsey *et al.*, 2002; Dick *et al.*, 2004; Zoccal *et al.*, 2008). The most compelling evidence that supports central respiratory-sympathetic coupling is the persistence of phrenic-locked sympathetic discharge after central respiratory drive has been decoupled from lung inflation (i.e. in artificially ventilated, bilaterally vagotomised preparations) (Barman & Gebber, 1980; Haselton & Guyenet, 1989a; Habler *et al.*, 1994). Coherence analysis of SNA and PNA from vagotomised and baroreceptor-denervated cats also supports this view (Zhong *et al.*, 1997). Furthermore, respiratory modulation in SNA has been demonstrated in the working heart brainstem preparation, in which no sensory input from the lungs is preserved (Pickering & Paton, 2006; Simms *et al.*, 2009).

Respiratory-sympathetic coupling under normal conditions

Under normal conditions (normoxia/normocapnia), maximal cervical and lumbar SNA occurs during the post-inspiratory phase, whereas splanchnic, cardiac, renal and adrenal SNA exhibit a biphasic respiratory modulation with peaks in both inspiratory and post-inspiratory phases (Numao *et al.*, 1987; Miyawaki *et al.*, 2002; Dick *et al.*, 2004). The functional role of respiratory-sympathetic coupling under normal physiological conditions remains obscure. It has been speculated that rhythmic inputs from the respiratory centre may play a role in facilitating synaptic transmission in sympathetic ganglia by synchronizing volleys of impulses in individual sympathetic preganglionic neurons (Habler *et al.*, 1994). The increase in heart rate during inspiration has been proposed to contribute to improving gas exchange efficiency (Hayano *et al.*, 1996), although *in silico* modelling suggests that the functional significance of these effects are minor (Ben-Tal *et al.*, 2012). Other researchers have proposed that the coupling of the two systems may allow for the adaption of complex patterns of activities under abnormal physiological challenges, such acute or chronic hypoxia (Dick *et al.*, 2014).

Pathological implications of respiratory-sympathetic coupling in the control of blood pressure

Enhancement of respiratory-sympathetic coupling has been observed in adult rats exposed to acute hypoxia (Dick *et al.*, 2004; Dick *et al.*, 2007), in juvenile rats submitted to chronic intermittent hypoxia (Zoccal *et al.*, 2008; Moraes *et al.*, 2012b), in congenital neurogenic hypertensive rats (Simms *et al.*, 2009), and in rats that were made hypertensive by systemic infusion of angiotensin II and feeding on high salt diet (Toney *et al.*, 2010). Based on the well-established correlation between elevated SNA and hypertension (reviewed by Guyenet, 2006; Malpas, 2010), it has been suggested that enhanced respiratory-sympathetic coupling could be a key contributor to the development of hypertension (Simms *et al.*, 2010).

Rats subjected to chronic intermittent hypoxia (CIH) are often used as animal models to mimic the physiological stress seen in patients with obstructive sleep apnea (OSA) (Fletcher *et al.*, 1992a). It has been found that patients with OSA have a high risk of developing hypertension as a result of repetitive episodes of hypoxia during sleep (Dempsey *et al.*, 2010). Exposure to CIH produces a sustained elevation of the arterial blood pressure in rats (Fletcher *et al.*, 1992b), and an over activation of the adrenergic and the renin-angiotensin systems were suggested to mediate the effect (Fletcher, 2001). Alternatively, Zoccal *et al.* (2007) observed that ganglionic blockade after systemic antagonism of the angiotensin II type 1 receptor produced a greater blood pressure fall in CIH rats than control rats and also observed elevated plasma catecholamines in CIH rats, suggesting that CIH-induced hypertension is determined by sympathetic overactivity. Moreover, SNA in CIH rats was shown to exhibit an elevated baseline discharge level, with an enhanced expiratory-locked activity (Zoccal *et al.*, 2008). As the augmented expiratory SNA was coincidental with CO₂-induced active expiration (i.e. activation of abdominal trunk muscles), it was initially suggested that CO₂-sensitive neurons from the RTN/pFRG, known to play a critical role in driving active expiration, may also play an important role in modulating SNA in CIH models (Molkov *et al.*, 2011). However, subsequent experiments showed that inhibition of the RTN region does not affect CIH-evoked sympathoexcitation (Moraes *et al.*, 2012a), suggesting that alternative sources of drive must be involved. Transection of the pons (Baekey *et al.*, 2008) abolished the respiratory gating of the baroreceptor reflex, and antagonism of glutamatergic transmission in the NTS (Costa-Silva *et al.*, 2010) or in the BötC (Moraes *et al.*, 2012c) abolished the sympathetic response to activation of the peripheral chemoreceptors. Such findings suggest that supramedullary inputs, and inputs from the NTS play important roles in normal coupling of central respiratory and cardiovascular outflows.

In contrast to the consistent post-inspiratory peak bursts in the SNA seen in normotensive Wistar-Kyoto rat (WKY) subjected to normoxia, hypoxia, hyperoxia, hyper- or hypocapnia and transection of carotid sinus nerves, the respiratory related peak discharge of SNA in the spontaneous hypertensive rat (SHR) is shifted from the post-inspiratory phase to the inspiratory phase under normoxia, and exhibits variable shifting under the different experimental conditions (Czyzyk-Krzeska & Trzebski, 1990). Simms *et al.* (2009) showed enhanced respiratory-sympathetic coupling in SHR at all ages compared to WKY, irrespective of inputs from peripheral baro- and chemo-receptors. Moreover, the augmented SNA drives larger Traube-Hering waves in SHR. Similarly, in a hypertensive model where hypertension is caused by chronic infusion of angiotensin II in combination with a high salt diet, amplified burst-firing was observed in RVLM neurons, and bursting frequency was entrained with respiratory rhythm (Toney *et al.*, 2010). The authors proposed that the elevated splanchnic sympathetic outflow and vascular resistance in this animal model maybe due to an enhanced central respiratory-sympathetic coupling in a subpopulation of the RVLM neurons.

Site of respiratory-sympathetic coupling

The RVLM contains a cluster of adrenaline-synthesizing cells, known as C1 neurons (Hökfelt *et al.*, 1973, 1974; Ross *et al.*, 1984). Although the majority (~70%) of bulbospinal RVLM neurons are C1 neurons (Schreihöfer & Guyenet, 1997), this population is not critical for maintaining sympathetic vasomotor tone. Depletion of up to 84% of bulbospinally projecting RVLM C1 neurons by anti-dopamine β -hydroxylase-saporin injected in the spinal cord does not change the baseline level of SNA (Madden *et al.*, 1999; Schreihöfer *et al.*, 2000). Instead, loss of C1 neurons severely attenuates the sympathetic baroreflex, suggesting a prominent role of C1 neurons in sympathoexcitatory reflexes (Schreihöfer & Guyenet, 2000).

Pharmacological blockade of excitatory amino acids and GABA transmission in the RVLM greatly attenuates respiratory-sympathetic coupling (Guyenet *et al.*, 1990), suggesting that the interaction site lies in the rostral tip of the region. Electrophysiological recordings from bulbospinal RVLM neurons indicate a variety of respiratory discharge patterns. In the rat, three patterns have been described, 1 inspiratory depression, 2 inspiratory peak, and 3 inspiratory depression followed by post-inspiratory peak, with no apparent predominance of any one pattern (Haselton & Guyenet, 1989a). Similar studies by Miyawaki *et al.* (1995) and Moraes *et al.* (2013) found comparable patterns in barosensitive RVLM neurons in rats and demonstrated that central respiratory drive not only affects basal activity of RVLM neurons, but also modulates their responsiveness to baroreceptor activation.

Finally, acute silencing of rostral C1 neurons in Sprague Dawley (SD) rats has been reported to reduce basal sympathetic vasomotor tone and causes a reversible 30% reduction of the respiratory-related SNA bursts (Marina *et al.*, 2011). Taken together, the RVLM C1 population is likely to be the cellular substrate that mediates respiratory-sympathetic coupling.

Sources of respiratory input to RVLM presympathetic neurons

Blockade of excitatory inputs to the RVLM abolished post-inspiratory modulation in splanchnic SNA and partially affected the inspiratory peak of SNA (Miyawaki *et al.*, 1996), suggesting an excitatory nature of the presumed respiratory inputs to the RVLM. Furthermore, blockade of GABA transmission in the RVLM elicited an exaggerated post-inspiratory activity in SNA, which has also been interpreted as evidence that phasic GABAergic inputs contribute to respiratory-sympathetic coupling (Miyawaki *et al.*, 2002). But what are the likely sources of excitatory and inhibitory respiratory-locked drive to RVLM premotor neurons? Intracellular recorded and labelled respiratory neurons in the VRC have axonal arborisations in the RVLM region, and inspiratory neurons of the VRC have been proposed to provide modulation of

bulbospinal RVLM neurons (Pilowsky *et al.*, 1990; Pilowsky, 1995). Pharmacological inhibition of neurons in the caudal ventrolateral medulla (CVLM), including preBötC and rVRG neurons, eliminates the respiratory modulation on vasomotor presympathetic cells in the RVLM (Koshiya & Guyenet, 1996). One interpretation of this finding would be a critical role of local respiratory inputs in the respiratory-sympathetic coupling, however the abolishment of respiratory modulation could also be due to the suppression of the rhythm generator in general. In addition to the coupling between neurons from the VRC and RVLM, neurons from the Kölliker-Fuse nucleus (KF), the lateral parabrachial nucleus (LPBN) and the A5 noradrenaline cells (A5) are suggested to play an important role in respiratory-sympathetic coupling as pontine transection eliminated respiratory modulation of SNA and vagal post inspiratory discharge in the *in situ* preparation (Baekey *et al.*, 2008; Dick *et al.*, 2009)

Electrophysiological and anatomical tracing studies have identified multiple brain regions that project to the RVLM (Table 1.1). However, inputs from regions immediately adjacent to the RVLM (such the VRC) have been omitted due to technical difficulties related to confident identification of retrogradely labelled neurons in close proximity to a tracer injection site. Moreover, the functional roles of local inputs are largely unknown, due to the difficulty in identifying and manipulating the input neurons exclusively.

Brain regions	References describing projections to the RVLM
<i>Cortex</i>	(Van Bockstaele <i>et al.</i> , 1989; Card <i>et al.</i> , 2011; Bowman <i>et al.</i> , 2013)
<i>MnPo</i>	(Card <i>et al.</i> , 2011; Bowman <i>et al.</i> , 2013)
<i>CeA</i>	(Cassell & Gray, 1989; Saha <i>et al.</i> , 2005; Bowman <i>et al.</i> , 2013)
<i>PVN</i>	(Dampney <i>et al.</i> , 1987; Van Bockstaele <i>et al.</i> , 1989; Granata & Chang, 1994; Milner <i>et al.</i> , 1996; Yang & Coote, 1998; Hardy, 2001; Card <i>et al.</i> , 2011; Bowman <i>et al.</i> , 2013; Dempsey, 2016)
<i>DMH</i>	(Lovick, 1986; Card <i>et al.</i> , 2011; Bowman <i>et al.</i> , 2013)
<i>LHA</i>	(Lovick, 1986; Dampney <i>et al.</i> , 1987; Van Bockstaele <i>et al.</i> , 1989; Granata & Chang, 1994; Card <i>et al.</i> , 2011; Bowman <i>et al.</i> , 2013)
<i>Colliculi</i>	(Van Bockstaele <i>et al.</i> , 1989; Bowman <i>et al.</i> , 2013; Stornetta <i>et al.</i> , 2015; Dempsey, 2016)
<i>PAG</i>	(Lovick, 1985; Carrive <i>et al.</i> , 1988; Van Bockstaele <i>et al.</i> , 1989; Bago & Dean, 2001; Card <i>et al.</i> , 2011; Bowman <i>et al.</i> , 2013; Stornetta <i>et al.</i> , 2015; Dempsey, 2016)
<i>LC</i>	(Van Bockstaele <i>et al.</i> , 1989; Card <i>et al.</i> , 2011; Bowman <i>et al.</i> , 2013)
<i>LBPN/KF</i>	(Dampney <i>et al.</i> , 1982; Lovick, 1986; Dampney <i>et al.</i> , 1987; Van Bockstaele <i>et al.</i> , 1989; Horiuchi <i>et al.</i> , 1999; Bowman <i>et al.</i> , 2013; Stornetta <i>et al.</i> , 2015; Dempsey, 2016)
<i>A5</i>	(Van Bockstaele <i>et al.</i> , 1989; Madden <i>et al.</i> , 1999; Card <i>et al.</i> , 2011; Bowman <i>et al.</i> , 2013)
<i>RVMM/Nucleus raphe magnus/raphe obscurus</i>	(Lovick, 1986; Van Bockstaele <i>et al.</i> , 1989; Nicholas & Hancock, 1990; Zagon, 1995; Milner <i>et al.</i> , 1996; Verberne <i>et al.</i> , 1999; Babic & Ciriello, 2004; Card <i>et al.</i> , 2011; Bowman <i>et al.</i> , 2013; Dempsey, 2016)
<i>LTF</i>	(Barman & Gebber, 1987; Gebber & Barman, 1988; Dempsey, 2016)
<i>RVLM/BötC</i>	(Dampney <i>et al.</i> , 1987; Nicholas & Hancock, 1991; Bryant <i>et al.</i> , 1993; Lipski <i>et al.</i> , 1995; Gaytan <i>et al.</i> , 1997; Sun <i>et al.</i> , 1997; Card <i>et al.</i> , 2011; Agassandian <i>et al.</i> , 2012; McMullan & Pilowsky, 2012; Bowman <i>et al.</i> , 2013; Stornetta <i>et al.</i> , 2015; Dempsey, 2016)

<i>NTS</i>	(Dampney <i>et al.</i> , 1982; Ross <i>et al.</i> , 1985; Lovick, 1986; Dampney <i>et al.</i> , 1987; Van Bockstaele <i>et al.</i> , 1989; Granata & Chang, 1994; Aicher <i>et al.</i> , 1996; Koshiya & Guyenet, 1996; Milner <i>et al.</i> , 1996; Horiuchi <i>et al.</i> , 1999; Bowman <i>et al.</i> , 2013; Stornetta <i>et al.</i> , 2015; Dempsey, 2016)
<i>A1/CVLM/CPA/preBötC/VRG</i>	(Willette <i>et al.</i> , 1984; Granata <i>et al.</i> , 1986; Dampney <i>et al.</i> , 1987; Blessing, 1988; Van Bockstaele <i>et al.</i> , 1989; Ellenberger & Feldman, 1990; Agarwal & Calaresu, 1991; Gieroba <i>et al.</i> , 1992; Li <i>et al.</i> , 1992; Gaytan <i>et al.</i> , 1997; Campos & McAllen, 1999; Tan <i>et al.</i> , 2010; Card <i>et al.</i> , 2011; Bowman <i>et al.</i> , 2013; Stornetta <i>et al.</i> , 2015; Dempsey, 2016)
<i>Contralateral RVLM/VRC/CVLM/CPA</i>	(Willette <i>et al.</i> , 1984; Gordon & McCann, 1988; Van Bockstaele <i>et al.</i> , 1989; Granata & Chang, 1994; Lipski <i>et al.</i> , 1995; Gaytan <i>et al.</i> , 1997; Sun & Panneton, 2002, 2005; Card <i>et al.</i> , 2006; Tan <i>et al.</i> , 2010; Card <i>et al.</i> , 2011; McMullan & Pilowsky, 2012; Bowman <i>et al.</i> , 2013; Turner <i>et al.</i> , 2013; Dempsey, 2016)

Table 1.1 Inputs to the RVLM. Left column shows the areas providing inputs to the RVLM supported by electrophysiology or tract tracing studies. Right column is the corresponding literature. MnPo: Median preoptic nucleus, LHA: lateral hypothalamic nucleus, LPBN: lateral parabrachial nucleus, KF: Kölliker-Fuse nucleus, A1/A5: A1/A5 noradrenaline cells, RTN/pFRG: retrotrapezoid nucleus/parafacial respiratory group, BötC: Bötzing complex, preBötC: preBötzing complex, VRG: ventral respiratory group, RVLM: rostral ventrolateral medulla, RVMM: rostral ventromedial medulla, CVLM: caudal ventrolateral medulla, LTF: Lateral tegmental field, NTS: nucleus of the solitary tract, PVN: paraventricular hypothalamic nucleus, DMH: dorsomedial hypothalamic nucleus, CeA: central nucleus of the amygdala, PAG: periaqueductal gray, LC: locus coeruleus, CPA: caudal pressor area.

Despite speculation of direct inputs from ‘classical’ respiratory neurons to RVLM sympathetic premotor neurons (McAllen, 1987; Haselton & Guyenet, 1989b; Zhou & Gilbey, 1992; Miyawaki *et al.*, 1995; Sun *et al.*, 1997), no sources of the respiratory input have yet been definitively established. Alternative schemes that do not directly involve classically defined respiratory neurons include a role for respiratory modulated CVLM neurons (Schreihofer & Guyenet, 2002; Mandel & Schreihofer, 2006), expiratory RTN neurons (particularly for the post inspiratory pattern observed in SNA under hypercapnia (Molkov *et al.*, 2011)), or direct input from the NTS (Braga *et al.*, 2007; Zoccal *et al.*, 2014). Examination of monosynaptic inputs to RVLM C1 neurons from neurons in functionally distinct respiratory regions, such as the BötC, the preBötC, the VRG, and the pontine respiratory group (PRG), is one of the key aims of the current thesis (Figure 1.2 B).

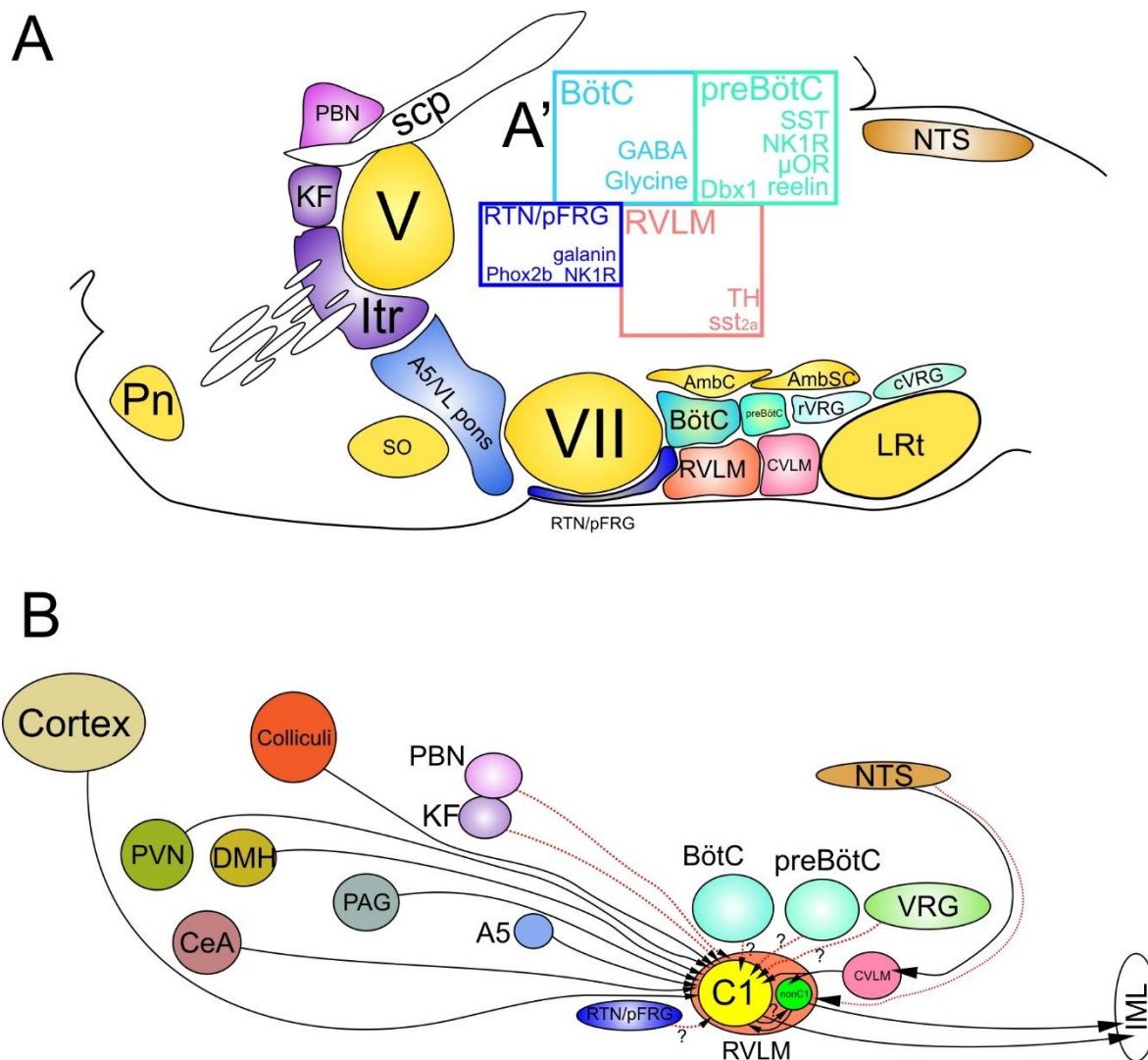


Figure 1.2 Inputs to the RVLM. A. Anatomy of respiratory and cardiovascular nuclei in the pons and medulla. A' Proposed chemical markers for the RTN/pFRG, BötC, and preBötC. B. Nuclei that project to the RVLM. Pn: pontine nuclei, PBN: parabrachial nucleus, KF: Kölliker-Fuse nucleus, Itr: intertrigeminal area, A5/VL pons: A5 noradrenaline cells/ventrolateral pons, SO: superior olive, V: trigeminal nucleus, scp: superior cerebellar peduncle, VII: facial nucleus, RTN/pFRG: retrotrapezoid nucleus/parafacial respiratory group, AmbC: nucleus ambiguus, compact part, AmbSC: nucleus ambiguus, subcompact part, BötC: Bötzinger complex, preBötC: preBötzinger complex, rVRG: rostral ventral respiratory group, cVRG: caudal ventral respiratory group, RVLM: rostral ventrolateral medulla, CVLM: caudal ventrolateral medulla, LRT: lateral reticular nucleus, NTS: nucleus of the solitary tract, PVN: paraventricular hypothalamic nucleus, DMH: dorsomedial hypothalamic nucleus, CeA: central nucleus of the amygdala, PAG: periaqueductal gray, IML: intermediolateral cell column.

Genetically restricted trans-synaptic tracing

Conventional anterograde and retrograde neuronal tracers have been used to collect information regarding brain connectivity. The retrograde tracer, cholera toxin subunit B (CTB) (Luppi *et al.*, 1987) has been extensively used to reveal neuroanatomical topography of neurons by their projection patterns (Goodchild *et al.*, 2000; Bowman *et al.*, 2013; Turner *et al.*, 2013). As a result of nonspecific labelling due to fibres passing through the injection field (Conte *et al.*, 2009), conventional tracers are not suitable for dissection of local interneuron connections. Furthermore, the non-selectivity of tracer uptake clouds interpretation of data pertaining to functionally heterogeneous brain regions, as there is no way to know to which functional subsets labelled neurons belong. As well, only half of the putative synaptic contacts identified by light microscopy following labelling with anterograde tracers are actually confirmed as synapses when examined under electron microscopy (Poulat *et al.*, 1992).

Trans-neuronal tracers were developed to overcome the ambiguity associated with identification of synaptic connections between neurons. Researchers initially deployed reagents such as the C-fragment of tetanus toxin (TTC), which is responsible for cell entry and trans-synaptic spread of tetanus toxin (Horn & Büttner-Ennever, 1990), or green fluorescent protein fused with TTC (Maskos *et al.*, 2002). Alternative approaches were to trace the progress of wheat germ agglutinin-conjugated horseradish peroxidase (Gonatas *et al.*, 1979). However, continued spread of these reagents across multiple synapses makes such tracers poorly suited for the investigation of monosynaptic connections (reviewed by Vercelli *et al.*, 2000; Callaway, 2008; Nassi *et al.*, 2015).

Natural neurotropic viruses, such as alpha-herpes virus (herpes simplex virus, pseudorabies) and rhabdoviruses (rabies virus, vesicular stomatitis virus), have been used for trans-synaptic tracing for decades (Strack *et al.*, 1989; Ugolini, 1995). Initially used to identify neuronal circuits connected to peripheral targets (e.g. skeletal muscle, adrenal gland), the utility of these

pathogens as research tools has been realised by the advent of modern molecular techniques, which have enabled their modification and redesign to restrict initial entry of virions to genetically targeted subpopulations of neurons and to limit trans-synaptic trafficking to a single order of the synaptic hierarchy. This technique, which has been applied to retrograde vesicular stomatitis virus and rabies virus (Wickersham *et al.*, 2007b; Beier *et al.*, 2011) is the foundation for the experimental series described in Chapter 4, and therefore merits a detailed overview.

The major advantage of rhabdoviruses over other viral vectors used for neuronal pathway tracing, such as a herpes virus, is that their mode of propagation is exclusively retrograde in the CNS (Ugolini, 1995; Kelly & Strick, 2000). Upon entering cells at the synaptic terminal, rabies virus is retrogradely transported to the cell body for transcription and replication, from which the virus spreads across chemical synapses to the next order of presynaptic neurons. As the cycle of retrograde transportation, transcription, and replication repeats, the rabies virus spreads to synaptically connected neurons order by order. This inherent limitation prevents differentiation of monosynaptic connections from polysynaptic connections that participate in a circuit.

An elegant solution to this limitation was developed by pseudotyping a recombinant rabies virus, in which the gene encoding the rabies glycoprotein was replaced with a sequence that encodes a fluorescent reporter (Wickersham *et al.*, 2007b) (Figure 1.3). Wild-type rabies virus contains a single negative strand of RNA which encodes five proteins, nucleoprotein (N), phosphoprotein (P), matrix protein (M), glycoprotein (G) and polymerase (L). The rabies glycoprotein is essential for mediating the trans-synaptic spread of the virus (Mebatsion *et al.*, 1996). In wild-type rabies, G is incorporated into the viral envelope, allowing it to interact with (as yet uncharacterised) presynaptic receptors (Lentz *et al.*, 1982; Schnell *et al.*, 2010). It is this interaction between rabies glycoprotein and receptors expressed on the presynaptic neuron that underlies the trans-synaptic trafficking of rabies. Although the exact mechanism is not fully

understood, deletion of the glycoprotein gene from the rabies genome renders the virus incapable of spreading from one neuron to another (Mebatsion *et al.*, 1996; Etessami *et al.*, 2000). Interestingly, so-called G deletion (or ΔG) does not affect the replication of the rabies virus within the infected cells, thus, a gene of interest such as a fluorescent reporter transgene (e.g. green fluorescent protein (GFP), yellow fluorescent protein (YFP)) can be inserted to replace the gene encoding G. Once the virus is introduced into cells, the reporter gene will be transcribed to produce fluorescent proteins to label the cell. This approach was originally developed using a rodent-specific strain of rabies that was developed in Berne in the 1970s (B19), which itself originated from the Street Alabama Dufferin rabies strain (SAD), isolated from a dog in 1935, and is thus known as SAD B19 ΔG rabies, often abbreviated to SAD ΔG (Geue *et al.*, 2008).

The trans-synaptic capabilities of G-deleted rabies virus can be temporarily rescued by expressing G in the infected cell. Genes that encode G can be supplied to cells in form of plasmid DNA via electroporation (Marshall *et al.*, 2010), via direct injection from a whole cell recording pipette (Rancz *et al.*, 2011), or using a genetically modified helper virus, such as adeno associated virus, herpes simplex virus or lentivirus (Wall *et al.*, 2010; Choi & Callaway, 2011; Yonehara *et al.*, 2011; Yonehara *et al.*, 2013). The glycoprotein supplied *in trans* restores the capacity of the virus to spread trans-synaptically. However, due to a lack of G in the secondarily infected neurons, the virus cannot spread beyond the first synapse (Wickersham *et al.*, 2007b).

In order to direct the G-deleted rabies virus into a defined starter cell population, Wickersham *et al.* (2007b) pseudotyped SAD ΔG with envelope protein (EnvA) from the subgroup A avian sarcoma and leucosis virus (ASLV-A). The EnvA protein specifically interacts with the cognate TVA receptor, which has no homologue in mammalian cells (Bates *et al.*, 1993; Young *et al.*, 1993; Federspiel *et al.*, 1994; Barnard *et al.*, 2006). By introducing the genes for TVA and

rabies G into a single neuron or neurons of interest and then applying SADΔG(EnvA), this two-step restricted monosynaptic trans-synaptic tracing system allows identification of presynaptic inputs to any defined neuronal population (reviewed by Ginger *et al.*, 2013; Callaway & Luo, 2015).

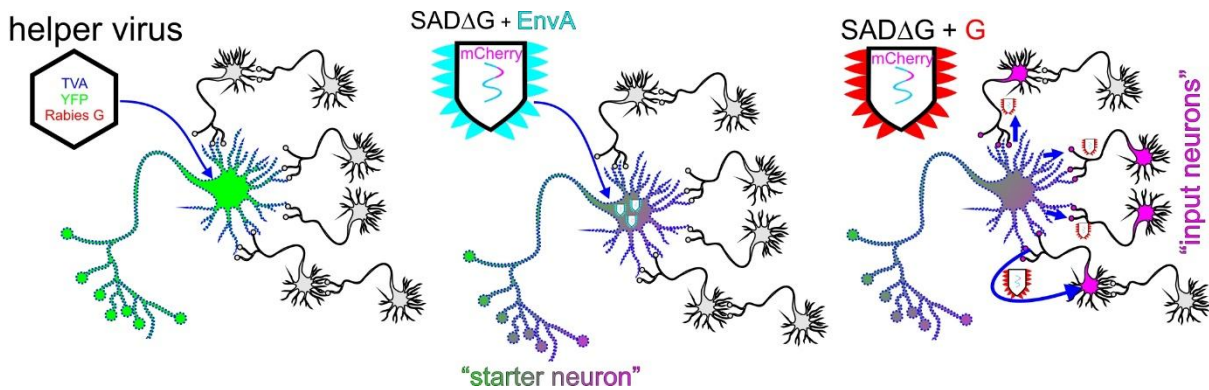


Figure 1.3 Monosynaptic tracing with glycoprotein-deleted EnvA-pseudotyped rabies (SADΔG(EnvA)). Neurons are transfected by helper virus containing genes encoding the cognate receptors for EnvA (TVA), the rabies glycoprotein (G) and reporter protein (YFP). SADΔG(EnvA) exclusively enter the infected neuron (starter neuron) via EnvA-TVA interaction, and subsequently spread retrogradely to the next order of synaptically connected neurons (input neurons). Due to lack of the G in the genome, SADΔG(EnvA) is unable to spread beyond the first order of the presynaptic hierarchy. Input neurons can be distinguished from the starter neurons by exclusively expressing the reporter gene from the rabies genome.

The field of connectomics in neuroscience

A major component of the field of neuroanatomy is the study of synaptic connections that link neurons and therefore underlie brain function. Ever since the pioneering work of Golgi and Cajal over a hundred years ago, generations of neuroscientists have attempted to generate comprehensive wiring diagrams of the brains of experimental animals and humans (reviewed by Catani *et al.*, 2013). The first nearly complete map of the entire nervous system of an individual species was made for the roundworm *C. elegans* (White *et al.*, 1986), and later completed by Varshney *et al.* (2011); this remains the only complete neural wiring diagram of an animal to date. The term “connectome” was later suggested by Sporns (2005) and Hagmann (2005) to refer to a completed map of neural connections within the brain. The field of connectomics has recently emerged as a standalone field of neuroscience due to advances in

neural tract tracing, imaging, and computational techniques, which make mapping mammalian brains possible.

Based on spatial resolution, the connectome can be used to refer to the brain connectivity at macro, meso, or microscales. In the Human Connectome Project, magnetic resonance imaging (MRI) is used to acquire structural and functional neural connections in the human brain at the macroscale level (a resolution of millimeters) (Toga *et al.*, 2012). At the other end of the scale, individual synaptic connections (at a resolution of nanometers) are mapped by imaging the brain using electron microscopy (White *et al.*, 1986; Bock *et al.*, 2011; Helmstaedter, 2013). Although the microscale connectome potentially offers comprehensive knowledge of every neural connection, the enormous time and resources required to collect, reconstruct, and analyse such connectomic data restrict its application in large mammalian brains. As a result of advanced imaging, computation, and emerging anterograde and retrograde viral tracers, the prospect of generating comprehensive connectomic maps to reveal both distant and local connections at the mesoscale is now becoming feasible (Pollak Dorocic *et al.*; Oh *et al.*, 2014; Schwarz *et al.*, 2015). However, controversy about the utility of extensive connectomic data remain unresolved (see the debates: Anothony Movshon vs Sebastian Seung in 2012 and vs Moritz Helmstardter in 2016). Taking for example the human genome project, people had doubts about the value of sequencing the whole human genome and questioned the exploratory nature of such a project. However, the completion of the human genome project not only dramatically advanced sequencing techniques, but also accelerated the incorporation of genetic techniques to biology at large (Lander, 2011). The connectomic data has already emerged as an important resource to guide neuroscience research. For example, the neural wiring diagram of *C. elegans* (White *et al.*, 1986) has helped researchers design experiments to understand the mechanism of thermosensing, chemosensing and egg-laying behaviour in the worm (Bargmann *et al.*, 1990; Shyn *et al.*, 2003; Kimura *et al.*, 2004). Although there are challenges for analysis

and interpretation of connectomic data (Lichtman *et al.*, 2014), novel connectomic technologies have already provided new insights into normal (Bota *et al.*, 2015; Petersen & Sporns, 2015) and pathological brain function, such as in stroke and psychiatric disorders (Silasi & Murphy, 2014; Fornito *et al.*, 2015).

Aims of this thesis

It is an ongoing task to fully characterize cardiovascular and respiratory neurons and appreciate their diversity at the anatomical, neurochemical and electrophysiological levels. Our initial objective was to map the neuronal connectomes of single functionally identified medullary respiratory or cardiovascular neurons, in order to identify detailed circuits and relate network architecture to functions *in vivo*, using the restricted monosynaptic tracing technique described above (Wickersham *et al.*, 2007a). In order to allow SADΔG(EnvA) to gain access to functionally characterized neurons, one major hurdle we had to overcome was to efficiently transfect recorded single neurons with plasmid DNA that encodes the TVA and the rabies glycoprotein. Inspired by the work from Marshel *et al.* (2010), which described a single neuronal monosynaptic network tracing strategy (although in their case they did not functionally identify neurons prior to transfection), we developed a method to genetically manipulate single electrophysiologically characterized brainstem neurons, as described in Chapter 2.

We first modified a conventional extracellular recording apparatus by connecting a constant voltage generator in parallel with the amplifier headstage, allowing us to apply high-voltage (up to 10 V) pulses across a recording electrode, temporarily causing dielectric breakdown of the cell membrane and simultaneous ejection of charged macromolecules, such as dyes or plasmid DNA, from the pipette tip. We then developed a protocol to guide the recording pipette into the optimized juxtacellular position, which is critical for the success of labelling or transfection of recorded neurons. When using small molecular dyes such as neurobiotin, our technique matches

the mainstream juxtacellular labelling technique (Pinault, 1996) in labelling quality and surpasses it in efficiency and ease of application. Although we achieved a promising success rate (~80%) in depositing plasmid DNA *in vitro* using this technique (and we had some success *in vivo*), this approach was ultimately too technically difficult and unreliable to use routinely for single cell gene delivery *in vivo* (Chapter 2).

Such technique proved simple and effective for dye delivery *in vivo*, and we applied this technique to test the hypothesis that expression of somatostatin _{2a} receptor (sst_{2a}) serves as a neurochemical marker for respiratory function in the VRC (Chapter 3). Numerous studies have demonstrated an inhibitory effect of somatostatin (SST) on respiration (Yamamoto *et al.*, 1988; Chen *et al.*, 1990; Pantaleo *et al.*, 2011), and electrophysiological evidence from our laboratory suggested SST exerts respiratory inhibition in a site specific and dose dependent manner (Burke *et al.*, 2010). Microinjection of SST delays phase transition from inspiration to expiration in the BötC, attenuates or abolishes respiratory frequency in the preBötC, and reduces phrenic nerve discharge amplitude when injected in the rVRG (Burke *et al.*, 2010). Further supported by anatomical evidence for high sst_{2a} expression in the ventral medulla region (Burke *et al.*, 2008; Spary *et al.*, 2008; Gray *et al.*, 2010), sst_{2a} was proposed to be a marker for respiratory neurons in the VRC. In Chapter 3, we directly tested this hypothesis by recording and labelling respiratory neurons in the VRC *in vivo*, and describing the distribution of sst_{2a} in the VRC respiratory cell groups with respect to widely used markers of respiratory function and on labelled respiratory neurons.

Due to the relatively low success rate of delivering genes to single neurons *in vivo*, we adopted an alternative strategy to map monosynaptic inputs to putative RVLM cardiovascular control neurons (Chapter 4). We used a lentiviral vector to drive the expression of YFP, TVA and rabies G in RVLM catecholaminergic neurons under the control of the PRSx8 promoter. We then subsequently injected SADΔG(EnvA)-mCherry in the same region to trace the

monosynaptically connected presynaptic neurons. In order to analyse the large connectomic dataset, we adapted a volumetric brain atlas and identified likely inputs from regions involved in respiratory rhythm genesis, phase transition and pattern modulation, thus providing a structural framework that may underlie the important physiological phenomenon of respiratory-sympathetic coupling.

Finally, in Chapter 5, the major findings of the studies are summarised with potential influence of the results in understanding the central control of cardiovascular and respiratory functions discussed, and potential approaches and ideas for future research proposed.

2.

Recording, labelling and
transfection of single neurons
in deep brain structures

Abstract

Genetic tools that permit functional or connectomic analysis of neuronal circuits are rapidly transforming neuroscience. The key to deployment of such tools is selective transfection of target neurons, but to date this has largely been achieved using transgenic animals or viral vectors that transduce subpopulations of cells chosen according to anatomical rather than functional criteria. Here we combine single-cell transfection with conventional electrophysiological recording techniques, resulting in three novel protocols that can be used for reliable delivery of conventional dyes or genetic material *in vitro* and *in vivo*. We report that techniques based on single cell electroporation yield reproducible transfection *in vitro*, and offer a simple, rapid and reliable alternative to established dye-labelling techniques *in vivo*, which are incompatible with targeted transfection in deep brain structures. In contrast, we show that intracellular electrophoresis of plasmid DNA transfects brainstem neurons recorded up to 9 mm deep in the anaesthetized rat. The protocols presented here require minimal, if any, modification to recording hardware, take seconds to deploy, and yield high recovery rates *in vitro* (dye labelling: 89%, plasmid transfection: 49%) and *in vivo* (dye labelling: 66%, plasmid transfection: 27%). They offer improved simplicity compared to the juxtacellular labelling technique and for the first time offer genetic manipulation of functionally characterized neurons in previously inaccessible brain regions.

Introduction

Techniques that combine electrophysiological recording of neuronal activity with dye labelling have been used to address fundamental questions about the relationship between neurochemistry, morphology, and cell behaviour (Schreihöfer & Guyenet, 1997; Bevan, 1998; Mileykovskiy *et al.*, 2005; Nosedá *et al.*, 2010; Jiang *et al.*, 2013). Historically, investigators have used three main strategies to introduce dye from a recording pipette to the cell interior. In the first, intracellular access is obtained by impalement of the neuron with a sharp electrode and fluorescent dyes or biotin conjugates are deposited by intracellular electrophoresis (Stretton & Kravitz, 1968; Horikawa & Armstrong, 1988). In the second, whole cell access is obtained using a low-resistance patch pipette and dye is passively dialyzed into the cell (Edwards *et al.*, 1989; Pickering *et al.*, 1991). In the third approach an extracellular recording electrode is positioned in close contact to the cell membrane (a “juxtacellular” position) and a train of 200 ms long positive current pulses up to 10 nA in amplitude is used to initiate and maintain membrane electroporation and simultaneously eject positively charged dyes, typically over a period of 2 – 30 minutes (Pinault, 1996; for review, see Pinault, 2011).

All three approaches are technically difficult and require experience and skill for efficient use, particularly *in vivo*. The quality of labelling obtained using the juxtacellular approach is generally inferior to that obtained using intracellular dye deposition; however, the technical difficulty associated with maintaining stable sharp recordings or obtaining whole cell access in deep brain regions *in vivo* has led to the ascendancy of Pinault’s juxtacellular technique as the gold-standard approach for labelling functionally identified neurons.

Recent advances in molecular biology have provided incentives for the development of single-cell labelling techniques that are compatible with intracellular nucleotide delivery. The major challenge associated with delivery of genetic material is the large molecular weight of gene constructs and the high copy number required for efficient transfection. For example, the

molecular weight of the plasmid that encodes yellow fluorescent protein, pCAG-YFP (MW 1.8 MDa) is approximately 6,000 times greater than that of neurobiotin (MW 286 Da). This obstacle has been overcome using two approaches. First, as with traditional dyes, plasmids can be dialyzed into neurons during low-resistance whole cell recordings (Rancz *et al.*, 2011). Although the transfection rate associated with this approach is high (56%: Rancz *et al.*, 2011) and the use of whole-cell patch recordings *in vivo* is becoming more commonplace, this approach is still restricted to more superficial brain regions as whole-cell recordings become difficult to obtain beyond about 2 mm deep (Margrie *et al.*, 2002; Schramm *et al.*, 2014).

An alternative approach combines conventional electrophysiological recording methods with single cell electroporation (SCE) (Haas *et al.*, 2001; Rae & Lewis, 2002; Rathenberg *et al.*, 2003; Bestman *et al.*, 2006a; Steinmeyer & Yanik, 2012). In common with the juxtacellular technique, SCE uses voltage trains to induce localized dielectric breakdown of the cell membrane and drive charged molecules from the pipette into the cell, but differs in terms of the duration (~ 1 ms), frequency (50 – 1000 Hz) and amplitude of pulses (~ 10 V, equivalent to ~ 500 nA assuming a series resistance of 20 M Ω). SCE is an efficient and quick transfection method, but suffers some limitations: first, it is critically dependent on gentle contact between the pipette and target cell, meaning its use is largely restricted to preparations in which direct visualization of the cell is possible (Rathenberg *et al.*, 2003; Kitamura *et al.*, 2008a; Judkewitz *et al.*, 2009). Furthermore, the voltages required for efficient SCE are beyond the limits of commercially available voltage-clamp amplifiers, meaning SCE cannot readily be combined with electrophysiological characterization of target neurons.

Three recent reports detail amplifier modifications and protocols that combine traditional electrophysiological recordings with SCE, allowing transfection of recorded neurons *in vitro* (Daniel *et al.*, 2013) or, within superficial layers of the cortex, *in vivo* (Cohen *et al.*, 2013; Oyama *et al.*, 2013). These achievements represent an important technical landmark that, in

common with the whole-cell transfection technique (Rancz *et al.*, 2011), may prove valuable to investigators studying neurons in easily accessible brain regions. However, their applicability to neurons in deep or fibrous regions of the adult brain is unproven.

Our group has a long-standing interest in the anatomy, behaviour, and network dynamics of autonomic and respiratory nuclei deep in the ventrolateral medulla of the rat (McMullan *et al.*, 2008; Sevigny *et al.*, 2008; Burke *et al.*, 2011). These neurons are located up to 9 mm deep to the cerebellar surface, lie intermingled with large fibre tracts, and are not amenable to whole-cell recordings in recovery experiments. The objective of the current study was to develop a technique that can be used for the targeted transfection of electrophysiologically profiled neurons in deep brain regions. We first independently developed an approach that combines extracellular recording of unit activity with SCE. We then validated its efficacy *in vitro* and extensively tested its suitability for transfection of neurons recorded >2 mm deep in the brainstem. We report that SCE-based approaches provide good transfection efficiency *in vitro* and can be used *in vivo* for dye-labelling as a simple and reliable alternative to the juxtacellular technique. However, in our hands SCE did not result in reliable transfection *in vivo*. To circumvent this limitation we describe a protocol for intracellular electrophoresis of DNA and show that this is a more useful approach.

Methods

Ethical Approval: All experiments were approved by Macquarie University Animal Ethics Committee and conformed to the Australian Code of Practice for the Care and Use of Animals for Scientific Purposes.

General Preparation

Preparation of brain slices for *in vitro* electroporation

P2-8 Sprague Dawley rat pups of either sex were anaesthetized with isoflurane and decapitated when areflexic. The head was submerged in ice-cold carbogen-bubbled artificial cerebrospinal fluid (ACSF, in mM: 125 NaCl, 25 NaHCO₃, 3 KCl, 1.25 NaH₂PO₄·H₂O, 10 glucose, 2 CaCl₂, 1 MgCl₂). The brain was dissected and 250 µm slices of hippocampus, cortex or brainstem were cut with a vibratome in ice-cold ACSF. Slices were maintained and recorded at 34°C in ACSF. In some cases spontaneous activity was enhanced by superfusing slices in 5-12 mM [K⁺] ACSF (Onimaru & Homma, 2007).

Organotypic slice cultures of hippocampus, cortex, brainstem and cerebellum were prepared as previously described (De Simoni & Yu, 2006). Cultures were maintained on organotypic culture mesh inserts (Millipore, PICM03050) in 6 well dishes, submerged in 1 ml of culture media. Slices were kept in a CO₂ incubator at 37°C, 5% CO₂ for at least 2 days prior to use.

Animal preparation: acute experiments

Adult Sprague Dawley rats of either sex (250 – 650 g) were anaesthetized with 10% urethane (1.3 g/kg i.p.) and prepared for single unit recording as previously described (Turner *et al.*, 2013). In brief, vascular access was obtained and rats were intubated and instrumented to record blood pressure, core temperature and end-tidal CO₂. Rats were positioned in a stereotaxic frame in the skull flat or nose-down (~30°) position. Bone overlying the brainstem was removed and the dura reflected. In experiments targeting respiratory neurons the caudal pole of the facial

nucleus, an anatomical landmark for the respiratory cell column, was mapped by antidromic field potentials as previously described (Brown & Guyenet, 1985). Diaphragmatic EMG was recorded as an index of respiratory phase via fine steel wire hook electrodes inserted through the thoracic wall into the diaphragm using a 26 gauge needle. When indicated by respiratory movements that interfered with recording stability, rats were artificially ventilated at parameters that maintained end-tidal CO₂ at 3.5 - 4.5% and movements suppressed by careful titration of pancuronium bromide (0.2 - 2 mg/kg i.v., AstraZeneca) such that diaphragmatic EMG was still observable. In long experiments hydration and electrolyte balance was maintained by intravenous infusion of 0.9% NaCl or 5% glucose (5 ml/kg/hr). Anaesthetic depth was carefully monitored by examining autonomic, respiratory and/or motor responses to firm pinch of the hindpaw; supplementary anaesthesia (10% initial dose) was provided as required.

Animal preparation: recovery experiments

Adult Sprague Dawley rats of either sex (85 – 605 g) were anaesthetized with intraperitoneal ketamine (75 mg/kg; Parnell Laboratories, Australia) mixed with medetomidine (0.5 mg/kg; Pfizer Animal Health, Australia). Prophylactic antibiotics (20 mg/kg Cephazolin sodium, i.m.; Mayne Pharma, Australia) and analgesia (2.5 mg/kg Carprofen, s.c.; Norbrook Pharmaceuticals, Australia) were administered and the left femoral artery and vein were cannulated under aseptic conditions. The brain was exposed as described above under minimally invasive conditions, medetomidine was reversed (atipamazole 1 mg; Pfizer Animal Health, Australia, s.c.), and anaesthesia switched to 1 – 3% isoflurane (Veterinary Companies of Australia Pty Ltd) in 100% oxygen and monitored as described above for the remainder of the procedure. In some experiments rats were artificially ventilated following endotracheal intubation with a 14 gauge cannula.

After conclusion of recordings, wounds were irrigated and the exposed brain covered with oxidized cellulose haemostat. Neck muscles were sutured and skin closed with stainless steel

suture clips. Femoral catheters were removed, vessels tied off and incisions closed. Anaesthesia was discontinued, rats were removed from the stereotaxic frame and, where applicable, extubated. Rats were monitored closely for up to 36 hours with additional analgesia as required.

Histology

At the conclusion of *in vivo* experiments rats were euthanized with pentobarbitone (>100 mg/kg i.v. (acute experiments) or i.p.

(recovery)), transcardially perfused with heparinised saline followed by 4% PFA, and the brain removed and postfixed in 4% PFA solution overnight. At the conclusion of *in vitro* experiments brain slices were briefly immersed in 4% PFA and transferred into TBPS until imaging.

Brainstems from *in vivo* experiments in which dextran or plasmids encoding fluorescent reporters were used were cut into 50 µm coronal sections with a vibrating microtome, wet-mounted and immediately visualized under epi-fluorescence. As part of a separate study, neurobiotin-labelled neurons were processed for ChAT and somatostatin 2A receptor immunoreactivity before visualization. Sections were washed in 0.01 M phosphate buffered saline containing 0.2% Triton-100 for 3x15 mins, and incubated in 0.01 M phosphate buffered saline containing 2% bovine serum albumin and 0.2% Triton-100 for 1 h at room temperature. Primary antibodies (Goat-anti-choline acetyltransferase, 1:800 (Chemicon, Millipore, Cat#AB144P), Rabbit anti-SST 2a receptor 1:100 (Bio-trend, ss-8000-rmc, Lot#a080826)), were added to the blocking buffer and sections were incubated for 48 h at 4 °C. Sections were washed in TPBS for 3x30mins and incubated in secondary antibodies (ExtrAvidin®-FITC 1:500 (Sigma-Aldrich, Cat#E2760), Cy3®-conjugated AffiniPure Donkey anti-Goat IgG (H+L) 1:250 (Jackson ImmunoResearch Laboratories, INC, Code#705-165-147, Lot#68839), Alexa Fluor® 647-AffiniPure Donkey Anti-Rabbit IgG (H+L) 1:250 (Jackson ImmunoResearch Laboratories, INC, Code#711-605-152, Lot#105115)) for 12 h at 4 °C.

Processed sections were washed again in TPBS for 3x30mins before being mounted in serial order on glass slides and coverslipped for imaging with Zeiss Z1 epifluorescent or Leica TCS SP5X confocal microscopes. In two cases CFP and EGFP immunoreactivity were enhanced using Rabbit-anti-GFP (1:1000, Life Technologies Cat# A-6455).

Recording parameters

Recordings were made using an Axoclamp 900A amplifier with HS-9AX1 headstage (Molecular Devices, USA) in current clamp mode. This model has several features that make it suitable: its high maximum current output (1000 nA) is convenient for constant-current electroporation, and the headstage is tolerant of externally generated voltages of up to 10 V.

Extracellular activity was simultaneously measured on two channels, one using conventional extracellular configuration (AC channel: Gain: 20 – 50, Band pass: 100-3000 Hz) and one configured for intracellular recordings (DC channel: Gain: 1, Band pass: DC-3000 Hz). Data were sampled at 10k (AC) or 5k (DC) samples/s using a 1401plus or power1401 running Spike 2 version 7 (Cambridge Electronic Design, UK). AC recordings were played back as an audio signal during experiments.

Pipettes were pulled from filamented borosilicate glass (external diameter 1 mm, internal diameter 0.5 mm) using a P-2000 pipette puller (Sutter Instruments). Pipettes with a long taper and tip diameter of approximately 1 μm (Resistance 10-20 M Ω when filled with 0.9% NaCl) were considered ideal for extracellular recordings. All pipettes were inspected using a microscope with a calibrated graticule.

Intracellular recordings were made using similar pipettes pulled to <1 μm tip diameters and filled with either Tris EDTA buffer or water containing freshly filtered plasmid DNA diluted to a concentration of 250 - 350 ng/ μl in 1M KCl.

Constant voltage switching circuit

A constant voltage generator (DS2A-mkII, Digitimer Ltd.) was connected in parallel to the recording pipette by connecting one pole of the stimulator to the pipette and the other to the experimental preparation. A high-impedance recording circuit was maintained by isolating the stimulator from the pipette assembly with an electromagnet-controlled reed switch. The increased capacitance (~ 7 pF) of the assembly was offset by the amplifier capacitance compensation. For electroporation the electromagnet was engaged with a 5 V TTL pulse and the stimulator triggered to produce the desired voltage train.

***In vitro* electroporation**

Experiments were performed on a patch electrophysiology rig under an Olympus microscope with differential interference contrast optics and immersion lenses. Pipettes were back loaded with plasmid DNA, fluorescent dextran (tetramethylrhodamine- or fluorescein-conjugated dextran (3000 MW, Invitrogen # D3307 and D3305 respectively, 1-3% in 0.9% NaCl) or neurobiotin (1 – 2% in 0.9% NaCl) and mounted on the recording headstage. Brain slices were placed in the recording chamber and perfused at 1-2 ml per minute. The pipette tip was guided onto the surface of the target cell until a dimple was formed. Pipette patency was maintained with positive pressure as required. Following electroporation the pipette was carefully retracted from the cell and reused until clogging occurred.

The same approach was used for transfection of neurons in organotypic culture, except pipettes were filled with freshly filtered plasmid DNA in 0.9% NaCl (0.3 – 3 $\mu\text{g}/\mu\text{l}$). SCE of organotypic cultures was typically completed within 15 minutes. Slices with transfected neurons were washed in fresh media and restored to the incubator for 24 – 48 hours before fixation and imaging of reporter-expressing neurons.

***In vivo* electroporation**

Pipettes were prepared as above, mounted on the recording headstage and slowly ($\sim 10 \mu\text{m/s}$) lowered into the brainstem using a piezo microstepper. For extracellular recordings, pipette pressure was maintained at $>200 \text{ mmHg}$ until the tip reached a depth of 2 mm at which point the pressure was reduced to 0 – 50 mmHg. The pipette was advanced in 3 μm steps until a spontaneously active neuron was isolated and pressure was released. In many cases no pressure was applied beyond 2 mm deep, without any apparent effect on dye labelling efficiency or quality. Positive pressure was always used in attempted extracellular transfection.

Correct pipette position was verified by induction of an open-cell response to single cell microstimulation. Once a recording from a single cell was isolated the pipette was withdrawn until spike amplitude was 0.2 - 0.5 mV and microstimulation was attempted. If no response was obtained the pipette was advanced and re-tested in 3 μm steps until a response was observed (interpreted as establishment of contact) or the spike height receded (interpreted as passage of the pipette past the cell without making contact).

Electroporation was generally only attempted in neurons in which normal neuronal activity resumed after responses to microstimulation, although electroporation before recovery was still associated with robust labelling (see Figure 2.5C). After electroporation the pipette was slowly withdrawn. Fresh pipettes were used for each track.

For the majority of intracellular recordings no pressure was applied during positioning of the pipette: it was lowered to a depth of 1.5 mm and then advanced in 1 - 5 μm steps until an extracellular recording of a spontaneously active neuron was isolated. A capacitive buzz was applied to gain intracellular access and the pipette was further maneuvered until a stable membrane potential was obtained. After electrophoresis the pipette was slowly withdrawn until the membrane potential returned to zero and was then withdrawn completely. New pipettes were used for each track.

Plasmid preparation

Plasmids encoding fluorescent reporter proteins were used to validate electroporation: pCAG-DsRed (Addgene: 11151), pCAG-YFP (Addgene: 11180), pCAG-EGFP (Addgene: 11150), pCAG-CFP (Addgene: 11179), pCBA-TdTomato (Addgene: 28017). Plasmids were amplified and purified according to the suppliers' recommendations, filtered, and stored at -20 °C until use.

Avoidance of inadvertent neuronal labelling

Partial blockage of recording pipettes is commonly resolved by passing a high-amplitude 'clearing' current through the pipette. In early experiments we occasionally observed false-positive dextran-labelled neurons at locations at which anionic 'clearing' currents had been used; this can be avoided using clearing currents opposite in polarity to that of the dye. As was the case with *in vitro* experiments, *in vivo* electroporation sometimes labelled more than one neuron. This rarely happened with TMR-dextran (2/79 recovered neurons, 2.5%), but occurred significantly more frequently with neurobiotin (7/51 neurons, 14%, $P = 0.03$, Fisher's exact test). Inadvertent labelling of neurons due to positive pressure ejection of dextran/neurobiotin was almost never seen; unintentionally labelled neurons were easily identified by their position dorsal to the end of the recording track.

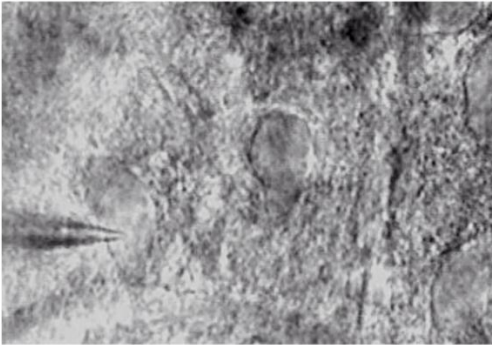
Results

Dye-labelling in vitro

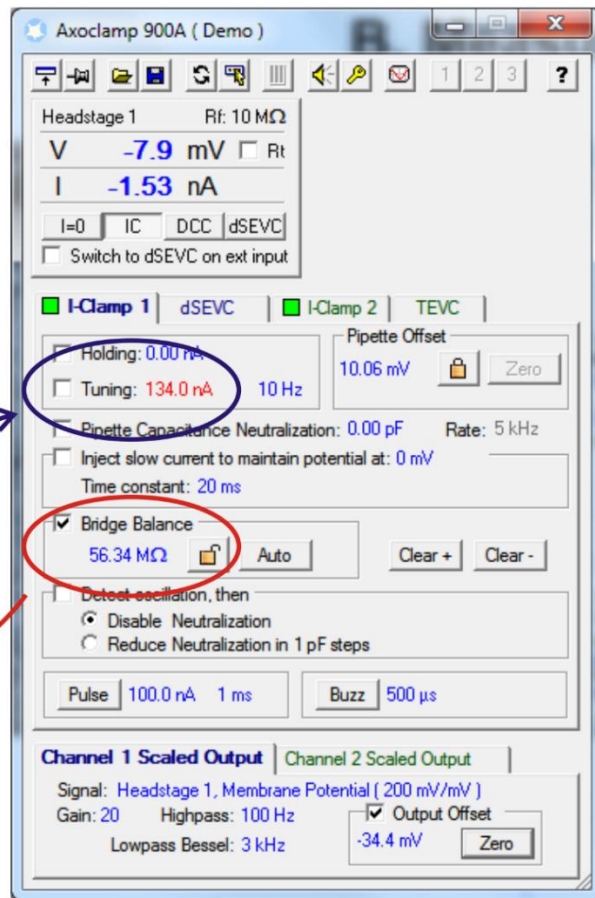
In pilot experiments performed on acute brain slices we first established that SCE was compatible with the micropipettes and recording amplifier used for extracellular recordings. Recording pipettes with a 1 μm tip diameter were filled with 0.9% NaCl containing 1-3% fluorescein- or tetramethylrhodamine-dextran (TMR-dextran: MW 3000, resistance = 8 – 20 M Ω) and electroporation currents were delivered by the amplifier current ejection system. The pipette was positioned in gentle contact with the target cell under optical guidance and series resistance (R_s) was measured using the amplifier bridge-balance function. The electroporation current (I_e) required to generate the target electroporation voltage (V_t) was calculated by Ohm's Law and programmed into the amplifier current-injection dialogue (Figure 2.1). As the amplitude of currents injected using this approach remain constant over the course of the electroporation train, we term this approach *constant-current electroporation*.

A. Approach cell

Record extracellular activity



B. Measure Rs



C. Calculate current

$$I_e = \frac{V_t}{R_s} = \frac{7.5}{5.6 \times 10^7} = 134 \text{ nA}$$

D. Program amplifier, trigger current train

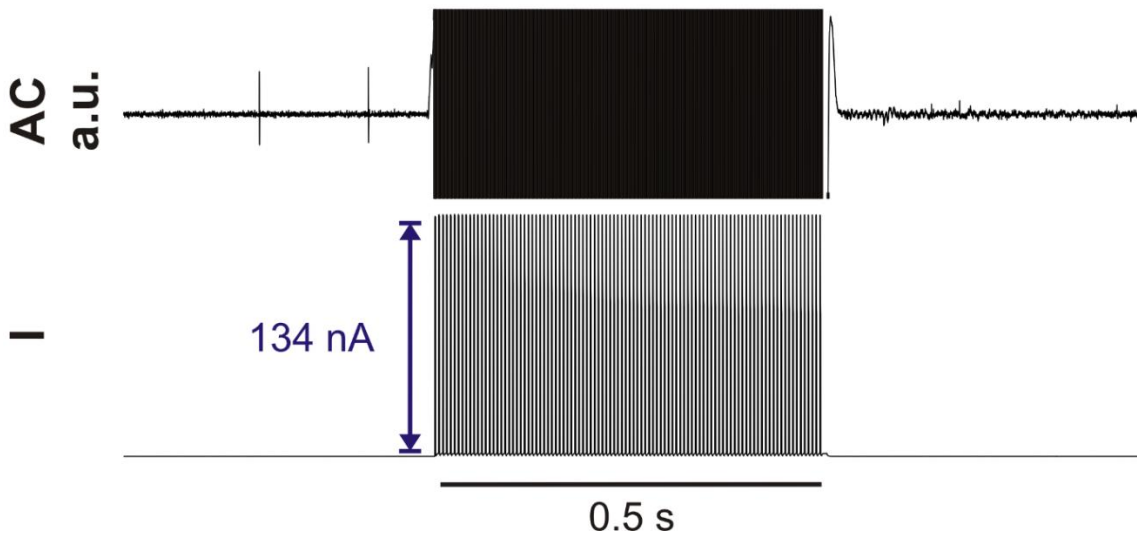


Figure 2.1 Illustration of workflow used for constant-current electroporation in vitro. A. Recording pipette is moved into gentle contact with the target cell under optical guidance. B. Immediately prior to electroporation R_s is measured using the amplifier bridge-balance function and C used to calculate the electroporation current (I_e) required to generate the target voltage (V_t ; in this example 7.5 V). D. The amplifier is programmed to deliver a train of current pulses at I_e .

Constant-current electroporation was compatible with high-quality recording of extracellular action potentials and resulted in labelling of the soma and dendritic tree using a wide range of train parameters: reproducible single-cell labelling was obtained with trains of 1 ms pulses delivered at 200 Hz for 0.5 s ($V_t = 7.5$ V: 36/48 cells labelled on the first attempt, Figure 2.2). Electroporation with even relatively low (<1%) concentrations of fluorescent dextrans resulted in extensive filling of fine axons and fibres, allowing resolution of fine morphological details (e.g dendritic spines) that were clearly observable under epifluorescent illumination in the live slice. Resolution was enhanced by increasing the concentration of dextran used. In the vast majority of cases electroporation (successful or unsuccessful) caused an immediate cessation of spontaneous firing that rarely recovered within 10 minutes (although resumption of firing was not systematically investigated).

Electroporation occasionally labelled more than one cell (3/129 cells, 2.4%). In such cases the intended target was always labelled too, and processes extending from the unintentionally filled cell were always observed in close proximity to the recording pipette, and were therefore presumably labelled *en passant*.

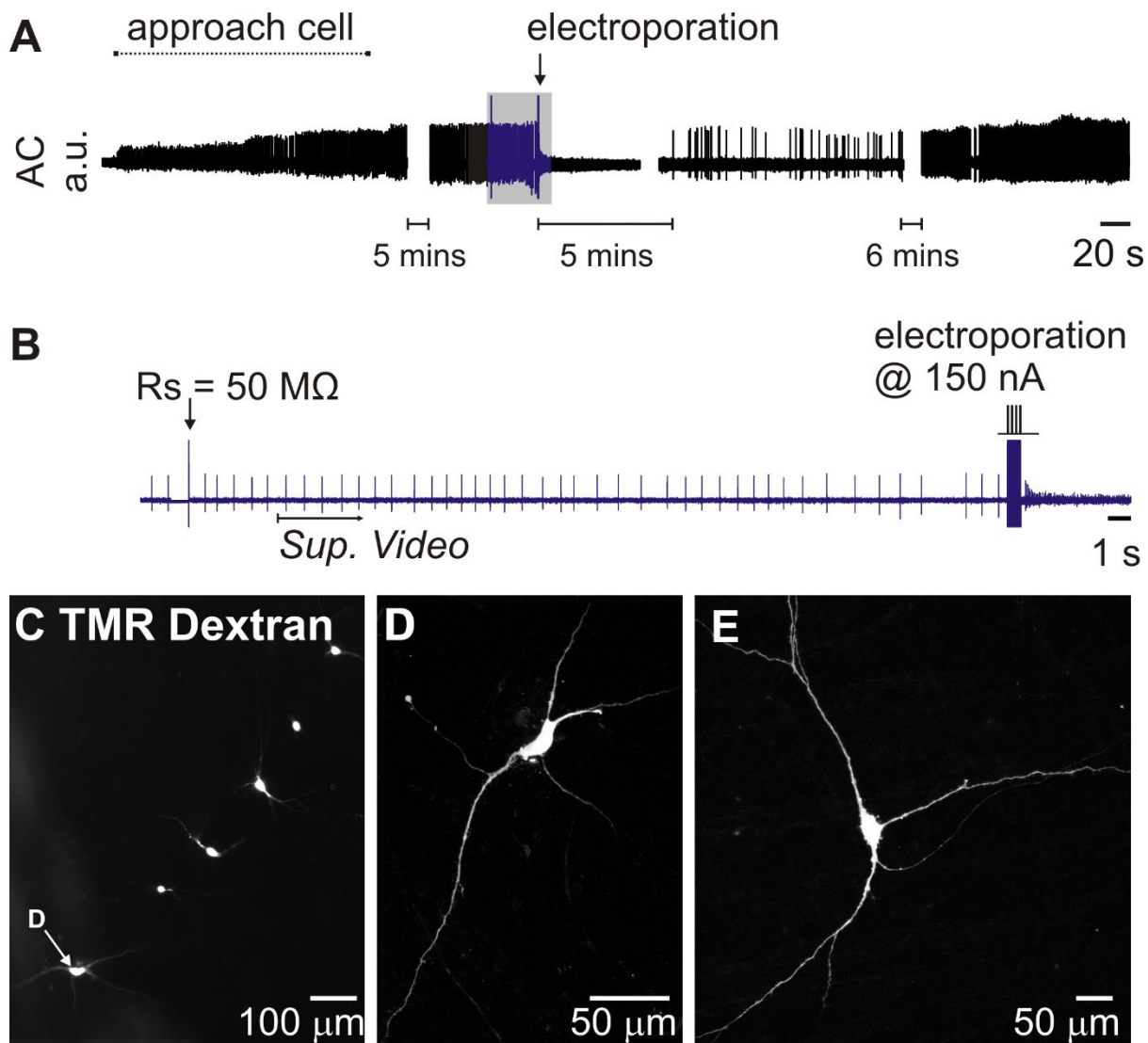


Figure 2.2 Extracellular recording and constant-current electroporation of a spontaneously active neuron in an acute brain slice. **A.** Overview of entire recording. **B.** Detailed view of portion indicated in blue in **A.** To electroporate, R_s was first measured using the amplifier bridge-balance function and used to calculate the appropriate electroporation current (see Figure 2.1). A 200 Hz train of 100 x 150 nA, 1 ms pulses immediately filled the cell with 1% tetramethylrhodamine (TMR)-dextran and abruptly halted its spontaneous discharge. Spontaneous activity returned after five minutes and was maintained for the remainder of the experiment. *Sup. Video* indicates starting point of Supplementary Video 1 (http://physreports.physiology.org/highwire/filestream/6846/field_highwire_adjunct_files/0/phy212246-sup-0001-VideoS1.wmv). **C.** Low-power fluorescence image of six dextran-filled neurons recorded and electroporated in a single slice **D.** Confocal image of the neuron indicated in **C.** **E.** Example of a neuron from a different experiment.

Single-cell transfection in vitro

Using the same approach we attempted to transfect neurons in organotypic cultures with plasmids that encode fluorescent proteins ($V_t = -10$ to -12 V, $100 \times 0.5 - 1$ ms pulses, 100 Hz, 1 s train). Although occasionally effective, this approach did not reliably result in protein transcription. As discussed in detail below, we postulated that low transfection efficiency may have resulted from voltage drop-off during pore formation, so we modified our pipette assembly to incorporate a constant-voltage source connected in parallel to the recording pipette by an electronic switch (“constant-voltage electroporation”, Figure 2.3 A).

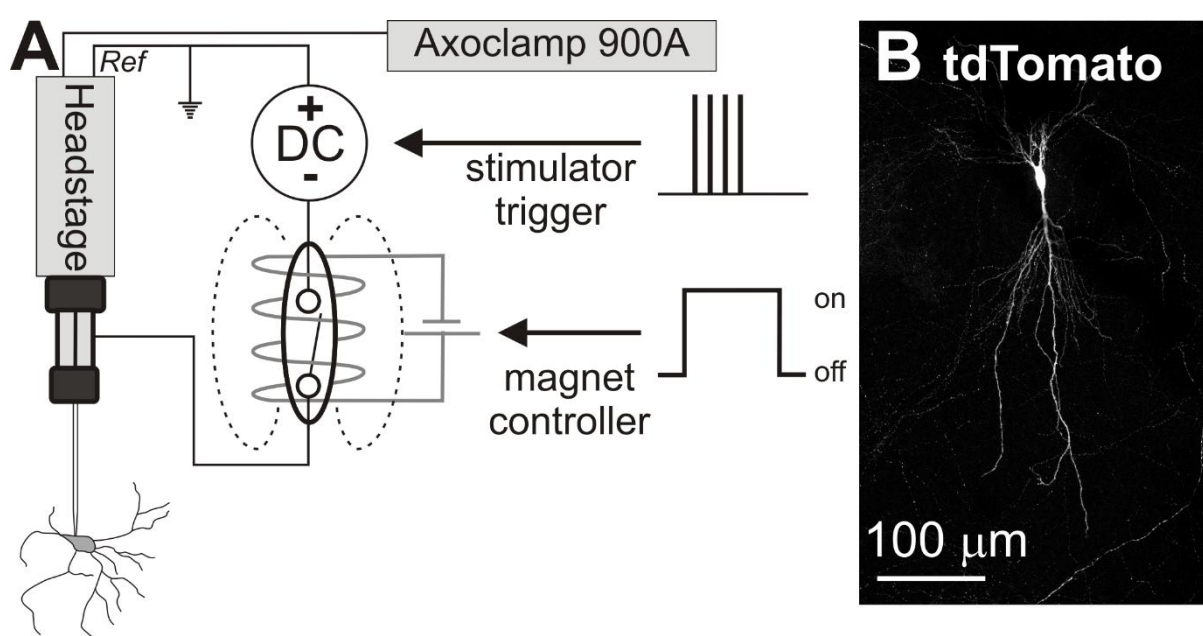


Figure 2.3 Circuit configuration used for recording and constant-voltage electroporation. A DC generator is connected in parallel to the recording and reference terminals of the amplifier headstage and is isolated from the recording electrode by a reed switch placed inside a cylindrical electromagnet. When the electromagnet is engaged the circuit is closed, allowing delivery of electroporation voltages. B. TdTomato fluorescence 24 hours after transfection of a hippocampal neuron in organotypic culture with pCBA-TdTomato.

This modification allows delivery of constant-voltage across the recording electrode (and headstage) when the switch is engaged, irrespective of R_s , but electrically isolates the voltage generator during when disengaged, preserving recording quality. This refinement improved the transfection efficiency achieved in organotypic cultures (reporter expression confirmed in 25/51 cells within 24 hours of electroporation, Figure 2.3 B), making it equivalent to a commercial

standalone SCE device (16/30 cells, Axoporation™, Fisher's Exact Test: $P = 0.82$) using the same electroporation parameters (-10 V, 100 Hz, 1 ms pulses, 1 s train). This modification also simplified the electroporation process, as it eliminated the requirement for measurement of R_s and calculation of I_e prior to electroporation. As described elsewhere, transfection of single neurons with plasmids that encode fluorescent reporters resulted in bright and complete filling of proximal and distal neuronal compartments, in most cases sufficient to clearly visualise fine branching of axons and dendrites, axonal varicosities and terminals, and dendritic spines (Haas *et al.*, 2001).

Establishing cell contact in blind recordings

SCE is critically dependent on gentle contact between the pipette and target neuron. In fields of view with a high cell density or recordings made deep in the slice it was often difficult to unambiguously determine when the recorded neuron had been correctly identified and contacted. Furthermore, in initial experiments *in vivo*, we were unable to achieve reliable electroporation when using changes in R_s to indicate cell contact (TMR-dextran: 2/29 cells recovered, $n = 4$ rats), although other investigators have recently reported success using this strategy (Oyama *et al.*, 2013).

To resolve this problem we developed a protocol that uses stereotypical responses to a single 50 - 100 nA, 1 ms pulse (“*single-cell microstimulation*”) to definitively identify contact between the recording pipette and soma. In acutely prepared brain slices this stimulus evoked electrophysiological responses characterized by four distinct elements (Figure 2.4): (1) Increased discharge rate and altered spike morphology that included (2) an increase in spike height and (3) adoption of an asymmetrical spike shape with a conspicuous after-hyperpolarization (4) a 1-20 mV reduction in potential recorded in DC mode. All four components were *always* apparent in spontaneously active cells, but sometimes transient

changes in pipette potential (with or without a short burst of action potentials) were the only features apparent in silent cells. Electrophysiological changes evoked by microstimulation typically recovered within 10 s and were never observed in the absence of physical contact between pipette and cell, confirmed as a dimpling of the cell membrane.

Although single-cell microstimulation was apparently innocuous *in vitro* (where gentle contact between pipette and cell were closely monitored), microstimulation of spontaneously active neurons *in vivo* was initially associated with loss of recordings and presumed cell rupture and death. This was mitigated by withdrawal of the pipette from the cell once stable recordings were established such that spikes were <0.5 mV in amplitude prior to microstimulation. Where no response to microstimulation was observed the pipette was advanced in 1-3 μm increments and stimulation repeated until a response was obtained. Using this approach transient responses, in which normal neuronal activity resumed within ~10 s, were achieved in approximately 50% of neurons (see Figure 2.4 & 2.5).

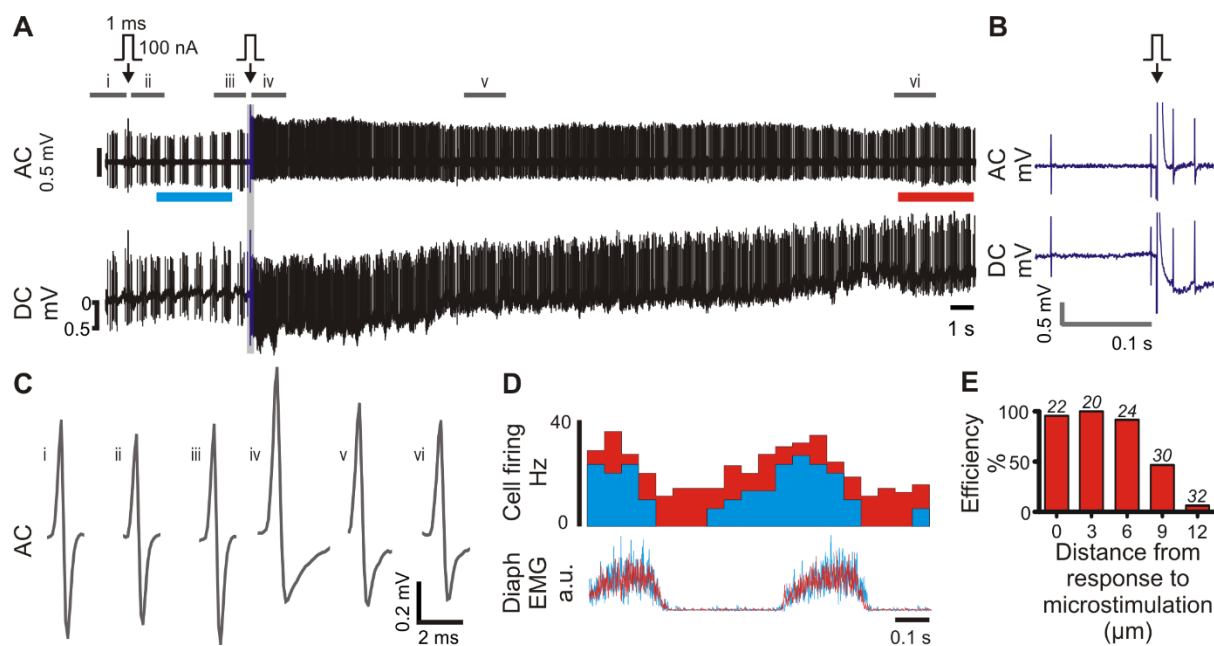


Figure 2.4 Single-cell microstimulation of a medullary respiratory neuron in vivo. **A.** 100 nA microstimulation (arrow) initially evoked no effect on neuronal firing. The pipette was advanced 3 μm and stimulation repeated. This time the stimulus evoked transient stereotypical changes in firing frequency, spike amplitude and spike shape, apparent in the AC trace, and a small hyperpolarization of the pipette, visible as a 1 mV shift in the DC trace. **B.** Expanded view of region drawn in blue in **A.** **C.** Average spike waveforms; source data indicated in **A.** **D.** Diaphragm-triggered histograms of neuronal firing before (cyan, bar indicated in **A.**) and after (red, bar indicated in **A.**) microstimulation: the firing pattern is maintained over the recording. **E.** Response to single-cell microstimulation (0 μm) is correlated with high labelling efficiency (TMR-dextran, *in vitro*), which decreases as the pipette is withdrawn from the cell membrane. Number of replicates shown over each series.

Responses to single-cell microstimulation were a reliable indicator of contact between the pipette and cell and were predictive of successful electroporation. Under blind conditions *in vitro*, the probability of achieving dextran labelling on the first attempt was 89% (55/62 cells) following a positive response to single-cell microstimulation, and rapidly declined as the pipette was withdrawn from the cell membrane (Figure 2.4, E). Positive responses to microstimulation were also correlated with successful constant-current electroporation in randomly sampled spontaneously active neurons encountered 0.3 – 9.7 mm deep *in vivo* (dextran electroporation in 82/137 neurons, 60%, $n = 26$ rats, $V_t = 5 - 10$ V, 200 Hz, 1 ms pulses, 0.5 s train). A similar proportion (49/74, 66%, $P = 0.37$, Fisher's exact test) were labelled using dextran or neurobiotin in a second cohort of experiments ($n = 21$ rats) in which neurons in the ventrolateral medulla with respiratory-related activity were preferentially targeted with constant-voltage electroporation (7.5 – 10 V, 200 Hz, 1 ms pulses, 0.5 s train: Figure 2.5).

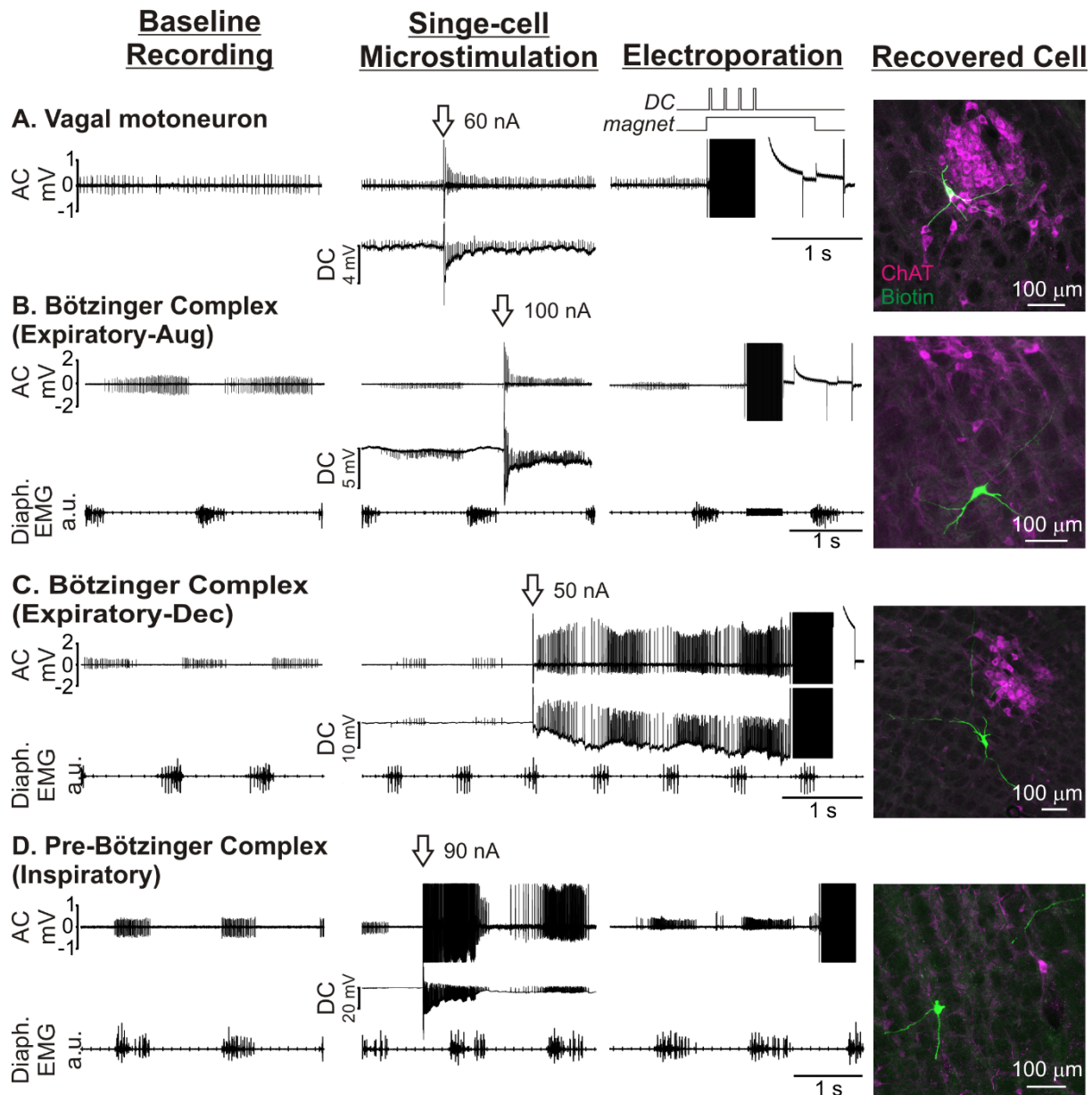


Figure 2.5 Examples of non-respiratory A. and respiratory B. - D. neurons recorded in extracellular mode in the ventrolateral medulla and labelled with neurobiotin by constant-voltage electroporation in vivo. After establishment of baseline recordings and repositioning of the recording pipette such that spike height was <0.5 mV, single-cell microstimulation (arrow) was used to verify cell contact. In most cases neurons were allowed to recover from microstimulation prior to electroporation (100 x 1 ms pulses, 200 Hz, +7.5 to +10 V). Photomicrographs show neurobiotin-filled neurons (green) recovered at the appropriate stereotaxic coordinates; magenta channel shows immunoreactivity for choline acetyl transferase (ChAT). Diaphragmatic EMG activity indicates inspiration, permitting functional identification of respiratory neurons. A. Tonically active ChAT-immunoreactive neuron in the nucleus ambiguus; B. Augmenting expiratory neuron recorded ventral to nucleus ambiguus; C. Decrementing expiratory neuron recorded ventral to nucleus ambiguus; D. inspiratory-locked neuron.

Single-cell transfection in vivo

Having verified that constant-voltage electroporation is capable of reliable single-cell transfection *in vitro* and established a protocol that results in reproducible dye-labelling *in vivo*, we then examined its suitability for single-cell transfection *in vivo*.

Brainstem neurons were recorded 1.6 – 9.8 mm deep in either non-recovery experiments, in which urethane anaesthesia was maintained for 12-18 hours after electroporation (n = 5 rats), or recovery experiments (n = 7 rats), in which anaesthesia was reversed at the conclusion of recording and rats were recovered for 1-2 days. Contact between the pipette and target neuron was first verified by observing a positive response to single-cell microstimulation, and neurons that recovered were electroporated at negative polarity (-10 V, 50 – 100 Hz, 0.5 – 1 ms pulses, 1 s). Regardless of surgical preparation, electroporation parameters, or plasmid construct used, this approach rarely resulted in reporter expression (6/87 neurons, 7%).

We initially hypothesized that the low success rate may have reflected an incorrect assumption regarding the predictive value of our microstimulation technique. We adopted an approach similar to that used for electroporation of superficial cortical neurons (Judkewitz *et al.*, 2009; Oyama *et al.*, 2013), in which the pipette is manoeuvred such that R_s is increased by 30%, and attempted SCE in 31 neurons in 5 recovery experiments; no transfected cells were subsequently identified.

Review of recordings from successfully transfected neurons revealed that microstimulation had in some cases resulted in full intracellular access prior to electroporation (5/6 neurons), suggesting that transfection could be achieved by direct intracellular plasmid electrophoresis. This hypothesis was examined in experiments in which brainstem neurons were targeted for intracellular recordings using semi-sharp pipettes (tip diameter: $<1\ \mu\text{m}$, resistance $18 \pm 3\ \text{M}\Omega$). This configuration was compatible with stable recording of unit activity in extracellular mode

prior to brief (typically <10 s) intracellular access and plasmid ejection (-10 V, 50 Hz, 1 ms pulses, 1 s train or -10 V, 1000 Hz, 0.1 ms pulses, 0.1 s train: Steinmeyer and Yanik (2012)). Transfection was achieved in 13/48 (27%) neurons in which intracellular access (membrane potential -30 to -70 mV) was obtained prior to electrophoresis (Figure 2.6). Transfected neurons were recorded 1.6 – 8.3 mm deep to the brain surface using pipettes between 8 and 37 M Ω in resistance. 3/13 neurons were silent; the remainder showed spontaneous activity between 1 and 20 Hz. Cross sectional areas of transfected neurons were 141 – 1178 μm^2 , equivalent to 13 – 39 μm in diameter.

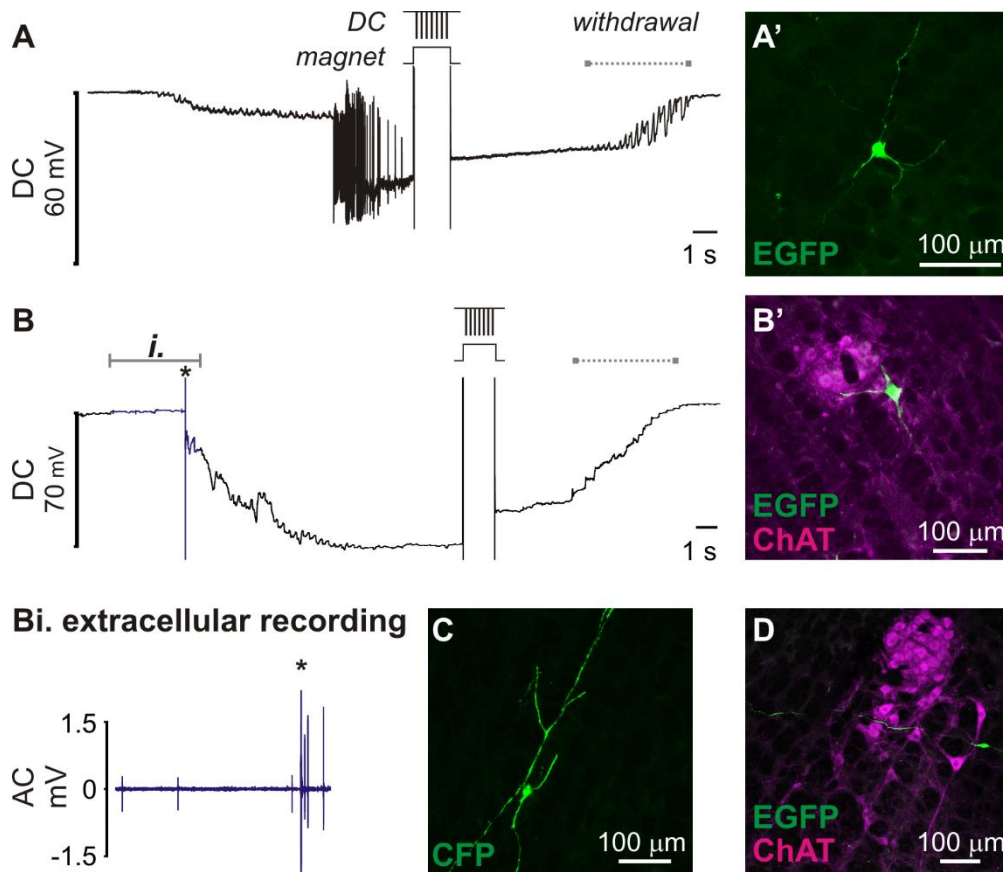


Figure 2.6 Transfection of ventrolateral brainstem neurons following intracellular penetration in vivo. Once membrane potential had stabilized, plasmid DNA encoding fluorescent protein was electrophoretically injected by -10 V pulses (50 x 1 ms pulses, 1 s). Membrane potential was retained after electrophoresis until withdrawal of the pipette (indicated by dashed lines). **A.** Electrophysiological recording from a silent neuron that started firing after penetration. **A'** shows EGFP-labelled neuron recovered at the corresponding stereotaxic coordinates. **B.** Slowly firing spontaneously active neuron: extracellular spikes (blue data, detailed in Bi.) were resolved prior to cell penetration (*). **B'** Colocalization of EGFP with ChAT immunoreactivity indicates that this example is a cholinergic motor neuron in nucleus ambiguus. **C.** & **D.** show examples of other neurons transfected using the same approach.

Discussion

The current study provides researchers with three novel protocols that can be used for dye-labelling or transfection of functionally identified neurons in deep brain regions *in vivo*. Constant-current electroporation can be performed without any customization of the recording amplifier and yields rapid and high quality dye labelling *in vitro* and *in vivo*. Constant-voltage electroporation requires minimal modification of hardware and yields *in vitro* transfection at efficiency equivalent to a widely-used proprietary device, but in our hands this approach was incompatible with high transfection efficiency *in vivo*. In contrast, we found that intracellular electrophoresis of genetic material may instead offer a more reliable method for transfection of functionally identified neurons in inaccessible brain regions.

In establishing our transfection methodology we developed dye-labelling techniques that offer some advantages to the juxtacellular method in terms of simplicity and speed. Successful juxtacellular labelling is indicated by ‘entrainment’ of neuronal firing to regular anodal pulsing of the recording pipette, which must be maintained for several minutes for reasonable labelling to occur. Longer periods of entrainment are associated with more complete labelling (up to 60 minutes: Nosedá *et al.*, 2010). Although the juxtacellular approach can yield efficient labelling in the hands of the technically elite (100/115 cells: Pinault, 1996; 45/50 cells: Guyenet & Wang, 2001), establishing and maintaining entrainment requires considerable finesse, and recordings are often lost before or during entrainment. It is notable that the number of neurons lost during attempted labelling is often omitted from reports that use this approach, perhaps boosting the apparent efficiency of the technique: in unpublished pilot experiments we found that recordings were lost before or during entrainment in 145/248 (58%) attempts.

In contrast to the imprecise cues used to guide entrainment over minutes of juxtacellular labelling, single-cell microstimulation provides an instant binary output; a cell either responds with an unambiguous electrophysiological signature, in which case it may be immediately

electroporated with a high probability of recovery, or does not, in which case the pipette is manoeuvred and stimulation repeated (in cases where there is no response) or another cell is sought (in cases where the recording is lost). This makes the protocol quick to perform and easy to learn: most of the experiments targeting respiratory neurons were performed by myself after learning the technique in a week, and I recovered two labelled neurons in my first experiment.

The increase in neuronal excitability and effects on spike shape and amplitude seen in response to microstimulation are consistent with induction of an “open-cell” state by the stimulus, a transient permeabilisation of the neuronal membrane evoked by its partial electroporation (Braeken *et al.*, 2012; Spira & Hai, 2013). Our observation that such responses only occur when the pipette is in contact with the neuron are supported by similar reports by Santos *et al.* (2007; 2009), who found that 30-100 nA, 1 ms pulses could be used to effectively stimulate spinal cord neurons in loose-seal mode, but not in the absence of physical contact between the pipette and cell. We conclude that single-cell microstimulation provides a reliable and objective indicator of contact between the pipette and neuron. The major shortcoming associated with using single-cell microstimulation to guide electroporation is its high attrition rate *in vivo*; this is most likely due to excessive contact between the pipette and target cell, as it does not seem to occur *in vitro* (where contact can be closely monitored), although factors such as cell size and pipette geometry may also contribute to the effect.

Constant-current and constant-voltage electroporation offer dye-labelling with similar efficiencies *in vitro* and *in vivo*; both result in labelling that is at least equivalent in quality to that offered by the juxtacellular technique *in vivo* and comparable to standard SCE *in vitro*, where fine morphological features such as dendritic spines and terminals are consistently revealed (Haas *et al.*, 2001; Umeda *et al.*, 2005). The quality of labelling obtained using the juxtacellular technique varies according to the brain region targeted and tissue processing procedures, hampering direct comparison with the protocols described here. However,

extensive filling of brainstem neurons juxtacellularly labelled with neurobiotin and visualised with fluorescent avidin conjugates is rare in the literature (Sartor & Verberne, 2003; Abbott *et al.*, 2009b; Kanbar *et al.*, 2011; Boucetta *et al.*, 2014; Iceman & Harris, 2014) and in our own experience (unpublished data). In contrast, although variability in labelling quality was observed using the approaches described here, we often saw extensively filled neurons that projected across dozens of histological sections in which fine morphological details were visible. We did not extensively investigate the quality of labelling possible using diaminobenzidine visualisation, but details such as terminals and dendritic spines were visible in one of three neurons processed that way. Constant-current electroporation may be conducted without modification to hardware provided the recording amplifier is capable of generating sufficiently high currents (400 - 800 nA), making it fast and cheap to adopt. However, we found it more convenient to use the constant-voltage approach, as it eliminates measurement of R_s and current calculation from the workflow, speeding up the protocol, and is compatible with single-cell transfection *in vitro*.

Why doesn't constant-current electroporation result in transfection? In constant-current mode the measured value of R_s has a critical influence on voltage output. Constant-current pulses may initially succeed in generating V_t for a given R_s ; however, pores are formed in the membrane within microseconds of voltage application (see DeBruin & Krassowska, 1999; Wang *et al.*, 2010), lowering membrane resistance and consequently R_s , resulting in a proportionate reduction in trans-membrane voltage. As a consequence of this voltage drop-off, constant-current electroporation may fail to sustain the voltages required for large and stable pore formation, which are crucial for efficient plasmid delivery (Rae & Levis, 2002).

In vitro transfection efficiency was restored by integration of a constant-voltage generator to the recording circuit. This modification allowed the delivery of up to ± 10 V without risk to the recording headstage (following advice from the manufacturer), and made transfection

efficiency equivalent to that obtained with a commercial single-cell electroporator and comparable to that reported elsewhere (Rae & Levis, 2002; Rathenberg *et al.*, 2003; Steinmeyer & Yanik, 2012). However, exhaustive attempts to translate it for single-cell gene delivery *in vivo* were fruitless. This is surprising, given the similarities between our approach and protocols recently described by other investigators, in which some level of transfection was observed under all parameters tested (Cohen *et al.*, 2013; Oyama *et al.*, 2013). Differences in the brain regions and, perhaps crucially, the depths at which neurons were targeted, may underlie this disparity, as Cohen *et al.* (2013) and Oyama *et al.* (2013) restricted their attempts to neurons within 450 μm or 1.5 mm of the brain surface respectively, where pipette patency is easier to manage.

We conclude that techniques based on SCE are unlikely to yield reliable transfection of neurons in deep brain structures, and speculate that blockage of pipettes is most likely responsible for the poor transfection efficiency seen *in vivo*. Despite applying high positive pressure to the internal solution during brain penetration and cell hunting, we rarely saw any evidence of dye leakage or hydraulic injury along pipette tracks, both of which indicate pipette patency *in vivo* (Rancz *et al.*, 2011), and the quality and efficiency of dye-labelling and reporter expression were consistently higher *in vitro* than *in vivo*. Although we were able to use SCE for efficient dye-labelling nearly 10 mm deep to the brain surface, this does not necessarily mean that recording pipettes were patent: in our experience electrophoretic ejection of fluorescent dextran is consistently possible from clogged pipettes in which no dextran may be pressure-ejected, and we were able to produce robust labelling with such pipettes *in vitro*. However, we and others have found that blocked pipettes absolutely preclude transfection by SCE (Haas *et al.*, 2001; Rae & Levis, 2002; Rathenberg *et al.*, 2003; Bestman *et al.*, 2006a; Kitamura *et al.*, 2008a; Judkewitz *et al.*, 2009).

If patency is the main issue affecting the efficiency of SCE in deep brain regions, pipette clogging probably reduces rather than completely obstructs plasmid ejection, as intracellular plasmid electrophoresis reproducibly transfected neurons up to 8.3 mm deep. Stable intracellular access is difficult to achieve even in acute preparations, where extensive craniotomy or pneumothoraces are commonly used to reduce movement. However, we found that brief access, sufficient for transfection, could be gained in minimally invasive preparations (although we found tracheal intubation with neuromuscular block and artificial ventilation useful) and that large neurons could be impaled and transfected using low-resistance pipettes. The current data provide a proof-of-principle that intracellular recording may be used to transfect neurons in deep brain regions, but the efficiency of the approach will ultimately be dependent on factors including operator experience, animal age, brain region targeted and the size of targeted neurons.

The current data provide relatively simple protocols that can be used for reliable and robust labelling of recorded neurons and a novel approach for transfection of neurons in deep brain regions. The clear-cut criteria used to guide electroporation and the rapidity at which labelling can be performed may prove particularly attractive to novice investigators, whereas the potential to select neurons for genetic modification based on their functional properties may prove useful to investigators interested in applying advanced connectome-tracing technologies at single-cell resolution (Wickersham *et al.*, 2007b; Marshel *et al.*, 2010; Rancz *et al.*, 2011)

3.

Somatostatin 2a receptors are
not expressed on functionally
identified respiratory neurons
in the ventral respiratory
column of the rat

Abstract

Microinjection of somatostatin (SST) causes site-specific effects on respiratory phase transition, frequency and amplitude when microinjected into the ventrolateral medulla (VLM) of the anaesthetized rat, suggesting selective expression of SST receptors on different functional classes of respiratory neurons. Of the six subtypes of SST receptors, somatostatin 2a (sst_{2a}) is the most prevalent in the VLM. Other investigators have suggested that glutamatergic neurons in the preBötzinger Complex (preBötC) that co-express neurokinin-1 receptor (NK1R), SST and sst_{2a} are critical for the generation of respiratory rhythm. However, quantitative data describing the distribution of sst_{2a} in respiratory compartments other than preBötC, or on functionally identified respiratory neurons, is absent. Here we examine the medullary expression of sst_{2a} with particular reference to glycinergic/expiratory neurons in the Bötzinger Complex (BötC) and NK1R-immunoreactive/inspiratory neurons in the preBötC. We found robust sst_{2a} expression at all rostrocaudal levels of the VLM, including a large proportion of catecholaminergic neurons, but no colocalization of sst_{2a} and glycine transporter 2 mRNA in the BötC. In the preBötC 54% of sst_{2a} immunoreactive neurons were also positive for NK1R. sst_{2a} was not observed in any of 52 dye-labelled respiratory interneurons, including 7 BötC expiratory-decrementing and 11 preBötC pre-inspiratory neurons. We conclude that sst_{2a} is not expressed on BötC respiratory neurons and that phasic respiratory activity is a poor predictor of sst_{2a} expression in the preBötC. Therefore sst_{2a} is unlikely to underlie responses to BötC SST injection, and is sparse or absent on respiratory neurons identified by classical functional criteria.

Introduction

Breathing is a fundamental motor function that is controlled by hierarchical arrays of spatially, functionally, and phenotypically compartmentalized groups of neurons in the brainstem and pons (for recent reviews see Feldman *et al.*, 2013; Smith *et al.*, 2013). The preBötzinger Complex (preBötC) located in the ventrolateral medulla (VLM) forms the essential kernel of the respiratory rhythm-generating apparatus. Rhythmic drive from preBötC neurons is necessary for the generation of activity in inspiratory motor nerves and is sufficient to maintain activity recorded in the hypoglossal nerve in medullary slices *in vitro* (Smith *et al.*, 1991). Respiratory interneurons in this area are active in the inspiratory phase of the respiratory cycle and contribute to inspiratory bursts via a combination of pacemaker activity and glutamatergic transmission (Koshiya & Smith, 1999; Del Negro *et al.*, 2002a; Wallen-Mackenzie *et al.*, 2006; Koizumi *et al.*, 2013).

preBötC glutamatergic neurons contain a number of other neurochemicals and transcription factors that may have particular functional significance. Of particular interest are subpopulations of glutamatergic neurons in this region that express neurokinin-1 receptors (NK1R), somatostatin (SST) and somatostatin 2a receptor (sst_{2a}), and these have been proposed as chemical markers for the preBötC (Guyenet & Wang, 2001; Stornetta *et al.*, 2003a; Gray *et al.*, 2010; Gray, 2013). Critical roles for these populations in the generation of normal respiratory activity are supported by targeted ablation and loss-of-function studies: extensive bilateral lesion of preBötC NK1R neurons leads to a severely ataxic breathing pattern (Gray *et al.*, 2001). Similarly, pharmacogenetic silencing of SSTergic preBötC neurons causes ataxic breathing and apnea (Tan *et al.*, 2008). However, it is important to note that although both NK1R and particularly SST (at least as mRNA) are extensively expressed throughout the VLM, neither is widely expressed in functionally identified respiratory neurons (Guyenet & Wang, 2001; Wang *et al.*, 2001; Stornetta *et al.*, 2003a).

The functional significance of SST release from putative preBötC neurons is unclear. Transgenic animals that lack SST (Low *et al.*, 2001) or SST receptors (Allen *et al.*, 2003; Qiu *et al.*, 2008; Rajput *et al.*, 2011) are not associated with an obvious respiratory phenotype. However, exogenous SST powerfully inhibits central respiratory drive *in vivo* (Yamamoto *et al.*, 1988; Chen *et al.*, 1990; Burke *et al.*, 2010; Pantaleo *et al.*, 2011) and *in vitro* (Llona *et al.*, 2004; Gray *et al.*, 2010; Ramirez-Jarquin *et al.*, 2012).

We have previously demonstrated that the respiratory effects of SST microinjection are site-specific and dose-dependent: SST microinjection in the Bötzing Complex (BötC) caused apneusis, characterized by a prolongation of phrenic burst duration (T_i) and ablation of post-inspiratory activity in vagal and sympathetic nerves. In contrast, preBötC SST injection evoked reductions in respiratory frequency (ultimately leading to apnea with higher doses) without significant effects on T_i or post-inspiratory activity (Burke *et al.*, 2010). We also found that SST evoked a reduction in phrenic nerve amplitude when injected into the rostral ventral respiratory group (rVRG). These results were consistent with an inhibitory effect of SST on inhibitory BötC neurons thought to terminate inspiration, presumably expiratory neurons with a decrementing firing pattern (E-Dec; Hayashi *et al.*, 1996), an inhibitory effect of SST on preBötC rhythm-generating neurons, and an inhibitory effect of SST on respiratory premotor neurons in the rVRG.

Taken together, the literature suggests that components of the respiratory circuits that subserve phase-transition, rhythm generation, and bulbospinal drive are directly sensitive to SST, and predicts the expression of SST receptors on subsets of respiratory neurons in the BötC (particularly E-Dec), preBötC (particularly pre-I) and rVRG compartments. That prediction is tested in the current study. Some colocalization of *sst_{2a}* with preBötC NK1R/SST/Dbx1 and tyrosine hydroxylase (TH)/pre-pro-enkephalin has previously been described (Burke *et al.*, 2008; Spary *et al.*, 2008; Gray *et al.*, 2010). However, no quantitative data regarding the

distribution of sst_{2a} on respiratory neurons are available. Here we comprehensively describe the distribution of sst_{2a} in VLM respiratory cell groups and on functionally identified respiratory neurons with a particular focus on the BötC and preBötC.

Methods

Animal experiments were approved by Macquarie University Animal Ethics Committee and adhered to the Australian code of practice for the care and use of animals for scientific purposes.

Electrophysiology experiments

Surgical procedures

Urethane-anaesthetized (1-1.3 g/kg i.p.) adult Sprague-Dawley rats of either sex (220-480g, ARC, Perth, Australia) were cannulated to allow intravenous access and recording of arterial blood pressure and intubated to permit artificial ventilation. Phrenic nerve activity (PNA, n = 7) or diaphragmatic EMG (n = 22) were recorded as an index of central respiratory drive. The phrenic nerve was isolated and recorded as previously described (McMullan *et al.*, 2009). Diaphragm EMG was recorded via Teflon-coated stainless steel wires inserted into the diaphragm at the lateral aspect of the inferior costal margin. Phrenic/EMG signals were differentially amplified and filtered (100 – 1000 Hz). In most experiments vagii were cut bilaterally at the cervical level to desynchronize central respiratory drive from mechanical ventilation; in three experiments vagii were left intact. Core temperature was maintained at 36 – 38 °C by a heating blanket controlled by a rectal thermometer and animals were moved into a stereotaxic frame in the nose-down position. The left facial nerve was exposed, the occipital bone removed and the brainstem exposed. The animal was artificially ventilated to maintain isocapnia, as indicated by end-tidal CO₂ (3.5 – 4.5%) or analysis of arterial blood gas samples. Neuromuscular blockade (pancuronium bromide, 0.1 – 0.4 mg i.v.) was used to reduce movements associated with ventilation while maintaining diaphragmatic EMG. Anaesthetic depth was regularly monitored by checking for motor, respiratory or pressor responses to noxious pinching of the tail or the hind paws. Supplementary anaesthetic (urethane 0.1 g/kg i.v.) was administered as required.

Identification and labelling of respiratory neurons *in vivo*

The caudal border of the facial nucleus was estimated by mapping antidromic facial field potentials using a borosilicate pipette filled with 3 M NaCl (resistance <2 MΩ) as previously described (Brown & Guyenet, 1984). Neuronal recordings were made using borosilicate glass pipettes filled with 0.9% NaCl containing 1-3 % tetramethylrhodamine-conjugated dextran (3000 MW, Invitrogen # D3307) or 2% neurobiotin (tip diameter, 1 μm, resistance 10-25 MΩ). Extracellular recordings were amplified (Axoclamp 900A, Molecular Devices) and simultaneously captured on two channels using differing filter sets, one configured for extracellular recording (AC: 100 – 3,000 Hz) and one for intracellular recordings (DC: DC-3,000 Hz, used to guide cell labelling: see below), and sampled by a Power1401 mk. II running Spike 2 software (Cambridge Electronic Design, UK, RRID: nlx_156886). Phrenic/diaphragm activity was sampled at 3k samples/s; extracellular activity at 10k samples/s; intracellular activity at 5k samples/s.

Neurons located 0 – 1.4 mm caudal to the caudal border of the facial nucleus, 1.6 – 2.0 mm lateral to midline, 2.1 – 3.7 mm and deep to the level of obex, with phasic spontaneous activity locked to phrenic or diaphragmatic discharge, were labelled using either conventional juxtacellular labelling (Pinault, 1996) or a modified single-cell electroporation technique in which labelling is achieved by a 0.5 s train of high voltage pulses (5 – 10 V, 200 Hz, 1 ms per pulse: Dempsey *et al.*, 2015). Gentle contact between the pipette and neuron was verified by observation of a stereotypical response to a single 50 – 100 nA, 1 ms current pulse (“*microstimulation*”) prior to electroporation. Positive responses to microstimulation were defined as a transient increase in firing frequency accompanied by an increase in spike amplitude, loss of spike symmetry, and a pipette hyperpolarization of 2 - 20 mV recorded in the DC channel (Figure 3.1). *In vitro* studies demonstrate that positive responses to microstimulation are strongly predictive of correct pipette position, and can be used as a reliable

indicator of juxtosomal contact when blindly approaching cells *in vivo* (Dempsey *et al.*, 2015). Once optimal pipette position was verified the neuron was immediately electroporated using a constant-voltage stimulator connected in parallel to the pipette. Positive pressure in the recording pipette (~200 mmHg) was used to prevent pipette blockage during initial brain penetration; in most cases pressure was reduced to zero once the pipette reached 2 mm deep, although in some cases low pressure (~30 mmHg) was maintained until a respiratory neuron was identified. Positive pressure in the pipette was not associated with unintentional labelling or dye leakage. Labelling was not attempted on neurons recorded within less than 300 μm of each other to ensure correct identification of recovered cells. Some of the data presented here contributed to the dataset that describes the development and validation of the modified electroporation technique (Dempsey *et al.*, 2015).

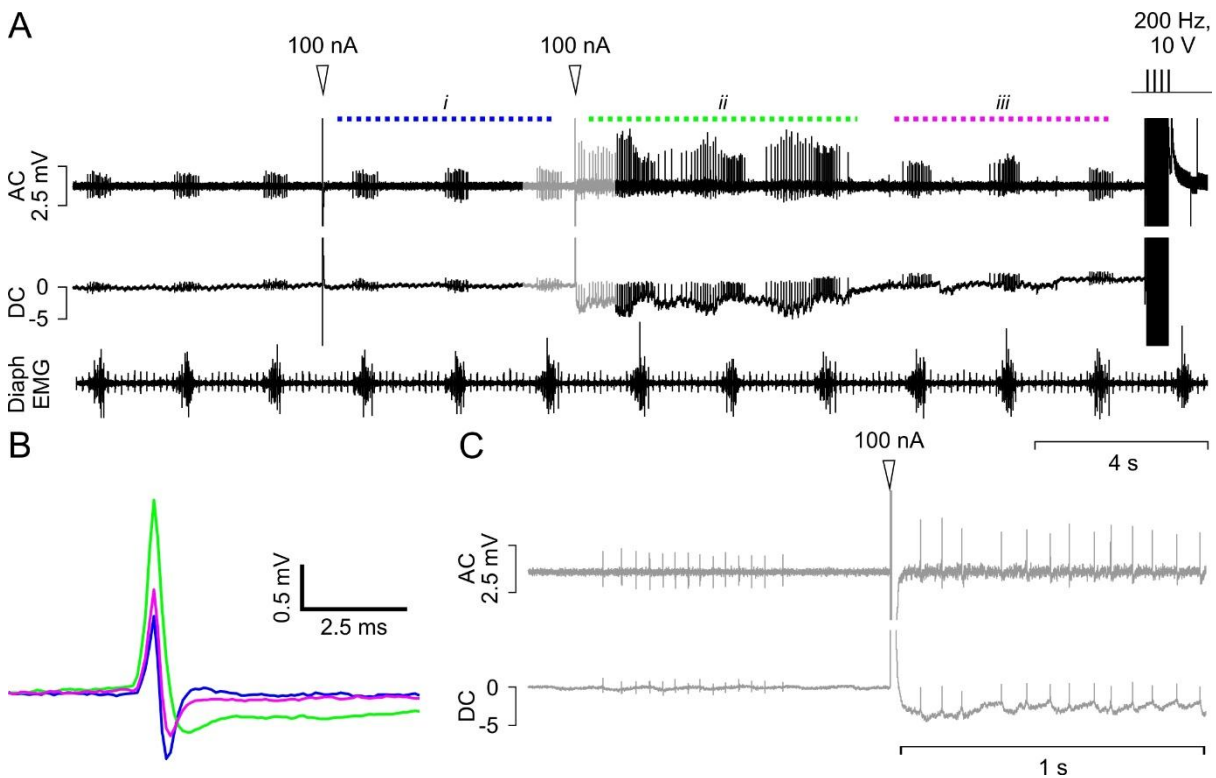


Figure 3.1 Electrophysiological recording and labelling of brainstem respiratory neuron. **A.** Following functional identification of an inspiratory-locked neuron in the preBötzinger Complex (preBötC) the pipette was gradually moved to a position at which 100 nA microstimulation evoked a transient increase in neuronal firing, a change in spike shape (**B**) and a -2 mV pipette potential. Note that the cell maintains its firing pattern for the duration of the recording. The cell was then electroporated with a 0.5 s train of 10 V 1 ms pulses at 200 Hz. Panel **B** shows average spike waveforms recorded in periods denoted in **A** *i*, *ii* and *iii*. Panel **C** shows an expanded view of data indicated in gray in Panel **A**.

Perfusion and tissue collection

Rats were euthanized with an overdose of sodium pentobarbitone (100 mg/kg i.p. or i.v.) or potassium chloride solution (3 M, 0.3 ml, i.v.) and transcardially perfused with 400 ml heparinized 0.9% NaCl followed by 400 ml freshly prepared fixative solution (4% paraformaldehyde/0.1 M phosphate buffer; pH 7.4; Sigma-Aldrich, Australia). Brains were removed under RNase free conditions and further fixed overnight in the same solution. Coronal or parasagittal brainstem sections (50 µm) were cut on a vibrating microtome, and collected in cryoprotectant or phosphate buffered saline containing 0.1% Tween-20 (PBT; Sigma-Aldrich, Australia).

Histology, in situ hybridization and immunohistochemistry

cRNA probe synthesis and ISH protocol

A non-radioactive *in situ* hybridization (ISH) digoxigenin (DIG)-11-UTP-labelled riboprobe was synthesized for the detection of glycine transporter 2 (GlyT2; *Rattus norvegicus* solute carrier family 6, member 5) mRNA. The riboprobe was directed at base pairs 5733-6543 (810 bp length) of the GlyT2 cDNA sequence (GeneBank accession number NM_203334.1). The sense cRNA probe was synthesized using an RNA polymerase SP6 promoter attached to the 5' end of the forward oligonucleotide primer (5'-GGATCCATTTAGGTGACACTATAGAAG aagcgtcttgccttagaa -3'). An anti-sense cRNA probe was synthesized with a T7 promoter attached to the 5' end of the reverse oligonucleotide primer (5'-GAATTCTAATACGACTCACTATAGGGAGA agcctgagcttgcttttcag-3'). A PCR-amplified cDNA template was generated using cDNA reverse transcribed from Sprague Dawley rat brainstem (at approximately -12.6 mm to -11.6 caudal to Bregma) total RNA. Following PCR, purified cDNA (QIAquick PCR Purification kit; 28104; Qiagen, Doncaster, Victoria, Australia) was *in vitro* transcribed using a T7 kit (AmpliScribe™ T7-Flash™ Transcription Kit; ASF 3257; Epicentre Biotechnologies, Madison, WI) incorporated with DIG-11-UTP (Roche).

Combined ISH and immunohistochemistry

Brainstem sections were incubated in pre-hybridization buffer (50% formamide, 5 x SSC, pH 7.0, 250 μ g/ml herring sperm DNA, 100 μ g/ml yeast tRNA, 100 μ g/ml heparin, 5% dextran sulphate, 1 x Denhardt's solution, 0.1% Tween-20) for 30 minutes at 37 °C then at 58 °C for 1 h before hybridization with cRNA riboprobe (final concentration 1000 ng/ml) for 12-18 h at 58 °C with gentle agitation. Sections were washed in 2 x SSC buffer with 0.1% Tween-20 followed by 0.2 x SSC buffer with 0.1% Tween-20 and then a wash of maleic acid buffer with 0.1% Tween-20. The tissue was then blocked in maleic acid buffer (0.1 M maleic acid, 0.15 M NaCl, 0.1% Tween-20) containing 2% Boehringer blocking reagent (Roche Applied Science; Mannheim, Germany) and 10% normal horse serum.

Primary antibodies were added to the blocking buffer and incubated for 24 h at 4 °C and 4 h at room temperature. Sections were washed in TPBS (Tris-HCl 10 mM, sodium phosphate buffer 10 mM, 0.9% NaCl, pH 7.4) buffer 3 x 30 min and incubated overnight with IgG secondary antibodies. DIG-labelled neurons were revealed colorimetrically by incubation in NTMT (0.1 M NaCl, 0.1 M Tris-HCl pH 9.5, 0.1 M $MgCl_2$), 0.1% Tween-20 (Sigma), 2 mM tetramisole HCl (Sigma) buffer containing nitro blue tetrazolium (Roche Applied Science), and 5-bromo-4-chloro-3-indolyl phosphate salts (Roche Applied Science). The reaction was stopped when DIG-labelling was intense with minimal background staining by 3 x 15 min wash in 0.1M Tris (pH 8.5)/ 1 mM EDTA solution. No labelling in any brain region was seen when the sense probe was substituted for the anti-sense probe.

For experiments in which no ISH was performed, sections were washed in PBT for 3 x 15 min and incubated in 0.01 M phosphate buffered saline containing 2% bovine serum albumin and 0.2% TritonX-100 or Tween-20 for 1 h at room temperature. Primary antibodies (see Table 4.1) were added to the blocking buffer and sections were incubated for 48 h at 4 °C. Sections were washed in TPBS (3 x 30 min) and incubated in IgG secondary antibodies (see Table 4.1) for 12

h at 4 °C. Processed sections were washed again in TPBS (3 x 30 min) before being mounted in serial order on glass slides and coverslipped for imaging.

Table 3.1 Antibodies

<i>Antibody name</i>	Immunogen	Manufacturer details	Concentration
Primary antibodies			
<i>Guinea pig anti-SST_{2a}</i>	C-terminus amino acid sequence 355–369 (ETQRTLLNGDLQTSI) of synthetic sst2a peptide	Gramsch Laboratories, Schwabhausen Germany Cat# SS-870 RRID: AB_2491104 Polyclonal	1:1,000
<i>Rabbit anti-SST_{2a}</i>	C-terminus amino acid sequence 355–369 (ETQRTLLNGDLQTSI) of synthetic sst2a peptide	Bio-trend Cat# ss-8000-rmc Lot# a080826 RRID: AB_2491103 monoclonal	1:100
<i>Goat-anti-choline acetyltransferase (ChAT)</i>	Human placental lysate	Chemicon, Millipore Cat# AB144P RRID: AB_2079751 Polyclonal	1:800
<i>Guinea pig anti-neurokinin 1 receptor (NK1R)</i>	C-terminus amino acid sequence 393–407 (KTMTESSSFYSNM LA) of synthetic rat NK1R peptide	Millipore Cat# AB15810 Lot# LV1587443 RRID: AB_992894 Polyclonal	1:1,000
<i>Rabbit anti-NK1R</i>	C-terminus amino acid sequence 393–407 (KTMTESSSFYSNM LA) of synthetic rat NK1R peptide	Sigma-Aldrich Cat# S8305 Lot# 67K4885 RRID: AB_261562 Polyclonal	1:5,000
<i>Mouse anti-tyrosine hydroxylase (TH)</i>	Rat tyrosine hydroxylase N-terminal region (approx. aa 9–16)	Sigma-Aldrich Cat# T1299 RRID: AB_477560 Monoclonal	1:8,000
<i>Rabbit anti-Phox2b</i>	14 amino acid C-terminal sequence (YFHRKPGPALKTNLF) of the rat/ mouse Phox2b protein	Jean Francois Brunet RRID: AB_2315161 Polyclonal	1:1,000
<i>Sheep anti-digoxigenin</i>	Digoxigenin, whole	Roche Applied Science Cat# 11093274910 RRID: AB_514497 Polyclonal	1:1,000
Secondary antibodies			

<i>ExtrAvidin-FITC</i>	n/a	Sigma-Aldrich Cat# E2761 RRID: AB_2492295	1:500
<i>Cy3- AffiniPure donkey antigoat IgG (H1L)</i>	Whole molecule goat IgG	Jackson ImmunoResearch Laboratories, INC Cat# 705-165-147 Lot# 68839 RRID: AB_2307351 Polyclonal	1:250
<i>Alexa Fluor 647-AffiniPure donkey antirabbit IgG (H1L)</i>	Whole molecule rabbit IgG	Jackson ImmunoResearch Laboratories, INC Cat# 711-605-152 Lot# 105115 RRID: AB_2492288 Polyclonal	1:250
<i>Alexa Fluor 647 donkey antirabbit IgG (H1L)</i>	Rabbit, IgG heavy & light chains	Life Technologies Cat# A31573 Lot# 1322326 RRID: AB_10561706 Polyclonal	1:250
<i>Alexa Fluor 488-AffiniPure donkey antiguinea pig IgG (H1L)</i>	Whole molecule guinea pig IgG	Jackson ImmunoResearch Laboratories, INC Cat# 706-545-148 Lot# 161406 RRID: AB_2340472 Polyclonal	1:250
<i>Alexa Fluor 647 goat antiguinea pig IgG (H1L)</i>	Domestic guinea pig, IgG heavy & light chains	Life Technologies Cat# A21450 Lot# 1235826 RRID: AB_10564076 Polyclonal	1:250
<i>Alexa Fluor 488 donkey antimouse IgG (H1L)</i>	Mouse, IgG heavy & light chains	Life Technologies Cat# A21202 RRID: AB_10049285 Polyclonal	1:250

Antibody characterization

Two different sst_{2a} antibodies were used in the current study: we used guinea pig antiserum raised against the C-terminus amino acid sequence 355-369 of rat sst_{2a} and a monoclonal rabbit anti- sst_{2a} antibody raised against the same amino acid sequence. Both antibodies have been extensively characterized by Western and dot blot assay; neither label sst₂ knock-out animals, and the rabbit antibody selectively labels HEK cells transfected with sst₂ (Schulz *et al.*, 1998a; Schulz *et al.*, 1998b; Korner *et al.*, 2005; Fischer *et al.*, 2008). As recently described, binding of both antisera is blocked by pre-absorption with the sst_{2a} antigen, and overlaps completely in tissue incubated with both primary antibodies, visualized with different fluorescent secondary antibodies (Bou Farah *et al.*, 2015).

For detection of neurokinin 1 receptor (NK1R) we used guinea pig and rabbit primary antibodies raised against a synthetic peptide that corresponds to amino acid sequence 393-407 of rat NK1R. The rabbit antibody has been validated in NK1R knock-out animals (Ptak *et al.*, 2002) and results in distinctive NK1R labelling in the brainstem and spinal cord (Al-Khater *et al.*, 2008; Bochorishvili *et al.*, 2012). The guinea pig antibody recognizes the same sequence, has been validated (by the manufacturers) by Western blot, and results in the expected pattern of immunolabelling (Yu *et al.*, 2009; Spirovski *et al.*, 2011).

A mouse anti-tyrosine hydroxylase (TH) monoclonal antibody was used to detect catecholaminergic neurons. This antibody has been widely used by other investigators (Berube-Carriere *et al.*, 2009; Forlano & Woolley, 2010; Lindemann *et al.*, 2013) and results in characteristic intense labelling of neurons in the brainstem C1, C3 and A1 groups.

A goat anti-choline acetyl transferase (ChAT) antibody was used to identify cranial motoneurons in the facial nucleus and nucleus ambiguus. Western blot analysis (by the manufacturer) reveals a single band at 70 kDa. Incubation with the antibody resulted in the expected pattern of immunolabelling.

Phox2b immunoreactivity was detected using a rabbit polyclonal antibody. Immunolabelling obtained using the same antibody colocalizes perfectly with Phox2b mRNA expression in the mouse (Pattyn *et al.*, 1997), is reported to be absent in Phox2b knockout animals, and overlaps with reporter expression in Phox2b-EGFP transgenic animals (Lazarenko *et al.*, 2009). The general pattern of labelling was consistent with previous reports, with high expression of Phox2b immunoreactivity in small neurons in the retrotrapezoid nucleus, high colocalization of Phox2b immunoreactivity with TH immunoreactivity in the C1 region, and Phox2b immunoreactivity in the facial nucleus and nucleus ambiguus compact formation.

Microscopy and analysis

Processed sections were mounted on glass slides in Vectashield (Vector Laboratories, cat#H-1000) or Dako fluorescence mounting medium (Dako, #S302380-2) and coverslipped for viewing using an AxioImager Z2 microscope under epifluorescence and brightfield illumination (Zeiss, Gottingen, Germany). Mosaic images of each coronal brainstem section were captured at 10x magnification and adjusted for brightness and contrast using ZEN software (2012 version, Carl Zeiss, RRID: SCR_013672). Color channels were overlayed in the resultant image file for analysis.

Definition of VLM respiratory compartments

BötC, preBötC and rVRG respiratory neurons are distributed in overlapping and adjacent regions of the brainstem. Electrophysiologists are in general agreement that the highest proportion of BötC neurons are found within 500 μ m caudal of the caudal pole of the facial nucleus, as determined by electrophysiological mapping of facial field potentials (Sun *et al.*, 1998; Schreihofer *et al.*, 1999). The majority of inspiratory putative preBötC neurons are found 500 – 1,100 μ m caudal to facial, with a transition zone of intermingled BötC and preBötC neurons that lies 500 – 700 μ m caudal to the facial nucleus (Sun *et al.*, 1998; Wang *et al.*, 2001;

Stornetta *et al.*, 2003a). This corresponds well with the anatomical distribution of SST, a putative marker of preBötC (Stornetta *et al.*, 2003a). A population of bulbospinal inspiratory locked neurons, many of which express NK1R, emerges beyond 1,000 μm caudal to the facial nucleus and extends for about 600 μm (Guyenet *et al.*, 2002; Stornetta *et al.*, 2003a; Stornetta *et al.*, 2003b). This population is thought to represent excitatory premotor neurons of the rVRG, as defined by trans-synaptic labelling of phrenic motoneurons (Dobbins & Feldman, 1994).

In the current study we have defined BötC as residing 0-500 μm caudal to the facial nucleus, preBötC as residing 600 – 1,100 μm caudal to the facial nucleus, and rVRG as residing 1,200 – 1,800 μm caudal to the facial nucleus. Rostro-caudal co-ordinates are presented with reference to the caudal pole of the facial nucleus as mapped in electrophysiology experiments or identified in histological experiments; the most caudal position at which facial motor neurons are clearly discernable corresponds to -12.0 mm caudal to Bregma according to the stereotaxic atlas of Paxinos and Watson (2006).

For quantification of sst_{2a}, NK1R and TH colocalization, regions that contained the preBötC (1 – 3 samples each from 4 rats, 13 images in total) were scanned using a confocal microscope under x10 objective (TCS SP5 X, Leica, Germany). The balance and contrast of the images were adjusted to include all information-containing pixels using ZEN or LAS AF software (RRID: SCR_013673). Figures were prepared using Coreldraw and Corel Photopaint X4 (RRID: SCR_013674).

For quantification of overall sst_{2a} distribution, sst_{2a}-immunoreactive neurons lying within the ventrolateral medulla between 0 and 2.4 mm caudal to the facial nucleus were counted bilaterally in six rats. Three to six sections were quantified at each rostrocaudal level indicated in Figure 3.2 B (2 images per section (one on each side), 131 images in total). We observed a shift in the dorso-ventral position of sst_{2a}-immunoreactive neurons at different Bregma levels, so divided the VLM into dorsal and ventral compartments. The dorsal compartment was defined

as a 500 x 500 μm box that lay center-aligned and immediately ventral to nucleus ambiguus. The ventral compartment was defined as a 500 μm high x 750 μm wide box that lay immediately ventral to the dorsal compartment (see Figure 3.2). In sections in which the compact formation of nucleus ambiguus could not be clearly distinguished both compartments were aligned to 1.8 mm lateral of midline.

The size of biotin- or dextran-labelled neurons was estimated by measuring the long and short axis of each neuron in the center of its focal plane, from which its cross-sectional area was estimated. Size data are presented as standardized diameter i.e. the diameter of a circle with the same cross sectional area.

Results

General pattern of sst_{2a} immunoreactivity

sst_{2a} immunoreactive neurons and fibers were identified throughout the ventral medulla. Particularly dense expression was found on cell bodies in the nucleus raphe magnus, in neurons immediately dorsal, medial and lateral to the compact formation of nucleus ambiguus, and in a single contiguous band that started at the ventral aspect of the facial nucleus and extended caudally for several millimetres. As the distance from the facial nucleus increased, sst_{2a} immunoreactive neurons concentrated more dorsally (Figure 3.2).

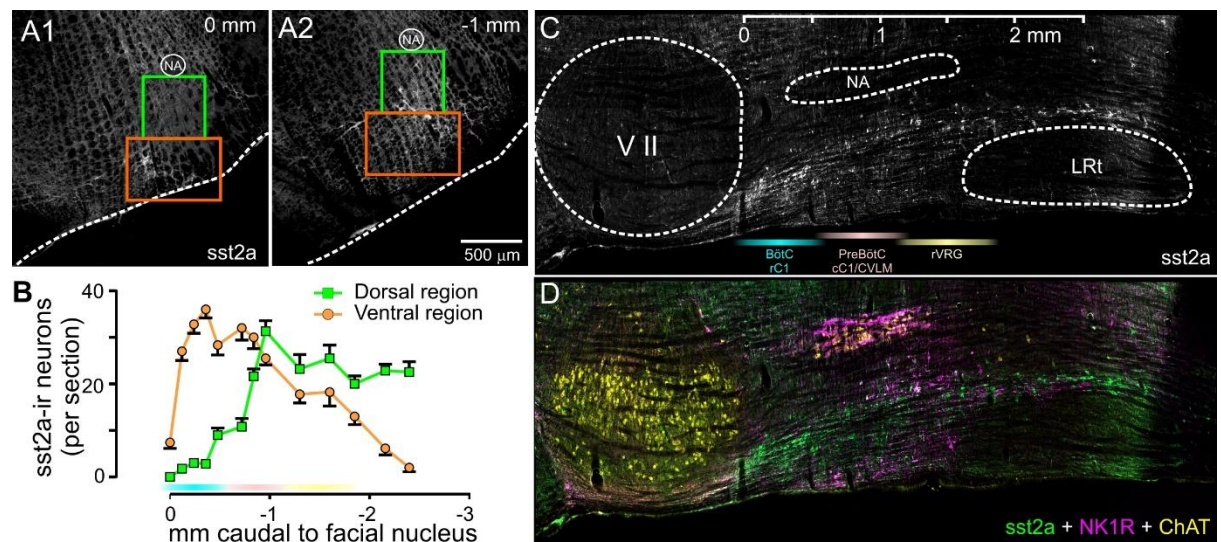


Figure 3.2 sst_{2a} - immunoreactive cells are distributed along the ventrolateral medulla. Cells residing in dorsal (green) or ventral (orange) regions of interest were counted and plotted against rostral co-ordinates. A1 and A2 illustrate sst_{2a} immunoreactivity and boxes used to define regions of interest at co-ordinates corresponding to the caudal pole of the facial nucleus (0 mm) and preBötC (1 mm). B shows pooled data from 6 rats. C. Parasagittal section shows the extent of sst_{2a} labelling within the ventrolateral medulla. D. Same section overlaid with NK1R and ChAT immunoreactivity. NA: compact formation of nucleus ambiguus. VII: facial nucleus; LRt: reticular formation; BötC: Bötzing Complex; rC1: rostral C1 group; cC1: caudal C1 group; CVLM: caudal ventrolateral medulla; rVRG: rostral ventral respiratory group.

sst_{2a} immunoreactive neurons are present in the RVLM C1 region but not Böttinger Complex

Within 500 µm of the facial nucleus, sst_{2a}-immunoreactivity was densely expressed in the portion of the ventrolateral medulla closest to the ventral surface of the brainstem, overlapping closely with the distribution of catecholaminergic C1 neurons, but was largely absent in the dorsal compartment of the VLM, corresponding to the BötC (Figures 3.2 & 3.3). In the rostral C1 (rC1) region and retrotrapezoid nucleus/parafacial respiratory group region (RTN/pFRG, data not shown) sst_{2a} immunoreactivity often co-localized with TH-immunoreactivity (Figure 3.3A). TH-immunoreactive neurons that were Phox2b-immunoreactive were often sst_{2a}-positive (Figure 3.3, A5), but Phox2b neurons that were TH-negative were almost never sst_{2a}-immunoreactive (data not shown). The pattern of sst_{2a}-immunoreactivity in the RVLM rC1 region and its co-localization with TH immunoreactivity was qualitatively similar to that previously reported (Burke *et al.*, 2008), and is therefore not presented in detail.

The BötC was defined as the region immediately ventral to the nucleus ambiguus compact formation containing dense glycine transporter-2 (GlyT2) mRNA expression (Schreihofer *et al.*, 1999). In contrast to the high sst_{2a} immunoreactivity observed in the RVLM C1 region, sst_{2a} immunofluorescence was absent in the BötC. Expression of GlyT2 mRNA and sst_{2a} was quantified in one representative BötC section from three rats using the same segregation into dorsal and ventral regions illustrated in Figure 3.2A. The dorsal compartment contained 115 ± 9 GlyT2-positive neurons per section and 4 ± 1 sst_{2a} immunoreactive neurons, none of which colocalized with GlyT2 (Figure 3.3B). The ventral compartment contained 46 ± 9 GlyT2-positive neurons and 36 ± 4 sst_{2a} neurons; one double labelled neuron was encountered.

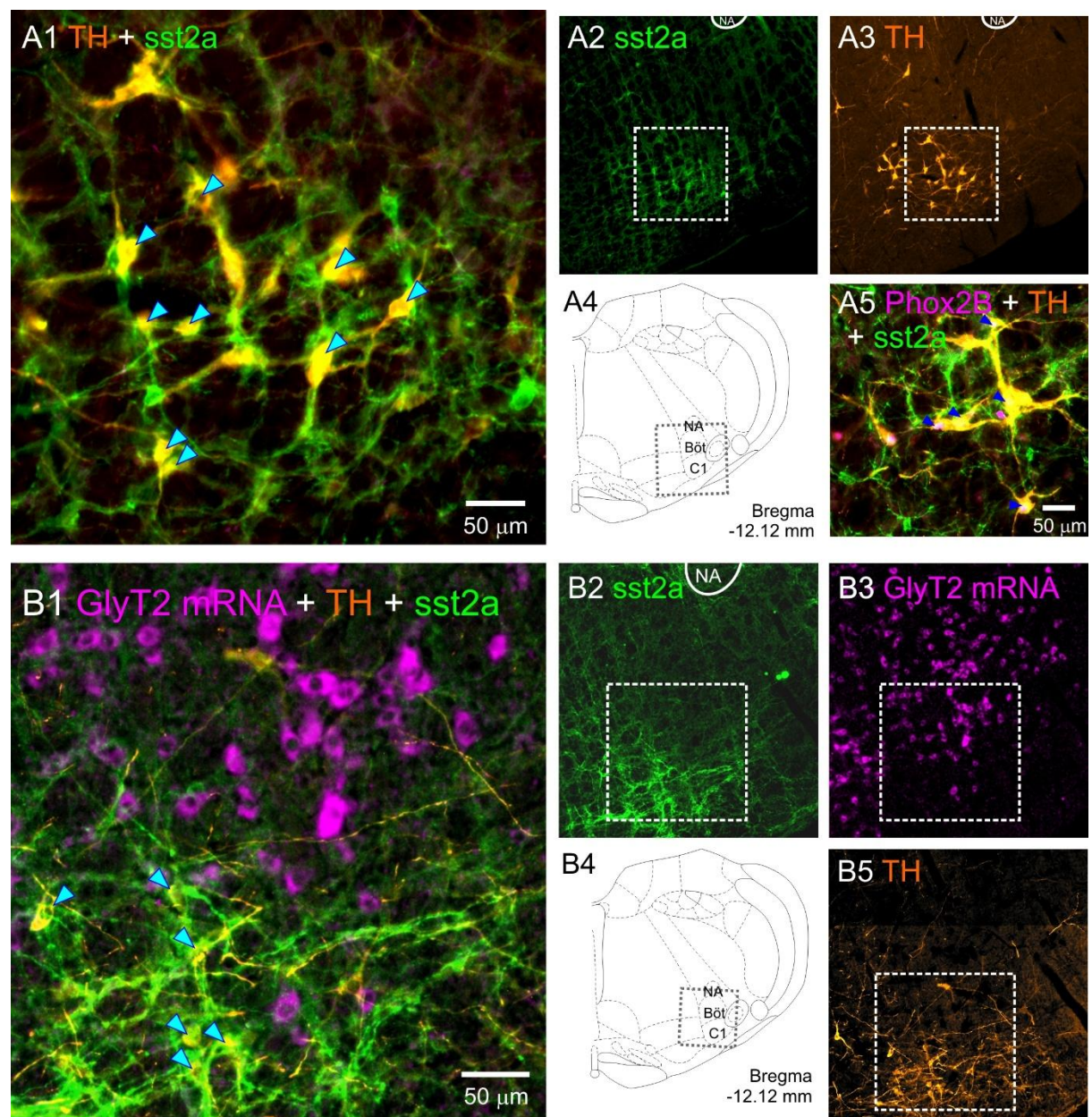


Figure 3.3 *sst2a* expression is colocalized with markers of cardiovascular but not respiratory function in the RVLM/BötC. **A.** Epifluorescent photomicrographs show colocalization of *sst2a*- with TH-immunoreactivity (A1, arrowheads). Region shown in A1 indicated by hatched boxes in individual channel images (A2, A3). Similarly, region illustrated in A2 + A3 indicated by hatched boxes in stereotaxic reference image (A4). A5 shows colocalization of *sst2a* with Phox2b and TH (arrowheads) in another experiment. **B.** *sst2a* immunoreactivity does not colocalize with GlyT2 *in-situ* hybridization (ISH) product in the BötC. No GlyT2-positive *sst2a*-positive neurons were ever identified. B1 shows pseudocolored inverted ISH signal overlaid with TH and *sst2a* immunoreactivity. Arrowheads indicate double labelled TH/*sst2a*-positive neurons. Region shown in B1 indicated by hatched boxes in individual channel images (B2, B3 & B5), and in stereotaxic reference image (B4).

sst_{2a} immunoreactive neurons in the preBötzinger Complex are either NK1R- or TH-immunoreactive

The difference in dorso-ventral distribution of sst_{2a} immunoreactivity seen in the rC1/BötC was not observed in confocal images containing the preBötC (13 ± 2 (dorsal) vs. 14 ± 1 (ventral) neurons per image, $P = 0.4$, $t = 1.03$, $df = 3$, $n = 13$ images from 4 rats, paired t-test). The distribution of sst_{2a}-immunoreactive neurons partially overlapped with the expression of NK1R-immunoreactivity in both compartments (Figure 3.4), with a significantly greater proportion of sst_{2a}-positive neurons expressing NK1R in the dorsal region (corresponding to preBötC) compared to the ventral region (corresponding to the caudal C1 (cC1)/CVLM region, 54 ± 5 vs. $20 \pm 2\%$ respectively, $P = 0.003$, $t = 8.5$, $df = 3$, $n = 4$, paired t-test). Difficulties in accurately quantifying the total number of NK1R-positive neurons precluded reliable estimates of the total fraction of NK1R-immunoreactive cells that were also sst_{2a}-positive, but many NK1R-immunoreactive neurons were sst_{2a}-negative.

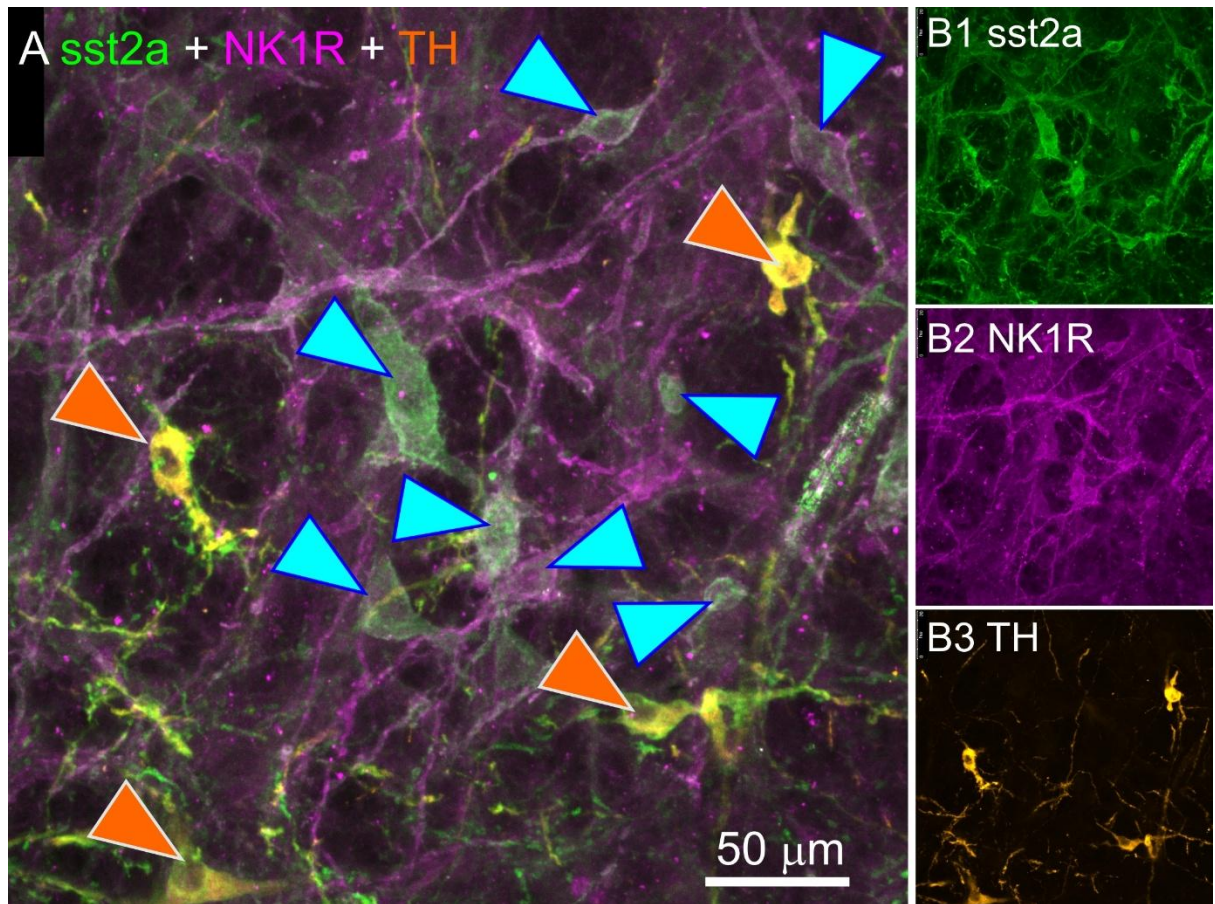


Figure 3.4 *sst2a* immunoreactivity in the preBötC is partially colocalized with NK1R and TH. **A:** Merged confocal stack showing colocalization of *sst2a* with NK1R (blue arrowheads) and TH (orange arrowheads). Individual channel images are shown in B1-3. Catecholaminergic neurons continued to account for a significant portion of *sst2a*-positive neurons in the preBötC and cC1/CVLM regions (27 ± 1 and $33 \pm 2\%$ respectively), with *sst2a* immunoreactivity identified in 57 ± 4 of dorsal compartment and $46 \pm 4\%$ of ventral compartment TH-immunoreactive neurons. No co-expression of NK1R with TH was detected (although we have previously reported a marginal co-expression of NK1R with TH in the RVLM: Makeham *et al.*, 2001): preBötC and cC1/CVLM *sst2a*-positive neurons that co-express NK1R or TH therefore accounted for $81 \pm 4\%$ of the total *sst2a*-positive population. In the rVRG, *sst2a* immunoreactive cells formed a dense cluster that colocalized with TH neurons (data not shown).

sst_{2a} immunoreactivity on functionally identified respiratory neurons

52 respiratory neurons (electroporated: 45, juxtacellularly labelled: 7) were evenly filled with neurobiotin ($n = 42$) or dextran ($n = 10$), with dendritic/axonal filling also visible. A further 4 recovered respiratory neurons were positive for ChAT immunoreactivity (and sst_{2a}-negative), identifying them as respiratory motoneurons, and were excluded from the current data set. ChAT-negative cells were considered as respiratory interneurons or pre-motor neurons. In nine cases two neurons were recovered in close proximity to each other when a single labelling attempt had been made. In all cases in which multiple neurons were labelled, both were negative for sst_{2a} immunoreactivity, so the data were included and counted as a single cell but excluded from morphometric analysis.

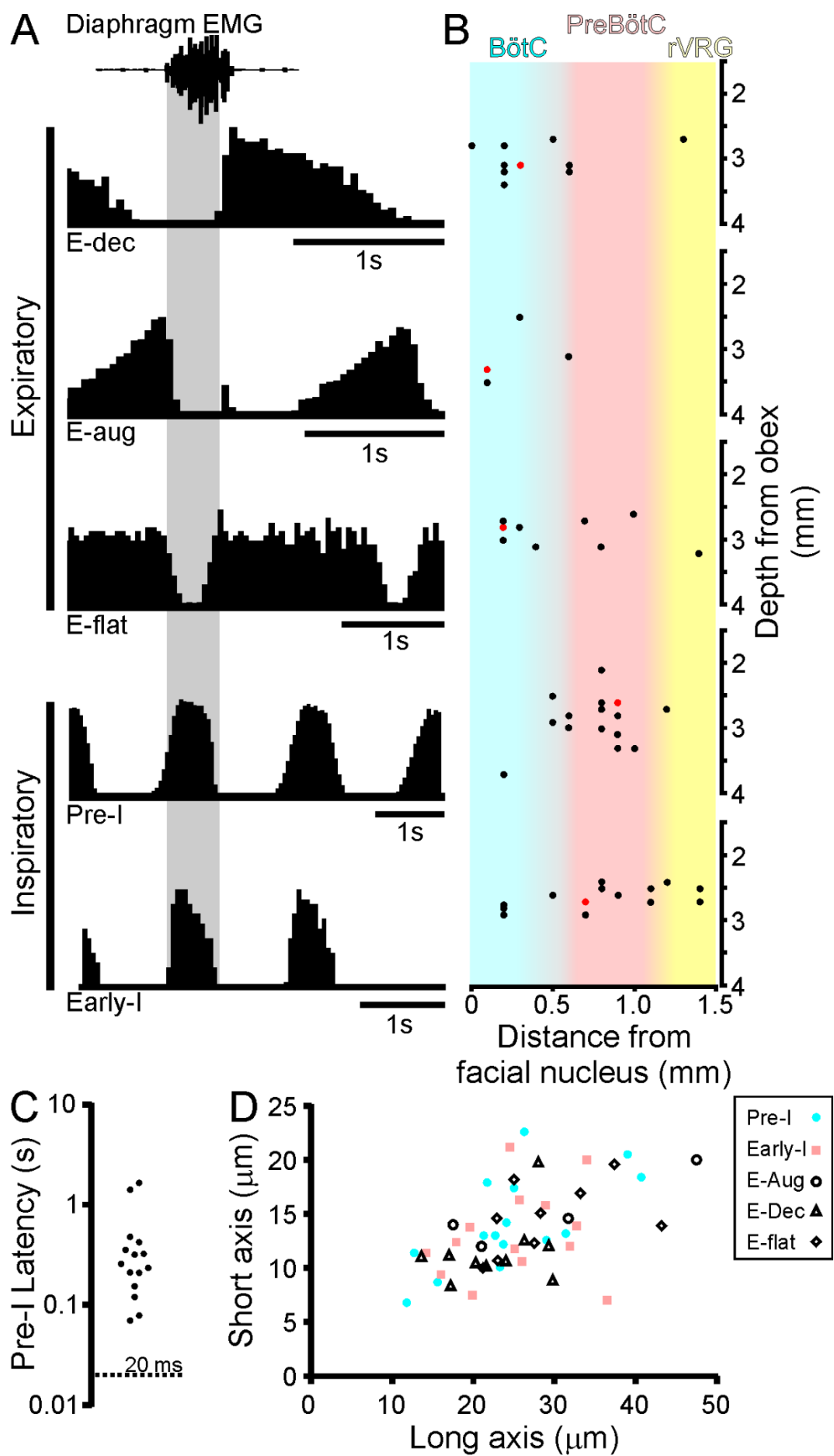


Figure 3.5 Functional classifications and anatomical locations of recovered respiratory neurons. A. Cycle-triggered histograms illustrating different functional classes of respiratory neurons and B. stereotaxic coordinates at which neurons of each class were recorded and recovered. X-axis of each histogram was adjusted such that inspiratory period in each recording is equivalent to the width of the grey band. Red dots in B indicate cells illustrated in Figure 3.6. C. Latencies between the onset of neuronal firing and the onset of the phrenic/diaphragmatic burst in neurons classified as pre-inspiratory. Dashed line indicates threshold for classification. The two neurons with pre-I latencies of >1 s were recorded in one experiment, in which the respiratory period was unusually long. Each data point represents the average value recorded in 6 – 10 consecutive respiratory cycles. D. Dimensions of recovered neurons, classified by functional properties.

Cycle-triggered averages of unit firing with respect to diaphragmatic/phrenic nerve activity were used to classify neurons according to the functional criteria described by Smith *et al.* (2007) (Figure 3.5): expiratory decrementing neurons (E-dec: $n = 10$), expiratory augmenting neurons (E-aug: $n = 4$), expiratory tonic discharge neurons (E-flat: $n = 9$), pre-inspiratory neurons (pre-I: $n = 15$) and early inspiratory neurons (early-I: $n = 14$). Most E-dec and E-aug neurons (10/14) were located within 500 μm of the caudal pole of the facial nucleus, with an average depth of 3.04 ± 0.08 mm from the level of obex, anatomically consistent with being within the confines of the BötC (Sun *et al.*, 1998). The distribution of E-flat neurons was more spread out through the VRC. According to the criteria described by Guyenet and Wang (2001), neurons were considered pre-I when the first action potential recorded in each respiratory cycle consistently preceded the phrenic/diaphragmatic inspiratory burst by >20 ms and discharge continued to the peak of phrenic/diaphragmatic discharge. The ‘pre-I latencies’ of neurons classified as pre-inspiratory are presented in Figure 3.5C. 17/29 pre-I and early-I neurons were recorded between 600-1100 μm caudal to the facial nucleus, anatomically consistent with the preBötC.

Size estimates of recovered biotin- or dextran-labeled respiratory neurons are presented in Figure 3.5D. Excluding data in which multiple neurons were labelled in a single attempt, diameters of E-dec, E-aug, E-flat, pre-I and early-I neurons were 17.1 ± 1.3 ($n = 10$), 22.5 ± 3.5 ($n = 4$), 21.5 ± 1.4 ($n = 9$), 19.3 ± 1.4 ($n = 15$) and 19.4 ± 1.1 ($n = 14$) μm respectively. No recovered neurons were sst_{2a}-immunoreactive. In some cases, dye-labelled neurons were recovered in close proximity to sst_{2a}-immunoreactive cell bodies or fibers, and in all cases sst_{2a}-positive labelling was apparent on the same sections, but clear evidence of sst_{2a} expression was absent (Figure 3.6).

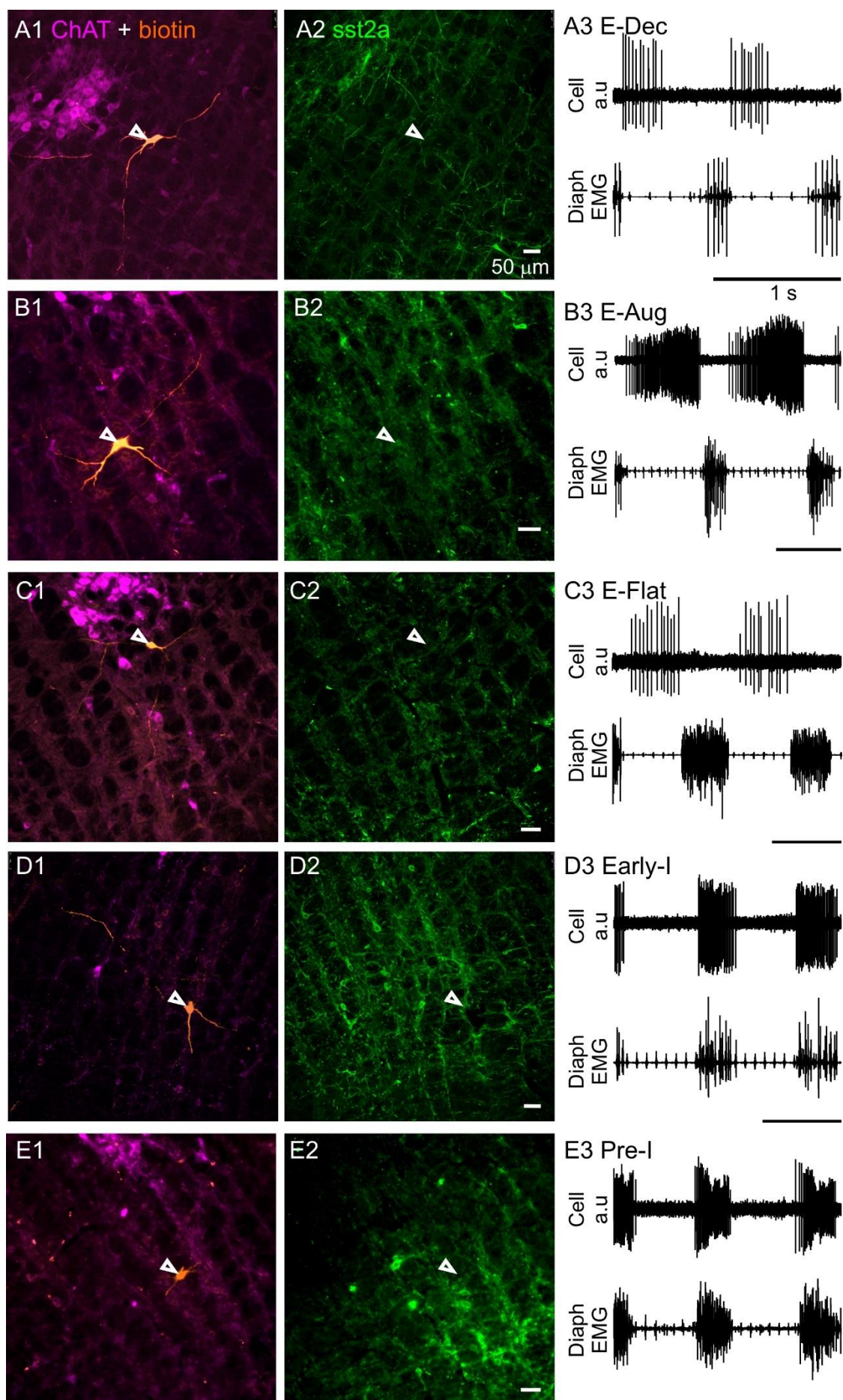


Figure 3.6 Medullary respiratory neurons do not express sst2a. A. – E. Examples of neurobiotin labelled respiratory neurons that were processed for sst_{2a} immunoreactivity. Panel 1 shows neurobiotin labelling (orange) and choline acetyl transferase (ChAT: magenta) immunoreactivity; none of the neurons shown are ChAT-positive, and are therefore considered to be respiratory interneurons. In each case sst_{2a}-positive fibers or somata were visible in the region of the recovered neuron (Panel 2), but no neurobiotin-labelled cells (*n* = 52) were sst_{2a}-positive. Panel 3 shows corresponding electrophysiological recordings from each neuron. Photomicrographs are taken in the coronal plane with the ventral surface towards the bottom of the field of view; nucleus ambiguus is visible as a cluster of cholinergic neurons in panels A, B, C & E. Scale bars in photomicrographs denote 50 μ m; scale bars in electrophysiological recordings denote 1 s. Electrical noise in EMG trace shown in E3 has been edited to aid clarity.

Discussion

The current study provides a detailed description of the distribution of sst_{2a} expressing neurons in the VLM with reference to functionally and neurochemically distinct respiratory compartments. We report that sst_{2a} is distributed across a contiguous region of the ventral brainstem that encompasses the RTN, RVLM C1 group, preBötC and rVRG, but that colocalization of sst_{2a} with markers of respiratory function, as defined by anatomical location and neurochemical phenotype, is sparse or absent in all but the preBötC, where substantial colocalization of sst_{2a} with NK1R was identified. These findings were supported by electrophysiological experiments in which neurons were selected by anatomical and functional criteria and recovered for sst_{2a} immunohistochemistry: no sst_{2a}-positive neurons were identified. Taken together, the findings suggest that somatic expression of sst_{2a} is rare on classically defined respiratory neurons, and challenges the mechanisms previously proposed to account for the effects of SST administration on respiratory rhythm generation and pattern formation.

Somatic expression of sst_{2a} receptor is absent in the Bötzing Complex

One of the specific aims of the current study was to examine the hypothesis that sst_{2a} is marker for BötC E-Dec neurons. This population is, along with other subsets of BötC expiratory neurons, largely glycinergic (Schreihofer *et al.*, 1999; Ezure *et al.*, 2003a), and is proposed to play a role in inspiratory-to-expiratory phase transition and generation of post-inspiratory activity (Ezure & Manabe, 1988; Smith *et al.*, 2013; Dutschmann *et al.*, 2014). Our hypothesis was based on the observation that microinjection of SST into the BötC evokes apneusis and loss of post-inspiratory activity in vagal (and sympathetic) nerve activities (Burke *et al.*, 2010), suggestive of a specific inhibitory effect on E-Dec neurons. We found that sst_{2a} immunoreactivity was closely associated with the C1 cell group, which lies immediately ventral

to the BötC, but sparse in the BötC, with no colocalization with GlyT2 mRNA, the distribution of which was similar to that described in previous investigations (Schreihofer *et al.*, 1999; Ezure *et al.*, 2003a; Tanaka *et al.*, 2003). No sst_{2a} immunoreactivity was detected in 15 expiratory-locked BötC neurons, of which 7 had a decrementing firing pattern. We conclude that somatic expression of sst_{2a} is absent from the BötC, and therefore not a marker BötC E-Dec neurons.

sst_{2a} is associated with preBötzinger Complex NK1R neurons but not widely expressed on functionally identified neurons

In contrast to the BötC, high levels of sst_{2a} expression were consistently observed in the preBötC. Most sst_{2a}-positive neurons in this region were also immunoreactive for either NK1R (54%) or TH (27%), leaving the neurochemical phenotype of only 19% of sst_{2a}-positive neurons unaccounted for. The association between sst_{2a} and NK1R expression in the preBötC has not previously been quantified, but our findings are consistent with qualitative studies of neonatal mice (Gray *et al.*, 2010; Gray, 2013), which propose that glutamatergic neurons which express NK1R, sst_{2a} and/or SST are an anatomical marker for the ‘core’ of the preBötC.

We observed no expression of sst_{2a} on 18 neurons recorded within the strict anatomical boundaries of the preBötC, of which eleven exhibited the pre-inspiratory discharge that is a signature for putative pacemaker neurons. We therefore conclude that, despite a relatively high expression of sst_{2a} within the preBötC, the expression of sst_{2a} on inspiratory-locked neurons, or at least those neurons amenable to extracellular recording *in vivo*, is unexpectedly low.

Technical considerations

There are two caveats to our conclusion that sst_{2a} is rarely expressed on preBötC inspiratory neurons. First, it may be that sst_{2a} is present on some, but expressed at levels too low to detect using immunohistochemistry. Second, it may be that sst_{2a}-expressing respiratory neurons are abundant, but difficult to record and/or label.

The monoclonal anti-sst_{2a} antibody used in the current study resulted in robust labelling of neuronal cell bodies in regions in which sst_{2a} immunoreactivity has previously been observed using other well-validated anti-sst_{2a} antibodies (Burke *et al.*, 2008; Spary *et al.*, 2008; Gray *et al.*, 2010), and resulted in labelling of fibers in brainstem regions in which little or no somatic labelling was visible, suggesting a reasonable level of sensitivity. The specificity of this antibody has previously been verified to a high standard, including artificial expression and knockout animals (Fischer *et al.*, 2008), and the antibody has been recommended as a gold standard tool for the clinical detection of sst_{2a}-expressing tumors (Korner *et al.*, 2012). We have recently shown that binding of the rabbit monoclonal anti-sst_{2a} antibody correlates well with SST sensitivity in RVLM bulbospinal neurons recorded *in vitro* (Bou Farah *et al.*, 2015), and therefore interpret sst_{2a} labelling as reliable evidence of sst_{2a} protein expression, although it is possible that low levels of sst_{2a} expression remained undetected.

Alternatively, it may be that sst_{2a}-expressing neurons contribute to the generation of respiratory drive, but that their activity profile does not conform to the expected phasic bursting pattern used to select putative respiratory neurons for labelling, or that their morphologies or size make them unamenable to stable recording (Humphrey & Schmidt, 1990). Although we observed no obvious influence of cell size on labelling efficiency when developing our single-cell electroporation technique *in vitro* (Dempsey *et al.*, 2015), the size range of respiratory neurons labelled in the current study indicates a bias towards larger neurons, probably reflecting a limitation of the extracellular recording technique rather than a deficiency in the approach used to label them. This may be problematic when considering putative pre-inspiratory neurons in the preBötC, as SST is largely restricted to smaller neurons (typically 10 x 18 µm: Stornetta *et al.*, 2003a; Wei *et al.*, 2012). Indeed, the same argument has been proposed to explain the absence of SST in functionally identified preBötC neurons (Stornetta *et al.*, 2003a). Although some of the labelled preBötC neurons fell within that range, most were larger, with average

dimensions of $14.1 \pm 1.1 \times 23.7 \pm 1.9 \mu\text{m}$ ($n = 17$). Another possibility is that sst_{2a} is expressed on a small minority of respiratory neurons, and that our sample size was insufficient to detect the sst_{2a} -positive population. The Monte Carlo model presented by Del Negro *et al.* (2002b) is useful for calculating the statistical power of strings of binary observations, such as sequences of coin-tosses. Applied to our observation that sst_{2a} was undetectable in all 17 preBötC neurons, their model indicates a 96% probability that sst_{2a} is expressed on less than 20% of preBötC neurons (assuming that sst_{2a} -positive and sst_{2a} -negative neurons are equally likely to be labelled) and, extended to include all 52 neurons recovered in the current study, <5.5% of VRC respiratory neurons overall (95% confidence).

Functional implications

Based on our previous findings (Burke *et al.*, 2010) we hypothesized that the expression of SST receptors on BötC E-Dec neurons likely mediates the apneusis evoked by BötC SST microinjection at doses above 6 pmol. The results of the current study unambiguously indicate that sst_{2a} expression is not associated with glycinergic or expiratory-locked BötC neurons. We therefore conclude that the effects evoked by SST microinjection in the BötC are probably not mediated by somatic expression of sst_{2a} on respiratory neurons, and may instead indicate expression of other SST receptor isoforms or effects on neurons presynaptically connected to BötC neurons. Given that RVLM sympathetic premotor neurons lie immediately adjacent to BötC neurons (Kanjhan *et al.*, 1995), are inhibited by exogenous SST application (Burke *et al.*, 2008; Bou Farah *et al.*, 2015), and have been recently shown to accelerate respiration frequency when optogenetically activated (Abbott *et al.*, 2013; Abbott *et al.*, 2014; Burke *et al.*, 2014), it is conceivable that withdrawal of excitatory drive from RVLM C1 neurons contributes to the apneustic breathing previously observed following microinjection of SST in the BötC.

We focused on the sst_{2a} receptor isoform following numerous surveys of SST receptor protein and mRNA expression that consistently identified high levels of sst_{2a} in the VLM. However, of the 5 other SST receptor isoforms, only sst₃ and sst₅ have been reported as completely absent, with sst₁, sst_{2b} and sst₄ expressed at variable levels (Burke *et al.*, 2008; Spary *et al.*, 2008; Ramirez-Jarquin *et al.*, 2012). Functional studies support a key role for sst₂ in driving responses to exogenous SST in the C1 region and preBötC, as they are abolished by sst₂ blockade and mimicked by the sst₂-selective agonist BIM23014c (Burke *et al.*, 2008; Ramirez-Jarquin *et al.*, 2012). However, to date no agents with selectivity for the sst_{2a} or sst_{2b} splice variants have been used to define SST-sensitive populations of respiratory neurons, and no subtype-specific agents have been used to assess SST sensitivity in respiratory compartments other than preBötC, leaving potential roles for other SST receptor isoforms in mediating responses to exogenous SST.

The intersection of the sst_{2a}-, NK1R- and somatostatin-positive populations is widely believed to represent the core rhythm-generating kernel of the preBötC (Stornetta *et al.*, 2003a; Gray *et al.*, 2010; Feldman *et al.*, 2013; Smith *et al.*, 2013). This hypothesis is based on the restricted distribution of this group and observations that selective silencing of SSTergic, SST-, or substance P-sensitive preBötC neurons profoundly inhibits respiratory rhythmogenesis (Gray *et al.*, 2001; McKay *et al.*, 2005; McKay & Feldman, 2008; Tan *et al.*, 2008; Burke *et al.*, 2010). However, a logical prediction of this hypothesis is that neurons with a pre-inspiratory activity profile should express NK1R, SST, or sst_{2a}, and this does not seem to be the case. NK1R is only expressed on a minority of electrophysiologically characterized preBötC pre-inspiratory neurons (~34%: Guyenet & Wang, 2001). The same investigators were unable to detect evidence of SST expression in 36 respiratory neurons labelled in the same region (Stornetta *et al.*, 2003a), and we report here that sst_{2a} was not detected on inspiratory preBötC neurons. Taken

together, these findings suggest that modification of the existing hypotheses regarding the neurochemical phenotype of the rhythm-generating core may be necessary.

Given the low prevalence of NK1/SST/sst_{2a} expression in phasic preBötC neurons, we support the proposal that NK1/SST/sst_{2a}-positive neurons may possess an electrophysiological signature that is tonic, not phasic, as previously postulated (Gray *et al.*, 1999; Stornetta *et al.*, 2003a). This would allow them to contribute to the rhythm-generating circuit while eluding electrophysiological characterization as ‘respiratory’ neurons. Such properties would explain the discord between predicted neurochemical and functional phenotype, and are consistent with some older models of respiratory rhythm generation, in which tonic excitatory drive regulates the excitability of the rhythmogenic kernel (Smith *et al.*, 2000). Alternatively, it may be that input from this group is not required by the rhythm generating core of the preBötC, but instead represents a peripheral component of the rhythm generating network. This view is supported by recent work by Tupal *et al.* (2014), who found that elimination of glutamate release from SSTergic preBötC neurons is not associated with any respiratory phenotype, as would be predicted if this population contained the pacemaking kernel.

In the current study we describe widespread expression of sst_{2a} immunoreactivity that spans regions of the VLM associated with respiratory function. However, the association between sst_{2a} and neurochemical markers of respiratory function is poor, and we were unable to find any evidence of sst_{2a} expression in neurons with phasic respiratory discharge. We therefore conclude that somatic sst_{2a} expression is a poor marker of respiratory function in this region.

4.

The connectome of rostral
ventrolateral medulla C1
neurons

Abstract

In normal animals, basal sympathetic nerve activity (SNA) exhibits a bursting firing pattern that is synchronized with specific phases of the respiratory motor cycle. The respiratory modulation is augmented in neurogenic or artificially induced hypertensive animal models, suggesting an abnormal interaction between the respiratory and sympathetic neural network could be causal to the development of hypertension. Evidence suggests that the rostral ventrolateral medulla (RVLM) is a site of convergence in mediating respiratory-sympathetic coupling. However, the cellular sources of respiratory drive have not been identified. RVLM C1 neurons are thought to play a key role in transmission of vasomotor sympathetic drive and mediation of multiple reflex pathways that modulate SNA. Elucidating the organization of the circuits that control these neurons is a key research objective. Here we present brain-wide connectomic maps of neurons that provide monosynaptic drive to RVLM C1 neurons, generated using a two-step restricted trans-synaptic viral tracing strategy. C1 neurons were first transduced with a lentiviral vector to express a cassette containing the cognate avian receptor TVA and rabies G-protein under the control of a C1 neuron preferring promoter: PRSx8. TVA-expressing neurons were then selectively infected with a reporter-expressing rabies variant, SADΔG (EnvA)-mCherry, which retrogradely and trans-synaptically labelled neurons that provide monosynaptic drive to RVLM C1 neurons. We observed reproducible patterns of inputs arising from the dorsal, contralateral, and midline medulla, as well as local RVLM interneurons and neurons likely to reside within the Bötzing, pre-Bötzing, and ventral respiratory groups. Distant inputs were identified in the pons and midbrain, and included previously suspected sites of monosynaptic drive such as the paraventricular nucleus of the hypothalamus.

Introduction

The correlation between elevated sympathetic nerve activity (SNA) and essential hypertension is well documented in both human and animals studies (for reviews see Grassi, 1998; Guyenet, 2006). Measurement of SNA in humans using microneurography or noradrenaline spill-over demonstrated elevated SNA in hypertensive and pre-hypertensive patients (Esler, 2000; Schlaich *et al.*, 2004). Furthermore, the contribution of an over activated sympathetic system to the initiation and development of essential hypertension has been extensively demonstrated in animal models (Judy & Farrell, 1979; Lee *et al.*, 1987). The mechanisms of initiation and development of elevated SNA are not well understood. Dysfunction of noradrenaline release or reuptake (Cabassi *et al.*, 1998) and attenuated and depressed development of the baroreceptor reflex (Struyker-Boudier *et al.*, 1982; Head, 1995) have been historically proposed as a cause of the elevated SNA observed in spontaneous hypertensive rats (SHR). However, the role of the baroreflex in long term regulation of blood pressure has since been largely discredited (for review see Cowley, 1992).

Another possible mechanism that could potentiate SNA is via enhanced respiratory-sympathetic coupling (for review see Zoccal *et al.*, 2009). It has long been recognized that sympathetic nerve activity exhibits phasic bursts that are synchronized with the respiratory cycle (Adrian *et al.*, 1932). Many studies have been conducted to investigate this interaction at the circuit and single neuron level (Haselton & Guyenet, 1989a; Mandel & Schreihof, 2006). Synchronization of SNA and respiratory activity seems to be of central origin as denervation of peripheral mechanical and chemoreceptor afferents does not alter the coupling. Also, systemic hypoxia and hypercapnia challenges affect the temporal relationship and magnitude of respiratory-sympathetic coupling, but do not abolish the synchronization in SHR or normotensive Wistar-Kyoto rats (Czyzyk-Krzeska & Trzebski, 1990). Enhanced respiratory-sympathetic coupling was observed in juvenile Sprague-Dawley (SD) rats made hypertensive via chronic intermittent

hypoxia treatment (Zoccal *et al.*, 2008). Simms *et al.* (2009) showed an augmented respiratory modulation of SNA presenting in neonatal SHR, moreover, they demonstrated this augmented respiratory-sympathetic coupling to be a causal factor in producing increased Traube-Hering arterial pressure waves prior to the establishment of hypertension. These findings suggest that enhanced coupling with the central respiratory generator may drive the elevation of SNA and therefore contribute to the development of essential hypertension.

The neural circuits that underlie respiratory-sympathetic coupling have not been conclusively demonstrated. Single neuron studies show that individual neurons in the RVLM exhibit a diversity of respiratory modulated discharge patterns (Haselton & Guyenet, 1989b; Miyawaki *et al.*, 1995; Moraes *et al.*, 2013). 40 - 70% of bulbospinal presympathetic RVLM neurons contain the enzyme phenylethanolamine N-methyltransferase (PNMT) to synthesize adrenaline and are known as C1 neurons (Hökfelt *et al.*, 1973, 1974; Blessing *et al.*, 1981; Ross *et al.*, 1981; Goodchild *et al.*, 1984; Stornetta *et al.*, 2002). C1 neurons also contain other catecholamine synthesizing enzymes for the production of adrenaline (i.e. tyrosine hydroxylase (TH) and dopamine beta-hydroxylase (D β H) (Phillips *et al.*, 2001)). Although bulbospinal barosensitive neurons in the C1 region appear to include both C1 and non-C1 phenotypes (Lipski *et al.*, 1995; Schreihöfer & Guyenet, 1997), C1 adrenergic RVLM neurons exhibit a more pronounced respiratory modulation in vagal intact rats (Haselton & Guyenet, 1989b; Moraes *et al.*, 2013; Moraes *et al.*, 2014), and exhibit the same level of respiratory modulation in vagotomised rats (Haselton & Guyenet, 1989a). The above observation supports the theory that RVLM C1 presympathetic neurons are potentially a major convergent site of respiratory-sympathetic coupling (Guyenet *et al.*, 1990).

Retrograde tracing studies indicate that the RVLM region is a site of termination for several brain regions that are involved in respiratory control, such as the Kölliker fuse (KF), lateral parabrachial nucleus (LPBN) in the pons, and the nucleus of the solitary tract (NTS),

retrotrapezoid nucleus (RTN), and midline raphe (Van Bockstaele *et al.*, 1989; Bowman *et al.*, 2013). None of these regions are considered to be essential for respiratory rhythm genesis (Smith *et al.*, 1991). Pontine respiratory neurons have been shown to play a limited role in respiratory-sympathetic coupling as pontomedullary transection attenuates but does not abolish the respiratory modulation of SNA (Baekey *et al.*, 2008). A more feasible candidate that can provide direct drive to modulate SNA would be respiratory neurons in the ventral respiratory column (VRC), especially neurons located in the areas adjacent to the RVLM, known as the Bötzinger complex (BötC), and preBötzinger complex (preBötC). The VRC contains key circuits that generate respiratory rhythm (for reviews see Smith *et al.*, 2012; Feldman *et al.*, 2013). However, because respiratory neurons and cardiovascular neurons are intermingled in the ventral medulla (Ellenberger & Feldman, 1990; Pilowsky *et al.*, 1990), it is almost impossible to reveal potential sources of respiratory input to the RVLM arising from the VRC using conventional tracing techniques.

The aim of the current study is to address the question of whether putative respiratory neurons in the BötC, preBötC, or ventral respiratory group (VRG) are a source of monosynaptic drive to RVLM sympathetic premotor neurons. To examine this question we used a recombinant rabies virus, SADΔG(EnvA)-mCherry, in which cell entry and trans-synaptic spread are restricted to neurons that express the receptor TVA and rabies glycoprotein (G) respectively (Callaway & Luo, 2015; Nassi *et al.*, 2015). In brief, this tracing strategy exploits the retrograde trans-synaptic infection mechanism used by the rabies virus and the critical role played by the rabies glycoprotein in mediating that mechanism. As previously described (Wickersham *et al.*, 2007a; Wickersham *et al.*, 2007b), two critical modifications were made to wild-type rabies to generate SADΔG(EnvA)-mCherry: first, the gene encoding rabies glycoprotein, was deleted from the genome and replaced with a gene encoding the fluorescent protein mCherry. This modification renders the virus incapable of infecting naive neurons and renders it incapable of

trans-synaptic spread (Mebatsion *et al.*, 1996), but does not impair the ability of the virus to replicate. The key concept at the heart of the tracing strategy is that the capacity to trans-synaptically spread can be temporally rescued by supplying the rabies glycoprotein *in trans* (Marshall *et al.*, 2010; Liu *et al.*, 2013; Takatoh *et al.*, 2013): the glycoprotein is incorporated as the virus self-assembles, enabling it to travel retrogradely to the next order of connected neurons. However, lacking the glycoprotein gene, the virus replicates within the second tier of the synaptic hierarchy but can spread no further. The second modification is that glycoprotein-deleted rabies is pseudotyped (coated) with an envelope protein (EnvA) derived from an avian sarcoma and leucosis virus. The cognate receptor for EnvA is the TVA receptor, which has no mammalian homologue. This modification enables targeted introduction of the rabies virus into cells that express TVA. By driving both the expression of TVA and the rabies glycoprotein on selected populations of neurons, the entry and trans-synaptic spread of SADΔG(EnvA)-mCherry can be restricted to targeted cell types.

In the current study we used a lentiviral vector (Lv-PRSx8-YTB) to introduce a cassette (YTB) that drives the expression of rabies glycoprotein, TVA, and YFP in RVLM catecholaminergic neurons. Expression of the gene cassette was controlled with the PRSx8 promoter, which has been widely used to target RVLM C1 neurons by other researchers (Abbott *et al.*, 2009a; Kanbar *et al.*, 2010; Marina *et al.*, 2011). We then infected TVA-expressing C1 neurons with SADΔG(EnvA)-mCherry and mapped the distribution of monosynaptically connected input neurons.

Methods

Animal experiments were approved by Macquarie University Animal Ethics Committee and adhered to the Australian code of practice for the care and use of animals for scientific purposes.

Vector preparation

A lentiviral vector that drives YFP along with TVA and rabies G, required for cell entry and trans-synaptic spread respectively, was manufactured by sub-cloning a plasmid that contains all three sequences, pCAG-YTB (Addgene 26721) into a lentiviral backbone under the control of the PRSx8 promoter (Chen *et al.*, 2010). Unpseudotyped SADΔG-mCherry and SADΔG(EnvA)-mCherry were produced and titrated as described by Osakada and Callaway (2013); the titers used for injections were 2×10^9 and 6.8×10^7 IU/ml respectively. SADΔG(EnvA)-mCherry purity was determined by infection of naïve HEK cells and determined to contain approximately 5.3×10^3 unpseudotyped virions per ml (i.e. <1 virion/100 nl injection). Vectors were stored in 3 µl aliquots at -80 °C until experiments. Injection of SADΔG(EnvA)-mCherry in the absence of YTB expression resulted in no labelling in two control experiments (Data not shown).

Vector injections

Adult male SD rats (250-350 g) were anaesthetised with intraperitoneal ketamine (75 mg/kg; Parnell Laboratories, Australia) mixed with medetomidine (0.75 mg/kg; Pfizer Animal Health, Australia). Prophylactic antibiotics (100 mg/kg Cephazolin sodium, i.m.; Mayne Pharma, Australia) and analgesia (2.5-10 mg/kg Carprofen, s.c.; Norbrook Pharmaceuticals, Australia) were administered. A satisfactory depth of anaesthesia was indicated by a lack of motor responses to firm pinching of the hind paws. Rats were shaved on the head and the left cheek, and the skin was cleaned three times with 10% povidone-iodine solution (Betadine™ Mayne Pharma, Australia). Core temperature was monitored by a rectal thermometer and maintained

at 36 - 38 °C by a heating pad. Anaesthetic depth was regularly monitored by checking motor and respiratory responses to noxious pinching of the hind paws. Supplementary anaesthetic (ketamine 7.5 mg/kg i.p.) was administered as required. Rats were positioned in a stereotaxic frame with the incisor bar adjusted 3.3 mm below the ear bar to achieve a head flat position. The left facial nerve was exposed. A midline incision was made along the skull, and a hole, approximately 4x4 mm, was made in the occipital bone 2 mm lateral to midline. The dura was cut with a 26G needle and cerebellum exposed. The caudal border of the facial nucleus was determined by mapping antidromic facial field potentials using a borosilicate pipette filled with viral vector in PBS (resistance <2 MΩ) as previously described (Brown & Guyenet, 1984). 50 nl Lv-PRSx8-YTB was microinjected 100-200 µm caudal to the caudal border of the facial nucleus at a depth equivalent to the most ventral depth where the evoked field potential was detected in the facial nucleus. The pipette was held in place for 5 minutes after the injection to prevent backflow of the vector and slowly withdrawn. Wounds were irrigated with sterile saline, covered with oxidized cellulose haemostat and closed with sutures or surgical clips. Anaesthesia was reversed with atipamazole (0.4 mg/kg, s.c.; Pfizer Animal Health, Australia). Animals were closely monitored until ambulatory and returned to the home cage with twice-daily monitoring and additional analgesia as required until fully recovered.

4 - 6 weeks after injection of Lv-PRSx8-YTB, rats were re-anaesthetized and treated with analgesia and prophylactic antibiotics as described above. The same surgical procedure was performed and 50 nl of SADΔG(EnvA)-mCherry was microinjected into the same location as Lv-PRSx8-YTB. Wounds were closed and anaesthesia reversed as described above. Rats were allowed to recover for 7 - 10 days before being sacrificed (Figure 3.2 A).

Perfusion and tissue collection

Rats were euthanized with sodium pentobarbitone (100 mg/kg i.p.) and immediately perfused with 400 ml heparinized 0.9% NaCl followed by 400 ml freshly prepared fixative solution (4% paraformaldehyde/0.1 M phosphate buffer; pH 7.4; Sigma-Aldrich, Australia). Brains were removed under RNase free conditions and further fixed overnight in the same solution.

The whole brain was mounted and coronal or sagittal brain sections (50 μ m) were cut on a vibrating microtome and collected in 4 pots in 0.01 M Tris-phosphate buffered saline (TPBS). Sections containing the RVLm region were selected for YFP and TH immunohistochemistry. Remaining sections from the same pot were mounted directly onto glass slides in order. Slices in the remaining pots were transferred to cryoprotectant solution (500 μ M polyvinylpyrrolidone, 76.7 mM Na₂HPO₄, 26.6 mM NaH₂PO₄, 876 mM sucrose, 5 mM ethylene glycol) for storage at - 20 °C or to phosphate buffered saline containing 0.1% Tween-20 (PBT; Sigma-Aldrich, Australia) for further immunohistochemistry.

Histology, in situ hybridization and immunohistochemistry

Synthesis of cRNA probe and *in situ* hybridization were performed as previously described (Parker *et al.*, 2013; Le *et al.*, 2016). Detailed protocols are in the Methods section in Chapter 3.

For fluorescent immunohistochemistry, brain sections were washed in PBT for 3 x 15 min and incubated in 0.01 M phosphate buffered saline containing 2% bovine serum albumin and 0.2% TritonX-100 or Tween-20 for 1 h at room temperature. Primary antibodies (Table 2.1) were added to the blocking buffer and sections were incubated for 48 h at 4 °C. Sections were washed in TPBS (3 x 30 min) and incubated in IgG secondary antibodies for 12 h at 4 °C. Processed sections were washed again in TPBS (3 x 30 min) before being mounted in serial order on glass slides and coverslipped with Dako fluorescence mounting medium (Dako, #S302380-2) for imaging.

Table 4.1 Antibodies

<i>Antibody name</i>	Immunogen	Manufacturer details	Concentration
Primary antibodies			
<i>Guinea pig anti-neurokinin 1 receptor (NK1R)</i>	C-terminus amino acid sequence 393–407 (KTMTESSSFYSNML A) of synthetic rat NK1R peptide	Millipore Cat# AB15810 Lot# LV1587443 RRID: AB_992894 Polyclonal	1:1,000
<i>Rabbit anti-NK1R</i>	C-terminus amino acid sequence 393–407 (KTMTESSSFYSNML A) of synthetic rat NK1R peptide	Sigma-Aldrich Cat# S8305 Lot# 67K4885 RRID: AB_261562 Polyclonal	1:5,000
<i>Mouse anti-tyrosine hydroxylase (TH)</i>	Rat tyrosine hydroxylase N-terminal region (approx. aa 9–16)	Sigma-Aldrich Cat# T1299 RRID: AB_477560 Monoclonal	1:8,000
<i>Sheep anti-digoxigenin</i>	Digoxigenin, whole	Roche Applied Science Cat# 11093274910 RRID: AB_514497 Polyclonal	1:1,000
Secondary antibodies			
<i>Cy3- AffiniPure donkey antigoat IgG (H1L)</i>	Whole molecule goat IgG	Jackson ImmunoResearch Laboratories,INC Cat# 705-165-147 Lot# 68839 RRID: AB_2307351 Polyclonal	1:250
<i>Alexa Fluor 647-AffiniPure donkey antirabbit IgG (H1L)</i>	Whole molecule rabbit IgG	Jackson ImmunoResearch Laboratories,INC Cat# 711-605-152 Lot# 105115 RRID: AB_2492288 Polyclonal	1:250
<i>Alexa Fluor 647 donkey antirabbit IgG (H1L)</i>	Rabbit, IgG heavy & light chains	Life Technologies Cat# A31573 Lot# 1322326 RRID: AB_10561706 Polyclonal	1:250
<i>Alexa Fluor 488-AffiniPure donkey antiguinea pig IgG (H1L)</i>	Whole molecule guinea pig IgG	Jackson ImmunoResearch Laboratories,INC Cat# 706-545-148 Lot# 161406 RRID: AB_2340472 Polyclonal	1:250
<i>Alexa Fluor 647 goat antiguinea pig IgG (H1L)</i>	Domestic guinea pig, IgG heavy & light chains	Life Technologies Cat# A21450 Lot# 1235826 RRID: AB_10564076 Polyclonal	1:250

<i>Alexa Fluor 488 donkey antimouse IgG (H1L)</i>	Mouse, IgG heavy & light chains	Life Technologies Cat# A21202 RRID: AB_10049285 Polyclonal	1:250
---	---------------------------------	---	-------

Imaging

Slices from pot 1 with rabies-labelled neurons were imaged under epifluorescence (Zeiss AxioImager Z2 microscope, 10x/0.30 NA M27 objective lens running ZEN 2012). Neurons containing both YFP and mCherry were categorized as starter neurons and further sub-categorized as TH-positive (C1 starter neurons) or -negative (non-C1 starter neurons) according to their immunoreactivity to tyrosine hydroxylase.

Confocal images were taken using a Leica TCS SP5X confocal microscope (Leica Microsystems Pty Ltd, North Ryde, NSW, Australia) and acquired using Leica Application Suite Advanced Fluorescence software (LAS:AF, Leica, Germany). Images were optimised using ImageJ and FIJI plugin package (NIH, Bethesda, Maryland, USA) and figures prepared using CorelDraw x4.

Data analysis

Image annotation

Images containing starter or input neurons were manually annotated using Zen software (Figure 4.1 A). Metadata containing the x,y, pixel coordinates of each annotated neuron and the height and width of the image were extracted using ImageJ/FIJI package (NIH, Bethesda, Maryland, USA) and organised in tables using Microsoft Excel.

Image alignment and anchoring

2D histological images were manually aligned with an interactive MRI whole brain dataset obtained from a male Sprague Dawley rat (Papp *et al.*, 2014) as previously described (Dempsey, 2016). An overview of image alignment workflow is provided in Figure 4.1. In brief, micrographs of brain sections were contrast-optimised for differentiation of grey and white matter and uploaded to navigator-3 (N3) platform in virtual tissue blocks. Image alignment and anchoring was achieved using a beta version of the AlignNII tool embedded in N3. Histological sections were aligned to the corresponding MRI image by manually adjusting the angles and

scales of the MRI virtual plane. Once each image was optimally aligned to its MRI equivalent the image was considered ‘anchored’; geometric vectors corresponding to the rostrocaudal level of the image origin, deviation from the vertical and horizontal planes, scaling and rotation were calculated by the anchoring tool in the N3 platform and exported as metadata. With this information the position of any point in a histological image could be converted to 3-dimensional Waxholm co-ordinates in Microsoft Excel. Waxholm co-ordinates are by convention presented in the xyz format (lateral, rostrocaudal, dorsoventral) with a voxel resolution of 39 μm . The interested reader is directed towards CutNii, a freely downloadable explorer and custom-angle slicer for the Waxholm dataset (Csucs & Bjaalie, 2015), which is similar to the N3 tool used for image alignment (although it does not allow overlay or anchoring of histological images).

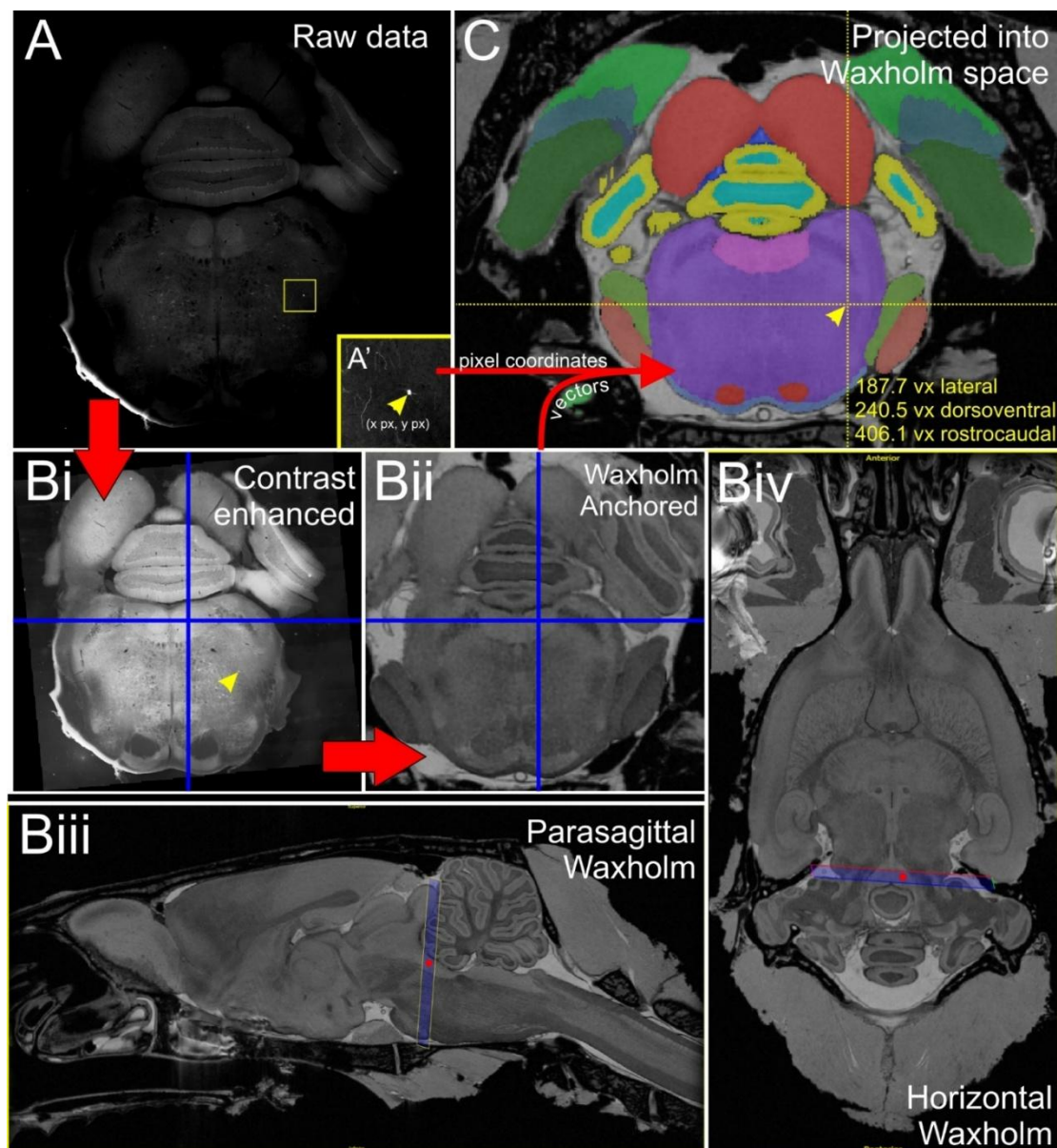


Figure 4.1 Anchoring workflow. A. Original coronal epifluorescence image showing the location of a single rabies-labelled input neuron (yellow box, inset in A'). Following manual annotation, the pixel coordinates of the neuron were exported to a spreadsheet and the image contrast adjusted for optimal visualization of anatomical landmarks (Bi). The image was then aligned to a corresponding section plane through the Waxholm atlas template (Bii) using a beta version of an image alignment/anchoring tool embedded in the Navigator-3 system. The anchoring tool allowed accurate positioning of the image plane in the MRI-derived atlas template. The orientation of the plane of the image is close to coronal, as shown in the blue frames in Biii and Biv. (The parasagittal plane through the atlas template shown in Biii corresponds to the vertical blue line in Bi and Bii, whereas the horizontal plane in Biv corresponds to the horizontal blue lines in Bi and Bii. The red dots in Biii and Biv represent the intersections with the horizontal and parasagittal planes, respectively. Anchoring vectors generated by Navigator-3 were then used to translate the pixel co-ordinates of annotated neurons into xyz Waxholm coordinates and integrated into the Waxholm segmentation model (C).

Volumetric brain modelling

The segmentation model of the Waxholm Sprague Dawley dataset was downloaded from the International Neuroinformatics Coordinating Facility Software Center (Papp et al., 2015) and imported into Imaris volumetric imaging software (Version 8.1, Bitplane AG, Switzerland) following conversion to the Biorad format in ImageJ. Each segmented area was individually rendered using the Imaris 'contour surface' function, resulting in a surface-rendered model that incorporates all of the regions demarcated in Waxholm space. Tabulated Waxholm coordinates of input, non-C1 starter, and C1 starter neurons were then imported using a Python script ('CreateSpotsFromFile', <http://open.bitplane.com/tabid/235/Default.aspx?id=70>), resulting in a 3d model of the Waxholm brain populated with points corresponding to identified neurons. Another script was then used to automatically quantify the number of input neurons that lay within each segmented region ('Spots split into surface objects', <http://open.bitplane.com/tabid/235/Default.aspx?id=19>).

Segmentation of the RVLM in Waxholm space

The Waxholm segmentation model does not differentiate brainstem subnuclei. We used the locations of bulbospinal TH-immunoreactive RVLM neurons to define the anatomical boundaries of the RVLM in Waxholm space, as previously described (Dempsey, 2016). In brief, data were obtained from six rats in which neurons projecting to the T2 and or T10 spinal segments were labelled using a recombinant herpes virus with a retrograde tropism, HSV-hCMV-GFP or HSV-hCMV-mCherry. Vector injections were performed under ketamine-medetomidine anaesthesia as described above and directed towards the intermediolateral column (IML) of the spinal cord. 4 – 7 days later rats were euthanized and tissue processed and imaged as described above. TH-positive bulbospinal RVLM neurons ($n = 273$) were annotated and anchored in Waxholm space. The lateral co-ordinates of all neurons were represented as being on both sides of the brainstem for segmentation; two-dimensional contour maps indicating the density of labelling were then generated for each dorsoventral level using the

Plotly visualization tool (<https://plot.ly>, 10 voxel resolution). Contours enclosing pixels that contained >2 neurons/10 pixel radius in the horizontal plane were converted to an image stack, imported the virtual Waxholm rat brain using Imaris, and surface rendered.

The geometric epicenter of the region containing C1 bulbospinal neurons was located at Waxholm coordinates 198 lateral, 313 rostrocaudal, 182 dorsoventral, corresponding to a position 1.78 mm lateral to the midline, 117 μ m rostral to the caudal pole of the facial nucleus, and 339 μ m dorsal to the ventral surface of the medulla immediately beneath the epicenter. As indicated by the 5th and 95th percentiles of this dataset, RVLM sympathetic premotor neurons spanned Waxholm co-ordinates 185 - 210 lateral (2.28 – 1.31 mm lateral to midline), 301 – 324 rostrocaudal (351 μ m caudal to 546 μ m rostral to caudal pole of the facial nucleus) and 178 – 193 dorsoventral (117 – 702 μ m from the ventral surface of the brainstem). The RVLM segmented model generated from these co-ordinates is density-encoded, and therefore differs slightly from the geometric boundaries indicated above. Our segmentation encloses a dorsoventrally flattened ovoid in which the long axis runs medial in more rostral sections and spans Waxholm coordinates 176 – 218 lateral (2.6 – 1 mm lateral to midline), 287 - 327 rostrocaudal (900 μ m caudal to 663 μ m rostral to caudal pole of the facial nucleus) and 174 – 198 dorsoventral (39 μ m ventral – 897 μ m from the ventral surface of the brainstem). This region contained 86% of TH-positive bulbospinal neurons (n = 236).

Segmentation of the facial nucleus, nucleus ambiguus, Bötzing and preBötzing Complex in Waxholm space

Surface objects were created using Imaris contour drawing tools. The facial nucleus and NA were identified directly from the MRI images (rostrocaudal co-ordinates 318 - 350, and 304 - 318 respectively). BötC and preBötC regions were defined as longitudinal cylinders (diameter = 13.4 voxel, equivalent to 522 μ m) situated directly beneath the NA. The segmentation of the BötC was created between 303 – 318 voxels rostrocaudally (spaning ~585 μ m); the preBötC

segmentation was created immediately caudal to the BötC from 291 – 303 voxels (spanning 468 μm) (Le *et al.*, 2016).

Results

Starter neurons are located within the rostral RVLM and are immunoreactive to tyrosine hydroxylase.

Neurons co-expressing YFP (from Lv-PRSx8-YTB) and mCherry (from SADΔG(EnvA)-mCherry) were identified as starter neurons, of which $46.9 \pm 6.7\%$ ($n = 5$) were catecholaminergic (TH-ir, Figure 4.2 B). Lightly labelled TH-immunoreactive starter neurons were under-represented when imaged under 10x epifluorescence magnification. Reimaging of five sections (from five rats) containing starter neurons under higher power (20x objective, Confocal Leica TCS SP5X) indicated that our standard imaging underestimated TH-immunoreactive starter neurons by an average of 12% (epi: $46.2 \pm 4.6\%$ vs confocal: $58.2 \pm 7.8\%$ ($n = 5$)). Starter neurons were confined to within $\sim 600 \mu\text{m}$ of the caudal pole of the facial motor nucleus immediately ventral to the BötC (Figure 4.2 D, E), corresponding to the rostral RVLM pressor region (Goodchild & Moon, 2009). 495 starter neurons (99 (72 – 138) [mean (range)] per animal) were identified counting every fourth section from 5 animals. When imported into the Waxholm brain atlas, 86% (61 - 96%) of starter neurons and 90% (58% - 100%) of C1 starter neurons fell into the RVLM segmentation (Dempsey, 2016) (Figure 4.2 C, D). Approximately 10% of the non-C1 starter neurons lay in the region immediately ventral and caudal to the caudal pole of the facial nucleus and therefore overlapped with the caudal region of the retrotrapezoid nucleus (RTN) (Figure 4.3). Occasionally non-C1 starter neurons were found in the marginal layer of the ventral medullary surface (Figure 4.3 A'), corresponding to the location of chemosensitive RTN neurons (Mulkey *et al.*, 2004), but such examples were rare.

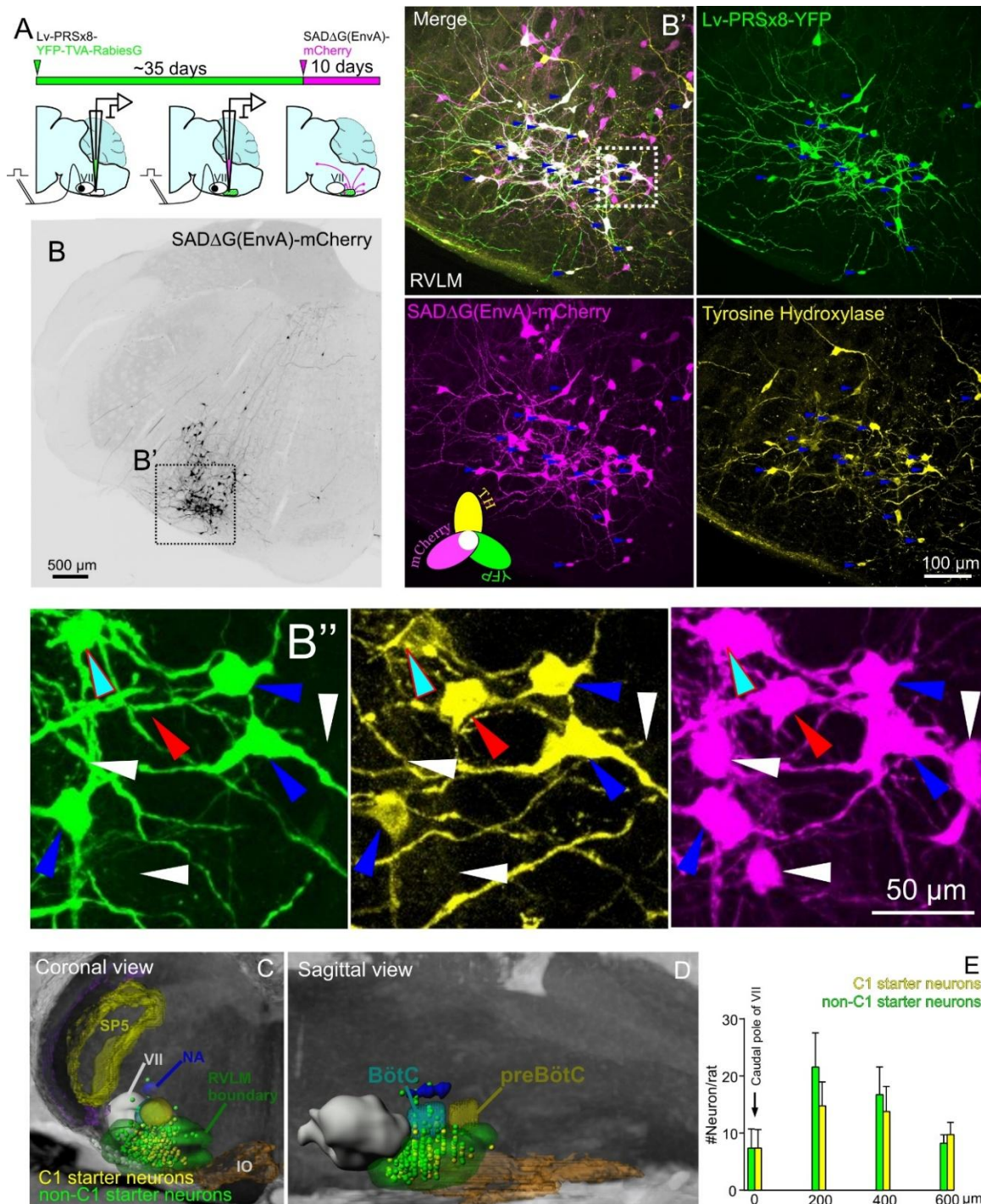


Figure 4.2 Distribution and phenotype of starter neurons. A. Experimental strategy: Lv-PRSx8-YTB was injected at RVLM, driving expression of YFP, TVA, and rabies glycoprotein. SADΔG(EnvA)-mCherry was subsequently injected into the same location. B. Coronal brainstem section at the level of the RVLM with mCherry labelled neurons. B'. Confocal images of region boxed in B with magnified examples (B'') showing immunoreactivity to TH and YFP. C1 starter neurons are defined by colocalization of YFP, mCherry, and TH (blue arrowheads). Non-C1 starter neurons are defined by colocalization of YFP and mCherry but not TH (cyan arrowhead). Input neurons are defined by expression of mCherry only (white arrowheads); red arrowhead indicates position of a rare TH-immunoreactive input neuron. Distribution of C1 starter neurons from 5 animals plotted in Waxholm space, shown from coronal (C) and sagittal perspectives (D) and boundaries of the following anatomical regions: facial nucleus (VII), nucleus ambiguus (NA), Bötzing complex (Böt), preBötzing complex (preBöt) and RVLM. E. Rostrocaudal distribution of starter neurons per rat (n = 5) with respect to the caudal pole of the facial nucleus, bin size = 200μm.

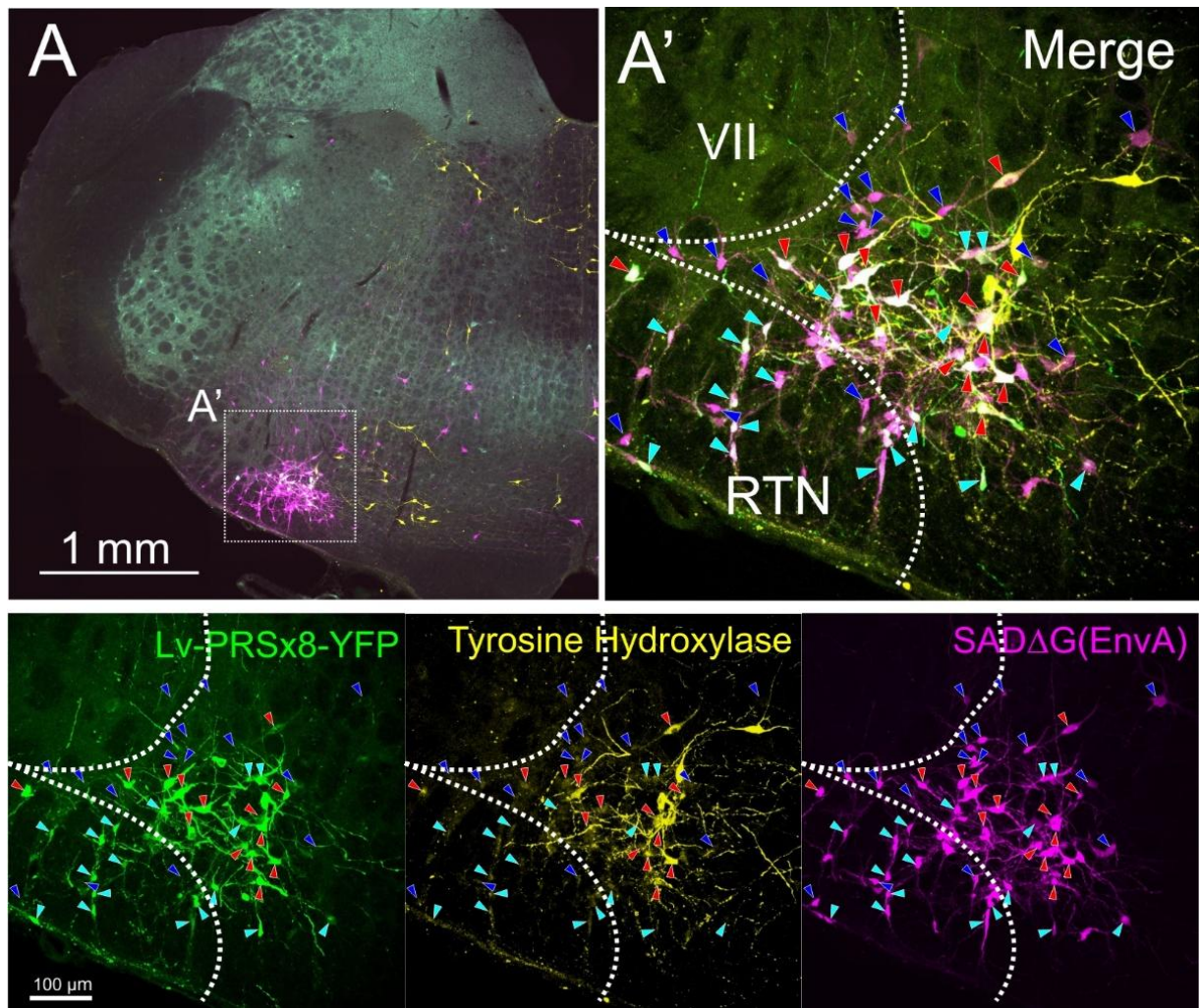


Figure 4.3 Starter and input neurons occasionally extended into the retrotrapezoid nucleus (RTN). **A.** Coronal brainstem section at the level of the RTN processed for immunoreactivity to TH and YFP. Magnified confocal images (**A'**) with examples of non-C1 starter neurons (cyan head arrows), C1 starter neurons (red head arrows), and input neurons (blue head arrows). **VII:** facial nucleus.

The majority of inputs to the RVLM C1 neurons arise from the medulla

3728 input neurons (746 (264 – 1928) per animal) were identified from 5 animals that were analysed in detail. The ratio of input : starter neurons was 7.1 (3.2 – 16.4). The overall distribution of input neurons was consistent between animals (Figure 4.4 F) . Neurons were seen from the optic chiasm (Bregma -0.84 mm) to the most caudal pole of the inferior olive (Bregma -14.6mm), with a large majority of input neurons located within the brainstem (Figure 4.4 A). 77% (67% - 86%) of input neurons were located ipsilateral to the injection site (Figure 4.4 C), with 85% (78% - 96%) lying caudal to the facial nerve tract (Bregma -10.08 mm, Figure 4.4 D, E). Input neurons were also encountered in the cervical and thoracic spinal cord, but these data were not quantified in the current dataset.

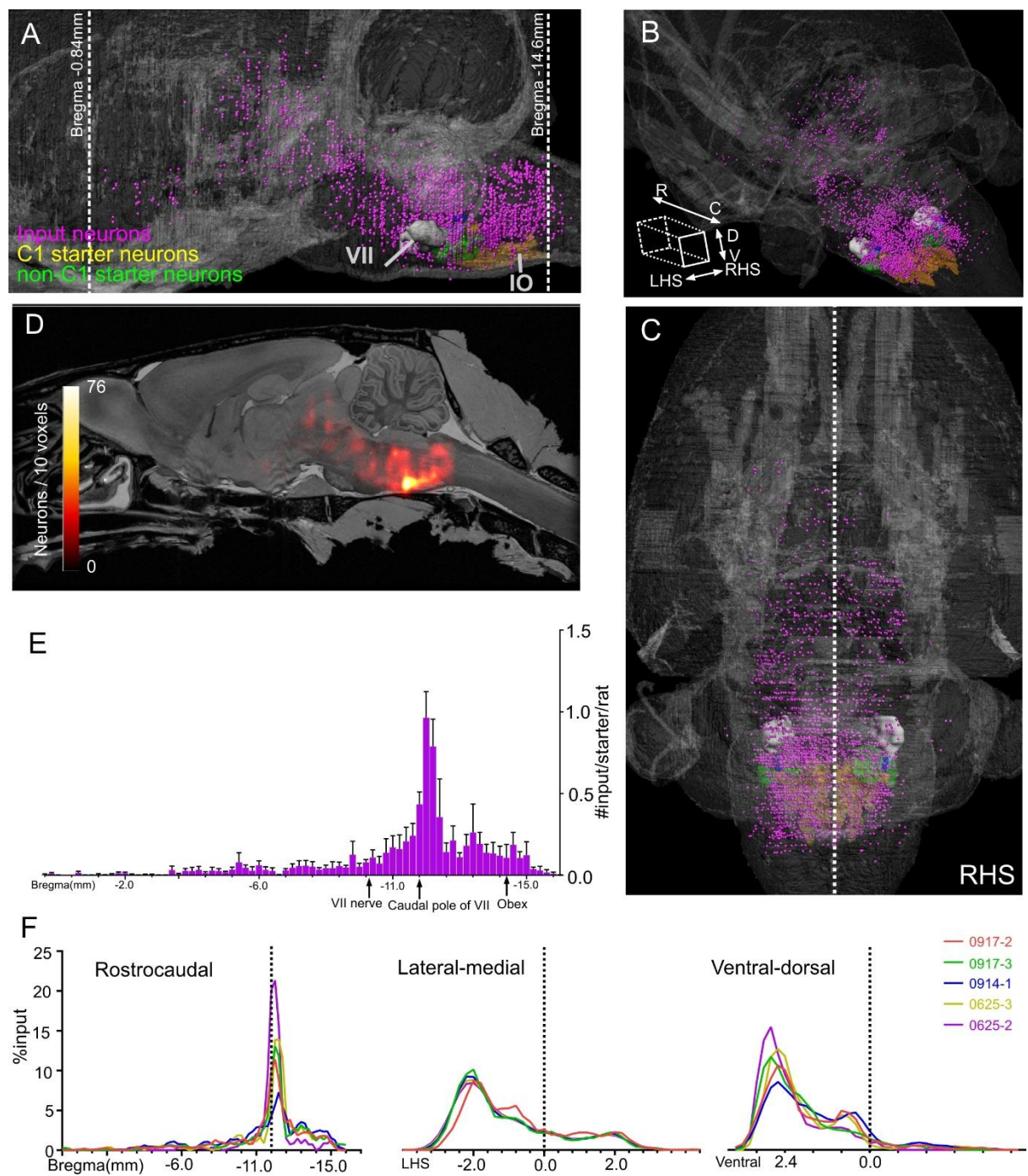


Figure 4.4 Distribution of monosynaptic input neurons. Input neurons were plotted in Waxholm space in sagittal view (A), overview (B), and birds-eye view (C), Dotted line in A indicating the Bregma level of optic chiasm and the caudal pole of the inferior olive (IO) respectively. Dotted line in C indicating midline. VII: facial nucleus. D. Heat map showing input neuron density superimposed on sagittal Waxholm MRI image. Scale indicates number of neurons per 10 voxels. E. Rostrocaudal distribution of mean number of input neurons per starter neuron per rat with SEM (n = 5 rats). Bin size = 200μm. F. Normalised input densities for individual experiments, dotted lines in each panel indicating the caudal pole of facial nucleus, midline, and the horizontal level of obex respectively.

Input neurons from the RVLM, the BötC, and the preBötC

Quantification was performed using Waxholm rat brain segmentations described above. Within the medulla, in contrast to our expectation of distinct clusters of inputs, rabies labelled neurons diffusely spread bilaterally and concentrated into longitudinal columns that extended across multiple medullary subnuclei. On average, $89.47 \pm 2.08\%$ ($n = 5$) of inputs were located in the brainstem with a high density of inputs within the RVLM, BötC, preBötC, and nucleus ambiguus (Table 2.2). The ipsilateral RVLM itself was a notable hot-spot of inputs (Figure 4.4 D), containing 629 input neurons. The inputs from the contralateral RVLM were consistent, but significantly lower than the ipsilateral side (contralateral: 0.10 ± 0.04 vs. ipsilateral: 1.24 ± 0.23 (#inputs per starter) respectively, $P = 0.0037$, $t = 6.099$, $df = 4$, $n = 5$, paired t-test). We rarely observed input neurons immunoreactive to TH, a rare example shown in Figure 4.2 B''.

Brain Region/Nuclei	# input neurons (n = 5rats)	Input percentage (regional inputs/total inputs %, mean \pm SEM)	Volume of region (Kvoxels)	Normalised input density (regional inputs/starter/M voxels, mean \pm SEM)	
Forebrain	25	0.56 ± 0.17			
Thalamus	15	0.34 ± 0.12	1390	0.02 ± 0.01	
Basal Forebrain region	10	0.22 ± 0.13	1250	0.01 ± 0.01	
Midbrain	154	2.94 ± 0.97			
Hypothalamus	15	0.26 ± 0.13	388	0.07 ± 0.04	
Periaqueductal Gray	63	1.25 ± 0.41	269	0.44 ± 0.25	
Superior Colliculus	67	1.28 ± 0.46	489.8	0.26 ± 0.15	
Inferior Colliculus	5	0.11 ± 0.06	451	0.02 ± 0.01	
Substantia Nigra	4	0.04 ± 0.04	113.6	0.06 ± 0.06	
Brainstem	3231	89.47 ± 2.08			
Pyramidal tract/corticofugal pathway	7	0.09 ± 0.06	461	0.03 ± 0.02	
Periventricular Grey	128	2.98 ± 0.84	226	1.11 ± 0.56	
Inferior Olive	6	0.12 ± 0.06	33.1	0.35 ± 0.17	
Spinal Trigeminal Nucleus	59	1.43 ± 0.60	249	0.42 ± 0.16	
Spinal Trigeminal Tract	4	0.1 ± 0.07	1551	0	
Facial nucleus/perifacial region	11	0.27 ± 0.16	30.2	0.63 ± 0.26	
Nucleus ambiguus	7	0.4 ± 0.37	0.495	34.91 ± 27.17	
Bötzinger complex	134	5.42 ± 1.77	3.041	92.94 ± 18.74	
preBötzinger complex	41	1.17 ± 0.47	2.466	35.45 ± 16.52	
RVLM	681	22.57 ± 4.14	45.6	29.38 ± 5.85	
Medulla (not specified)	2153	54.91 ± 2.85	3343.4	1.26 ± 0.46	
Other not specified regions	318	7.02 ± 1.12			
Whole brain	3728		40600	0.18 ± 0.06	

Table 4.2 Input neurons segregated by brain structures in Waxholm rat brain atlas

Input neurons were encountered bilaterally in the preBötC and BötC (Figure 4.6 E&F). The BötC contained the highest concentration of inputs of any region quantified (Table 4.2: 92.94 ± 18.74 inputs per starter neurons per million voxels) with a prominent ipsilateral bias (0.27 ± 0.05 vs. 0.01 ± 0.01 (# inputs per starter) respectively, $P = 0.0078$, $t = 4.943$, $df = 4$, $n = 5$, paired t-test, Figure 4.5 A'). Some BötC input neurons expressed mRNA for glycine transporter 2 (GlyT2, Figure 4.5 B), but the GlyT2 positive neurons mostly lay outside the classical BötC and were instead closer to the overlapping border between the BötC and RVLM. The absolute numbers of input neurons seen in the preBötC were relatively low compared to the numbers in the BötC (8.2 ± 3.7 vs. 26.8 ± 6.3 , $n=5$, bilateral), with no statistically significant difference between the number of inputs arising from each side (left: 0.06 ± 0.02 vs. right: 0.03 ± 0.02 (# inputs per starter) respectively, $P = 0.0937$, $t = 2.190$, $df = 4$, $n = 5$, paired t-test). $5.5 \pm 2.9\%$ (3 out of 72 neurons from 10 sections from 5 rats) of preBötC input neurons were immunoreactive for neurokinin receptor-1 (NK1R, Figure 4.5 C), a putative respiratory function marker (Guyenet & Wang, 2001). A small number of input neurons were seen in the nucleus ambiguus; the exceptionally high input density seen in NA from Table 2.2 was due to the small volume of the region. Low numbers of input neurons were seen from the RTN region, however, due to overlapping with rostral C1 region, input neurons were partially intermingled with non-C1 starter neurons (Figure 4.3 A').

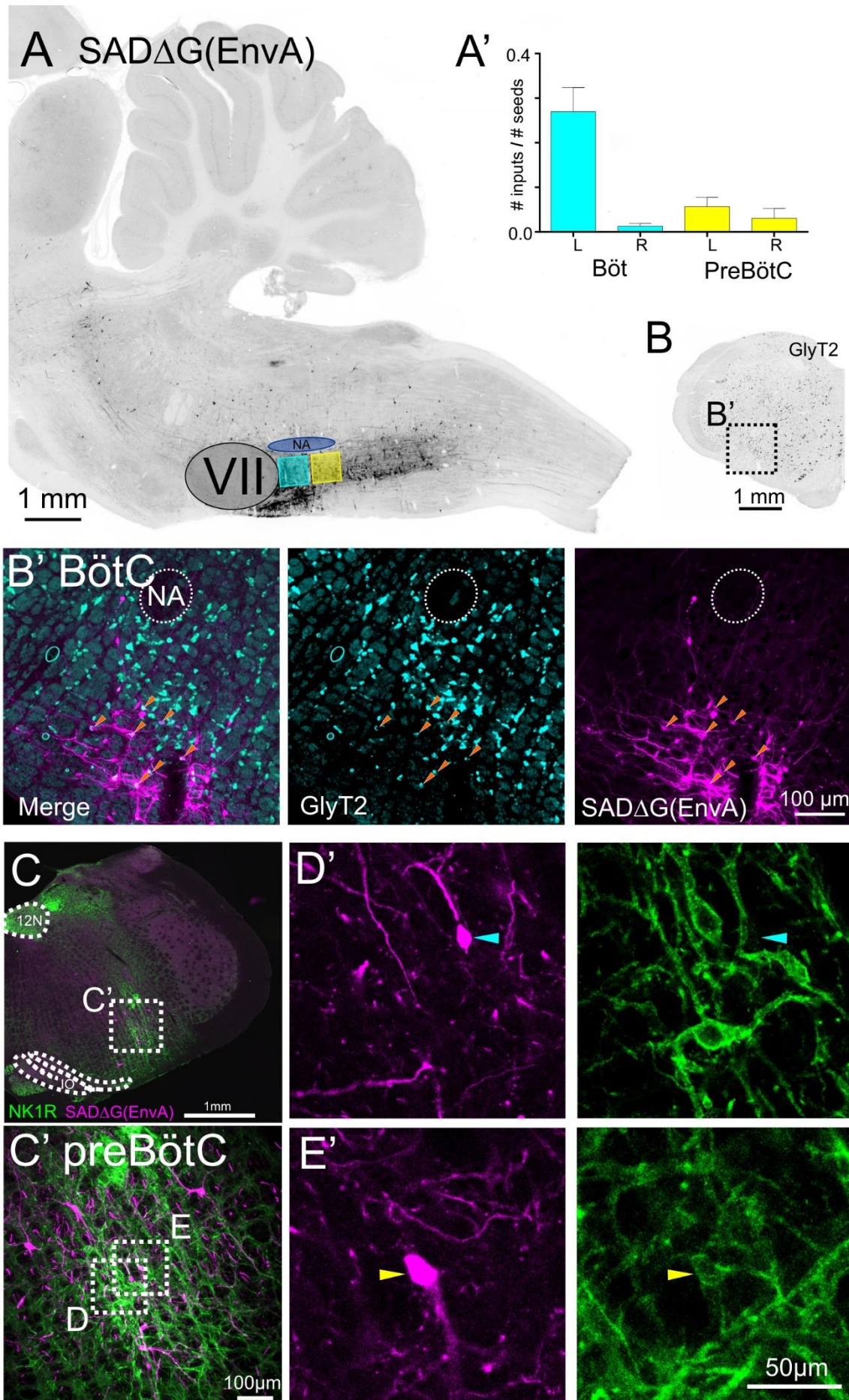


Figure 4.5 Neurochemical phenotypes of input neurons in the BötC & preBötC. A. Inverted epifluorescence image of input neurons in the pons and medulla. Cyan and yellow box illustrating BötC and preBötC respectively. Inset (A') the number of input neurons (normalised against the number of starter neurons per rat, n = 5) lying within the BötC and preBötC Waxholm segmentations. B. Low power photomicrograph of *in situ* hybridization illustrating expression of glycine transport 2 (Gly T2) mRNA in the BötC region. Inset (B') highlights input neurons that contain Gly T2 mRNA (orange arrow heads). C. Confocal image of neurokinin 1 receptor (NK1R)/mCherry labelling in the preBötC with magnified region (C',D, E) showing examples of NK1R-negative (D', cyan arrowhead) and NK1R-immunoreactive (E', yellow arrowhead) preBötC input neurons. VII: facial nucleus, NA: nucleus ambiguus, 12N: hypoglossal nucleus.

Input neurons from other medullary nuclei

Clusters of input neurons were seen in the caudal NTS, mainly in the commissural and dorsolateral parts (Figure 4.6 A - C, A', B', C'). Input neurons were encountered in the VRG and A1 regions with neurons more concentrated in the caudal part of those regions (Figure 4.6 A – D, A'', B''). High input density was observed in the caudal C1 and CVLM regions (Figure 4.6 C, D, C'', D''). A cluster of neurons with small somata were consistently seen at the ventral boundary of the nucleus prepositus and midline raphe (Figure 4.6 G). However, due to the incomplete segmentation available in the Waxholm space, no quantification has been performed for these regions.

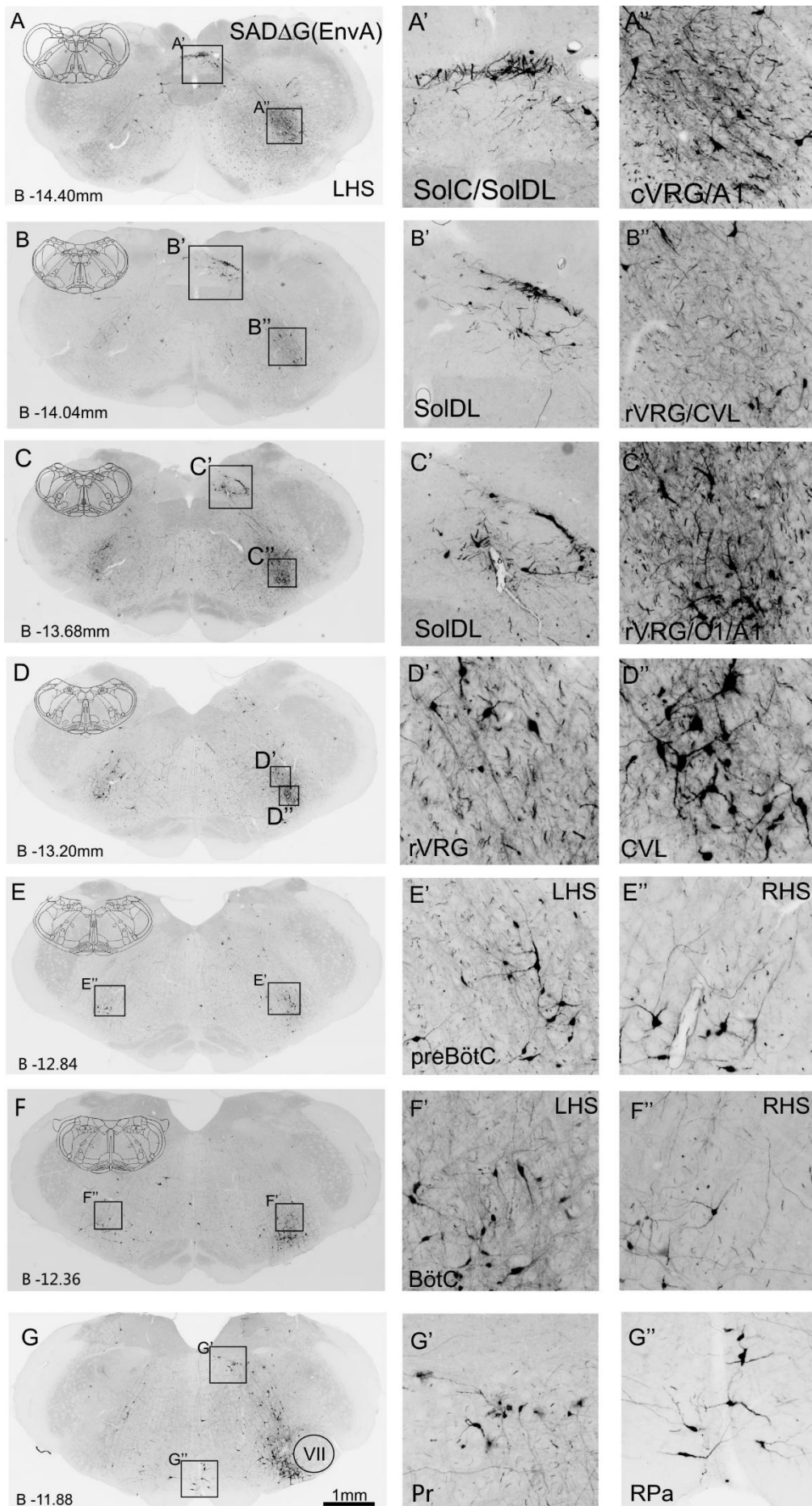


Figure 4.6 Medullary input neurons to RVLM C1 neurons. Inverted epifluorescence images with magnified insets of boxed regions illustrating monosynaptic input neurons in the commissural (SolC: A) and dorsolateral (SolDL: A - C) nucleus of the solitary tract, caudal ventral respiratory group (cVRG: A), rostral respiratory group (rVRG: B - D), A1 region (A - C), caudal C1 group (C), caudal ventrolateral medulla (CVL: B, D), preBötzinger complex (preBötC: E), Bötzing complex (BötC: F), the prepositus nucleus (Pr: G) and the midline raphe magnus nucleus (RPa: G). LHS: left hand side.

Input neurons from the supramedullary regions

Supramedullary input neurons were diffuse and relatively sparse, with the majority of neurons located in the midbrain. The pontine respiratory group provided a moderate level of inputs, with most seen from the Kölliker-Fuse nucleus (KF, Figure 4.7 F & G). In the midbrain, inputs were dispersed across the superior and inferior colliculi with most found in the superior colliculus, and in the periaqueductal gray. Although small in number, we consistently encountered clusters of neurons in the paraventricular hypothalamic nucleus (PVN, Figure 4.7 A & B) and the dorsomedial hypothalamic nucleus (DMH, Figure 4.7 A & C). In addition, we consistently observed a cluster of input neurons in the region corresponding to the contralateral retrorubral nucleus (RR, Figure 4.7 D, E).

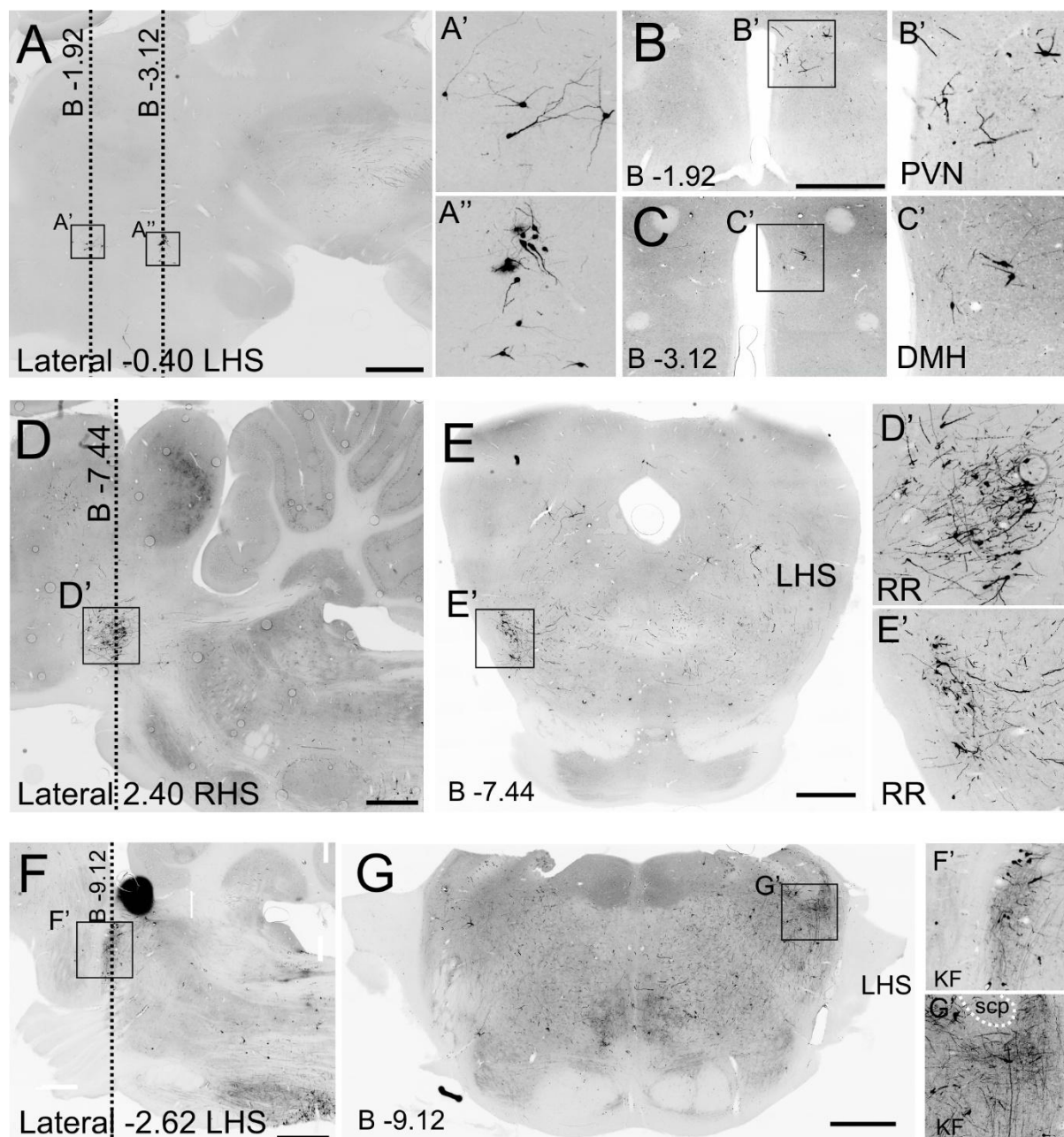


Figure 4.7 Supramedullary input neurons to RVLM C1 neurons. **A.** Sagittal inverted epifluorescence photomicrograph with insets (**A'**, **A''**) indicating input neurons from the paraventricular hypothalamic nucleus (PVN) and the dorsomedial hypothalamic nucleus (DMH). Coronal sections (**B** & **C**) at the Bregma levels indicated in **A** illustrate input neurons from the same regions. Input neurons from the retrorubral nucleus (RR) are illustrated in sagittal (**D**) and coronal (**E**) sections with enlarged insets (**D'**, **E'**). **F** & **G.** Sagittal and coronal sections illustrating input neurons from the Kölliker-Fuse nucleus (KF). scp: superior cerebellar peduncle. Scale bar = 1 mm.

Discussion

In the current study we used a two-step restricted viral tracing technique to generate brain wide maps of neurons that provide monosynaptic input to RVLM C1 neurons, with a focus on revealing the inputs from respiratory-related nuclei. The data reveal inputs from multiple brain regions that play roles in the generation of central respiratory drive; the ipsilateral BötC, bilateral preBötC, bilateral VRG, and the ipsilateral KF. In addition, we observed inputs arising from brain nuclei long-associated with the generation and modulation of sympathetic nerve activity (NTS, CVLM, VPN, DMH), and observed clusters of inputs from two brain structures not conventionally associated with sympathetic functions, the retrorubal and prepositus nuclei, as well as substantial (~ 20% of the total input) numbers of neurons arising from within the RVLM itself. Monosynaptic connections from respiratory nuclei, particularly the BötC and the preBötC, may form the core of the neural circuitry that underlies the central interaction between respiratory and sympathetic networks. The functional implication of the inputs identified in the current study and their relationship with conventional tracing data is discussed below.

Inputs from respiratory related nuclei

Previous electrophysiological studies showed that RVLM C1 neurons are likely to be the converging site of respiratory-sympathetic coupling (Marina *et al.*, 2011; Moraes *et al.*, 2013). Conventional tracing studies have previously demonstrated the existence of inputs to the RVLM region from respiratory-related nuclei in distant brain regions such as the LPB, KF and cVRG (Horiuchi *et al.*, 1999; Len & Chan, 1999; Bowman *et al.*, 2013), which may or may not target RVLM C1 neurons, but direct inputs from the adjacent ventral respiratory column have not previously been convincingly demonstrated. In the current study we observed consistent inputs from the region immediately ventral to the nucleus ambiguus, corresponding to the VRC, which

contains the key components for respiratory rhythm generation and phase transition (Smith *et al.*, 2012).

preBötC

The respiratory modulation of SNA is dependent on glutamatergic transmission in the RVLM (Guyenet *et al.*, 1990; Miyawaki *et al.*, 2002), suggesting that phasic excitatory input to RVLM sympathetic premotor neurons from a population of respiratory interneurons underlies respiratory-sympathetic coupling. Although the pattern of respiratory modulation in RVLM sympathetic premotor neurons is diverse (Haselton & Guyenet, 1989a; Miyawaki *et al.*, 1995), a subpopulation of C1 neurons specifically exhibit inspiratory-locked excitation, suggestive of excitatory input during the inspiratory phase of the respiratory cycle (Moraes *et al.*, 2013; Moraes *et al.*, 2014).

Many inspiratory interneurons reside in the preBötC (Smith *et al.*, 1991; Sun *et al.*, 1998), of which many are thought to be glutamatergic (Stornetta *et al.*, 2003a; Gray *et al.*, 2010; Koizumi *et al.*, 2013) and about 30% of which are NK1R immunoreactive (Guyenet & Wang, 2001). In the current study, monosynaptic input neurons were frequently encountered in the preBötC, including many neurons that were intermingled with NK1R neurons, a widely used regional marker of the preBötC (Wang *et al.*, 2001; Stornetta *et al.*, 2003a; Gray *et al.*, 2010). We also positively identified NK1R in a small number of input preBötC input neurons, directly supporting a potential role for preBötC inspiratory neuron inputs in the generation of respiratory-sympathetic drives. However, preBötC inspiratory neurons are neurochemically heterogeneous, containing inhibitory neurotransmitters such as glycine and GABA in addition to glutamate (Koizumi *et al.*, 2013), and so the input neurons we observed in the preBötC may also include inhibitory preBöt neurons in addition to the presumably excitatory NK1R neurons we identified. The relatively minor input from identified NK1R neurons suggest a limited role of NK1R expressing preBötC neurons in generating respiratory-sympathetic interaction, in

contrast to the supposedly important role these neurons play in central rhythm generation (Gray *et al.*, 1999; Gray *et al.*, 2001; although see Tupal *et al.*, 2014).

BötC

BötC neurons are thought to be responsible for phase transition from inspiration to expiration (Smith *et al.*, 2009), and have extensive connections with other respiratory neurons (Jiang & Lipski, 1990; Bryant *et al.*, 1993; Duffin & Douse, 1993; Tian *et al.*, 1999). Glycine has been identified as the neurotransmitter used by subpopulations of E-Aug and Post-I neurons (Ezure *et al.*, 2003a), and is often used as a chemical marker for BötC expiratory neurons (Stornetta, 2008). One previous study found that over 50% of electrophysiologically characterised BötC neurons project towards the RVLM and have axonal varicosities that appose RVLM bulbospinal neurons (Sun *et al.*, 1997), suggesting a potential role for BötC neurons in the generation of respiratory-sympathetic coupling. Baekey *et al.* (2010) proposed direct involvement of BötC neurons in the respiratory modulation of the SNA, based on electrophysiological experiments and sophisticated computational modelling.

However, although we found extensive evidence of inputs within the BötC, the majority of these neurons did not express GlyT2. The small number of labelled glycinergic neurons was mostly located in the overlapping area between the RVLM and BötC. Supported by the finding that blockade of glycinergic transmission in the RVLM has no measurable effect on the amplitude of respiratory-sympathetic coupling (Guyenet *et al.*, 1990), we suggest that glycinergic BötC neurons are unlikely to be the major respiratory source of bursting activities in the SNA. The phenotype of the BötC input neurons seen in the current study remains unidentified, we suspect a proportion of these could be GABAergic (Ellenberger, 1999).

RTN/pFRG

Neurons in the RTN/pFRG region play an important role in central CO₂ sensing and are proposed as likely central chemoreceptors (Guyenet *et al.*, 2010). The function of the RTN in

regulating respiratory and cardiovascular outflows has been recently reviewed in detail (Guyenet, 2011; Guyenet & Bayliss, 2015). Presympathetic RVLM neurons are activated by hypercapnia despite blockade of the peripheral chemoreflex pathway, inputs from the CVLM, and inhibition of the caudal regions of the VRC including the preBötC (Moreira *et al.*, 2006). Since the firing properties of RVLM C1 neurons are unaffected by CO₂ *in vitro* (Lazarenko *et al.*, 2009), an excitatory input from the RTN (direct or via RVLM interneurons) is hypothesized. However, late-expiratory RTN/pFRG neurons are probably not involved in modulating sympathetic responses to peripheral chemoreceptor activation (Moraes *et al.*, 2012a). In the current dataset, input neurons were rarely (if ever) seen in the lateral parafacial region recently proposed to mediate active expiration (Huckstepp *et al.*, 2015), but were encountered in the region of the RTN classically defined as containing CO₂-sensitive Phox2b-positive neurons (i.e. running rostrally from the caudal pole of the facial nucleus immediately ventral to the facial nucleus (Abbott *et al.*, 2009a; Abbott *et al.*, 2011; Kumar *et al.*, 2015). However, technical limitations confound the interpretation of this observation because Phox2b chemosensitive RTN neurons are intermingled with rostral RVLM C1 sympathetic premotor neurons, which are also Phox2b-positive, and are transduced by the PRSx8 promoter used in the current study. Although the numbers of starter neurons encountered in the RTN were relatively low, we cannot entirely dismiss the possibility that some input neurons may reflect monosynaptic inputs to RTN chemosensors.

VRG

The VRG contains bulbospinal respiratory neurons clustered in predominantly inspiratory (rVRG) and expiratory (cVRG) groups (Alheid & McCrimmon, 2008). Glycine was identified as the major neurotransmitter used by decrementing expiratory cVRG neurons (Ezure *et al.*, 2003a), some of which have intramedullary projections to unknown target populations (Saito *et al.*, 2002). GABA-immunoreactive I-aug neurons were also found in the rVRG and cVRG

(Okazaki *et al.*, 2001). Blockade of glycine receptors via strychnine microinjection in the RVLM has been found to have no effect on respiratory-sympathetic coupling, but GABA_A receptor blockade increases the overall activity level of SNA. This increase is proportionally equal in different phases of the respiratory cycle (Guyenet *et al.*, 1990), suggesting GABAergic inputs may exert a tonic rather than a phasic effect on respiratory-sympathetic coupling. Regardless of the phenotype of the inputs (glycinergic, GABAergic, or both) in the cVRG, it is unlikely to provide a phasic influence on the SNA.

KF

The pontine respiratory circuits, which include the KF nucleus, are important in eupneic breathing and, in particular, regulating inspiration – expiration phase transition (Alheid *et al.*, 2004; Dutschmann & Dick, 2012). Descending fibres from the KF travel through the medullary reticular formation and project to the NTS, the ventrolateral medulla and the thoracic spinal cord (Saper & Loewy, 1980; Fulwiler & Saper, 1984; Herbert *et al.*, 1990), and inputs from the pontine respiratory network appear to play a role in mediating respiratory-sympathetic coupling, since it is abolished by pontomedullary transection (Baekey *et al.*, 2008). We encountered a small number of input neurons in the KF but not the PBN or A5 regions, supporting a potential role for the KF in contributing to respiratory-sympathetic coupling. However, the KF is also implicated in cardiovascular roles other than respiratory-sympathetic coupling, such as involvement in mediating cardiovascular components of the diving reflex (Browaldh *et al.*, 2015), complicating interpretation of this finding. Furthermore, as physical removal or pharmacological lesion of the KF region abolishes post-inspiratory motor output (Smith *et al.*, 2007) and evokes apneusis (i.e. a reconfiguration of respiratory pattern) (Dutschmann & Herbert, 2006; Bautista & Dutschmann, 2014), any effects of KF efferent neurons on respiratory-sympathetic coupling could be secondary to modulation of presynaptic respiratory neurons in the VRC.

Inputs from cardiovascular related nuclei

RVLM

The RVLM region itself was a major source of synaptic drive to RVLM C1 neurons. The majority of RVLM interneurons were located on the ipsilateral side, but inputs were also seen on the contralateral side consistent with previous studies (McMullan & Pilowsky, 2012; Turner *et al.*, 2013). Most inputs were not immunoreactive to TH, and included some glycinergic neurons, but complete neurochemical phenotyping of RVLM input neurons was beyond the scope of the current study. The functional significance of local RVLM input neurons has been a subject of speculation for some years and remains unknown (Ito & Sved, 1997; Dampney *et al.*, 2003; Guyenet, 2006). However, the relatively large fraction of the total connectome of RVLM C1 neurons that is located within the ipsilateral RVLM supports a likely critical role for these neurons in the generation of sympathetic nerve activity.

CVLM

In agreement with previous studies (Sved & Gordon, 1994; Suzuki *et al.*, 1997; Bowman *et al.*, 2013), we confirmed that the CVLM is a major source of monosynaptic input to RVLM C1 neurons. The CVLM is thought to provide direct tonic and phasic GABAergic inhibitory control of RVLM sympathetic premotor neurons (Minson *et al.*, 1997; Chan & Sawchenko, 1998; Schreihofer & Guyenet, 2003). CVLM inhibitory interneurons are perhaps best known for their critical role in mediating the sympathetic baroreflex (Pilowsky & Goodchild, 2002), but it is also the case that the activity of CVLM barosensitive neurons, including confirmed GABAergic neurons, is entrained with central respiratory rhythm (Mandel & Schreihofer, 2006). Thus, it is possible that the respiratory-modulation of RVLM sympathetic premotor neurons is transmitted through CVLM barosensitive neurons, a possibility supported by the observation that inhibition of the CVLM abolished inspiratory depression pattern in some presympathetic RVLM neurons and increased the expiratory modulation in others (Miyawaki *et al.*, 1996). Although the close

proximity of the CVLM to the preBötC/rVRG means that non-specific pharmacological interventions that target one are likely to also affect the other, tempering the interpretation of that observation..

NTS

The NTS plays a key role in integrating visceral afferent drive, and the caudal two thirds of the NTS are thought to regulate cardiovascular and respiratory reflexes due the relay of inputs from the baroreceptors of the carotid sinus and carotid arch, chemoreceptors of the carotid body, and the mechano- and chemoreceptors from the heart and lungs (reviewed by Andresen & Kunze, 1994; Zoccal *et al.*, 2014). The NTS projects to many brain regions that are involved in autonomic function, including the PVN (Affleck *et al.*, 2012), LC (Van Bockstaele *et al.*, 1999), CVLM (Aicher *et al.*, 1995; Aicher *et al.*, 1996), PBN region (Herbert *et al.*, 1990), and RVLM (Ross *et al.*, 1985). In the current study we confirmed direct projections from the NTS to RVLM C1 neurons, as previously described (Hancock, 1988; Aicher *et al.*, 1996), with a focal concentration in the commissural and dorsolateral regions.

PVN and DMH

The PVN in the hypothalamus play an important role in long term regulation of blood pressure and regulating tonic SNA (Kenney *et al.*, 2003; Dampney *et al.*, 2005). Neurons in the PVN have been hypothesised to directly regulate SNA via putative projections to the RVLM (Shafton *et al.*, 1998) and to sympathetic preganglionic neurons in the spinal cord (Hosoya *et al.*, 1991), in particular in response to plasma osmolality (Pyner & Coote, 2000; Stocker *et al.*, 2004a; Stocker *et al.*, 2008). The evidence for PVN contribution to resting SNA under normal conditions is conflicting (Ito *et al.*, 2003; Stocker *et al.*, 2004b; Dampney *et al.*, 2005), but bilateral inhibition of the PVN decreased the blood pressure in both spontaneous hypertensive rats and high salt- induced hypertensive rats (Allen, 2002; Ito *et al.*, 2003). These findings suggest overactivation of the PVN-RVLM/spinal cord pathway in models of hypertension: our

consistent observation of clusters of monosynaptically connected PVN neurons confirms the previously speculated direct input from PVN to RVLM C1 neurons, but provides no indication of whether such inputs are active under resting conditions. However, the number of neurons encountered was low (2 – 3 neurons per section).

The DMH is thought to mediate cardiovascular responses to emotional stress (DiMicco *et al.*, 2002; Dampney *et al.*, 2005; Fontes *et al.*, 2011). Although there is no direct evidence to support the idea that the DMH plays a role in the long term regulation of sympathetic nerve activity in normal animals, a recent study demonstrated a critical role of leptin receptor-expressing neurons of the DMH in regulating blood pressure associated with obesity (Simonds *et al.*, 2014). Our finding of a direct connection between the DMH and RVLM C1 populations support previously proposed neuroanatomical schemes (Fontes *et al.*, 2001).

Inputs from other nuclei

Nucleus prepositus

We observed input neurons in a region immediately ventral to the nucleus prepositus of brainstem, in agreement with findings from another tracing study targeting bulbospinal RVLM neurons (Dempsey, 2016). These neurons usually had small somata and a distinctive multi-dendritic structure that is similar to one type of prepositus neuron described previously (McCrea & Baker, 1985). This nucleus has been associated with control of horizontal eye movement, gaze stabilization and vestibulo-ocular reflex (Cannon & Robinson, 1987; Robinson *et al.*, 1994; Dale & Cullen, 2013; Yoder & Taube, 2014). Observations from human patients with brainstem infarctions that predominantly involved the prepositus nucleus suggested a possible role of the prepositus nucleus in regulating vestibular function (Seo *et al.*, 2004; Cho *et al.*, 2008). Moreover, lesions of the vestibular system affect both respiratory and cardiovascular controls, in particular during movement or changes in posture (see review (Yates & Bronstein, 2005), and a decreased functionality of the vestibular system causes blood pressure instability in

astronauts returning from space (Hallgren *et al.*, 2015). In rats, electrical stimulation of, or glutamate microinjection to the prepositus nucleus elicited an increase in arterial blood pressure and bradycardia, which are thought to be mediated via axonal projections passing the fastigial nucleus (Talman & Robertson, 1991). Our findings provide direct evidence that the prepositus nucleus regulates cardiovascular function via monosynaptic projections to the RVLM. This pathway may play an important role in regulating blood pressure during posture changes.

Retrochubral nucleus

A distinct cluster of input neurons was seen in the region of the contralateral retrochubral nucleus, a region that is coincident with the urotensin II binding site (Bucharles *et al.*, 2014) and the location of the urotensin receptor (Jegou *et al.*, 2006). Urotensin II is a cyclic undecapeptide whose structure is related to somatostatin, and possibly derived from the same ligand-receptor pair (Tostivint *et al.*, 2014). Intracerebroventricular administration of urotensin II increases heart rate and blood pressure (Lin *et al.*, 2003), and also increases release of epinephrine and adrenocorticotrophic hormone (ACTH) (Watson *et al.*, 2003). Pressor and depressor responses were observed when urotensin II was microinjected into the medullary A1 region and the PVN respectively (Lu *et al.*, 2002). To the best knowledge of the author, no studies have previously associated this region with sympathetic regulation. The functional implication of this cluster of input neurons we identified in the current study requires further investigation.

Technical consideration

Targeting of RVLM C1 neurons using Lv-PRSx8-YTB

The PRSx8 promoter is a synthetic promoter constructed from a noradrenergic-specific cis-regulatory element identified in the human D β H promoter (Hwang *et al.*, 2001). This promoter has a binding site for the transcription factor Phox2a/Phox2b (Kim *et al.*, 1998; Yang *et al.*, 1998). These transcription factors are essential for activating the D β H promoter, and therefore are critical for the differentiation of noradrenergic neurons and the expression of the

catecholaminergic phenotype (Pattyn *et al.*, 2000; Seo *et al.*, 2002). The PRSx8 promoter has been used to drive gene expression in noradrenergic neurons in the locus coeruleus (LC) (Hwang *et al.*, 2001), and various catecholaminergic cell groups (Kasparov *et al.*, 2004; Lonergan *et al.*, 2005), including RVLM C1 neurons (Abbott *et al.*, 2009a; Kanbar *et al.*, 2010; Marina *et al.*, 2011). However, neighbouring chemosensitive Phox2b-expressing RTN neurons also activate the promoter, and indeed the PRSx8 promoter has also been used to target this population (Kanbar *et al.*, 2010; Marina *et al.*, 2010). By optimising the injection site, carefully titrating the injection volume, and rejecting data from experiments in which potential contamination of starter neurons by neurons outside of the RVLM was apparent, we restricted the spread of the vector to the RVLM. However, a small scatter of starter neurons was found in the RTN region, and therefore we cannot totally exclude the possibility that some of the input neurons we identified are monosynaptically connected with the Phox2b-expressing RTN neurons.

Variability in rabies spread

The current monosynaptic tracing strategy does not label all input neurons. In studies of cortical pyramidal neurons, transfecting the starter neurons via different techniques, such as single cell electroporation (Marshel *et al.*, 2010), viral vector transfection (Miyamichi *et al.*, 2011), or whole cell recording (Rancz *et al.*, 2011), resulted a huge variability in numbers of input neurons labelled (range from 14 – 500 inputs per starter cell). In a recent comparable study, bulbospinal C1 neurons were primed as starter cells using Cre-dependent viral vectors, using the same strain of rabies we used in the current study, the investigators yielded an inputs : starter cells ratio of 1.7 (Stornetta *et al.*, 2015). On average, 7.1 input neurons per starter cell were labelled in the current study, and a similar number (9.8 input neurons per starter cell) was seen from another experiment conducted in our laboratory using herpes virus to transfect the starter

neurons (Dempsey, 2016). We consider this ratio to be reasonable and appropriate for quantification analysis.

The mechanisms of the differential spread pattern of the rabies virus is not fully understood (Callaway & Luo, 2015). It was suggested the spread is independent of the activity level of synapses, as incubation of cultured neurons in tetrodotoxin doesn't affect spreading of the rabies virus (Brennand *et al.*, 2011). Rather, the rabies virus may bias strongly connected synapses for trans-synaptic spread (Ugolini, 2008). Furthermore, distance between the inputs and starter neurons had limited effects on the trans-synaptic efficiency of the rabies virus, as input neurons far away from the starter cells were labelled effectively (Schwarz *et al.*, 2015). Therefore, the proportion of input neurons labelled in the PVN and DMH in the current study should match the overall labelling efficiency.

Summary and future direction

Taking advantage of the monosynaptic tracing technique, we generated a brain-wide connectomic map of RVLM C1 neurons. With a focus on respiratory related circuitry, we mapped inputs from the BötC, the preBötC, the VRG, the NTS and the KF nucleus. As respiratory-sympathetic coupling relies on excitatory transmission rather than inhibitory transmission (Guyenet *et al.*, 1990; Miyawaki *et al.*, 1996; Miyawaki *et al.*, 2002), and the phasic modulation of SNA is in the period of inspiration (Bainton *et al.*, 1985; Numao *et al.*, 1987), we proposed that the monosynaptic input neurons we frequently encountered in the preBötC are most likely to provide the excitatory respiratory modulation of the SNA. Our data suggests a limited involvement of NK1R expressing preBötC neurons in the respiratory-sympathetic coupling, and indicate a need to further identify the phenotypes of these input neurons. More sophisticated manipulation of these neurons, such as introducing channelrhodopsin in the presynaptic population revealed by the rabies tracing (Petreanu *et al.*,

2007; Weissbourd *et al.*, 2014), would provide a way to elicit and assess the functional responses.

5.

General discussion

Chapters 2&3

Characterizing the electrophysiological signatures of individual neurons in intact neural networks has been an ongoing research objective in the field of neurophysiology, either by recording single neurons or recording fields of neurons via multi-channel microelectrode arrays (Obien *et al.*, 2014). However, the methodology required to correlate the functional properties of recorded neurons to their morphological and molecular identities remains largely unchanged over the years. In Chapter 2, we describe a protocol that allowed us to introduce dyes into single electrophysiologically characterised neurons more effectively compared to the gold standard juxtacellular labelling technique. Application of our approach for the introduction of plasmid DNA into functionally characterized cells was promising, but not yet refined enough to be practical: in our hands, it worked very well *in vitro*, but effective transfection of cells *in vivo* was technically difficult. We speculate that blockage of the recording pipette is the most likely cause for the reduced efficiency *in vivo*.

The findings in Chapter 3 show that sst_{2a} is widely expressed on neurons in regions of the VLM associated with respiratory and cardiovascular function, and partially colocalized with NK1R in the preBötC. However, no evidence of sst_{2a} expression in functionally identified respiratory neurons was found. As the electrophysiological identities of sst_{2a} neurons remain unknown, our findings undermine the postulate that sst_{2a} expressing respiratory neurons account for the inhibitory effects of SST on respiratory functions (Burke *et al.*, 2010). One caveat of this study is the sensitivity of sst_{2a} detection. The antibodies used in this study are well validated (Burke *et al.*, 2008; Bou Farah *et al.*, 2016), but we cannot exclude the possibility that neurons expressing sst_{2a} at a level below our detection threshold may still be able to mediate functional responses. Like all single neuron sampling techniques, we did not exhaust the sample pool, therefore, strictly speaking, absence of evidence does not equate to evidence of absence. More sophisticated experiments may be required to reveal the functional identities of these neurons.

Exclusive access to the cells that express sst_{2a} may be achievable. For example, modifying the HI loop of adenoviral capsid proteins to incorporate SST has been shown to drive transgene expression in sst_{2a}-expressing cells (Lecolle *et al.*, 2013). Similarly, fusion of SST with the viral envelope glycoprotein of the Maloney murine leukemia virus also enabled preferential retroviral transfection of cells expressing somatostatin receptors *in vitro* (Li *et al.*, 2012). Alternatively, introducing a gene of interest under the control of an sst_{2a} specific promoter may be possible. Gray *et al.* (2013) identified that RVLM sst_{2a}-expressing neurons were derived from progenitors expressing transcription factor *Ptf1a* (pancreas specific transcription factor 1a). Cre-dependent expression of microbial opsins such as channelrhodopsin, halorhodopsin, and archaerhodopsin (Flytzanis *et al.*, 2014; Grosenick *et al.*, 2015; Rajasethupathy *et al.*, 2016) in sst_{2a} expressing neurons can be achieved by microinjection of a viral vector, such as AAV-DIO-ChR2-mCherry (Cardin *et al.*, 2010), into *Ptf1a-Cre* mice (Kawaguchi *et al.*, 2002). Furthermore, long term single cell recording can be performed from optogenetically identified subpopulations of neurons (Moore & Wehr, 2014) to further characterize the functional properties of sst_{2a} expressing neurons.

Another approach that might be useful for determining the functional properties of sst_{2a}-expressing VLM neurons would be to selectively express voltage or calcium-sensitive reporters, such as the GCaMP family of genetically encoded calcium indicators (Tian *et al.*, 2009; Chen *et al.*, 2013), in neurons that express sst_{2a}. As with the optogenetic approaches described above, this technique is limited by the availability of transgenic mice that express recombinase or GFP in sst_{2a}-synthesizing neurons.

Chapter 4

Substantial evidence supports the view that chronic activation of the sympathetic nervous system participates in the initiation, development, and maintenance of essential hypertension

(Esler, 2000; Osborn, 2005; Esler *et al.*, 2010). However, the definitive cause or causes of sympathetic hyperactivity have yet to be determined: in recent years hypoperfusion of the brainstem during development (Paton *et al.*, 2009), carotid body overactivity (Abdala *et al.*, 2012; McBryde *et al.*, 2013), and reconfiguration of the interaction between brainstem respiratory and cardiovascular circuits (Simms *et al.*, 2010; Moraes *et al.*, 2012b) have all been proposed as potential critical mechanisms. The results of Chapter 4 provide structural evidence of neurons within core regions of the central respiratory rhythm generator that directly innervate RVLM C1 neurons. Further characterization of the neurochemical and functional profiles of these putative respiratory neurons may provide insights into the mechanisms through which the respiratory rhythm generator influences sympathetic outflow and the identity of the critical populations involved, which can be used as a basis for target selection in future functional experiments designed to specifically manipulate the same populations. Furthermore, comparing the distribution pattern, phenotype composition, and electrophysiological signatures of input neurons originating from the same starter populations between healthy and diseased animals may provide new insights into the most influential respiratory neurons. Ongoing experiments in our laboratory will directly test this hypothesis by comparing connectomic maps of inputs to C1 neurons in normotensive animals to those with a hypertensive phenotype; although not included in the current thesis due to time constraints, our preliminary data look promising and suggest quantifiable changes of the compositions of inputs that may underlie the enhanced respiratory-sympathetic coupling observed in these animals.

Another surprising observation of our study is that, in contrast to our expectation that input neurons would lie in discrete and well-defined nuclei, the distribution of inputs instead seemed quite diffuse, with a conspicuous predominance of inputs from the immediate vicinity of the RVLM. The distribution of distances that input neurons lie from the RVLM is in striking accordance with the nodal edge-length distribution of the mouse mesoscale connectome (Oh *et*

al., 2014). Henriksen *et al.* (2016) have proposed two general principles governing neural network organization at the mesoscale level: 1. proximal attachment, suggesting that outgoing connections are more likely to attach to nearby targets than to distant ones. 2. source growth, proposing that new outgoing connections are more likely to originate from nodes with many existing outgoing connections. Our data indicate that the distribution of the RVLM connectome follows the same rules, at least the first rule “proximal attachment”. This is particularly intriguing, as respiratory neurons are spatially close to, or overlap with cardiovascular RVLM C1 neurons, therefore it would seem that neurons in the VRC are ideally located to exert a powerful influence on cardiovascular functions.

Continuous refinement of the tools used to target specific cell types with more accuracy (Fenno *et al.*, 2014), coupled with ongoing modification of rabies G to boost trans-synaptic efficiency (Kim *et al.*, 2016), and generating new mutant strains of the rabies virus (Reardon *et al.*, 2016), suggests that the future of the connectomic approach is bright and likely to become increasingly effective. However, the tools used to quantify, analyse and compare connectomic datasets is underdeveloped (Lichtman *et al.*, 2014). We established an easy-to-apply method to transfer histological image data into Cartesian coordinates in a volumetric brain atlas, and have demonstrated the suitability and effectiveness of using this platform to analyse and quantify large connectomic datasets. With further development and refinement of the segmentation models in the Waxholm brain atlas, we expect a sharable, open platform for researchers to compare connectomic data with minimum subjective judgement.

Final thoughts

The research focus given to the field of autonomic neuroscience is not commensurate with the importance of autonomic nervous systems. To new researchers, the stereotypical functions of the autonomic nervous system, such as respiration and blood pressure regulation, may look less

interesting compared to higher brain functions, such as memory, cognition, and motor controls. However, researchers are now beginning to appreciate the role of autonomic dysfunction, and brainstem circuitries in contributing to diseases such as Alzheimer's disease, Parkinson's disease, and autism (Grinberg *et al.*, 2011; Cheshire, 2012). Furthermore, the advance of molecular tools, such as transgenic mice, genetically modified viral vectors, as well as vast improvement in imaging and computing techniques are helping to overcome the technical difficulties in elucidation of neural networks buried deep in the brainstem. One of the major challenges in the field is to specifically manipulate one substrate of interwoven cardiovascular or respiratory neurons without affecting others. In addition to targeting cell types using specific promoters to test their functional roles (Abbott *et al.*, 2009a; Burke *et al.*, 2014), connectomic approaches open the possibility to control cells defined by their specific connectivity, and to study the causal linkages between different populations (Packer *et al.*, 2013; Deisseroth, 2014). This will further our understanding of how interactive functions emerge from intermingled neurons.

References

- Abbott SB, DePuy SD, Nguyen T, Coates MB, Stornetta RL & Guyenet PG. (2013). Selective optogenetic activation of rostral ventrolateral medullary catecholaminergic neurons produces cardiorespiratory stimulation in conscious mice. *The Journal of neuroscience : the official journal of the Society for Neuroscience* **33**, 3164-3177.
- Abbott SB, Holloway BB, Viar KE & Guyenet PG. (2014). Vesicular glutamate transporter 2 is required for the respiratory and parasympathetic activation produced by optogenetic stimulation of catecholaminergic neurons in the rostral ventrolateral medulla of mice in vivo. *The European journal of neuroscience* **39**, 98-106.
- Abbott SB, Stornetta RL, Coates MB & Guyenet PG. (2011). Phox2b-expressing neurons of the parafacial region regulate breathing rate, inspiration, and expiration in conscious rats. *The Journal of neuroscience : the official journal of the Society for Neuroscience* **31**, 16410-16422.
- Abbott SB, Stornetta RL, Fortuna MG, Depuy SD, West GH, Harris TE & Guyenet PG. (2009a). Photostimulation of retrotrapezoid nucleus phox2b-expressing neurons in vivo produces long-lasting activation of breathing in rats. *The Journal of neuroscience : the official journal of the Society for Neuroscience* **29**, 5806-5819.
- Abbott SB, Stornetta RL, Socolovsky CS, West GH & Guyenet PG. (2009b). Photostimulation of channelrhodopsin-2 expressing ventrolateral medullary neurons increases sympathetic nerve activity and blood pressure in rats. *The Journal of physiology* **587**, 5613-5631.
- Abdala AP, McBryde FD, Marina N, Hendy EB, Engelman ZJ, Fudim M, Sobotka PA, Gourine AV & Paton JF. (2012). Hypertension is critically dependent on the carotid body input in the spontaneously hypertensive rat. *The Journal of physiology* **590**, 4269-4277.
- Abdala AP, Paton JF & Smith JC. (2015). Defining inhibitory neurone function in respiratory circuits: opportunities with optogenetics? *The Journal of physiology* **593**, 3033-3046.
- Adrian ED, Bronk DW & Phillips G. (1932). Discharges in mammalian sympathetic nerves. *The Journal of physiology* **74**, 115-133.
- Affleck VS, Coote JH & Pyner S. (2012). The projection and synaptic organisation of NTS afferent connections with presympathetic neurons, GABA and nNOS neurons in the paraventricular nucleus of the hypothalamus. *Neuroscience* **219**, 48-61.
- Agarwal SK & Calaresu FR. (1991). Monosynaptic connection from caudal to rostral ventrolateral medulla in the baroreceptor reflex pathway. *Brain research* **555**, 70-74.
- Agassandian K, Shan Z, Raizada M, Sved AF & Card JP. (2012). C1 Catecholamine Neurons form Local Circuit Synaptic Connections Within the Rostroventrolateral Medulla of Rat. *Neuroscience* **227**, 247-259.

- Aicher SA, Kurucz OS, Reis DJ & Milner TA. (1995). Nucleus tractus solitarius efferent terminals synapse on neurons in the caudal ventrolateral medulla that project to the rostral ventrolateral medulla. *Brain research* **693**, 51-63.
- Aicher SA, Saravay RH, Cravo S, Jeske I, Morrison SF, Reis DJ & Milner TA. (1996). Monosynaptic projections from the nucleus tractus solitarii to C1 adrenergic neurons in the rostral ventrolateral medulla: comparison with input from the caudal ventrolateral medulla. *The Journal of comparative neurology* **373**, 62-75.
- Al-Khater KM, Kerr R & Todd AJ. (2008). A quantitative study of spinothalamic neurons in laminae I, III, and IV in lumbar and cervical segments of the rat spinal cord. *The Journal of comparative neurology* **511**, 1-18.
- Alexander RS. (1946). Tonic and reflex functions of medullary sympathetic cardiovascular centers. *Journal of neurophysiology* **9**, 205-217.
- Alheid GF & McCrimmon DR. (2008). The chemical neuroanatomy of breathing. *Respir Physiol Neurobiol* **164**, 3-11.
- Alheid GF, Milsom WK & McCrimmon DR. (2004). Pontine influences on breathing: an overview. *Respir Physiol Neurobiol* **143**, 105-114.
- Allen AM. (2002). Inhibition of the hypothalamic paraventricular nucleus in spontaneously hypertensive rats dramatically reduces sympathetic vasomotor tone. *Hypertension* **39**, 275-280.
- Allen JP, Hathway GJ, Clarke NJ, Jowett MI, Topps S, Kendrick KM, Humphrey PP, Wilkinson LS & Emson PC. (2003). Somatostatin receptor 2 knockout/lacZ knockin mice show impaired motor coordination and reveal sites of somatostatin action within the striatum. *The European journal of neuroscience* **17**, 1881-1895.
- Amiel J, Dubreuil V, Ramanantsoa N, Fortin G, Gallego J, Brunet JF & Goridis C. (2009). PHOX2B in respiratory control: lessons from congenital central hypoventilation syndrome and its mouse models. *Respir Physiol Neurobiol* **168**, 125-132.
- Amiel J, Laudier B, Attie-Bitach T, Trang H, de Pontual L, Gener B, Trochet D, Etchevers H, Ray P, Simonneau M, Vekemans M, Munnich A, Gaultier C & Lyonnet S. (2003). Polyalanine expansion and frameshift mutations of the paired-like homeobox gene PHOX2B in congenital central hypoventilation syndrome. *Nature genetics* **33**, 459-461.
- Andresen MC & Kunze DL. (1994). Nucleus tractus solitarius--gateway to neural circulatory control. *Annual review of physiology* **56**, 93-116.

- Babic T & Ciriello J. (2004). Medullary and spinal cord projections from cardiovascular responsive sites in the rostral ventromedial medulla. *The Journal of comparative neurology* **469**, 391-412.
- Baekey DM, Dick TE & Paton JF. (2008). Pontomedullary transection attenuates central respiratory modulation of sympathetic discharge, heart rate and the baroreceptor reflex in the in situ rat preparation. *Experimental physiology* **93**, 803-816.
- Baekey DM, Molkov YI, Paton JF, Rybak IA & Dick TE. (2010). Effect of baroreceptor stimulation on the respiratory pattern: insights into respiratory-sympathetic interactions. *Respir Physiol Neurobiol* **174**, 135-145.
- Bago M & Dean C. (2001). Sympathoinhibition from ventrolateral periaqueductal gray mediated by 5-HT(1A) receptors in the RVLM. *American journal of physiology Regulatory, integrative and comparative physiology* **280**, R976-984.
- Bainton CR, Richter DW, Seller H, Ballantyne D & Klein JP. (1985). Respiratory modulation of sympathetic activity. *Journal of the autonomic nervous system* **12**, 77-90.
- Bargmann CI, Thomas JH & Horvitz HR. (1990). Chemosensory cell function in the behavior and development of *Caenorhabditis elegans*. *Cold Spring Harbor symposia on quantitative biology* **55**, 529-538.
- Barman SM & Gebber GL. (1980). Sympathetic nerve rhythm of brain stem origin. *The American journal of physiology* **239**, R42-47.
- Barman SM & Gebber GL. (1987). Lateral tegmental field neurons of cat medulla: a source of basal activity of ventrolateral medullospinal sympathoexcitatory neurons. *Journal of neurophysiology* **57**, 1410-1424.
- Barnard RJ, Elleder D & Young JA. (2006). Avian sarcoma and leukosis virus-receptor interactions: from classical genetics to novel insights into virus-cell membrane fusion. *Virology* **344**, 25-29.
- Bates P, Young JA & Varmus HE. (1993). A receptor for subgroup A Rous sarcoma virus is related to the low density lipoprotein receptor. *Cell* **74**, 1043-1051.
- Bautista TG & Dutschmann M. (2014). Inhibition of the pontine Kölliker-Fuse nucleus abolishes eupneic inspiratory hypoglossal motor discharge in rat. *Neuroscience* **267**, 22-29.
- Beier KT, Saunders A, Oldenburg IA, Miyamichi K, Akhtar N, Luo L, Whelan SP, Sabatini B & Cepko CL. (2011). Anterograde or retrograde transsynaptic labeling of CNS neurons with vesicular stomatitis virus vectors. *Proceedings of the National Academy of Sciences of the United States of America* **108**, 15414-15419.

- Ben-Tal A, Shamilov SS & Paton JF. (2012). Evaluating the physiological significance of respiratory sinus arrhythmia: looking beyond ventilation-perfusion efficiency. *The Journal of physiology* **590**, 1989-2008.
- Berner J, Shvarev Y, Lagercrantz H, Bilkei-Gorzo A, Hokfelt T & Wickstrom R. (2007). Altered respiratory pattern and hypoxic response in transgenic newborn mice lacking the tachykinin-1 gene. *Journal of applied physiology (Bethesda, Md : 1985)* **103**, 552-559.
- Berube-Carriere N, Riad M, Dal Bo G, Levesque D, Trudeau LE & Descarries L. (2009). The dual dopamine-glutamate phenotype of growing mesencephalic neurons regresses in mature rat brain. *The Journal of comparative neurology* **517**, 873-891.
- Bestman JE, Ewald RC, Chiu S-L & Cline HT. (2006a). In vivo single-cell electroporation for transfer of DNA and macromolecules. *Nat Protocols* **1**, 1267-1272.
- Bestman JE, Ewald RC, Chiu SL & Cline HT. (2006b). In vivo single-cell electroporation for transfer of DNA and macromolecules. *Nature protocols* **1**, 1267-1272.
- Bevan MD. (1998). Selective innervation of neostriatal interneurons by a subclass of neuron in the globus pallidus of the rat. *J Neurosci* **18**, 9438-9452.
- Bianchi AL, Denavit-Saubie M & Champagnat J. (1995). Central control of breathing in mammals: neuronal circuitry, membrane properties, and neurotransmitters. *Physiological reviews* **75**, 1-45.
- Billman GE. (2011). Heart rate variability - a historical perspective. *Frontiers in physiology* **2**, 86.
- Blessing WW. (1988). Depressor neurons in rabbit caudal medulla act via GABA receptors in rostral medulla. *The American journal of physiology* **254**, H686-692.
- Blessing WW, Goodchild AK, Dampney RA & Chalmers JP. (1981). Cell groups in the lower brain stem of the rabbit projecting to the spinal cord, with special reference to catecholamine-containing neurons. *Brain research* **221**, 35-55.
- Bochorishvili G, Stornetta RL, Coates MB & Guyenet PG. (2012). Pre-Botzinger complex receives glutamatergic innervation from galaninergic and other retrotrapezoid nucleus neurons. *The Journal of comparative neurology* **520**, 1047-1061.
- Bock DD, Lee W-CA, Kerlin AM, Andermann ML, Hood G, Wetzel AW, Yurgenson S, Soucy ER, Kim HS & Reid RC. (2011). Network anatomy and in vivo physiology of visual cortical neurons. *Nature* **471**, 177-182.

- Bota M, Sporns O & Swanson LW. (2015). Architecture of the cerebral cortical association connectome underlying cognition. *Proceedings of the National Academy of Sciences* **112**, E2093-E2101.
- Bou Farah L, Bowman BR, Bokinić P, Karim S, Le S, Goodchild AK & McMullan S. (2015). Somatostatin in the rat rostral ventrolateral medulla: Origins and mechanism of action. *The Journal of comparative neurology* **In Press**.
- Bou Farah L, Bowman BR, Bokinić P, Karim S, Le S, Goodchild AK & McMullan S. (2016). Somatostatin in the rat rostral ventrolateral medulla: Origins and mechanism of action. *The Journal of comparative neurology* **524**, 323-342.
- Boucetta S, Cisse Y, Mainville L, Morales M & Jones BE. (2014). Discharge profiles across the sleep-waking cycle of identified cholinergic, GABAergic, and glutamatergic neurons in the pontomesencephalic tegmentum of the rat. *The Journal of neuroscience : the official journal of the Society for Neuroscience* **34**, 4708-4727.
- Bouvier J, Thoby-Brisson M, Renier N, Dubreuil V, Ericson J, Champagnat J, Pierani A, Chedotal A & Fortin G. (2010). Hindbrain interneurons and axon guidance signaling critical for breathing. *Nat Neurosci* **13**, 1066-1074.
- Bowman BR, Kumar NN, Hassan SF, McMullan S & Goodchild AK. (2013). Brain sources of inhibitory input to the rat rostral ventrolateral medulla. *The Journal of comparative neurology* **521**, 213-232.
- Braeken D, Jans D, Huys R, Stassen A, Collaert N, Hoffman L, Eberle W, Peumans P & Callewaert G. (2012). Open-cell recording of action potentials using active electrode arrays. *Lab on a Chip - Miniaturisation for Chemistry and Biology* **12**, 4397-4402.
- Braga VA, Soriano RN, Braccialli AL, de Paula PM, Bonagamba LG, Paton JF & Machado BH. (2007). Involvement of L-glutamate and ATP in the neurotransmission of the sympathoexcitatory component of the chemoreflex in the commissural nucleus tractus solitarii of awake rats and in the working heart-brainstem preparation. *The Journal of physiology* **581**, 1129-1145.
- Brecht M, Schneider M, Sakmann B & Margrie TW. (2004). Whisker movements evoked by stimulation of single pyramidal cells in rat motor cortex. *Nature* **427**, 704-710.
- Brennand KJ, Simone A, Jou J, Gelboin-Burkhart C, Tran N, Sangar S, Li Y, Mu Y, Chen G, Yu D, McCarthy S, Sebat J & Gage FH. (2011). Modelling schizophrenia using human induced pluripotent stem cells. *Nature* **473**, 221-225.
- Browaldh N, Bautista TG, Dutschmann M & Berkowitz RG. (2015). The Kolliker-Fuse nucleus: a review of animal studies and the implications for cranial nerve function in humans. *Eur Arch Otorhinolaryngol*.

- Brown DL & Guyenet PG. (1984). Cardiovascular neurons of brain stem with projections to spinal cord. *The American journal of physiology* **247**, R1009-1016.
- Brown DL & Guyenet PG. (1985). Electrophysiological study of cardiovascular neurons in the rostral ventrolateral medulla in rats. *Circulation research* **56**, 359-369.
- Bryant TH, Yoshida S, de Castro D & Lipski J. (1993). Expiratory neurons of the bötzing complex in the rat: A morphological study following intracellular labeling with biocytin. *The Journal of comparative neurology* **335**, 267-282.
- Bucharles C, Bizet P, Arthaud S, Arabo A, Leprince J, Lefranc B, Cartier D, Anouar Y & Lihmann I. (2014). Concordant localization of functional urotensin II and urotensin II-related peptide binding sites in the rat brain: Atypical occurrence close to the fourth ventricle. *The Journal of comparative neurology* **522**, 2634-2649.
- Burke PG, Abbott SB, Coates MB, Viar KE, Stornetta RL & Guyenet PG. (2014). Optogenetic stimulation of adrenergic C1 neurons causes sleep state-dependent cardiorespiratory stimulation and arousal with sighs in rats. *Am J Respir Crit Care Med* **190**, 1301-1310.
- Burke PG, Li Q, Costin ML, McMullan S, Pilowsky PM & Goodchild AK. (2008). Somatostatin 2A receptor-expressing presympathetic neurons in the rostral ventrolateral medulla maintain blood pressure. *Hypertension* **52**, 1127-1133.
- Burke PG, Neale J, Korim WS, McMullan S & Goodchild AK. (2011). Patterning of somatosympathetic reflexes reveals nonuniform organization of presympathetic drive from C1 and non-C1 RVLM neurons. *American journal of physiology Regulatory, integrative and comparative physiology* **301**, R1112-1122.
- Burke PGR, Abbott SBG, McMullan S, Goodchild AK & Pilowsky PM. (2010). Somatostatin selectively ablates post-inspiratory activity after injection into the Bötzing complex. *Neuroscience* **167**, 528-539.
- Burke PGR, Kanbar R, Viar KE, Stornetta RL & Guyenet PG. (2015). Selective optogenetic stimulation of the retrotrapezoid nucleus in sleeping rats activates breathing without changing blood pressure or causing arousal or sighs. *Journal of Applied Physiology* **118**, 1491-1501.
- Cabassi A, Vinci S, Calzolari M, Bruschi G & Borghetti A. (1998). Regional sympathetic activity in pre-hypertensive phase of spontaneously hypertensive rats. *Life sciences* **62**, 1111-1118.
- Callaway EM. (2008). Transneuronal circuit tracing with neurotropic viruses. *Current opinion in neurobiology* **18**, 617-623.

- Callaway EM & Luo L. (2015). Monosynaptic Circuit Tracing with Glycoprotein-Deleted Rabies Viruses. *The Journal of neuroscience : the official journal of the Society for Neuroscience* **35**, 8979-8985.
- Campos RR & McAllen RM. (1999). Tonic drive to sympathetic premotor neurons of rostral ventrolateral medulla from caudal pressor area neurons. *The American journal of physiology* **276**, R1209-1213.
- Cannon SC & Robinson DA. (1987). Loss of the neural integrator of the oculomotor system from brain stem lesions in monkey. *Journal of neurophysiology* **57**, 1383-1409.
- Carandini M. (2012). From circuits to behavior: A bridge too far? *Nature Neuroscience* **15**, 507-509.
- Card JP, Kobiler O, McCambridge J, Ebdlahad S, Shan Z, Raizada MK, Sved AF & Enquist LW. (2011). Microdissection of neural networks by conditional reporter expression from a Brainbow herpesvirus. *Proceedings of the National Academy of Sciences of the United States of America* **108**, 3377-3382.
- Card JP, Sved JC, Craig B, Raizada M, Vazquez J & Sved AF. (2006). Efferent projections of rat rostroventrolateral medulla C1 catecholamine neurons: Implications for the central control of cardiovascular regulation. *The Journal of comparative neurology* **499**, 840-859.
- Cardin JA, Carlén M, Meletis K, Knoblich U, Zhang F, Deisseroth K, Tsai L-H & Moore CI. (2010). Targeted optogenetic stimulation and recording of neurons in vivo using cell-type-specific expression of Channelrhodopsin-2. *Nature protocols* **5**, 247-254.
- Carrive P, Bandler R & Dampney RA. (1988). Anatomical evidence that hypertension associated with the defence reaction in the cat is mediated by a direct projection from a restricted portion of the midbrain periaqueductal grey to the subretrofacial nucleus of the medulla. *Brain research* **460**, 339-345.
- Cassell MD & Gray TS. (1989). The amygdala directly innervates adrenergic (C1) neurons in the ventrolateral medulla in the rat. *Neuroscience letters* **97**, 163-168.
- Catani M, Thiebaut de Schotten M, Slater D & Dell'Acqua F. (2013). Connectomic approaches before the connectome. *NeuroImage* **80**, 2-13.
- Chamberlin NL. (2004). Functional organization of the parabrachial complex and intertrigeminal region in the control of breathing. *Respir Physiol Neurobiol* **143**, 115-125.

- Chan RK & Sawchenko PE. (1998). Organization and transmitter specificity of medullary neurons activated by sustained hypertension: implications for understanding baroreceptor reflex circuitry. *The Journal of neuroscience : the official journal of the Society for Neuroscience* **18**, 371-387.
- Chen D, Bassi JK, Walther T, Thomas WG & Allen AM. (2010). Expression of angiotensin type 1A receptors in C1 neurons restores the sympathoexcitation to angiotensin in the rostral ventrolateral medulla of angiotensin type 1A knockout mice. *Hypertension* **56**, 143-150.
- Chen TW, Wardill TJ, Sun Y, Pulver SR, Renninger SL, Baohan A, Schreiter ER, Kerr RA, Orger MB, Jayaraman V, Looger LL, Svoboda K & Kim DS. (2013). Ultrasensitive fluorescent proteins for imaging neuronal activity. *Nature* **499**, 295-300.
- Chen ZB, Hedner T & Hedner J. (1990). Local application of somatostatin in the rat ventrolateral brain medulla induces apnea. *Journal of applied physiology (Bethesda, Md : 1985)* **69**, 2233-2238.
- Cheshire WP. (2012). Highlights in clinical autonomic neuroscience: new insights into autonomic dysfunction in autism. *Autonomic neuroscience : basic & clinical* **171**, 4-7.
- Cho HJ, Choi HY, Kim YD, Seo SW & Heo JH. (2008). The clinical syndrome and etiological mechanism of infarction involving the nucleus prepositus hypoglossi. *Cerebrovascular diseases (Basel, Switzerland)* **26**, 178-183.
- Choi J & Callaway EM. (2011). Monosynaptic inputs to ErbB4-expressing inhibitory neurons in mouse primary somatosensory cortex. *The Journal of comparative neurology* **519**, 3402-3414.
- Cohen L, Koffman N, Meiri H, Yarom Y, Lampl I & Mizrahi A. (2013). Time-lapse electrical recordings of single neurons from the mouse neocortex. *Proceedings of the National Academy of Sciences of the United States of America* **110**, 5665-5670.
- Conte WL, Kamishina H & Reep RL. (2009). Multiple neuroanatomical tract-tracing using fluorescent Alexa Fluor conjugates of cholera toxin subunit B in rats. *Nat Protocols* **4**, 1157-1166.
- Costa-Silva JH, Zoccal DB & Machado BH. (2010). Glutamatergic antagonism in the NTS decreases post-inspiratory drive and changes phrenic and sympathetic coupling during chemoreflex activation. *Journal of neurophysiology* **103**, 2095-2106.
- Cowley AW, Jr. (1992). Long-term control of arterial blood pressure. *Physiological reviews* **72**, 231-300.

- Cui Y, Kam K, Sherman D, Janczewski Wiktor A, Zheng Y & Feldman Jack L. Defining preBotzinger Complex Rhythm- and Pattern-Generating Neural Microcircuits In Vivo. *Neuron* **91**, 602-614.
- Cui Y, Kam K, Sherman D, Janczewski WA, Zheng Y & Feldman JL. (2016). Defining preBotzinger Complex Rhythm- and Pattern-Generating Neural Microcircuits In Vivo. *Neuron* **91**, 602-614.
- Czyzyk-Krzeska MF & Trzebski A. (1990). Respiratory-related discharge pattern of sympathetic nerve activity in the spontaneously hypertensive rat. *The Journal of physiology* **426**, 355-368.
- Dale A & Cullen KE. (2013). The nucleus prepositus predominantly outputs eye movement-related information during passive and active self-motion. *Journal of neurophysiology* **109**, 1900-1911.
- Dampney RA. (1994). Functional organization of central pathways regulating the cardiovascular system. *Physiological reviews* **74**, 323-364.
- Dampney RA, Coleman MJ, Fontes MA, Hirooka Y, Horiuchi J, Li YW, Polson JW, Potts PD & Tagawa T. (2002). Central mechanisms underlying short- and long-term regulation of the cardiovascular system. *Clinical and experimental pharmacology & physiology* **29**, 261-268.
- Dampney RA, Czachurski J, Dembowski K, Goodchild AK & Seller H. (1987). Afferent connections and spinal projections of the pressor region in the rostral ventrolateral medulla of the cat. *Journal of the autonomic nervous system* **20**, 73-86.
- Dampney RA, Goodchild AK, Robertson LG & Montgomery W. (1982). Role of ventrolateral medulla in vasomotor regulation: a correlative anatomical and physiological study. *Brain research* **249**, 223-235.
- Dampney RA, Horiuchi J, Killinger S, Sheriff MJ, Tan PS & McDowall LM. (2005). Long-term regulation of arterial blood pressure by hypothalamic nuclei: some critical questions. *Clinical and experimental pharmacology & physiology* **32**, 419-425.
- Dampney RA, Horiuchi J, Tagawa T, Fontes MA, Potts PD & Polson JW. (2003). Medullary and supramedullary mechanisms regulating sympathetic vasomotor tone. *Acta physiologica Scandinavica* **177**, 209-218.
- Dampney RA & Moon EA. (1980). Role of ventrolateral medulla in vasomotor response to cerebral ischemia. *The American journal of physiology* **239**, H349-358.

- Daniel J, Polder HR, Lessmann V & Brigadski T. (2013). Single-cell juxtacellular transfection and recording technique. *Pflugers Archiv : European journal of physiology* **465**, 1637-1649.
- De Burgh Daly M. (2011). Interactions Between Respiration and Circulation. In *Comprehensive Physiology*. John Wiley & Sons, Inc.
- De Simoni A & Yu LM. (2006). Preparation of organotypic hippocampal slice cultures: interface method. *Nature protocols* **1**, 1439-1445.
- DeBruin KA & Krassowska W. (1999). Modeling electroporation in a single cell. I. Effects Of field strength and rest potential. *Biophysical journal* **77**, 1213-1224.
- Deisseroth K. (2014). Circuit dynamics of adaptive and maladaptive behaviour. *Nature* **505**, 309-317.
- Del Negro CA, Koshiya N, Butera RJ, Jr. & Smith JC. (2002a). Persistent sodium current, membrane properties and bursting behavior of pre-botzinger complex inspiratory neurons in vitro. *Journal of neurophysiology* **88**, 2242-2250.
- Del Negro CA, Morgado-Valle C & Feldman JL. (2002b). Respiratory rhythm: an emergent network property? *Neuron* **34**, 821-830.
- Del Negro CA, Morgado-Valle C, Hayes JA, Mackay DD, Pace RW, Crowder EA & Feldman JL. (2005). Sodium and calcium current-mediated pacemaker neurons and respiratory rhythm generation. *The Journal of neuroscience : the official journal of the Society for Neuroscience* **25**, 446-453.
- Dempsey B, Turner AJ, Le S, Sun Q-J, Bou Farah L, Allen AM, Goodchild AK & McMullan S. (2015). Recording, labeling, and transfection of single neurons in deep brain structures. *Physiological Reports* **3**, n/a-n/a.
- Dempsey BR. (2016). The connectome of medullary sympathetic premotor neurons. In *Faculty of Medicine and Health Science*. Macquarie University.
- Dempsey JA, Sheel AW, St Croix CM & Morgan BJ. (2002). Respiratory influences on sympathetic vasomotor outflow in humans. *Respir Physiol Neurobiol* **130**, 3-20.
- Dempsey JA, Veasey SC, Morgan BJ & O'Donnell CP. (2010). Pathophysiology of sleep apnea. *Physiological reviews* **90**, 47-112.
- Denk W, Briggman KL & Helmstaedter M. (2012). Structural neurobiology: Missing link to a mechanistic understanding of neural computation. *Nature Reviews Neuroscience* **13**, 351-358.

- Dick TE, Baekey DM, Paton JF, Lindsey BG & Morris KF. (2009). Cardio-respiratory coupling depends on the pons. *Respir Physiol Neurobiol* **168**, 76-85.
- Dick TE, Hsieh Y-H, Dhingra RR, Baekey DM, Galán RF, Wehrwein E & Morris KF. (2014). Cardiorespiratory Coupling: Common Rhythms in Cardiac, Sympathetic, and Respiratory Activities. *Progress in brain research* **209**, 191-205.
- Dick TE, Hsieh Y-H, Wang N & Prabhakar N. (2007). Acute intermittent hypoxia increases both phrenic and sympathetic nerve activities in the rat. *Experimental physiology* **92**, 87-97.
- Dick TE, Hsieh YH, Morrison S, Coles SK & Prabhakar N. (2004). Entrainment pattern between sympathetic and phrenic nerve activities in the Sprague-Dawley rat: hypoxia-evoked sympathetic activity during expiration. *American journal of physiology Regulatory, integrative and comparative physiology* **286**, R1121-1128.
- Dick TE & Morris KF. (2004). Quantitative analysis of cardiovascular modulation in respiratory neural activity. *The Journal of physiology* **556**, 959-970.
- Dick TE, Shannon R, Lindsey BG, Nuding SC, Segers LS, Baekey DM & Morris KF. (2005). Arterial pulse modulated activity is expressed in respiratory neural output. *Journal of applied physiology (Bethesda, Md : 1985)* **99**, 691-698.
- DiMicco JA, Samuels BC, Zaretskaia MV & Zaretsky DV. (2002). The dorsomedial hypothalamus and the response to stress: part renaissance, part revolution. *Pharmacology, biochemistry, and behavior* **71**, 469-480.
- Dobbins EG & Feldman JL. (1994). Brainstem network controlling descending drive to phrenic motoneurons in rat. *The Journal of comparative neurology* **347**, 64-86.
- Dubreuil V, Ramanantsoa N, Trochet D, Vaubourg V, Amiel J, Gallego J, Brunet JF & Golidis C. (2008). A human mutation in Phox2b causes lack of CO2 chemosensitivity, fatal central apnea, and specific loss of parafacial neurons. *Proceedings of the National Academy of Sciences of the United States of America* **105**, 1067-1072.
- Duffin J & Douse MA. (1993). Botzinger expiratory neurones inhibit propriobulbar decrementing inspiratory neurones. *Neuroreport* **4**, 1215-1218.
- Dutschmann M & Dick TE. (2012). Pontine mechanisms of respiratory control. *Comprehensive Physiology* **2**, 2443-2469.
- Dutschmann M & Herbert H. (2006). The Kolliker-Fuse nucleus gates the postinspiratory phase of the respiratory cycle to control inspiratory off-switch and upper airway resistance in rat. *The European journal of neuroscience* **24**, 1071-1084.

- Dutschmann M, Jones SE, Subramanian HH, Stanic D & Bautista TG. (2014). The physiological significance of postinspiration in respiratory control. *Prog Brain Res* **212**, 113-130.
- Eckberg DL, Nerhed C & Wallin BG. (1985). Respiratory modulation of muscle sympathetic and vagal cardiac outflow in man. *The Journal of physiology* **365**, 181-196.
- Edwards FA, Konnerth A, Sakmann B & Takahashi T. (1989). A thin slice preparation for patch clamp recordings from neurones of the mammalian central nervous system. *Pflugers Arch* **414**, 600-612.
- Ellenberger HH. (1999). Distribution of bulbospinal gamma-aminobutyric acid-synthesizing neurons of the ventral respiratory group of the rat. *The Journal of comparative neurology* **411**, 130-144.
- Ellenberger HH & Feldman JL. (1990). Subnuclear organization of the lateral tegmental field of the rat. I: Nucleus ambiguus and ventral respiratory group. *The Journal of comparative neurology* **294**, 202-211.
- Esler M. (2000). The sympathetic system and hypertension. *American journal of hypertension* **13**, 99S-105S.
- Esler M, Lambert E & Schlaich M. (2010). Point: Chronic activation of the sympathetic nervous system is the dominant contributor to systemic hypertension. *Journal of applied physiology (Bethesda, Md : 1985)* **109**, 1996-1998; discussion 2016.
- Etessami R, Conzelmann KK, Fadaei-Ghotbi B, Natelson B, Tsiang H & Ceccaldi PE. (2000). Spread and pathogenic characteristics of a G-deficient rabies virus recombinant: an in vitro and in vivo study. *The Journal of general virology* **81**, 2147-2153.
- Ezure K & Manabe M. (1988). Decrementing expiratory neurons of the Botzinger complex. II. Direct inhibitory synaptic linkage with ventral respiratory group neurons. *Experimental brain research* **72**, 159-166.
- Ezure K, Manabe M & Yamada H. (1988). Distribution of medullary respiratory neurons in the rat. *Brain research* **455**, 262-270.
- Ezure K, Tanaka I & Kondo M. (2003a). Glycine is used as a transmitter by decrementing expiratory neurons of the ventrolateral medulla in the rat. *The Journal of neuroscience : the official journal of the Society for Neuroscience* **23**, 8941-8948.
- Ezure K, Tanaka I & Saito Y. (2003b). Brainstem and spinal projections of augmenting expiratory neurons in the rat. *Neuroscience research* **45**, 41-51.

- Farmer DG, Dutschmann M, Paton JF, Pickering AE & McAllen RM. (2016). Brainstem sources of cardiac vagal tone and respiratory sinus arrhythmia. *The Journal of physiology*.
- Federspiel MJ, Bates P, Young JA, Varmus HE & Hughes SH. (1994). A system for tissue-specific gene targeting: transgenic mice susceptible to subgroup A avian leukosis virus-based retroviral vectors. *Proceedings of the National Academy of Sciences of the United States of America* **91**, 11241-11245.
- Feldman JL & Del Negro CA. (2006). Looking for inspiration: new perspectives on respiratory rhythm. *Nat Rev Neurosci* **7**, 232-242.
- Feldman JL, Del Negro CA & Gray PA. (2013). Understanding the rhythm of breathing: So near, yet so far. In *Annual review of physiology*, pp. 423-452.
- Feldman JL & Ellenberger HH. (1988). Central coordination of respiratory and cardiovascular control in mammals. *Annual review of physiology* **50**, 593-606.
- Feldman JL & Kam K. (2014). Facing the challenge of mammalian neural microcircuits: Taking a few breaths may help. *The Journal of physiology*.
- Fenno LE, Mattis J, Ramakrishnan C, Hyun M, Lee SY, He M, Tucciarone J, Selimbeyoglu A, Berndt A, Grosenick L, Zalocusky KA, Bernstein H, Swanson H, Perry C, Diester I, Boyce FM, Bass CE, Neve R, Huang ZJ & Deisseroth K. (2014). Targeting cells with single vectors using multiple-feature Boolean logic. *Nature methods* **11**, 763-772.
- Fischer T, Doll C, Jacobs S, Kolodziej A, Stumm R & Schulz S. (2008). Reassessment of sst2 Somatostatin Receptor Expression in Human Normal and Neoplastic Tissues Using the Novel Rabbit Monoclonal Antibody UMB-1. *The Journal of Clinical Endocrinology & Metabolism* **93**, 4519-4524.
- Fishman RA. (1994). Origins of neuroscience: A history of explorations into brain function. By Stanley Finger, New York, Oxford University Press, 1994, 462 pp, illustrated, \$75.00. *Annals of Neurology* **36**, 807-807.
- Fletcher EC. (2001). Invited review: Physiological consequences of intermittent hypoxia: systemic blood pressure. *Journal of applied physiology (Bethesda, Md : 1985)* **90**, 1600-1605.
- Fletcher EC, Lesske J, Behm R, Miller CC, 3rd, Stauss H & Unger T. (1992a). Carotid chemoreceptors, systemic blood pressure, and chronic episodic hypoxia mimicking sleep apnea. *Journal of applied physiology (Bethesda, Md : 1985)* **72**, 1978-1984.
- Fletcher EC, Lesske J, Qian W, Miller CC, 3rd & Unger T. (1992b). Repetitive, episodic hypoxia causes diurnal elevation of blood pressure in rats. *Hypertension* **19**, 555-561.

- Flytzanis NC, Bedbrook CN, Chiu H, Engqvist MKM, Xiao C, Chan KY, Sternberg PW, Arnold FH & Gradinaru V. (2014). Archaelhodopsin variants with enhanced voltage-sensitive fluorescence in mammalian and *Caenorhabditis elegans* neurons. *Nat Commun* **5**.
- Fontes MA, Tagawa T, Polson JW, Cavanagh SJ & Dampney RA. (2001). Descending pathways mediating cardiovascular response from dorsomedial hypothalamic nucleus. *American journal of physiology Heart and circulatory physiology* **280**, H2891-2901.
- Fontes MA, Xavier CH, de Menezes RC & Dimicco JA. (2011). The dorsomedial hypothalamus and the central pathways involved in the cardiovascular response to emotional stress. *Neuroscience* **184**, 64-74.
- Forlano PM & Woolley CS. (2010). Quantitative analysis of pre- and postsynaptic sex differences in the nucleus accumbens. *The Journal of comparative neurology* **518**, 1330-1348.
- Fornito A, Zalesky A & Breakspear M. (2015). The connectomics of brain disorders. *Nat Rev Neurosci* **16**, 159-172.
- Friedman L, Dick TE, Jacono FJ, Loparo KA, Yeganeh A, Fishman M, Wilson CG & Strohl KP. (2012). Cardio-ventilatory coupling in young healthy resting subjects. *Journal of applied physiology (Bethesda, Md : 1985)* **112**, 1248-1257.
- Fulwiler CE & Saper CB. (1984). Subnuclear organization of the efferent connections of the parabrachial nucleus in the rat. *Brain research* **319**, 229-259.
- Funk GD, Smith JC & Feldman JL. (1993). Generation and transmission of respiratory oscillations in medullary slices: role of excitatory amino acids. *Journal of neurophysiology* **70**, 1497-1515.
- Galletly DC & Larsen PD. (1997). Cardioventilatory coupling during anaesthesia. *British journal of anaesthesia* **79**, 35-40.
- Gaytan SP, Calero F, Nunez-Abades PA, Morillo AM & Pasaro R. (1997). Pontomedullary efferent projections of the ventral respiratory neuronal subsets of the rat. *Brain research bulletin* **42**, 323-334.
- Gebber GL & Barman SM. (1988). Studies on the origin and generation of sympathetic nerve activity. *Clinical and experimental hypertension Part A, Theory and practice* **10 Suppl 1**, 33-44.
- Gestreau C, Heitzmann D, Thomas J, Dubreuil V, Bandulik S, Reichold M, Bendahhou S, Pierson P, Sterner C, Peyronnet-Roux J, Benfriha C, Tegtmeier I, Ehnes H, Georgieff

- M, Lesage F, Brunet JF, Goridis C, Warth R & Barhanin J. (2010). Task2 potassium channels set central respiratory CO₂ and O₂ sensitivity. *Proceedings of the National Academy of Sciences of the United States of America* **107**, 2325-2330.
- Geue L, Schares S, Schnick C, Kliemt J, Beckert A, Freuling C, Conraths FJ, Hoffmann B, Zanoni R, Marston D, McElhinney L, Johnson N, Fooks AR, Tordo N & Muller T. (2008). Genetic characterisation of attenuated SAD rabies virus strains used for oral vaccination of wildlife. *Vaccine* **26**, 3227-3235.
- Gieroba ZJ, Li YW & Blessing WW. (1992). Characteristics of caudal ventrolateral medullary neurons antidromically activated from rostral ventrolateral medulla in the rabbit. *Brain research* **582**, 196-207.
- Ginger M, Haberl M, Conzelmann K-K, Schwarz MK & Frick A. (2013). Revealing the secrets of neuronal circuits with recombinant rabies virus technology. *Frontiers in Neural Circuits* **7**, 2.
- Gonatas NK, Harper C, Mizutani T & Gonatas JO. (1979). Superior sensitivity of conjugates of horseradish peroxidase with wheat germ agglutinin for studies of retrograde axonal transport. *The journal of histochemistry and cytochemistry : official journal of the Histochemistry Society* **27**, 728-734.
- Goodchild AK, Llewellyn-Smith IJ, Sun QJ, Chalmers J, Cunningham AM & Pilowsky PM. (2000). Calbindin-immunoreactive neurons in the reticular formation of the rat brainstem: catecholamine content and spinal projections. *The Journal of comparative neurology* **424**, 547-562.
- Goodchild AK & Moon EA. (2009). Maps of cardiovascular and respiratory regions of rat ventral medulla: focus on the caudal medulla. *Journal of chemical neuroanatomy* **38**, 209-221.
- Goodchild AK, Moon EA, Dampney RA & Howe PR. (1984). Evidence that adrenaline neurons in the rostral ventrolateral medulla have a vasopressor function. *Neuroscience letters* **45**, 267-272.
- Gordon FJ & McCann LA. (1988). Pressor responses evoked by microinjections of L-glutamate into the caudal ventrolateral medulla of the rat. *Brain research* **457**, 251-258.
- Granata AR & Chang HT. (1994). Relationship of calbindin D-28k with afferent neurons to the rostral ventrolateral medulla in the rat. *Brain research* **645**, 265-277.
- Granata AR, Numao Y, Kumada M & Reis DJ. (1986). A1 noradrenergic neurons tonically inhibit sympathoexcitatory neurons of C1 area in rat brainstem. *Brain research* **377**, 127-146.

- Grassi G. (1998). Role of the sympathetic nervous system in human hypertension. *Journal of hypertension* **16**, 1979-1987.
- Gray PA. (2013). Transcription factors define the neuroanatomical organization of the medullary reticular formation. *Frontiers in neuroanatomy* **7**, 7.
- Gray PA, Hayes JA, Ling GY, Llona I, Tupal S, Picardo MC, Ross SE, Hirata T, Corbin JG, Eugenin J & Del Negro CA. (2010). Developmental origin of preBotzinger complex respiratory neurons. *The Journal of neuroscience : the official journal of the Society for Neuroscience* **30**, 14883-14895.
- Gray PA, Janczewski WA, Mellen N, McCrimmon DR & Feldman JL. (2001). Normal breathing requires preBotzinger complex neurokinin-1 receptor-expressing neurons. *Nat Neurosci* **4**, 927-930.
- Gray PA, Rekling JC, Bocchiaro CM & Feldman JL. (1999). Modulation of respiratory frequency by peptidergic input to rhythmogenic neurons in the preBotzinger complex. *Science* **286**, 1566-1568.
- Grinberg LT, Rueb U & Heinsen H. (2011). Brainstem: Neglected Locus in Neurodegenerative Diseases. *Frontiers in Neurology* **2**, 42.
- Grosenick L, Marshel JH & Deisseroth K. (2015). Closed-loop and activity-guided optogenetic control. *Neuron* **86**, 106-139.
- Guertzenstein PG & Silver A. (1974). Fall in blood pressure produced from discrete regions of the ventral surface of the medulla by glycine and lesions. *Journal of Physiology* **242**, 489-503.
- Guyenet PG. (2006). The sympathetic control of blood pressure. *Nat Rev Neurosci* **7**, 335-346.
- Guyenet PG. (2011). Regulation of Breathing and Autonomic Outflows by Chemoreceptors. In *Comprehensive Physiology*. John Wiley & Sons, Inc.
- Guyenet Patrice G & Bayliss Douglas A. (2015). Neural Control of Breathing and CO2 Homeostasis. *Neuron* **87**, 946-961.
- Guyenet PG, Darnall RA & Riley TA. (1990). Rostral ventrolateral medulla and sympathorespiratory integration in rats. *The American journal of physiology* **259**, R1063-1074.
- Guyenet PG, Sevigny CP, Weston MC & Stornetta RL. (2002). Neurokinin-1 receptor-expressing cells of the ventral respiratory group are functionally heterogeneous and

- predominantly glutamatergic. *The Journal of neuroscience : the official journal of the Society for Neuroscience* **22**, 3806-3816.
- Guyenet PG, Stornetta RL & Bayliss DA. (2010). Central respiratory chemoreception. *The Journal of comparative neurology* **518**, 3883-3906.
- Guyenet PG & Wang H. (2001). Pre-Botzinger neurons with preinspiratory discharges "in vivo" express NK1 receptors in the rat. *Journal of neurophysiology* **86**, 438-446.
- Haas K, Sin WC, Javaherian A, Li Z & Cline HT. (2001). Single-cell electroporation for gene transfer in vivo. *Neuron* **29**, 583-591.
- Habler HJ, Janig W & Michaelis M. (1994). Respiratory modulation in the activity of sympathetic neurones. *Prog Neurobiol* **43**, 567-606.
- Hagmann P. (2005). From diffusion MRI to brain connectomics. EPFL.
- Hallgren E, Migeotte PF, Kornilova L, Deliere Q, Fransen E, Glukhikh D, Moore ST, Clement G, Diedrich A, MacDougall H & Wuyts FL. (2015). Dysfunctional vestibular system causes a blood pressure drop in astronauts returning from space. *Scientific reports* **5**, 17627.
- Halliburton WD. (1919). TRAUBE WAVES AND MAYER WAVES. *Quarterly Journal of Experimental Physiology* **12**, 227-229.
- Hancock MB. (1988). Evidence for direct projections from the nucleus of the solitary tract onto medullary adrenaline cells. *The Journal of comparative neurology* **276**, 460-467.
- Hardy SGP. (2001). Hypothalamic projections to cardiovascular centers of the medulla. *Brain research* **894**, 233-240.
- Haselton JR & Guyenet PG. (1989a). Central respiratory modulation of medullary sympathoexcitatory neurons in rat. *The American journal of physiology* **256**, R739-750.
- Haselton JR & Guyenet PG. (1989b). Electrophysiological characterization of putative C1 adrenergic neurons in the rat. *Neuroscience* **30**, 199-214.
- Hayano J, Yasuma F, Okada A, Mukai S & Fujinami T. (1996). Respiratory sinus arrhythmia. A phenomenon improving pulmonary gas exchange and circulatory efficiency. *Circulation* **94**, 842-847.

- Hayashi F, Coles SK & McCrimmon DR. (1996). Respiratory neurons mediating the Breuer-Hering reflex prolongation of expiration in rat. *The Journal of neuroscience : the official journal of the Society for Neuroscience* **16**, 6526-6536.
- Head GA. (1995). Baroreflexes and cardiovascular regulation in hypertension. *Journal of cardiovascular pharmacology* **26 Suppl 2**, S7-16.
- Helmstaedter M. (2013). Cellular-resolution connectomics: challenges of dense neural circuit reconstruction. *Nature methods* **10**, 501-507.
- Henriksen S, Pang R & Wronkiewicz M. (2016). A simple generative model of the mouse mesoscale connectome. *eLife* **5**, e12366.
- Herbert H, Moga MM & Saper CB. (1990). Connections of the parabrachial nucleus with the nucleus of the solitary tract and the medullary reticular formation in the rat. *The Journal of comparative neurology* **293**, 540-580.
- Hökfelt T, Fuxe K, Goldstein M & Johansson O. (1973). Evidence for adrenaline neurons in the rat brain. *Acta physiologica Scandinavica* **89**, 286-288.
- Hökfelt T, Fuxe K, Goldstein M & Johansson O. (1974). Immunohistochemical evidence for the existence of adrenaline neurons in the rat brain. *Brain research* **66**, 235-251.
- Horikawa K & Armstrong WE. (1988). A versatile means of intracellular labeling: injection of biocytin and its detection with avidin conjugates. *Journal of neuroscience methods* **25**, 1-11.
- Horiuchi J, Potts PD, Polson JW & Dampney RA. (1999). Distribution of neurons projecting to the rostral ventrolateral medullary pressor region that are activated by sustained hypotension. *Neuroscience* **89**, 1319-1329.
- Horn AKE & Büttner-Ennever JA. (1990). The time course of retrograde transsynaptic transport of tetanus toxin fragment C in the oculomotor system of the rabbit after injection into extraocular eye muscles. *Experimental brain research* **81**, 353-362.
- Hosoya Y, Sugiura Y, Okado N, Loewy AD & Kohno K. (1991). Descending input from the hypothalamic paraventricular nucleus to sympathetic preganglionic neurons in the rat. *Experimental brain research* **85**, 10-20.
- Houweling AR & Brecht M. (2008). Behavioural report of single neuron stimulation in somatosensory cortex. *Nature* **451**, 65-68.
- Huckstepp RT, Cardoza KP, Henderson LE & Feldman JL. (2015). Role of parafacial nuclei in control of breathing in adult rats. **35**, 1052-1067.

- Huckstepp RTR, Henderson LE, Cardoza KP & Feldman JL. (2016). Interactions between respiratory oscillators in adult rats. *eLife* **5**, e14203.
- Humphrey DR & Schmidt EM. (1990). Extracellular Single-Unit Recording Methods. In *Neuromethods: Neurophysiological Techniques Applications to Neural Systems*, ed. Boulton AA, Baker GB & Vanderwolf CH, pp. 1-64.
- Hwang DY, Carlezon WA, Jr., Isacson O & Kim KS. (2001). A high-efficiency synthetic promoter that drives transgene expression selectively in noradrenergic neurons. *Human gene therapy* **12**, 1731-1740.
- Iceman KE & Harris MB. (2014). A group of non-serotonergic cells is CO₂-stimulated in the medullary raphe. *Neuroscience* **259**, 203-213.
- Iscue S. (1998). Control of abdominal muscles. *Progress in Neurobiology* **56**, 433-506.
- Ito S, Hiratsuka M, Komatsu K, Tsukamoto K, Kanmatsuse K & Sved AF. (2003). Ventrolateral medulla AT₁ receptors support arterial pressure in Dahl salt-sensitive rats. *Hypertension* **41**, 744-750.
- Ito S & Sved AF. (1997). Tonic glutamate-mediated control of rostral ventrolateral medulla and sympathetic vasomotor tone. *The American journal of physiology* **273**, R487-494.
- Janczewski WA & Feldman JL. (2006). Distinct rhythm generators for inspiration and expiration in the juvenile rat. *The Journal of physiology* **570**, 407-420.
- Janczewski WA, Tashima A, Hsu P, Cui Y & Feldman JL. (2013). Role of inhibition in respiratory pattern generation. *The Journal of neuroscience : the official journal of the Society for Neuroscience* **33**, 5454-5465.
- Jegou S, Cartier D, Dubessy C, Gonzalez BJ, Chatenet D, Tostivint H, Scalbert E, LePrince J, Vaudry H & Lihmann I. (2006). Localization of the urotensin II receptor in the rat central nervous system. *The Journal of comparative neurology* **495**, 21-36.
- Jiang C & Lipski J. (1990). Extensive monosynaptic inhibition of ventral respiratory group neurons by augmenting neurons in the Botzinger complex in the cat. *Experimental brain research* **81**, 639-648.
- Jiang X, Wang G, Lee AJ, Stornetta RL & Zhu JJ. (2013). The organization of two new cortical interneuronal circuits. *Nature Neuroscience* **16**, 210-218.
- Johnson SM, Smith JC, Funk GD & Feldman JL. (1994). Pacemaker behavior of respiratory neurons in medullary slices from neonatal rat. *Journal of neurophysiology* **72**, 2598-2608.

- Judkewitz B, Rizzi M, Kitamura K & Häusser M. (2009). Targeted single-cell electroporation of mammalian neurons in vivo. *Nature protocols* **4**, 862-869.
- Judy WV & Farrell SK. (1979). Arterial baroreceptor reflex control of sympathetic nerve activity in the spontaneously hypertensive rat. *Hypertension* **1**, 605-614.
- Kanbar R, Depuy SD, West GH, Stornetta RL & Guyenet PG. (2011). Regulation of visceral sympathetic tone by A5 noradrenergic neurons in rodents. *The Journal of physiology* **589**, 903-917.
- Kanbar R, Stornetta RL, Cash DR, Lewis SJ & Guyenet PG. (2010). Photostimulation of Phox2b medullary neurons activates cardiorespiratory function in conscious rats. *Am J Respir Crit Care Med* **182**, 1184-1194.
- Kanjhan R, Lipski J, Kruszevska B & Rong W. (1995). A comparative study of pre-sympathetic and Botzinger neurons in the rostral ventrolateral medulla (RVLM) of the rat. *Brain research* **699**, 19-32.
- Karemaker JM. (1999). Autonomic integration: the physiological basis of cardiovascular variability. *The Journal of physiology* **517**, 316-316.
- Kasparov S, Teschemacher AG, Hwang DY, Kim KS, Lonergan T & Paton JF. (2004). Viral vectors as tools for studies of central cardiovascular control. *Progress in biophysics and molecular biology* **84**, 251-277.
- Kawaguchi Y, Cooper B, Gannon M, Ray M, MacDonald RJ & Wright CV. (2002). The role of the transcriptional regulator Ptf1a in converting intestinal to pancreatic progenitors. *Nature genetics* **32**, 128-134.
- Kelly RM & Strick PL. (2000). Rabies as a transneuronal tracer of circuits in the central nervous system. *Journal of neuroscience methods* **103**, 63-71.
- Kenney MJ, Weiss ML & Haywood JR. (2003). The paraventricular nucleus: an important component of the central neurocircuitry regulating sympathetic nerve outflow. *Acta physiologica Scandinavica* **177**, 7-15.
- Kim EJ, Jacobs MW, Ito-Cole T & Callaway EM. (2016). Improved Monosynaptic Neural Circuit Tracing Using Engineered Rabies Virus Glycoproteins. *Cell reports*.
- Kim HS, Seo H, Yang C, Brunet JF & Kim KS. (1998). Noradrenergic-specific transcription of the dopamine beta-hydroxylase gene requires synergy of multiple cis-acting elements including at least two Phox2a-binding sites. *The Journal of neuroscience : the official journal of the Society for Neuroscience* **18**, 8247-8260.

- Kimura KD, Miyawaki A, Matsumoto K & Mori I. (2004). The C. elegans thermosensory neuron AFD responds to warming. *Current biology : CB* **14**, 1291-1295.
- Kitamura K, Judkewitz B, Kano M, Denk W & Hausser M. (2008a). Targeted patch-clamp recordings and single-cell electroporation of unlabeled neurons in vivo. *Nature methods* **5**, 61-67.
- Kitamura K, Judkewitz B, Kano M, Denk W & Hausser M. (2008b). Targeted patch-clamp recordings and single-cell electroporation of unlabeled neurons in vivo. *Nat Methods* **5**, 61-67.
- Koizumi H, Koshiya N, Chia JX, Cao F, Nugent J, Zhang R & Smith JC. (2013). Structural-Functional Properties of Identified Excitatory and Inhibitory Interneurons within Pre-Botzinger Complex Respiratory Microcircuits. *The Journal of neuroscience : the official journal of the Society for Neuroscience* **33**, 2994-3009.
- Koizumi H, Mosher B, Tariq MF, Zhang R, Koshiya N & Smith JC. (2016a). Voltage-Dependent Rhythmogenic Property of Respiratory Pre-Botzinger Complex Glutamatergic, Dbx1-Derived, and Somatostatin-Expressing Neuron Populations Revealed by Graded Optogenetic Inhibition. *eNeuro* **3**.
- Koizumi H, Mosher B, Tariq MF, Zhang R, Koshiya N & Smith JC. (2016b). Voltage-Dependent Rhythmogenic Property of Respiratory Pre-Bötzing Complex Glutamatergic, Dbx1-Derived, and Somatostatin-Expressing Neuron Populations Revealed by Graded Optogenetic Inhibition. *eneuro* **3**.
- Korner M, Eltschinger V, Waser B, Schonbrunn A & Reubi JC. (2005). Value of immunohistochemistry for somatostatin receptor subtype sst2A in cancer tissues: lessons from the comparison of anti-sst2A antibodies with somatostatin receptor autoradiography. *The American journal of surgical pathology* **29**, 1642-1651.
- Korner M, Waser B, Schonbrunn A, Perren A & Reubi JC. (2012). Somatostatin receptor subtype 2A immunohistochemistry using a new monoclonal antibody selects tumors suitable for in vivo somatostatin receptor targeting. *The American journal of surgical pathology* **36**, 242-252.
- Koshiya N & Guyenet PG. (1996). Tonic sympathetic chemoreflex after blockade of respiratory rhythmogenesis in the rat. *The Journal of physiology* **491**, 859-869.
- Koshiya N & Smith JC. (1999). Neuronal pacemaker for breathing visualized in vitro. *Nature* **400**, 360-363.
- Kumar NN, Velic A, Soliz J, Shi Y, Li K, Wang S, Weaver JL, Sen J, Abbott SB, Lazarenko RM, Ludwig MG, Perez-Reyes E, Mohebbi N, Bettoni C, Gassmann M, Suply T, Seuwen K, Guyenet PG, Wagner CA & Bayliss DA. (2015). *PHYSIOLOGY*.

Regulation of breathing by CO₂ requires the proton-activated receptor GPR4 in retrotrapezoid nucleus neurons. *Science* **348**, 1255-1260.

Lander ES. (2011). Initial impact of the sequencing of the human genome. *Nature* **470**, 187-197.

Larsen PD & Galletly DC. (1999). Cardioventilatory coupling in the anaesthetised rabbit, rat and guinea-pig. *Pflugers Archiv : European journal of physiology* **437**, 910-916.

Lazarenko RM, Milner TA, Depuy SD, Stornetta RL, West GH, Kievits JA, Bayliss DA & Guyenet PG. (2009). Acid sensitivity and ultrastructure of the retrotrapezoid nucleus in Phox2b-EGFP transgenic mice. *The Journal of comparative neurology* **517**, 69-86.

Le S, Turner AJ, Parker LM, Burke PG, Kumar NN, Goodchild AK & McMullan S. (2016). Somatostatin 2a receptors are not expressed on functionally identified respiratory neurons in the ventral respiratory column of the rat. *The Journal of comparative neurology* **524**, 1384-1398.

Lecolle K, Begard S, Caillierez R, Demeyer D, Grellier E, Loyens A, Csaba Z, Beauvillain JC, D'Halluin JC, Baroncini M, Lejeune JP, Sharif A, Prevot V, Dournaud P, Buee L & Colin M. (2013). Sstr2A: a relevant target for the delivery of genes into human glioblastoma cells using fiber-modified adenoviral vectors. *Gene Ther* **20**, 283-297.

Lee RM, Triggle CR, Cheung DW & Coughlin MD. (1987). Structural and functional consequence of neonatal sympathectomy on the blood vessels of spontaneously hypertensive rats. *Hypertension* **10**, 328-338.

Len WB & Chan JY. (1999). Glutamatergic projection to RVLM mediates suppression of reflex bradycardia by parabrachial nucleus. *The American journal of physiology* **276**, H1482-1492.

Lentz TL, Burrage TG, Smith AL, Crick J & Tignor GH. (1982). Is the acetylcholine receptor a rabies virus receptor? *Science* **215**, 182-184.

Li A, Randall M & Nattie EE. (1999). CO₂ microdialysis in retrotrapezoid nucleus of the rat increases breathing in wakefulness but not in sleep. *Journal of applied physiology (Bethesda, Md : 1985)* **87**, 910-919.

Li C-yT, Poo M-m & Dan Y. (2009). Burst Spiking of a Single Cortical Neuron Modifies Global Brain State. *Science (New York, NY)* **324**, 643-646.

Li F, Ryu BY, Krueger RL, Heldt SA & Albritton LM. (2012). Targeted Entry via Somatostatin Receptors Using a Novel Modified Retrovirus Glycoprotein That Delivers Genes at Levels Comparable to Those of Wild-Type Viral Glycoproteins. *Journal of virology* **86**, 373-381.

- Li P, Janczewski WA, Yackle K, Kam K, Pagliardini S, Krasnow MA & Feldman JL. (2016). The peptidergic control circuit for sighing. *Nature* **530**, 293-297.
- Li YW, Wesselingh SL & Blessing WW. (1992). Projections from rabbit caudal medulla to C1 and A5 sympathetic premotor neurons, demonstrated with phaseolus leucoagglutinin and herpes simplex virus. *The Journal of comparative neurology* **317**, 379-395.
- Lichtman JW, Pfister H & Shavit N. (2014). The big data challenges of connectomics. *Nat Neurosci* **17**, 1448-1454.
- Lin Y, Tsuchihashi T, Matsumura K, Abe I & Iida M. (2003). Central cardiovascular action of urotensin II in conscious rats. *Journal of hypertension* **21**, 159-165.
- Lindemann C, Alam M, Krauss JK & Schwabe K. (2013). Neuronal activity in the medial associative-limbic and lateral motor part of the rat subthalamic nucleus and the effect of 6-hydroxydopamine-induced lesions of the dorsolateral striatum. *The Journal of comparative neurology* **521**, 3226-3240.
- Lindsey BG, Rybak IA & Smith JC. (2012). Computational models and emergent properties of respiratory neural networks. *Comprehensive Physiology* **2**, 1619-1670.
- Lipski J, Kanjhan R, Kruszewska B & Smith M. (1995). Barosensitive neurons in the rostral ventrolateral medulla of the rat in vivo: morphological properties and relationship to C1 adrenergic neurons. *Neuroscience* **69**, 601-618.
- Liu YJ, Ehrenguber MU, Negwer M, Shao HJ, Cetin AH & Lyon DC. (2013). Tracing inputs to inhibitory or excitatory neurons of mouse and cat visual cortex with a targeted rabies virus. *Current biology : CB* **23**, 1746-1755.
- Livingston CA & Berger AJ. (1989). Immunocytochemical localization of GABA in neurons projecting to the ventrolateral nucleus of the solitary tract. *Brain research* **494**, 143-150.
- Llona I, Ampuero E & Eugenin JL. (2004). Somatostatin inhibition of fictive respiration is modulated by pH. *Brain research* **1026**, 136-142.
- Lonergan T, Teschemacher AG, Hwang DY, Kim KS, Pickering AE & Kasparov S. (2005). Targeting brain stem centers of cardiovascular control using adenoviral vectors: impact of promoters on transgene expression. *Physiological genomics* **20**, 165-172.
- Lopez-Munoz F, Boya J & Alamo C. (2006). Neuron theory, the cornerstone of neuroscience, on the centenary of the Nobel Prize award to Santiago Ramon y Cajal. *Brain research bulletin* **70**, 391-405.

- Lovick TA. (1985). Projections from the diencephalon and mesencephalon to nucleus paragigantocellularis lateralis in the cat. *Neuroscience* **14**, 853-861.
- Lovick TA. (1986). Projections from brainstem nuclei to the nucleus paragigantocellularis lateralis in the cat. *Journal of the autonomic nervous system* **16**, 1-11.
- Low MJ, Otero-Corchon V, Parlow AF, Ramirez JL, Kumar U, Patel YC & Rubinstein M. (2001). Somatostatin is required for masculinization of growth hormone-regulated hepatic gene expression but not of somatic growth. *The Journal of clinical investigation* **107**, 1571-1580.
- Lu Y, Zou CJ, Huang DW & Tang CS. (2002). Cardiovascular effects of urotensin II in different brain areas. *Peptides* **23**, 1631-1635.
- Luo L, Callaway EM & Svoboda K. (2008). Genetic Dissection of Neural Circuits. *Neuron* **57**, 634-660.
- Luppi PH, Sakai K, Salvert D, Fort P & Jouvet M. (1987). Peptidergic hypothalamic afferents to the cat nucleus raphe pallidus as revealed by a double immunostaining technique using unconjugated cholera toxin as a retrograde tracer. *Brain research* **402**, 339-345.
- Madden CJ, Ito S, Rinaman L, Wiley RG & Sved AF. (1999). Lesions of the C1 catecholaminergic neurons of the ventrolateral medulla in rats using anti-DbetaH-saporin. *The American journal of physiology* **277**, R1063-1075.
- Makeham JM, Goodchild AK & Pilowsky PM. (2001). NK1 receptor and the ventral medulla of the rat: Bulbosplinal and catecholaminergic neurons. *NeuroReport* **12**, 3663-3667.
- Malpas SC. (1998). The rhythmicity of sympathetic nerve activity. *Prog Neurobiol* **56**, 65-96.
- Malpas SC. (2010). Sympathetic nervous system overactivity and its role in the development of cardiovascular disease. *Physiological reviews* **90**, 513-557.
- Mandel DA & Schreihof AM. (2006). Central respiratory modulation of barosensitive neurones in rat caudal ventrolateral medulla. *The Journal of physiology* **572**, 881-896.
- Marchenko V, Koizumi H, Mosher B, Koshiya N, Tariq MF, Bezdudnaya TG, Zhang R, Molkov YI, Rybak IA & Smith JC. (2016). Perturbations of Respiratory Rhythm and Pattern by Disrupting Synaptic Inhibition within Pre-Botzinger and Botzinger Complexes. *eNeuro* **3**.
- Margrie TW, Brecht M & Sakmann B. (2002). In vivo, low-resistance, whole-cell recordings from neurons in the anaesthetized and awake mammalian brain. *Pflügers Archiv : European journal of physiology* **444**, 491-498.

- Marina N, Abdala AP, Korsak A, Simms AE, Allen AM, Paton JF & Gourine AV. (2011). Control of sympathetic vasomotor tone by catecholaminergic C1 neurones of the rostral ventrolateral medulla oblongata. *Cardiovascular research* **91**, 703-710.
- Marina N, Abdala AP, Trapp S, Li A, Nattie EE, Hewinson J, Smith JC, Paton JF & Gourine AV. (2010). Essential role of Phox2b-expressing ventrolateral brainstem neurons in the chemosensory control of inspiration and expiration. *The Journal of neuroscience : the official journal of the Society for Neuroscience* **30**, 12466-12473.
- Marshall JH, Mori T, Nielsen KJ & Callaway EM. (2010). Targeting single neuronal networks for gene expression and cell labeling in vivo. *Neuron* **67**, 562-574.
- Maskos U, Kiss K, St Clément C & Brulet P. (2002). Retrograde trans-synaptic transfer of green fluorescent protein allows the genetic mapping of neuronal circuits in transgenic mice. *Proceedings of the National Academy of Sciences of the United States of America* **99**, 10120-10125.
- McAllen RM. (1987). Central respiratory modulation of subretrofacial bulbospinal neurones in the cat. *The Journal of physiology* **388**, 533-545.
- McBryde FD, Abdala AP, Hendy EB, Pijacka W, Marvar P, Moraes DJ, Sobotka PA & Paton JF. (2013). The carotid body as a putative therapeutic target for the treatment of neurogenic hypertension. *Nat Commun* **4**, 2395.
- McCrea RA & Baker R. (1985). Cytology and intrinsic organization of the perihypoglossal nuclei in the cat. *The Journal of comparative neurology* **237**, 360-376.
- McKay LC & Feldman JL. (2008). Unilateral ablation of pre-Bötzinger complex disrupts breathing during sleep but not wakefulness. *Am J Respir Crit Care Med* **178**, 89-95.
- McKay LC, Janczewski WA & Feldman JL. (2005). Sleep-disordered breathing after targeted ablation of pre-Bötzinger complex neurons. *Nat Neurosci* **8**, 1142-1144.
- McMullan S, Dick TE, Farnham MM & Pilowsky PM. (2009). Effects of baroreceptor activation on respiratory variability in rat. *Respir Physiol Neurobiol* **166**, 80-86.
- McMullan S, Pathmanandavel K, Pilowsky PM & Goodchild AK. (2008). Somatic nerve stimulation evokes qualitatively different somatosympathetic responses in the cervical and splanchnic sympathetic nerves in the rat. *Brain research* **1217**, 139-147.
- McMullan S & Pilowsky PM. (2010). The effects of baroreceptor stimulation on central respiratory drive: A review. *Respiratory Physiology & Neurobiology* **174**, 37-42.

- McMullan S & Pilowsky PM. (2012). Sympathetic premotor neurones project to and are influenced by neurones in the contralateral rostral ventrolateral medulla of the rat in vivo. *Brain research* **1439**, 34-43.
- Mebatsion T, König M & Conzelmann K-K. (1996). Budding of Rabies Virus Particles in the Absence of the Spike Glycoprotein. *Cell* **84**, 941-951.
- Migliore M & Shepherd GM. (2005). An integrated approach to classifying neuronal phenotypes. *Nat Rev Neurosci* **6**, 810-818.
- Miles R & Wong RK. (1983). Single neurones can initiate synchronized population discharge in the hippocampus. *Nature* **306**, 371-373.
- Mileykovskiy BY, Kiyashchenko LI & Siegel JM. (2005). Behavioral correlates of activity in identified hypocretin/orexin neurons. *Neuron* **46**, 787-798.
- Milner TA, Reis DJ & Giuliano R. (1996). Afferent sources of substance P in the C1 area of the rat rostral ventrolateral medulla. *Neuroscience letters* **205**, 37-40.
- Minson JB, Llewellyn-Smith IJ, Chalmers JP, Pilowsky PM & Arnolda LF. (1997). c-fos identifies GABA-synthesizing barosensitive neurons in caudal ventrolateral medulla. *Neuroreport* **8**, 3015-3021.
- Mitra PP. (2014). The circuit architecture of whole brains at the mesoscopic scale. *Neuron* **83**, 1273-1283.
- Miyamichi K, Amat F, Moussavi F, Wang C, Wickersham I, Wall NR, Taniguchi H, Tasic B, Huang ZJ, He Z, Callaway EM, Horowitz MA & Luo L. (2011). Cortical representations of olfactory input by trans-synaptic tracing. *Nature* **472**, 191-196.
- Miyawaki T, Goodchild AK & Pilowsky PM. (2002). Evidence for a tonic GABA-ergic inhibition of excitatory respiratory-related afferents to presympathetic neurons in the rostral ventrolateral medulla. *Brain research* **924**, 56-62.
- Miyawaki T, Minson J, Arnolda L, Chalmers J, Llewellyn-Smith I & Pilowsky P. (1996). Role of excitatory amino acid receptors in cardiorespiratory coupling in ventrolateral medulla. *The American journal of physiology* **271**, R1221-1230.
- Miyawaki T, Pilowsky P, Sun QJ, Minson J, Suzuki S, Arnolda L, Llewellyn-Smith I & Chalmers J. (1995). Central inspiration increases barosensitivity of neurons in rat rostral ventrolateral medulla. *The American journal of physiology* **268**, R909-918.
- Molkov YI, Zoccal DB, Moraes DJ, Paton JF, Machado BH & Rybak IA. (2011). Intermittent hypoxia-induced sensitization of central chemoreceptors contributes to sympathetic

- nerve activity during late expiration in rats. *Journal of neurophysiology* **105**, 3080-3091.
- Monnier A, Alheid GF & McCrimmon DR. (2003). Defining ventral medullary respiratory compartments with a glutamate receptor agonist in the rat. *The Journal of physiology* **548**, 859-874.
- Montandon G & Horner RL. (2013). State-dependent contribution of the hyperpolarization-activated Na⁺/K⁺ and persistent Na⁺ currents to respiratory rhythmogenesis in vivo. *The Journal of neuroscience : the official journal of the Society for Neuroscience* **33**, 8716-8728.
- Moore AK & Wehr M. (2014). A Guide to In vivo Single-unit Recording from Optogenetically Identified Cortical Inhibitory Interneurons. *Journal of visualized experiments : JoVE*, e51757-e51757.
- Moraes DJ, da Silva MP, Bonagamba LG, Mecawi AS, Zoccal DB, Antunes-Rodrigues J, Varanda WA & Machado BH. (2013). Electrophysiological properties of rostral ventrolateral medulla presympathetic neurons modulated by the respiratory network in rats. *The Journal of neuroscience : the official journal of the Society for Neuroscience* **33**, 19223-19237.
- Moraes DJ, Dias MB, Cavalcanti-Kwiatkoski R, Machado BH & Zoccal DB. (2012a). Contribution of the retrotrapezoid nucleus/parafacial respiratory region to the expiratory-sympathetic coupling in response to peripheral chemoreflex in rats. *Journal of neurophysiology* **108**, 882-890.
- Moraes DJ, Machado BH & Paton JF. (2014). Specific respiratory neuron types have increased excitability that drive presympathetic neurones in neurogenic hypertension. *Hypertension* **63**, 1309-1318.
- Moraes DJ, Zoccal DB & Machado BH. (2012b). Medullary respiratory network drives sympathetic overactivity and hypertension in rats submitted to chronic intermittent hypoxia. *Hypertension* **60**, 1374-1380.
- Moraes DJ, Zoccal DB & Machado BH. (2012c). Sympathoexcitation during chemoreflex active expiration is mediated by L-glutamate in the RVLM/Botzinger complex of rats. *Journal of neurophysiology* **108**, 610-623.
- Moreira TS, Takakura AC, Colombari E & Guyenet PG. (2006). Central chemoreceptors and sympathetic vasomotor outflow. *The Journal of physiology* **577**, 369-386.
- Mulkey DK, Stornetta RL, Weston MC, Simmons JR, Parker A, Bayliss DA & Guyenet PG. (2004). Respiratory control by ventral surface chemoreceptor neurons in rats. *Nat Neurosci* **7**, 1360-1369.

- Nassi JJ, Cepko CL, Born RT & Beier KT. (2015). Neuroanatomy goes viral! *Frontiers in neuroanatomy* **9**, 80.
- Nattie EE & Li A. (2002). Substance P-saporin lesion of neurons with NK1 receptors in one chemoreceptor site in rats decreases ventilation and chemosensitivity. *The Journal of physiology* **544**, 603-616.
- Nicholas AP & Hancock MB. (1990). Evidence for projections from the rostral medullary raphe onto medullary catecholamine neurons in the rat. *Neuroscience letters* **108**, 22-28.
- Nicholas AP & Hancock MB. (1991). Projections from the rostral ventrolateral medulla to brainstem monoamine neurons in the rat. *Neuroscience letters* **122**, 91-95.
- Nosedá R, Kainz V, Jakubowski M, Gooley JJ, Saper CB, Digre K & Burstein R. (2010). A neural mechanism for exacerbation of headache by light. *Nat Neurosci* **13**, 239-245.
- Numao Y, Koshiya N, Gilbey MP & Spyer KM. (1987). Central respiratory drive-related activity in sympathetic nerves of the rat: the regional differences. *Neuroscience letters* **81**, 279-284.
- Obien MEJ, Deligkaris K, Bullmann T, Bakkum DJ & Frey U. (2014). Revealing neuronal function through microelectrode array recordings. *Frontiers in Neuroscience* **8**, 423.
- Oh SW, Harris JA, Ng L, Winslow B, Cain N, Mihalas S, Wang Q, Lau C, Kuan L, Henry AM, Mortrud MT, Ouellette B, Nguyen TN, Sorensen SA, Slaughterbeck CR, Wakeman W, Li Y, Feng D, Ho A, Nicholas E, Hirokawa KE, Bohn P, Joines KM, Peng H, Hawrylycz MJ, Phillips JW, Hohmann JG, Wornoutka P, Gerfen CR, Koch C, Bernard A, Dang C, Jones AR & Zeng H. (2014). A mesoscale connectome of the mouse brain. *Nature* **508**, 207-214.
- Okazaki M, Takeda R, Haji A & Yamazaki H. (2001). Glutamic acid decarboxylase-immunoreactivity of bulbar respiratory neurons identified by intracellular recording and labeling in rats. *Brain research* **914**, 34-47.
- Onimaru H & Homma I. (1987). Respiratory rhythm generator neurons in medulla of brainstem-spinal cord preparation from newborn rat. *Brain research* **403**, 380-384.
- Onimaru H & Homma I. (2003). A novel functional neuron group for respiratory rhythm generation in the ventral medulla. *The Journal of neuroscience : the official journal of the Society for Neuroscience* **23**, 1478-1486.

- Onimaru H & Homma I. (2007). Spontaneous oscillatory burst activity in the piriform-amygdala region and its relation to in vitro respiratory activity in newborn rats. *Neuroscience* **144**, 387-394.
- Onimaru H, Kumagawa Y & Homma I. (2006). Respiration-Related Rhythmic Activity in the Rostral Medulla of Newborn Rats. *Journal of neurophysiology* **96**, 55-61.
- Osakada F & Callaway EM. (2013). Design and generation of recombinant rabies virus vectors. *Nature protocols* **8**, 1583-1601.
- Osborn JW. (2005). HYPOTHESIS: SET-POINTS and LONG-TERM CONTROL OF ARTERIAL PRESSURE. A THEORETICAL ARGUMENT FOR A LONG-TERM ARTERIAL PRESSURE CONTROL SYSTEM IN THE BRAIN RATHER THAN THE KIDNEY. *Clinical and Experimental Pharmacology and Physiology* **32**, 384-393.
- Oyama K, Ohara S, Sato S, Karube F, Fujiyama F, Isomura Y, Mushiake H, Iijima T & Tsutsui KI. (2013). Long-lasting single-neuron labeling by in vivo electroporation without microscopic guidance. *Journal of neuroscience methods* **14**, 00221-00225.
- Pace RW, Mackay DD, Feldman JL & Del Negro CA. (2007a). Inspiratory bursts in the preBotzinger complex depend on a calcium-activated non-specific cation current linked to glutamate receptors in neonatal mice. *The Journal of physiology* **582**, 113-125.
- Pace RW, Mackay DD, Feldman JL & Del Negro CA. (2007b). Role of persistent sodium current in mouse preBotzinger Complex neurons and respiratory rhythm generation. *The Journal of physiology* **580**, 485-496.
- Packer AM, Roska B & Hausser M. (2013). Targeting neurons and photons for optogenetics. *Nat Neurosci* **16**, 805-815.
- Pantaleo T, Mutolo D, Cinelli E & Bongianni F. (2011). Respiratory responses to somatostatin microinjections into the Bötzing complex and the pre-Bötzing complex of the rabbit. *Neuroscience letters* **498**, 26-30.
- Papp EA, Leergaard TB, Calabrese E, Johnson GA & Bjaalie JG. (2014). Waxholm Space atlas of the Sprague Dawley rat brain. *NeuroImage* **97**, 374-386.
- Parker LM, Kumar NN, Lonergan T, McMullan S & Goodchild AK. (2013). Distribution and neurochemical characterization of neurons in the rat ventrolateral medulla activated by glucoprivation. *Brain structure & function*.

- Paton JF, Dickinson CJ & Mitchell G. (2009). Harvey Cushing and the regulation of blood pressure in giraffe, rat and man: introducing 'Cushing's mechanism'. *Experimental physiology* **94**, 11-17.
- Pattyn A, Goridis C & Brunet JF. (2000). Specification of the central noradrenergic phenotype by the homeobox gene Phox2b. *Molecular and cellular neurosciences* **15**, 235-243.
- Pattyn A, Morin X, Cremer H, Goridis C & Brunet JF. (1997). Expression and interactions of the two closely related homeobox genes Phox2a and Phox2b during neurogenesis. *Development* **124**, 4065-4075.
- Paxinos G & Watson C. (2006). *The Rat Brain in Stereotaxic Coordinates*. Academic Press.
- Petersen Steven E & Sporns O. (2015). Brain Networks and Cognitive Architectures. *Neuron* **88**, 207-219.
- Petreanu L, Huber D, Sobczyk A & Svoboda K. (2007). Channelrhodopsin-2-assisted circuit mapping of long-range callosal projections. *Nat Neurosci* **10**, 663-668.
- Phillips JK, Goodchild AK, Dubey R, Sesiasvili E, Takeda M, Chalmers J, Pilowsky PM & Lipski J. (2001). Differential expression of catecholamine biosynthetic enzymes in the rat ventrolateral medulla. *The Journal of comparative neurology* **432**, 20-34.
- Picardo MC, Weragalaarachchi KT, Akins VT & Del Negro CA. (2013). Physiological and morphological properties of Dbx1-derived respiratory neurons in the pre-Botzinger complex of neonatal mice. *The Journal of physiology* **591**, 2687-2703.
- Pickering AE & Paton JF. (2006). A decerebrate, artificially-perfused in situ preparation of rat: utility for the study of autonomic and nociceptive processing. *Journal of neuroscience methods* **155**, 260-271.
- Pickering AE, Spanswick D & Logan SD. (1991). Whole-cell recordings from sympathetic preganglionic neurons in rat spinal cord slices. *Neuroscience letters* **130**, 237-242.
- Pilowsky P. (1995). Good vibrations? Respiratory rhythms in the central control of blood pressure. *Clinical and experimental pharmacology & physiology* **22**, 594-604.
- Pilowsky PM & Goodchild AK. (2002). Baroreceptor reflex pathways and neurotransmitters: 10 years on. *Journal of hypertension* **20**, 1675-1688.
- Pilowsky PM, Jiang C & Lipski J. (1990). An intracellular study of respiratory neurons in the rostral ventrolateral medulla of the rat and their relationship to catecholamine-containing neurons. *The Journal of comparative neurology* **301**, 604-617.

- Pinault D. (1996). A novel single-cell staining procedure performed in vivo under electrophysiological control: morpho-functional features of juxtacellularly labeled thalamic cells and other central neurons with biocytin or Neurobiotin. *Journal of neuroscience methods* **65**, 113-136.
- Pinault D. (2011). The juxtacellular recording-labeling technique. In *Electrophysiological Recording Techniques*, ed. Vertes RP & Stackman RW, pp. 41-75. Springer Science+Business Media, LLC.
- Pollak Dorocic I, Fürth D, Xuan Y, Johansson Y, Pozzi L, Silberberg G, Carlén M & Meletis K. A Whole-Brain Atlas of Inputs to Serotonergic Neurons of the Dorsal and Median Raphe Nuclei. *Neuron* **83**, 663-678.
- Poulat P, Sandillon F, Marlier L, Rajaofetra N, Oliver C & Privat A. (1992). Distribution of thyrotropin-releasing hormone in the rat spinal cord with special reference to sympathetic nuclei: a light- and electron-microscopic immunocytochemical study. *Journal of neurocytology* **21**, 157-170.
- Ptak K, Burnet H, Blanchi B, Sieweke M, De Felipe C, Hunt SP, Monteau R & Hilaire G. (2002). The murine neurokinin NK1 receptor gene contributes to the adult hypoxic facilitation of ventilation. *The European journal of neuroscience* **16**, 2245-2252.
- Pyner S & Coote JH. (2000). Identification of branching paraventricular neurons of the hypothalamus that project to the rostroventrolateral medulla and spinal cord. *Neuroscience* **100**, 549-556.
- Qiu C, Zeyda T, Johnson B, Hochgeschwender U, de Lecea L & Tallent MK. (2008). Somatostatin receptor subtype 4 couples to the M-current to regulate seizures. *The Journal of neuroscience : the official journal of the Society for Neuroscience* **28**, 3567-3576.
- Rae JL & Levis RA. (2002). Single-cell electroporation. *Pflugers Archiv : European journal of physiology* **443**, 664-670.
- Rajasethupathy P, Ferenczi E & Deisseroth K. (2016). Targeting Neural Circuits. *Cell* **165**, 524-534.
- Rajput PS, Kharmate G, Norman M, Liu SH, Sastry BR, Brunicardi CF & Kumar U. (2011). Somatostatin receptor 1 and 5 double knockout mice mimic neurochemical changes of Huntington's disease transgenic mice. *PloS one* **6**, e24467.
- Ramanantsoa N, Hirsch MR, Thoby-Brisson M, Dubreuil V, Bouvier J, Ruffault PL, Matrot B, Fortin G, Brunet JF, Gallego J & Goridis C. (2011). Breathing without CO(2) chemosensitivity in conditional Phox2b mutants. *The Journal of neuroscience : the official journal of the Society for Neuroscience* **31**, 12880-12888.

- Ramirez-Jarquin JO, Lara-Hernandez S, Lopez-Guerrero JJ, Aguilera MA, Rivera-Angulo AJ, Sampieri A, Vaca L, Ordaz B & Pena-Ortega F. (2012). Somatostatin modulates generation of inspiratory rhythms and determines asphyxia survival. *Peptides* **34**, 360-372.
- Rancz EA, Franks KM, Schwarz MK, Pichler B, Schaefer AT & Margrie TW. (2011). Transfection via whole-cell recording in vivo: bridging single-cell physiology, genetics and connectomics. *Nat Neurosci* **14**, 527-532.
- Rathenberg J, Nevian T & Witzemann V. (2003). High-efficiency transfection of individual neurons using modified electrophysiology techniques. *Journal of neuroscience methods* **126**, 91-98.
- Reardon TR, Murray AJ, Turi GF, Wirblich C, Croce KR, Schnell MJ, Jessell TM & Losonczy A. (2016). Rabies Virus CVS-N2c(DeltaG) Strain Enhances Retrograde Synaptic Transfer and Neuronal Viability. *Neuron* **89**, 711-724.
- Reiner A. (1990). The Triune Brain in Evolution. Role in Paleocerebral Functions. Paul D. MacLean. Plenum, New York, 1990. xxiv, 672 pp., illus. \$75. *Science* **250**, 303-305.
- Rekling JC, Champagnat J & Denavit-Saubie M. (1996). Electroresponsive properties and membrane potential trajectories of three types of inspiratory neurons in the newborn mouse brain stem in vitro. *Journal of neurophysiology* **75**, 795-810.
- Ricardo JA & Koh ET. (1978). Anatomical evidence of direct projections from the nucleus of the solitary tract to the hypothalamus, amygdala, and other forebrain structures in the rat. *Brain research* **153**, 1-26.
- Richter DW & Smith JC. (2014). Respiratory rhythm generation in vivo. *Physiology (Bethesda)* **29**, 58-71.
- Richter DW & Spyer KM. (2001). Studying rhythmogenesis of breathing: comparison of in vivo and in vitro models. *Trends in neurosciences* **24**, 464-472.
- Robinson FR, Phillips JO & Fuchs AF. (1994). Coordination of gaze shifts in primates: brainstem inputs to neck and extraocular motoneuron pools. *The Journal of comparative neurology* **346**, 43-62.
- Rose MF, Ren J, Ahmad KA, Chao H-T, Klisch TJ, Flora A, Greer JJ & Zoghbi HY. (2009). Math1 Is Essential for the Development of Hindbrain Neurons Critical for Perinatal Breathing. *Neuron* **64**, 341-354.
- Ross CA, Armstrong DM, Ruggiero DA, Pickel VM, Joh TH & Reis DJ. (1981). Adrenaline neurons in the rostral ventrolateral medulla innervate thoracic spinal cord: a combined

immunocytochemical and retrograde transport demonstration. *Neuroscience letters* **25**, 257-262.

- Ross CA, Ruggiero DA, Park DH, Joh TH, Sved AF, Fernandez-Pardal J, Saavedra JM & Reis DJ. (1984). Tonic vasomotor control by the rostral ventrolateral medulla: effect of electrical or chemical stimulation of the area containing C1 adrenaline neurons on arterial pressure, heart rate, and plasma catecholamines and vasopressin. *The Journal of neuroscience : the official journal of the Society for Neuroscience* **4**, 474-494.
- Ross CA, Ruggiero DA & Reis DJ. (1985). Projections from the nucleus tractus solitarii to the rostral ventrolateral medulla. *The Journal of comparative neurology* **242**, 511-534.
- Ruangkittisakul A, Kottick A, Picardo MCD, Ballanyi K & Del Negro CA. (2014). Identification of the pre - Bötzing complex inspiratory center in calibrated “sandwich” slices from newborn mice with fluorescent Dbx1 interneurons. *Physiological Reports* **2**.
- Ruffault PL, D'Autreaux F, Hayes JA, Nomaksteinsky M, Autran S, Fujiyama T, Hoshino M, Hagglund M, Kiehn O, Brunet JF, Fortin G & Goridis C. (2015). The retrotrapezoid nucleus neurons expressing Atoh1 and Phox2b are essential for the respiratory response to CO(2). *Elife* **4**.
- Saha S, Drinkhill MJ, Moore JP & Batten TF. (2005). Central nucleus of amygdala projections to rostral ventrolateral medulla neurones activated by decreased blood pressure. *The European journal of neuroscience* **21**, 1921-1930.
- Saito Y, Tanaka I & Ezure K. (2002). Morphology of the decrementing expiratory neurons in the brainstem of the rat. *Neuroscience research* **44**, 141-153.
- Santos SF, Luz LL, Szucs P, Lima D, Derkach VA & Safronov BV. (2009). Transmission efficacy and plasticity in glutamatergic synapses formed by excitatory interneurons of the substantia gelatinosa in the rat spinal cord. *PloS one* **4**, e8047.
- Santos SF, Rebelo S, Derkach VA & Safronov BV. (2007). Excitatory interneurons dominate sensory processing in the spinal substantia gelatinosa of rat. *The Journal of physiology* **581**, 241-254.
- Saper CB & Loewy AD. (1980). Efferent connections of the parabrachial nucleus in the rat. *Brain research* **197**, 291-317.
- Sartor DM & Verberne AJM. (2003). Phenotypic identification of rat rostroventrolateral medullary presympathetic vasomotor neurons inhibited by exogenous cholecystokinin. *Journal of Comparative Neurology* **465**, 467-479.

- Schlaich MP, Lambert E, Kaye DM, Krozowski Z, Campbell DJ, Lambert G, Hastings J, Aggarwal A & Esler MD. (2004). Sympathetic augmentation in hypertension: role of nerve firing, norepinephrine reuptake, and Angiotensin neuromodulation. *Hypertension* **43**, 169-175.
- Schnell MJ, McGettigan JP, Wirblich C & Papaneri A. (2010). The cell biology of rabies virus: using stealth to reach the brain. *Nat Rev Micro* **8**, 51-61.
- Schramm AE, Marinazzo D, Gener T & Graham LJ. (2014). The touch and zap method for in vivo whole-cell patch recording of intrinsic and visual responses of cortical neurons and glial cells. *PloS one* **9**, e97310.
- Schreihöfer AM & Guyenet PG. (1997). Identification of C1 presympathetic neurons in rat rostral ventrolateral medulla by juxtacellular labeling in vivo. *The Journal of comparative neurology* **387**, 524-536.
- Schreihöfer AM & Guyenet PG. (2000). Sympathetic reflexes after depletion of bulbospinal catecholaminergic neurons with anti-DbetaH-saporin. *American journal of physiology Regulatory, integrative and comparative physiology* **279**, R729-742.
- Schreihöfer AM & Guyenet PG. (2002). The baroreflex and beyond: control of sympathetic vasomotor tone by GABAergic neurons in the ventrolateral medulla. *Clinical and experimental pharmacology & physiology* **29**, 514-521.
- Schreihöfer AM & Guyenet PG. (2003). Baro-activated neurons with pulse-modulated activity in the rat caudal ventrolateral medulla express GAD67 mRNA. *Journal of neurophysiology* **89**, 1265-1277.
- Schreihöfer AM, Stornetta RL & Guyenet PG. (1999). Evidence for glycinergic respiratory neurons: Botzinger neurons express mRNA for glycinergic transporter 2. *The Journal of comparative neurology* **407**, 583-597.
- Schreihöfer AM, Stornetta RL & Guyenet PG. (2000). Regulation of sympathetic tone and arterial pressure by rostral ventrolateral medulla after depletion of C1 cells in rat. *The Journal of physiology* **529 Pt 1**, 221-236.
- Schulz S, Schreff M, Schmidt H, Händel M, Przewlocki R & Höllt V. (1998a). Immunocytochemical localization of somatostatin receptor sst2A in the rat spinal cord and dorsal root ganglia. *European Journal of Neuroscience* **10**, 3700-3708.
- Schulz S, Schulz S, Schmitt J, Wiborny D, Schmidt H, Olbricht S, Weise W, Roessner A, Gramsch C & Höllt V. (1998b). Immunocytochemical detection of somatostatin receptors sst1 sst(2A), sst(2B), and sst3 in paraffin-embedded breast cancer tissue using subtype- specific antibodies. *Clinical Cancer Research* **4**, 2047-2052.

- Schwarz LA, Miyamichi K, Gao XJ, Beier KT, Weissbourd B, DeLoach KE, Ren J, Ibanes S, Malenka RC, Kremer EJ & Luo L. (2015). Viral-genetic tracing of the input-output organization of a central noradrenaline circuit. *Nature* **524**, 88-92.
- Seo H, Hong SJ, Guo S, Kim HS, Kim CH, Hwang DY, Isacson O, Rosenthal A & Kim KS. (2002). A direct role of the homeodomain proteins Phox2a/2b in noradrenaline neurotransmitter identity determination. *J Neurochem* **80**, 905-916.
- Seo SW, Shin HY, Kim SH, Han SW, Lee KY, Kim SM & Heo JH. (2004). Vestibular imbalance associated with a lesion in the nucleus prepositus hypoglossi area. *Archives of neurology* **61**, 1440-1443.
- Sevigny CP, Bassi J, Teschemacher AG, Kim KS, Williams DA, Anderson CR & Allen AM. (2008). C1 neurons in the rat rostral ventrolateral medulla differentially express vesicular monoamine transporter 2 in soma and axonal compartments. *European Journal of Neuroscience* **28**, 1536-1544.
- Shafton AD, Ryan A & Badoer E. (1998). Neurons in the hypothalamic paraventricular nucleus send collaterals to the spinal cord and to the rostral ventrolateral medulla in the rat. *Brain research* **801**, 239-243.
- Shvarev Y, Berner J, Bilkei-Gorzo A, Lagercrantz H & Wickstrom R. (2010). Acute morphine effects on respiratory activity in mice with target deletion of the tachykinin 1 gene (Tac1^{-/-}). *Advances in experimental medicine and biology* **669**, 129-132.
- Shyn SI, Kerr R & Schafer WR. (2003). Serotonin and Go Modulate Functional States of Neurons and Muscles Controlling C. elegans Egg-Laying Behavior. *Current Biology* **13**, 1910-1915.
- Silasi G & Murphy Timothy H. (2014). Stroke and the Connectome: How Connectivity Guides Therapeutic Intervention. *Neuron* **83**, 1354-1368.
- Simms AE, Paton JF, Pickering AE & Allen AM. (2009). Amplified respiratory-sympathetic coupling in the spontaneously hypertensive rat: does it contribute to hypertension? *The Journal of physiology* **587**, 597-610.
- Simms AE, Paton JFR, Allen AM & Pickering AE. (2010). Is augmented central respiratory-sympathetic coupling involved in the generation of hypertension? *Respiratory Physiology & Neurobiology* **174**, 89-97.
- Simonds Stephanie E, Pryor Jack T, Ravussin E, Greenway Frank L, Dileone R, Allen Andrew M, Bassi J, Elmquist Joel K, Keogh Julia M, Henning E, Myers Martin G, Licinio J, Brown Russell D, Enriori Pablo J, O'Rahilly S, Sternson Scott M, Grove Kevin L, Spanswick David C, Farooqi I S & Cowley Michael A. (2014). Leptin Mediates the Increase in Blood Pressure Associated with Obesity. *Cell* **159**, 1404-1416.

- Smith JC, Abdala AP, Borgmann A, Rybak IA & Paton JF. (2012). Brainstem respiratory networks: building blocks and microcircuits. *Trends in neurosciences*.
- Smith JC, Abdala AP, Borgmann A, Rybak IA & Paton JF. (2013). Brainstem respiratory networks: building blocks and microcircuits. *Trends in neurosciences* **36**, 152-162.
- Smith JC, Abdala AP, Koizumi H, Rybak IA & Paton JF. (2007). Spatial and functional architecture of the mammalian brain stem respiratory network: a hierarchy of three oscillatory mechanisms. *Journal of neurophysiology* **98**, 3370-3387.
- Smith JC, Abdala AP, Rybak IA & Paton JF. (2009). Structural and functional architecture of respiratory networks in the mammalian brainstem. *Philosophical transactions of the Royal Society of London Series B, Biological sciences* **364**, 2577-2587.
- Smith JC, Butera RJ, Koshiya N, Del Negro C, Wilson CG & Johnson SM. (2000). Respiratory rhythm generation in neonatal and adult mammals: the hybrid pacemaker-network model. *Respiration physiology* **122**, 131-147.
- Smith JC, Ellenberger HH, Ballanyi K, Richter DW & Feldman JL. (1991). Pre-Botzinger complex: a brainstem region that may generate respiratory rhythm in mammals. *Science* **254**, 726-729.
- Smith JC, Greer JJ, Liu GS & Feldman JL. (1990). Neural mechanisms generating respiratory pattern in mammalian brain stem-spinal cord in vitro. I. Spatiotemporal patterns of motor and medullary neuron activity. *Journal of neurophysiology* **64**, 1149-1169.
- Smith JC, Morrison DE, Ellenberger HH, Otto MR & Feldman JL. (1989). Brainstem projections to the major respiratory neuron populations in the medulla of the cat. *The Journal of comparative neurology* **281**, 69-96.
- Song G, Li Q & Shao FZ. (2000). GABAergic neurons in Kolliker-Fuse nucleus and Botzinger complex with axons projecting to phrenic nucleus. *Sheng li xue bao : [Acta physiologica Sinica]* **52**, 167-169.
- Spary EJ, Maqbool A & Batten TF. (2008). Expression and localisation of somatostatin receptor subtypes sst1-sst5 in areas of the rat medulla oblongata involved in autonomic regulation. *Journal of chemical neuroanatomy* **35**, 49-66.
- Spira ME & Hai A. (2013). Multi-electrode array technologies for neuroscience and cardiology. *Nature Nanotechnology* **8**, 83-94.
- Spirovski D, Li Q & Pilowsky PM. (2011). Brainstem galanin synthesising neurons are differentially activated by chemoreceptor stimuli and represent a subpopulation of respiratory neurons. *The Journal of comparative neurology*.

- Spirovski D, Li Q & Pilowsky PM. (2012). Brainstem galanin-synthesizing neurons are differentially activated by chemoreceptor stimuli and represent a subpopulation of respiratory neurons. *The Journal of comparative neurology* **520**, 154-173.
- Sporns O, Tononi G & Kötter R. (2005). The Human Connectome: A Structural Description of the Human Brain. *PLoS Computational Biology* **1**, e42.
- Steinmeyer JD & Yanik MF. (2012). High-throughput single-cell manipulation in brain tissue. *PloS one* **7**, e35603.
- Stocker SD, Cunningham JT & Toney GM. (2004a). Water deprivation increases Fos immunoreactivity in PVN autonomic neurons with projections to the spinal cord and rostral ventrolateral medulla. *American journal of physiology Regulatory, integrative and comparative physiology* **287**, R1172-1183.
- Stocker SD, Keith KJ & Toney GM. (2004b). Acute inhibition of the hypothalamic paraventricular nucleus decreases renal sympathetic nerve activity and arterial blood pressure in water-deprived rats. *American journal of physiology Regulatory, integrative and comparative physiology* **286**, R719-725.
- Stocker SD, Osborn JL & Carmichael SP. (2008). Forebrain osmotic regulation of the sympathetic nervous system. *Clinical and experimental pharmacology & physiology* **35**, 695-700.
- Stornetta RL. (2008). Identification of neurotransmitters and co-localization of transmitters in brainstem respiratory neurons. *Respir Physiol Neurobiol* **164**, 18-27.
- Stornetta RL, Inglis MA, Viar KE & Guyenet PG. (2015). Afferent and efferent connections of C1 cells with spinal cord or hypothalamic projections in mice. *Brain structure & function*.
- Stornetta RL, Moreira TS, Takakura AC, Kang BJ, Chang DA, West GH, Brunet JF, Mulkey DK, Bayliss DA & Guyenet PG. (2006). Expression of Phox2b by brainstem neurons involved in chemosensory integration in the adult rat. *The Journal of neuroscience : the official journal of the Society for Neuroscience* **26**, 10305-10314.
- Stornetta RL, Rosin DL, Wang H, Sevigny CP, Weston MC & Guyenet PG. (2003a). A group of glutamatergic interneurons expressing high levels of both neurokinin-1 receptors and somatostatin identifies the region of the pre-Botzinger complex. *The Journal of comparative neurology* **455**, 499-512.
- Stornetta RL, Sevigny CP & Guyenet PG. (2003b). Inspiratory augmenting bulbospinal neurons express both Glutamatergic and enkephalinergic phenotypes. *Journal of Comparative Neurology* **455**, 113-124.

- Stornetta RL, Seigny CP, Schreihof AM, Rosin DL & Guyenet PG. (2002). Vesicular glutamate transporter DNPI/VGLUT2 is expressed by both C1 adrenergic and nonaminergic presympathetic vasomotor neurons of the rat medulla. *The Journal of comparative neurology* **444**, 207-220.
- Stornetta RL, Spirovski D, Moreira TS, Takakura AC, West GH, Gwilt JM, Pilowsky PM & Guyenet PG. (2009). GALANIN IS A SELECTIVE MARKER OF THE RETROTRAPEZOID NUCLEUS IN RATS. *The Journal of comparative neurology* **512**, 373-383.
- Strack AM, Sawyer WB, Hughes JH, Platt KB & Loewy AD. (1989). A general pattern of CNS innervation of the sympathetic outflow demonstrated by transneuronal pseudorabies viral infections. *Brain research* **491**, 156-162.
- Stretton AO & Kravitz EA. (1968). Neuronal geometry: determination with a technique of intracellular dye injection. *Science* **162**, 132-134.
- Struyker-Boudier HA, Evenwel RT, Smits JF & Van Essen H. (1982). Baroreflex sensitivity during the development of spontaneous hypertension in rats. *Clinical science* **62**, 589-594.
- Sun QJ, Goodchild AK, Chalmers JP & Pilowsky PM. (1998). The pre-Botzinger complex and phase-spanning neurons in the adult rat. *Brain research* **809**, 204-213.
- Sun QJ, Minson J, Llewellyn-Smith IJ, Arnold L, Chalmers J & Pilowsky P. (1997). Botzinger neurons project towards bulbospinal neurons in the rostral ventrolateral medulla of the rat. *The Journal of comparative neurology* **388**, 23-31.
- Sun W & Panneton WM. (2002). The caudal pressor area of the rat: its precise location and projections to the ventrolateral medulla. *American journal of physiology Regulatory, integrative and comparative physiology* **283**, R768-778.
- Sun W & Panneton WM. (2005). Defining projections from the caudal pressor area of the caudal ventrolateral medulla. *The Journal of comparative neurology* **482**, 273-293.
- Suzuki T, Takayama K & Miura M. (1997). Distribution and projection of the medullary cardiovascular control neurons containing glutamate, glutamic acid decarboxylase, tyrosine hydroxylase and phenylethanolamine N-methyltransferase in rats. *Neuroscience research* **27**, 9-19.
- Sved A & Gordon F. (1994). Amino Acids as Central Neurotransmitters in the Baroreceptor Reflex Pathway. *Physiology* **9**, 243-246.

- Takato J, Nelson A, Zhou X, Bolton MM, Ehlers MD, Arenkiel BR, Mooney R & Wang F. (2013). New modules are added to vibrissal premotor circuitry with the emergence of exploratory whisking. *Neuron* **77**, 346-360.
- Talman WT & Robertson SC. (1991). Nucleus prepositus hypoglossi. A medullary pressor region. *Hypertension* **17**, 1173-1176.
- Tan W, Janczewski WA, Yang P, Shao XM, Callaway EM & Feldman JL. (2008). Silencing preBotzinger complex somatostatin-expressing neurons induces persistent apnea in awake rat. *Nat Neurosci* **11**, 538-540.
- Tan W, Pagliardini S, Yang P, Janczewski WA & Feldman JL. (2010). Projections of preBotzinger complex neurons in adult rats. *The Journal of comparative neurology* **518**, 1862-1878.
- Tan W, Sherman D, Turesson J, Shao XM, Janczewski WA & Feldman JL. (2012). Reelin demarcates a subset of pre-Botzinger complex neurons in adult rat. *The Journal of comparative neurology* **520**, 606-619.
- Tanaka I, Ezure K & Kondo M. (2003). Distribution of glycine transporter 2 mRNA-containing neurons in relation to glutamic acid decarboxylase mRNA-containing neurons in rat medulla. *Neuroscience research* **47**, 139-151.
- Taylor EW, Jordan D & Coote JH. (1999). Central Control of the Cardiovascular and Respiratory Systems and Their Interactions in Vertebrates. *Physiological reviews* **79**, 855-916.
- Thoby-Brisson M, Cauli B, Champagnat J, Fortin G & Katz DM. (2003). Expression of functional tyrosine kinase B receptors by rhythmically active respiratory neurons in the pre-Botzinger complex of neonatal mice. *The Journal of neuroscience : the official journal of the Society for Neuroscience* **23**, 7685-7689.
- Thoby-Brisson M & Ramirez JM. (2001). Identification of two types of inspiratory pacemaker neurons in the isolated respiratory neural network of mice. *Journal of neurophysiology* **86**, 104-112.
- Tian GF, Peever JH & Duffin J. (1998). Botzinger-complex expiratory neurons monosynaptically inhibit phrenic motoneurons in the decerebrate rat. *Experimental brain research* **122**, 149-156.
- Tian GF, Peever JH & Duffin J. (1999). Botzinger-complex, bulbospinal expiratory neurones monosynaptically inhibit ventral-group respiratory neurones in the decerebrate rat. *Experimental brain research* **124**, 173-180.

- Tian L, Hires SA, Mao T, Huber D, Chiappe ME, Chalasani SH, Petreanu L, Akerboom J, McKinney SA, Schreiter ER, Bargmann CI, Jayaraman V, Svoboda K & Looger LL. (2009). Imaging neural activity in worms, flies and mice with improved GCaMP calcium indicators. *Nature methods* **6**, 875-881.
- Toga AW, Clark KA, Thompson PM, Shattuck DW & Van Horn JD. (2012). Mapping the human connectome. *Neurosurgery* **71**, 1-5.
- Toney GM, Pedrino GR, Fink GD & Osborn JW. (2010). Does enhanced respiratory-sympathetic coupling contribute to peripheral neural mechanisms of angiotensinII-salt hypertension? *Experimental physiology* **95**, 587-594.
- Tostivint H, Ocampo Daza D, Bergqvist CA, Quan FB, Bougerol M, Lihrmann I & Larhammar D. (2014). Molecular evolution of GPCRs: Somatostatin/urotensin II receptors. *Journal of molecular endocrinology* **52**, T61-86.
- Tupal S, Rieger MA, Ling GY, Park TJ, Dougherty JD, Goodchild AK & Gray PA. (2014). Testing the role of preBotzinger Complex somatostatin neurons in respiratory and vocal behaviors. *The European journal of neuroscience* **40**, 3067-3077.
- Turner A, Kumar N, Farnham M, Lung M, Pilowsky P & McMullan S. (2013). Rostroventrolateral medulla neurons with commissural projections provide input to sympathetic premotor neurons: anatomical and functional evidence. *The European journal of neuroscience* **38**, 2504-2515.
- Tzeng YC, Larsen PD & Galletly DC. (2003). Cardioventilatory coupling in resting human subjects. *Experimental physiology* **88**, 775-782.
- Tzeng YC, Larsen PD & Galletly DC. (2007). Mechanism of cardioventilatory coupling: insights from cardiac pacing, vagotomy, and sinoaortic denervation in the anesthetized rat. *American Journal of Physiology - Heart and Circulatory Physiology* **292**, H1967-H1977.
- Ugolini G. (1995). Specificity of rabies virus as a transneuronal tracer of motor networks: transfer from hypoglossal motoneurons to connected second-order and higher order central nervous system cell groups. *The Journal of comparative neurology* **356**, 457-480.
- Ugolini G. (2008). Use of rabies virus as a transneuronal tracer of neuronal connections: implications for the understanding of rabies pathogenesis. *Developments in biologicals* **131**, 493-506.
- Umeda T, Ebihara T & Okabe S. (2005). Simultaneous observation of stably associated presynaptic varicosities and postsynaptic spines: morphological alterations of CA3-CA1 synapses in hippocampal slice cultures. *Molecular and cellular neurosciences* **28**, 264-274.

- Van Bockstaele EJ, Peoples J & Telegan P. (1999). Efferent projections of the nucleus of the solitary tract to peri-locus coeruleus dendrites in rat brain: evidence for a monosynaptic pathway. *The Journal of comparative neurology* **412**, 410-428.
- Van Bockstaele EJ, Pieribone VA & Aston-Jones G. (1989). Diverse afferents converge on the nucleus paragigantocellularis in the rat ventrolateral medulla: retrograde and anterograde tracing studies. *The Journal of comparative neurology* **290**, 561-584.
- Varshney LR, Chen BL, Paniagua E, Hall DH & Chklovskii DB. (2011). Structural Properties of the *Caenorhabditis elegans* Neuronal Network. *PLoS Computational Biology* **7**, e1001066.
- Verberne AJ, Sartor DM & Berke A. (1999). Midline medullary depressor responses are mediated by inhibition of RVLM sympathoexcitatory neurons in rats. *The American journal of physiology* **276**, R1054-1062.
- Vercelli A, Repici M, Garbossa D & Grimaldi A. (2000). Recent techniques for tracing pathways in the central nervous system of developing and adult mammals. *Brain research bulletin* **51**, 11-28.
- Wall NR, Wickersham IR, Cetin A, De La Parra M & Callaway EM. (2010). Monosynaptic circuit tracing in vivo through Cre-dependent targeting and complementation of modified rabies virus. *Proceedings of the National Academy of Sciences of the United States of America* **107**, 21848-21853.
- Wallen-Mackenzie A, Gezelius H, Thoby-Brisson M, Nygard A, Enjin A, Fujiyama F, Fortin G & Kullander K. (2006). Vesicular glutamate transporter 2 is required for central respiratory rhythm generation but not for locomotor central pattern generation. *The Journal of neuroscience : the official journal of the Society for Neuroscience* **26**, 12294-12307.
- Wang H, Germanson TP & Guyenet PG. (2002). Depressor and tachypneic responses to chemical stimulation of the ventral respiratory group are reduced by ablation of neurokinin-1 receptor-expressing neurons. *The Journal of neuroscience : the official journal of the Society for Neuroscience* **22**, 3755-3764.
- Wang H, Stornetta RL, Rosin DL & Guyenet PG. (2001). Neurokinin-1 receptor-immunoreactive neurons of the ventral respiratory group in the rat. *The Journal of comparative neurology* **434**, 128-146.
- Wang M, Orwar O, Olofsson J & Weber SG. (2010). Single-cell electroporation. *Analytical and Bioanalytical Chemistry* **397**, 3235-3248.
- Wang S, Benamer N, Zanella S, Kumar NN, Shi Y, Bévençut M, Penton D, Guyenet PG, Lesage F, Gestreau C, Barhanin J & Bayliss DA. (2013). TASK-2 Channels

Contribute to pH Sensitivity of Retrotrapezoid Nucleus Chemoreceptor Neurons. *The Journal of Neuroscience* **33**, 16033-16044.

Wang X & Hayes JA. (2014). Laser ablation of Dbx1 neurons in the pre-Botzinger complex stops inspiratory rhythm and impairs output in neonatal mice. **3**, e03427.

Watson AM, Lambert GW, Smith KJ & May CN. (2003). Urotensin II acts centrally to increase epinephrine and ACTH release and cause potent inotropic and chronotropic actions. *Hypertension* **42**, 373-379.

Weese-Mayer DE, Berry-Kravis EM, Ceccherini I & Rand CM. (2008). Congenital central hypoventilation syndrome (CCHS) and sudden infant death syndrome (SIDS): kindred disorders of autonomic regulation. *Respir Physiol Neurobiol* **164**, 38-48.

Wei XY, Zhao Y, Wong-Riley MT, Ju G & Liu YY. (2012). Synaptic relationship between somatostatin- and neurokinin-1 receptor-immunoreactive neurons in the pre-Botzinger complex of rats. *J Neurochem* **122**, 923-933.

Weissbourd B, Ren J, DeLoach KE, Guenther CJ, Miyamichi K & Luo L. (2014). Presynaptic partners of dorsal raphe serotonergic and GABAergic neurons. *Neuron* **83**, 645-662.

White JG, Southgate E, Thomson JN & Brenner S. (1986). The Structure of the Nervous System of the Nematode *Caenorhabditis elegans*. *Philosophical Transactions of the Royal Society of London B: Biological Sciences* **314**, 1-340.

Wickersham IR, Finke S, Conzelmann KK & Callaway EM. (2007a). Retrograde neuronal tracing with a deletion-mutant rabies virus. *Nature methods* **4**, 47-49.

Wickersham IR, Lyon DC, Barnard RJ, Mori T, Finke S, Conzelmann KK, Young JA & Callaway EM. (2007b). Monosynaptic restriction of transsynaptic tracing from single, genetically targeted neurons. *Neuron* **53**, 639-647.

Willette RN, Krieger AJ, Barcas PP & Sapru HN. (1983). Medullary gamma-aminobutyric acid (GABA) receptors and the regulation of blood pressure in the rat. *The Journal of pharmacology and experimental therapeutics* **226**, 893-899.

Willette RN, Punnen S, Krieger AJ & Sapru HN. (1984). Interdependence of rostral and caudal ventrolateral medullary areas in the control of blood pressure. *Brain research* **321**, 169-174.

Winter SM, Freseman J, Schnell C, Oku Y, Hirrlinger J & Hulsman S. (2009). Glycinergic interneurons are functionally integrated into the inspiratory network of mouse medullary slices. *Pflügers Archiv : European journal of physiology* **458**, 459-469.

- Yamamoto Y, Runold M, Prabhakar N, Pantaleo T & Lagercrantz H. (1988). Somatostatin in the control of respiration. *Acta physiologica Scandinavica* **134**, 529-533.
- Yang C, Kim HS, Seo H, Kim CH, Brunet JF & Kim KS. (1998). Paired-like homeodomain proteins, Phox2a and Phox2b, are responsible for noradrenergic cell-specific transcription of the dopamine beta-hydroxylase gene. *J Neurochem* **71**, 1813-1826.
- Yang Z & Coote JH. (1998). Influence of the hypothalamic paraventricular nucleus on cardiovascular neurones in the rostral ventrolateral medulla of the rat. *The Journal of physiology* **513** (Pt 2), 521-530.
- Yates BJ & Bronstein AM. (2005). The effects of vestibular system lesions on autonomic regulation: observations, mechanisms, and clinical implications. *Journal of vestibular research : equilibrium & orientation* **15**, 119-129.
- Yoder RM & Taube JS. (2014). The vestibular contribution to the head direction signal and navigation. *Frontiers in integrative neuroscience* **8**, 32.
- Yonehara K, Balint K, Noda M, Nagel G, Bamberg E & Roska B. (2011). Spatially asymmetric reorganization of inhibition establishes a motion-sensitive circuit. *Nature* **469**, 407-410.
- Yonehara K, Farrow K, Ghanem A, Hillier D, Balint K, Teixeira M, Jüttner J, Noda M, Neve RL, Conzelmann KK & Roska B. (2013). The first stage of cardinal direction selectivity is localized to the dendrites of retinal ganglion cells. *Neuron* **79**, 1078-1085.
- Young JA, Bates P & Varmus HE. (1993). Isolation of a chicken gene that confers susceptibility to infection by subgroup A avian leukosis and sarcoma viruses. *Journal of virology* **67**, 1811-1816.
- Yu YJ, Arttamangkul S, Evans CJ, Williams JT & von Zastrow M. (2009). Neurokinin 1 receptors regulate morphine-induced endocytosis and desensitization of mu-opioid receptors in CNS neurons. *The Journal of neuroscience : the official journal of the Society for Neuroscience* **29**, 222-233.
- Zagon A. (1995). Internal connections in the rostral ventromedial medulla of the rat. *Journal of the autonomic nervous system* **53**, 43-56.
- Zhong S, Zhou SY, Gebber GL & Barman SM. (1997). Coupled oscillators account for the slow rhythms in sympathetic nerve discharge and phrenic nerve activity. *The American journal of physiology* **272**, R1314-1324.
- Zhou SY & Gilbey MP. (1992). Respiratory-related activity of lower thoracic and upper lumbar sympathetic preganglionic neurones in the rat. *The Journal of physiology* **451**, 631-642.

- Zoccal DB, Bonagamba LG, Oliveira FR, Antunes-Rodrigues J & Machado BH. (2007). Increased sympathetic activity in rats submitted to chronic intermittent hypoxia. *Experimental physiology* **92**, 79-85.
- Zoccal DB, Furuya WI, Bassi M, Colombari DSA & Colombari E. (2014). The nucleus of the solitary tract and the coordination of respiratory and sympathetic activities. *Frontiers in physiology* **5**, 238.
- Zoccal DB, Paton JF & Machado BH. (2009). Do changes in the coupling between respiratory and sympathetic activities contribute to neurogenic hypertension? *Clinical and experimental pharmacology & physiology* **36**, 1188-1196.
- Zoccal DB, Simms AE, Bonagamba LG, Braga VA, Pickering AE, Paton JF & Machado BH. (2008). Increased sympathetic outflow in juvenile rats submitted to chronic intermittent hypoxia correlates with enhanced expiratory activity. *The Journal of physiology* **586**, 3253-3265.

Appendices

ANIMAL RESEARCH AUTHORITY (ARA)

AEC Reference No.: 2012/030 - 2

Date of Expiry: 15 June 2013

Full Approval Duration: 15 June 2012 to 14 June 2015 (36 Months)

This ARA remains in force until the Date of Expiry (unless suspended, cancelled or surrendered) and will only be renewed upon receipt of a satisfactory Progress Report before expiry (see Approval email for submission details).

Principal Investigator:

Dr Simon McMullan
Australian School of Advanced Medicine
Macquarie University NSW 2109
0402 073 146
simon.mcmullan@mq.edu.au

Associate Investigators:

Anita Turner 0411 283 223
Lama Bou Farah 0406 164 456
Bowen Dempsey 0403 831 090
Other people participating:
Sheng Le 0430 360 228

In case of emergency, please contact:

the Principal Investigator / Associate Investigator named above

or Manager, CAF: 9850 7780 / 0428 861 163 and Animal Welfare Officer: 9850 7758 / 0439 497 383

The above-named are authorised by MACQUARIE UNIVERSITY ANIMAL ETHICS COMMITTEE to conduct the following research:

Title of the project: Mapping the connectome that controls blood pressure in vivo

Purpose: 4: Human or Animal Biology

Aims: 1. Single cell electroporation of functionally identified neurons in vivo
2. Mapping presynaptic neurons using genetically modified rabies virus

Surgical Procedures category: 5. Major Surgery with Recovery

All procedures must be performed as per the AEC-approved protocol, unless stated otherwise by the AEC and/or AWO.

Maximum numbers approved (for the Full Approval Duration):

Species	Strain	Age/Sex/Weight	Total	Supplier/Source
Rat	any	any	40	ARC Perth or transferred from other approved protocols
Rat	SD	male	100	ARC Perth
		TOTAL	140	

Location of research:

Location	Full street address
Central Animal Facility	Building F9A, Research Park Drive, Macquarie University NSW 2109

Amendments approved by the AEC since initial approval:

- Addition of Sheng Le with conditions (Approved February 2013)
 - That the student attend the next Working With Research Animals Workshop on 21 February 2013 or provide evidence of attendance at a similar approved course in the ethical conduct of animal research
 - That the student attend courses in rodent handling, anaesthesia, surgery, and post mortem examination, provided by the Animal Welfare Officer
 - That there is supervision commensurate with the student's skill and knowledge.

Conditions of Approval: N/A

Being animal research carried out in accordance with the Code of Practice for a recognised research purpose and in connection with - animals (other than exempt animals) that have been obtained from the holder of an animal suppliers licence.



Dr. Kandy White (Deputy Chair, Animal Ethics Committee)

Approval Date: 14 February 2013

ANIMAL RESEARCH AUTHORITY (ARA)

AEC Reference No.: 2013/022 - 2

Date of Expiry: 18 July 2015

Full Approval Duration: 19 July 2013 to 18 July 2016 (36 Months)

This ARA remains in force until the Date of Expiry (unless suspended, cancelled or surrendered) and will only be renewed upon receipt of a satisfactory Progress Report before expiry (see Approval email for submission details).

Principal Investigator:

Dr Simon McMullan
School of Advanced Medicine
Macquarie University, NSW 2109
simon.mcmullan@mq.edu.au
0402 073 146

Associate Investigators:

Anita Turner 0411 283 223
Sheng Le 0430 360 228

In case of emergency, please contact:

the Principal Investigator / Associate Investigator named above

Or Manager, CAF: 9850 7780 / 0428 861 163 and **Animal Welfare Officer:** 9850 7758 / 0439 497 383

The above-named are authorised by MACQUARIE UNIVERSITY ANIMAL ETHICS COMMITTEE to conduct the following research:

Title of the project: Investigating the expression pattern of somatostatin 2a receptors in functionally identified respiratory neurons in the rat

Purpose: 4 - Research: Human or Animal Biology

Aims: To investigate the expression pattern of SST2aR on individual rat neurons that plays a role in the generation of respiration

Surgical Procedures category: 2 - Animal Unconscious without Recovery

All procedures must be performed as per the AEC-approved protocol, unless stated otherwise by the AEC and/or AWO.

Maximum numbers approved (for the Full Approval Duration):

Species	Strain	Weight	Total	Supplier/Source
02 - Rats	Sprague Dawley	250-300g	50	ARC Perth
		TOTAL	50	

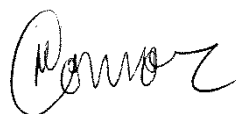
Location of research:

Location	Full street address
Central Animal Facility	Building F9A, Research Park Drive, Macquarie University, NSW 2109
ASAM	Level 1, F10A, 2 Technology Place, Macquarie University, NSW 2109

Amendments approved by the AEC since initial approval: N/A

Conditions of Approval: N/A

Being animal research carried out in accordance with the Code of Practice for a recognised research purpose and in connection with animals (other than exempt animals) that have been obtained from the holder of an animal suppliers licence.



Professor Mark Connor (Chair, Animal Ethics Committee)

Approval Date: 17 July 2014

ANIMAL RESEARCH AUTHORITY (ARA)

AEC Reference No.: 2014/028

Date of Expiry: 19 June 2015

Full Approval Duration: 20 June 2014 to 19 June 2017 (36 Months)

This ARA remains in force until the Date of Expiry (unless suspended, cancelled or surrendered) **and will only be renewed upon receipt of a satisfactory Progress Report before expiry (see Approval email for submission details).**

Principal Investigator:

Dr Simon McMullan
Australian School of Advanced Medicine
Macquarie University, NSW 2109
0402 073 146
Simon.McMullan@mq.edu.au

Associate Investigators:

Anita Turner	0411 283 223
Ann Goodchild	0410 601 302
Bowen Richard Dempsey	0403 831 090
Sheng Le	0430 360 228

In case of emergency, please contact:

the Principal Investigator / Associate Investigator named above

or Manager, CAF: 9850 7780 / 0428 861 163 and Animal Welfare Officer: 9850 7758 / 0439 497 383

The above-named are authorised by MACQUARIE UNIVERSITY ANIMAL ETHICS COMMITTEE to conduct the following research:

Title of the project: Viral tracing of brainstem cardiovascular and respiratory networks

Purpose: 5 - Research: Human or Animal Health and Welfare

Aims: To identify the circuitry that underlies cardiovascular and respiratory function by targeting populations of neurons with custom-made viral vectors, based on their anatomical location and neurochemistry, and then with rabies to provide a relatively high-throughput overview of cardiorespiratory circuit structure

Surgical Procedures category: 5 - Major Surgery with Recovery

All procedures must be performed as per the AEC-approved protocol, unless stated otherwise by the AEC and/or AWO.

Maximum numbers approved (for the Full Approval Duration):

Species	Strain	Age/Sex/Weight	Total	Supplier/Source
02 – Rattus	Sprague Dawley	Adult / 300g	70	ARC Perth
		TOTAL	70	

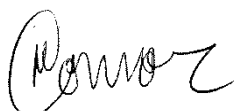
Location of research:

Location	Full street address
Central Animal Facility	Building F9A, Research Park Drive, Macquarie University, NSW 2109
ASAM	Level 1, F10A, 2 Technology Place, Macquarie University, NSW 2109

Amendments approved by the AEC since initial approval: N/A

Conditions of Approval: N/A

Being animal research carried out in accordance with the Code of Practice for a recognised research purpose and in connection with animals (other than exempt animals) that have been obtained from the holder of an animal suppliers licence.



Professor Mark Connor (Chair, Animal Ethics Committee)

Approval Date: 19 June 2014

Somatostatin 2a Receptors Are Not Expressed on Functionally Identified Respiratory Neurons in the Ventral Respiratory Column of the Rat

Sheng Le,¹ Anita J. Turner,¹ Lindsay M. Parker,² Peter G. Burke,³ Natasha N. Kumar,⁴ Ann K. Goodchild,¹ and Simon McMullan^{1*}

¹Faculty of Medicine & Health Sciences, Macquarie University, NSW, Australia

²ARC Center of Excellence for Nanoscale BioPhotonics, Macquarie University, NSW, Australia

³Neuroscience Research Australia, Randwick, NSW, Australia

⁴Department of Pharmacology, University of Virginia, Charlottesville, Virginia, USA

Microinjection of somatostatin (SST) causes site-specific effects on respiratory phase transition, frequency, and amplitude when microinjected into the ventrolateral medulla (VLM) of the anesthetized rat, suggesting selective expression of SST receptors on different functional classes of respiratory neurons. Of the six subtypes of SST receptor, somatostatin 2a (sst_{2a}) is the most prevalent in the VLM, and other investigators have suggested that glutamatergic neurons in the preBötzinger Complex (preBötC) that coexpress neurokinin-1 receptor (NK1R), SST, and sst_{2a} are critical for the generation of respiratory rhythm. However, quantitative data describing the distribution of sst_{2a} in respiratory compartments other than preBötC, or on functionally identified respiratory neurons, is absent. Here we examine the medullary expression of sst_{2a} with particular reference to glycinergic/expiratory neurons in the Böttinger Complex (BötC) and NK1R-immunoreactive/inspiratory neurons in

the preBötC. We found robust sst_{2a} expression at all rostro-caudal levels of the VLM, including a large proportion of catecholaminergic neurons, but no colocalization of sst_{2a} and glycine transporter 2 mRNA in the BötC. In the preBötC 54% of sst_{2a}-immunoreactive neurons were also positive for NK1R. sst_{2a} was not observed in any of 52 dye-labeled respiratory interneurons, including seven BötC expiratory-decrementing and 11 preBötC preinspiratory neurons. We conclude that sst_{2a} is not expressed on BötC respiratory neurons and that phasic respiratory activity is a poor predictor of sst_{2a} expression in the preBötC. Therefore, sst_{2a} is unlikely to underlie responses to BötC SST injection, and is sparse or absent on respiratory neurons identified by classical functional criteria. *J. Comp. Neurol.* 524:1384–1398, 2016.

© 2015 Wiley Periodicals, Inc.

INDEXING TERMS: respiratory neurons; preBötzinger Complex; somatostatin

Breathing is a fundamental motor function that is controlled by hierarchical arrays of spatially, functionally, and phenotypically compartmentalized groups of neurons in the brainstem and pons (for recent reviews, see Feldman et al., 2013; Smith et al., 2013). The preBötzinger Complex (preBötC) located in the ventrolateral medulla (VLM) forms the essential kernel of the respiratory rhythm-generating apparatus: rhythmic drive from preBötC neurons is necessary for the generation of activity in inspiratory motor nerves and sufficient to maintain activity recorded in the hypoglossal nerve in medullary slices *in vitro* (Smith et al., 1991). Respiratory interneurons in this area are active in the inspiratory phase of the respiratory cycle and contribute to inspiratory bursts via a combination of pacemaker activ-

ity and glutamatergic transmission (Koshiya and Smith, 1999; Del Negro et al., 2002a; Wallen-Mackenzie et al., 2006; Koizumi et al., 2013). preBötC glutamatergic neurons contain a number of other neurochemicals and transcription factors that may have particular functional significance. Of particular interest are subpopulations of glutamatergic neurons in this region that express

Grant sponsor: National Health and Medical Research Council; Grant numbers: 604002, APP1028183, APP1030301; Grant sponsor: Australian Research Council Discover; Grant number: Project DP120100920.

*CORRESPONDENCE TO: Simon McMullan, Faculty of Medicine & Health Sciences, Macquarie University, NSW 2109, Australia.
E-mail: simon.mcmullan@mq.edu.au

Received June 22, 2015; Revised October 9, 2015;
Accepted October 12, 2015.

DOI 10.1002/cne.23912

Published online November 7, 2015 in Wiley Online Library
(wileyonlinelibrary.com)

© 2015 Wiley Periodicals, Inc.

neurokinin-1 receptors (NK1R), somatostatin (SST), and somatostatin 2a receptor (sst_{2a}), and these have been proposed as chemical markers for the preBötC (Guyenet and Wang, 2001; Stornetta et al., 2003a; Gray et al., 2010; Gray, 2013). Critical roles for these populations in the generation of normal respiratory activity are supported by targeted ablation and loss-of-function studies: extensive bilateral lesion of preBötC NK1R neurons leads to a severely ataxic breathing pattern (Gray et al., 2001). Similarly, pharmacogenetic silencing of SSTergic preBötC neurons causes ataxic breathing and apnea (Tan et al., 2008). However, it is important to note that although both NK1R and particularly SST (at least as mRNA) are extensively expressed throughout the VLM, neither is widely expressed in functionally identified respiratory neurons (Guyenet and Wang, 2001; Wang et al., 2001; Stornetta et al., 2003a).

The functional significance of SST release from putative preBötC neurons is unclear. Transgenic animals that lack SST (Low et al., 2001) or SST receptors (Allen et al., 2003; Qiu et al., 2008; Rajput et al., 2011) are not associated with an obvious respiratory phenotype. However, exogenous SST powerfully inhibits central respiratory drive in vivo (Yamamoto et al., 1988; Chen et al., 1990; Burke et al., 2010; Pantaleo et al., 2011) and in vitro (Llona et al., 2004; Gray et al., 2010; Ramírez-Jarquín et al., 2012).

We have previously demonstrated that the respiratory effects of SST microinjection are site-specific and dose-dependent: SST microinjection in the Böttinger Complex (BötC) caused apneusis, characterized by a prolongation of phrenic burst duration (T_i) and ablation of postinspiratory activity in vagal and sympathetic nerves. In contrast, preBötC SST injection evoked reductions in respiratory frequency (ultimately leading to apnea with higher doses) without significant effects on T_i or postinspiratory activity (Burke et al., 2010). We also found that SST evoked a reduction in phrenic nerve amplitude when injected into the rostral ventral respiratory group (rVRG). These results were consistent with an inhibitory effect of SST on inhibitory BötC neurons thought to terminate inspiration, presumably expiratory neurons with a decrementing firing pattern (E-Dec; Hayashi et al., 1996), an inhibitory effect of SST on preBötC rhythm-generating neurons, and an inhibitory effect of SST on respiratory premotor neurons in the rVRG.

Taken together, the literature suggests that components of the respiratory circuits that subserve phase-transition, rhythm generation, and bulbospinal drive are directly sensitive to SST, and predicts the expression of SST receptors on subsets of respiratory neurons in the BötC (particularly E-Dec), preBötC (particularly pre-I), and rVRG compartments. That prediction is tested in the current study. Some colocalization of sst_{2a} with preBötC NK1R/SST/Dbx1 and tyrosine hydroxylase (TH)/pre-pro-

enkephalin has previously been described (Burke et al., 2008; Spary et al., 2008; Gray et al., 2010). However, no quantitative data regarding the distribution of sst_{2a} on respiratory neurons are available. Here we comprehensively describe the distribution of sst_{2a} in VLM respiratory cell groups and on functionally identified respiratory neurons with a particular focus on the BötC and preBötC.

MATERIALS AND METHODS

Animal experiments were approved by Macquarie University Animal Ethics Committee and adhered to the Australian code of practice for the care and use of animals for scientific purposes.

Electrophysiology experiments

Surgical procedures

Urethane-anesthetized (1–1.3 g/kg i.p.) adult Sprague-Dawley rats of either sex (220–480 g, ARC, Perth, Australia) were cannulated to allow intravenous access and recording of arterial blood pressure and intubated to permit artificial ventilation. Phrenic nerve activity (PNA, $n = 7$) or diaphragmatic electromyogram (EMG, $n = 22$) were recorded as an index of central respiratory drive. The phrenic nerve was isolated and recorded as previously described (McMullan et al., 2009). Diaphragm EMG was recorded via Teflon-coated stainless steel wires inserted into the diaphragm at the lateral aspect of the inferior costal margin. Phrenic/EMG signals were differentially amplified and filtered (100–1,000 Hz). In most experiments vagi were cut bilaterally at the cervical level to desynchronize central respiratory drive from mechanical ventilation; in three experiments vagi were left intact. Core temperature was maintained at 36–38°C by a heating blanket controlled by a rectal thermometer and animals were moved into a stereotaxic frame in the nose-down position. The left facial nerve was exposed, the occipital bone removed, and the brainstem exposed. The animal was artificially ventilated to maintain isocapnia, as indicated by end-tidal CO_2 (3.5–4.5%) or analysis of arterial blood gas samples. Neuromuscular blockade (pancuronium bromide, 0.1–0.4 mg i.v.) was used to reduce movements associated with ventilation while maintaining diaphragmatic EMG by careful titration. Anesthetic depth was regularly monitored by checking for motor, respiratory, or pressor responses to noxious pinching of the tail or the hind paws. Supplementary anesthetic (urethane 0.1 g/kg i.v.) was administered as required.

Identification and labeling of respiratory neurons in vivo

The caudal border of the facial nucleus was estimated by mapping antidromic facial field potentials

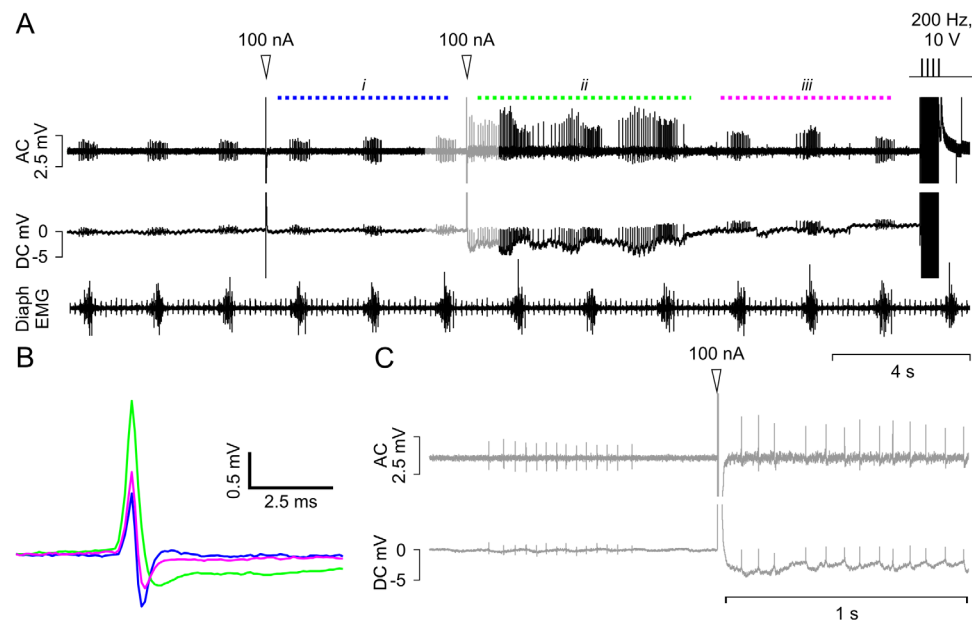


Figure 1. Electrophysiological recording and labeling of brainstem respiratory neuron. **A:** Following functional identification of an inspiratory-locked neuron in the preBötC the pipette was gradually moved to a position at which 100 nA microstimulation evoked a transient increase in neuronal firing, a change in spike shape (**B**) and a -2 mV pipette potential (**C**). Note that the cell maintains its firing pattern for the duration of the recording. The cell was then electroporated with a 0.5 s train of 10 V 1 ms pulses at 200 Hz. **B:** Average spike waveforms recorded in periods denoted in **A** i, ii, and iii. **C:** An expanded view of data indicated in gray in (**A**).

using a borosilicate pipette filled with 3 M NaCl (resistance <2 M Ω) as previously described (Brown and Guyenet, 1984). Neuronal recordings were made using borosilicate glass pipettes filled with 0.9% NaCl containing 1–3% tetramethylrhodamine-conjugated dextran (3000 MW, Invitrogen, La Jolla, CA, #D3307) or 2% neurobiotin (tip diameter, 1 μ m, resistance 10–25 M Ω). Extracellular recordings were amplified (Axoclamp 900A, Molecular Devices, Palo Alto, CA) and simultaneously captured on two channels using differing filter sets, one configured for extracellular recording (AC: 100–3,000 Hz) and one for intracellular recordings (DC: DC–3,000 Hz, used to guide cell labeling: see below), and sampled by a Power1401 mk. II running Spike 2 software (Cambridge Electronic Design, UK, RRID: nlx_156886). Phrenic/diaphragm activity was sampled at 3k samples/s; extracellular activity at 10k samples/s; intracellular activity at 5k samples/s.

Neurons located 0–1.4 mm caudal to the caudal border of the facial nucleus, 1.6–2.0 mm lateral to the midline, 2.1–3.7 mm deep to the level of obex with phasic spontaneous activity locked to phrenic or diaphragmatic discharge were labeled using either conventional juxtacellular labeling (Pinault, 1996) or a modified single-cell electroporation technique in which labeling is achieved by a 0.5-second train of high voltage pulses (5–10 V, 200 Hz, 1 ms per pulse: Dempsey et al., 2015). Gentle contact between the pipette and neuron was verified by

observation of a stereotypical response to a single 50–100 nA, 1 ms current pulse (“microstimulation”) prior to electroporation. Positive responses to microstimulation were defined as a transient increase in firing frequency accompanied by an increase in spike amplitude, loss of spike symmetry, and a pipette hyperpolarization of 2–20 mV recorded in the DC channel (Fig. 1). In vitro studies demonstrate that positive responses to microstimulation are strongly predictive of correct pipette position, and can be used as a reliable indicator of juxtacellular contact when blindly approaching cells *in vivo* (Dempsey et al., 2015). Once optimal pipette position was verified the neuron was immediately electroporated using a constant-voltage stimulator connected in parallel to the pipette. Positive pressure in the recording pipette (~ 200 mmHg) was used to prevent pipette blockage during initial brain penetration; in most cases pressure was reduced to zero once the pipette reached 2 mm deep, although in some cases low pressure (~ 30 mmHg) was maintained until a respiratory neuron was identified. Positive pressure in the pipette was not associated with unintentional labeling or dye leakage. Labeling was not attempted on neurons recorded within less than 300 μ m of each other to ensure correct identification of recovered cells. Some of the data presented here contributed to the dataset that describes the development and validation of the modified electroporation technique (Dempsey et al., 2015).

Perfusion and tissue collection

Rats were euthanized with an overdose of sodium pentobarbitone (100 mg/kg i.p. or i.v.) or potassium chloride solution (3 M, 0.3 ml, i.v.) and transcardially perfused with 400 ml heparinized 0.9% NaCl followed by 400 ml freshly prepared fixative solution (4% paraformaldehyde / 0.1 M phosphate buffer; pH 7.4; Sigma-Aldrich, Australia). Brains were removed under RNase-free conditions and further fixed overnight in the same solution. Coronal or parasagittal brainstem sections (50 μ m) were cut on a vibrating microtome and collected in cryoprotectant or phosphate-buffered saline containing 0.1% Tween-20 (PBT; Sigma-Aldrich, Australia).

Histology, in situ hybridization, and immunohistochemistry

cRNA probe synthesis and ISH protocol

A nonradioactive in situ hybridization (ISH) digoxigenin (DIG)-11-UTP-labeled riboprobe was synthesized for the detection of glycine transporter 2 (GlyT2; *Rattus norvegicus* solute carrier family 6, member 5) mRNA. The riboprobe was directed at basepairs 5733–6543 (810 bp length) of the GlyT2 cDNA sequence (GenBank accession number NM_203334.1). The sense cRNA probe was synthesized using an RNA polymerase SP6 promoter attached to the 5' end of the forward oligonucleotide primer (5'-GGATCCATTAGGTGACACTATAGAAG aagcgtcttgcccactagaa-3'). An antisense cRNA probe was synthesized with a T7 promoter attached to the 5' end of the reverse oligonucleotide primer (5'-GAATTCT AATACGACTCACTATAGGGAGA agcctgagcttgcttttcag-3'). A polymerase chain reaction (PCR)-amplified cDNA template was generated using cDNA reverse transcribed from Sprague–Dawley rat brainstem (at approximately –12.6 mm to –11.6 caudal to bregma) total RNA. Following PCR, purified cDNA (QIAquick PCR Purification kit; 28104; Qiagen, Doncaster, Victoria, Australia) was *in vitro* transcribed using a T7 kit (AmpliScribe T7-Flash Transcription Kit; ASF 3257; Epicentre Biotechnologies, Madison, WI) incorporated with DIG-11-UTP (Roche, Nutley, NJ).

Combined ISH and immunohistochemistry

Brainstem sections were incubated in prehybridization buffer (50% formamide, 5 \times SSC, pH 7.0, 250 μ g/ml herring sperm DNA, 100 μ g/ml yeast tRNA, 100 μ g/ml heparin, 5% dextran sulfate, 1 \times Denhardt's solution, 0.1% Tween-20) for 30 minutes at 37°C then at 58°C for 1 hour before hybridization with cRNA riboprobe (final concentration 1,000 ng/ml) for 12–18 hours at 58°C with gentle agitation. Sections were washed in 2 \times SSC buffer with 0.1% Tween-20 followed by 0.2 \times SSC buffer with 0.1%

Tween-20 and then a wash of maleic acid buffer with 0.1% Tween-20. The tissue was then blocked in maleic acid buffer (0.1 M maleic acid, 0.15 M NaCl, 0.1% Tween-20) containing 2% Boehringer blocking reagent (Roche Applied Science, Mannheim, Germany) and 10% normal horse serum.

Primary antibodies were added to the blocking buffer and incubated for 24 hours at 4°C and 4 hours at room temperature. Sections were washed in TPBS (Tris-HCl 10 mM, sodium phosphate buffer 10 mM, 0.9% NaCl, pH 7.4) buffer 3 \times 30 minutes and incubated overnight with IgG secondary antibodies. DIG-labeled neurons were revealed colorimetrically by incubation in NTMT (0.1 M NaCl, 0.1 M Tris-HCl pH 9.5, 0.1 M MgCl₂), 0.1% Tween-20 (Sigma), 2 mM tetramisole HCl (Sigma) buffer containing nitro blue tetrazolium (Roche Applied Science), and 5-bromo-4-chloro-3-indolyl phosphate salts (Roche Applied Science). The reaction was stopped when DIG-labeling was intense with minimal background staining by 3 \times 15 minutes wash in 0.1M Tris (pH 8.5) / 1 mM EDTA solution. No labeling in any brain region was seen when the sense probe was substituted for the antisense probe.

For experiments in which no ISH was performed, sections were washed in PBT for 3 \times 15 minutes and incubated in 0.01 M PBS containing 2% bovine serum albumin and 0.2% Triton X-100 or Tween-20 for 1 hour at room temperature. Primary antibodies (Table 1) were added to the blocking buffer and sections were incubated for 48 hours at 4°C. Sections were washed in TPBS (3 \times 30 minutes) and incubated in IgG secondary antibodies (see Table 1) for 12 hours at 4°C. Processed sections were washed again in TPBS (3 \times 30 min) before being mounted in serial order on glass slides and coverslipped for imaging.

Antibody characterization

Two different sst_{2a} antibodies were used in the current study: we used guinea pig antiserum raised against the C-terminus amino acid sequence 355–369 of rat sst_{2a} and a monoclonal rabbit anti-sst_{2a} antibody raised against the same amino acid sequence. Both antibodies have been extensively characterized by western and dot-blot assay; neither label sst₂ knockout animals, and the rabbit antibody selectively labels HEK cells transfected with sst₂ (Schulz et al., 1998a,b; Korner et al., 2005; Fischer et al., 2008). As recently described, binding of both antisera is blocked by preabsorption with the sst_{2a} antigen, and overlaps completely in tissue incubated with both primary antibodies, visualized with different fluorescent secondary antibodies (Bou Farah et al., 2015).

For detection of neurokinin 1 receptor (NK1R) we used guinea pig and rabbit primary antibodies raised

TABLE 1.
Antibody Details

Antibody name	Immunogen	Manufacturer details	Concentration
<i>Primary antibodies</i>			
Guinea pig anti-SST _{2a}	C-terminus amino acid sequence 355–369 (ETQRTLLNGDLQTSI) of synthetic sst2a peptide	Gramsch Laboratories, Schwabhausen Germany Cat# SS-870 RRID: AB_2491104 Polyclonal	1:1,000
Rabbit anti-SST _{2a}	C-terminus amino acid sequence 355–369 (ETQRTLLNGDLQTSI) of synthetic sst2a peptide	Bio-trend Cat# ss-8000-rmc Lot# a080826 RRID: AB_2491103 monoclonal	1:100
Goat-anti-choline acetyltransferase (ChAT)	Human placental lysate	Chemicon, Millipore Cat# AB144P RRID: AB_2079751 Polyclonal	1:800
Guinea pig anti-neurokinin 1 receptor (NK1R)	C-terminus amino acid sequence 393–407 (KTMTESSSFYSNMLA) of synthetic rat NK1R peptide	Millipore Cat# AB15810 Lot# LV1587443 RRID: AB_992894 Polyclonal	1:1,000
Rabbit anti-NK1R	C-terminus amino acid sequence 393–407 (KTMTESSSFYSNMLA) of synthetic rat NK1R peptide	Sigma-Aldrich Cat# S8305 Lot# 67K4885 RRID: AB_261562 Polyclonal	1:5,000
Mouse anti-tyrosine hydroxylase (TH)	Rat tyrosine hydroxylase N-terminal region (approx. aa 9–16)	Sigma-Aldrich Cat# T1299 RRID: AB_477560 Monoclonal	1:8,000
Rabbit anti-phox2b	14 amino acid C-terminal sequence (YFHRKPGPALKTNLF) of the rat/mouse Phox2b protein	Jean François Brunet RRID: AB_2315161 Polyclonal	1:1,000
Sheep anti-digoxigenin	Digoxigenin, whole	Roche Applied Science Cat# 11093274910 RRID: AB_514497 Polyclonal	1:1,000
<i>Secondary antibodies</i>			
ExtrAvidin-FITC	n/a	Sigma-Aldrich Cat# E2761 RRID: AB_2492295	1:500
Cy3- AffiniPure donkey antigoat IgG (H+L)	Whole molecule goat IgG	Jackson ImmunoResearch Laboratories, INC Cat# 705-165-147 Lot# 68839 RRID: AB_2307351 Polyclonal	1:250
Alexa Fluor 647-AffiniPure donkey antirabbit IgG (H+L)	Whole molecule rabbit IgG	Jackson ImmunoResearch Laboratories, INC Cat# 711-605-152 Lot# 105115 RRID: AB_2492288 Polyclonal	1:250
Alexa Fluor 647 donkey antirabbit IgG (H+L)	Rabbit, IgG heavy & light chains	Life Technologies Cat# A31573 Lot# 1322326 RRID: AB_10561706 Polyclonal	1:250
Alexa Fluor 488-AffiniPure donkey antiguinea pig IgG (H+L)	Whole molecule guinea pig IgG	Jackson ImmunoResearch Laboratories, INC Cat# 706-545-148 Lot# 161406 RRID: AB_2340472 Polyclonal	1:250
Alexa Fluor 647 goat antiguinea pig IgG (H+L)	Domestic guinea pig, IgG heavy & light chains	Life Technologies Cat# A21450 Lot# 1235826 RRID: AB_10564076 Polyclonal	1:250
Alexa Fluor 488 donkey antimouse IgG (H+L)	Mouse, IgG heavy & light chains	Life Technologies Cat# A21202 RRID: AB_10049285 Polyclonal	1:250

against a synthetic peptide that corresponds to amino acid sequence 393–407 of rat NK1R. The rabbit antibody has been validated in NK1R knockout animals (Ptak et al., 2002) and results in distinctive NK1R labeling in the brainstem and spinal cord (Al-Khater et al., 2008; Bochorishvili et al., 2012). The guinea pig antibody recognizes the same sequence, has been validated (by the manufacturers) by western blot, and results in the expected pattern of immunolabeling (Yu et al., 2009; Spirovski et al., 2012).

A mouse anti-tyrosine hydroxylase (TH) monoclonal antibody was used to detect catecholaminergic neurons. This antibody has been widely used by other investigators (Berube-Carriere et al., 2009; Forlano and Woolley, 2010; Lindemann et al., 2013) and results in characteristic intense labeling of neurons in the brainstem C1, C3, and A1 groups.

A goat anti-choline acetyl transferase (ChAT) antibody was used to identify cranial motoneurons in the facial nucleus and nucleus ambiguus. Western blot analysis (by the manufacturer) reveals a single band at 70 kDa. Incubation with the antibody resulted in the expected pattern of immunolabeling.

Phox2b immunoreactivity was detected using a rabbit polyclonal antibody. Immunolabeling obtained using the same antibody colocalizes perfectly with Phox2b mRNA expression in the mouse (Pattyn et al., 1997), is reported to be absent in Phox2b knockout animals, and overlaps with reporter expression Phox2b-EGFP transgenic animals (Lazarenko et al., 2009). The general pattern of labeling was consistent with previous reports, with high expression of Phox2b immunoreactivity in small neurons in the retrotrapezoid nucleus, high colocalization of Phox2b immunoreactivity with TH immunoreactivity in the C1 region, and Phox2b immunoreactivity in the facial nucleus and nucleus ambiguus compact formation.

Microscopy and analysis

Processed sections were mounted on glass slides in Vectashield (Vector Laboratories, Burlingame, CA, #H-1000) or Dako fluorescence mounting medium (Dako, Carpinteria, CA, #S302380-2) and coverslipped for viewing using an AxioImager Z2 microscope under epifluorescence and brightfield illumination (Zeiss, Gottingen, Germany). Mosaic images of each coronal brainstem section were captured at 10 \times magnification and adjusted for brightness and contrast using ZEN software (2012 version, Carl Zeiss, RRID: SCR_013672). Color channels were overlaid in the resultant image file for analysis.

Definition of VLM respiratory compartments

BötC, preBötC, and rVRG respiratory neurons are distributed in overlapping and adjacent regions of the brainstem. Electrophysiologists are in general agreement that the highest proportion of BötC neurons are found within 500 μ m caudal of the caudal pole of the facial nucleus, as determined by electrophysiological mapping of facial field potentials (Sun et al., 1998; Schreihofer et al., 1999). The majority of inspiratory putative preBötC neurons are found 500–1,100 μ m caudal to facial, with a transition zone of intermingled BötC and preBötC neurons that lies 500–700 μ m caudal to the facial nucleus (Sun et al., 1998; Wang et al., 2001; Stornetta et al., 2003a). This corresponds well with the anatomical distribution of SST, a putative marker of preBötC (Stornetta et al., 2003a). A population of bulbospinal inspiratory locked neurons, many of which express NK1R, emerges beyond 1,000 μ m caudal to the facial nucleus and extends for about 600 μ m (Guyenet et al., 2002; Stornetta et al., 2003a,b). This population is thought to represent excitatory premotor neurons of the rVRG, as defined by trans-synaptic labeling of phrenic motoneurons (Dobbins and Feldman, 1994).

In the current study we defined BötC as residing 0–500 μ m caudal to the facial nucleus, preBötC as residing 600–1,100 μ m caudal to the facial nucleus, and rVRG as residing 1,200–1,800 μ m caudal to the facial nucleus. Rostrocaudal coordinates are presented with reference to the caudal pole of the facial nucleus as mapped in electrophysiology experiments or identified in histological experiments; the most caudal position at which facial motor neurons are clearly discernable corresponds to \sim 12.0 mm caudal to bregma according to the stereotaxic atlas of Paxinos and Watson (2006).

For quantification of sst_{2a}, NK1R, and TH colocalization, regions that contained the preBötC (1–3 samples each from 4 rats, 13 images in total) were scanned using a confocal microscope under 10 \times objective (TCS SP5 X, Leica, Germany). The balance and contrast of the images were adjusted to include all information-containing pixels using ZEN or LAS AF software (RRID: SCR_013673). Figures were prepared using Coreldraw and Corel Photopaint X4 (Ottawa, Canada; RRID: SCR_013674).

For quantification of overall sst_{2a} distribution, sst_{2a}-immunoreactive neurons lying within the ventrolateral medulla between 0 and 2.4 mm caudal to the facial nucleus were counted bilaterally in six rats. Three to six sections were quantified at each rostrocaudal level indicated in Figure 2B (two images per section [one on

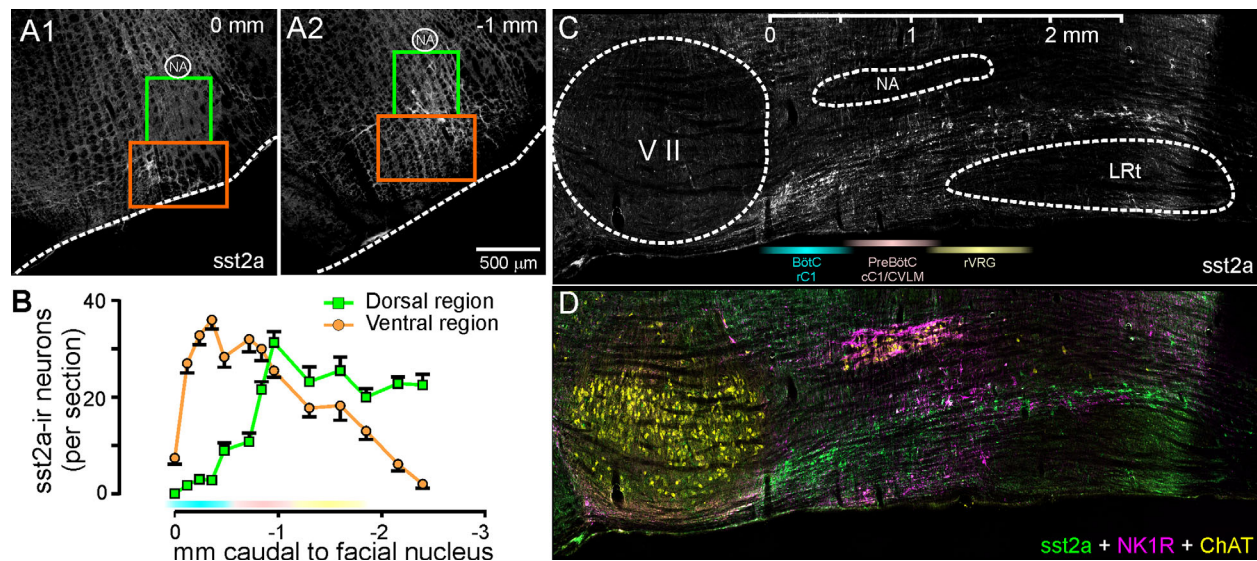


Figure 2. *sst*_{2a}-immunoreactive cells are distributed along the entire ventrolateral medulla. Cells residing in dorsal (green) or ventral (orange) regions of interest were counted and plotted against rostral coordinates. **A1,A2:** *sst*_{2a} immunoreactivity and boxes used to define regions of interest at coordinates corresponding to the caudal pole of the facial nucleus (0 mm) and preBötC (1 mm). **B:** Pooled data from six rats. **C:** Parasagittal section shows the extent of *sst*_{2a} labeling within the ventrolateral medulla. **D:** Same section overlaid with NK1R and ChAT immunoreactivity. NA: compact formation of nucleus ambiguus. VII: facial nucleus; LRt: reticular formation; BötC: Bötzingen Complex; rC1: rostral C1 group; cC1: caudal C1 group; CVLM: caudal ventrolateral medulla; rVRG: rostral ventral respiratory group.

each side], 131 images in total). We observed a shift in the dorsoventral position of *sst*_{2a}-immunoreactive neurons at different bregma levels, so we divided the VLM into dorsal and ventral compartments. The dorsal compartment was defined as a 500 × 500 μm box that lay center-aligned and immediately ventral to nucleus ambiguus. The ventral compartment was defined as a 500 μm high × 750 μm wide box that lay immediately ventral to the dorsal compartment (Fig. 2). In sections in which the compact formation of nucleus ambiguus could not be clearly distinguished both compartments were aligned to 1.8 mm lateral of midline.

The size of biotin- or dextran-labeled neurons was estimated by measuring the long and short axis of each neuron in the center of its focal plane, from which its cross-sectional area was estimated. Size data are presented as standardized diameter, i.e., the diameter of a circle with the same cross-sectional area.

RESULTS

General pattern of *sst*_{2a} immunoreactivity

*sst*_{2a}-immunoreactive neurons and fibers were identified throughout the ventral medulla. Particularly dense expression was found in cell bodies in the nucleus raphe magnus, in neurons immediately dorsal, medial, and lateral to the compact formation of nucleus ambiguus, and in a single contiguous band that started at the ventral aspect of the facial nucleus and extended

caudally for several millimeters. As the distance from the facial nucleus increased *sst*_{2a}-immunoreactive neurons concentrated more dorsally (Fig. 2).

*sst*_{2a}-immunoreactive neurons are present in the rostral ventrolateral medulla (RVLM) C1 region but not BötC

Within 500 μm of the facial nucleus *sst*_{2a} immunoreactivity was densely expressed in the portion of the ventrolateral medulla closest to the ventral surface of the brainstem, overlapping closely with the distribution of the catecholaminergic C1 neurons, but was largely absent in the dorsal compartment of the VLM, corresponding to the BötC (Figs. 2 and 3)). In the rostral C1 (rC1) region and retrotrapezoid nucleus/parafacial respiratory region (RTN/pFRG, data not shown) *sst*_{2a} immunoreactivity often colocalized with TH immunoreactivity (Fig. 3A). TH-immunoreactive neurons that were Phox2b-immunoreactive were often *sst*_{2a}-positive (Fig. 3A5), but Phox2b neurons that were TH-negative were almost never *sst*_{2a}-immunoreactive (data not shown). The pattern of *sst*_{2a} immunoreactivity in the RVLM rC1 region and its colocalization with TH immunoreactivity was qualitatively similar to that previously reported (Burke et al., 2008), and is therefore not presented in detail.

The BötC was defined as the region immediately ventral to nucleus ambiguus compact formation containing dense glycine transporter-2 (GlyT2) mRNA expression (Schreihofer et al., 1999). In contrast to the high *sst*_{2a}

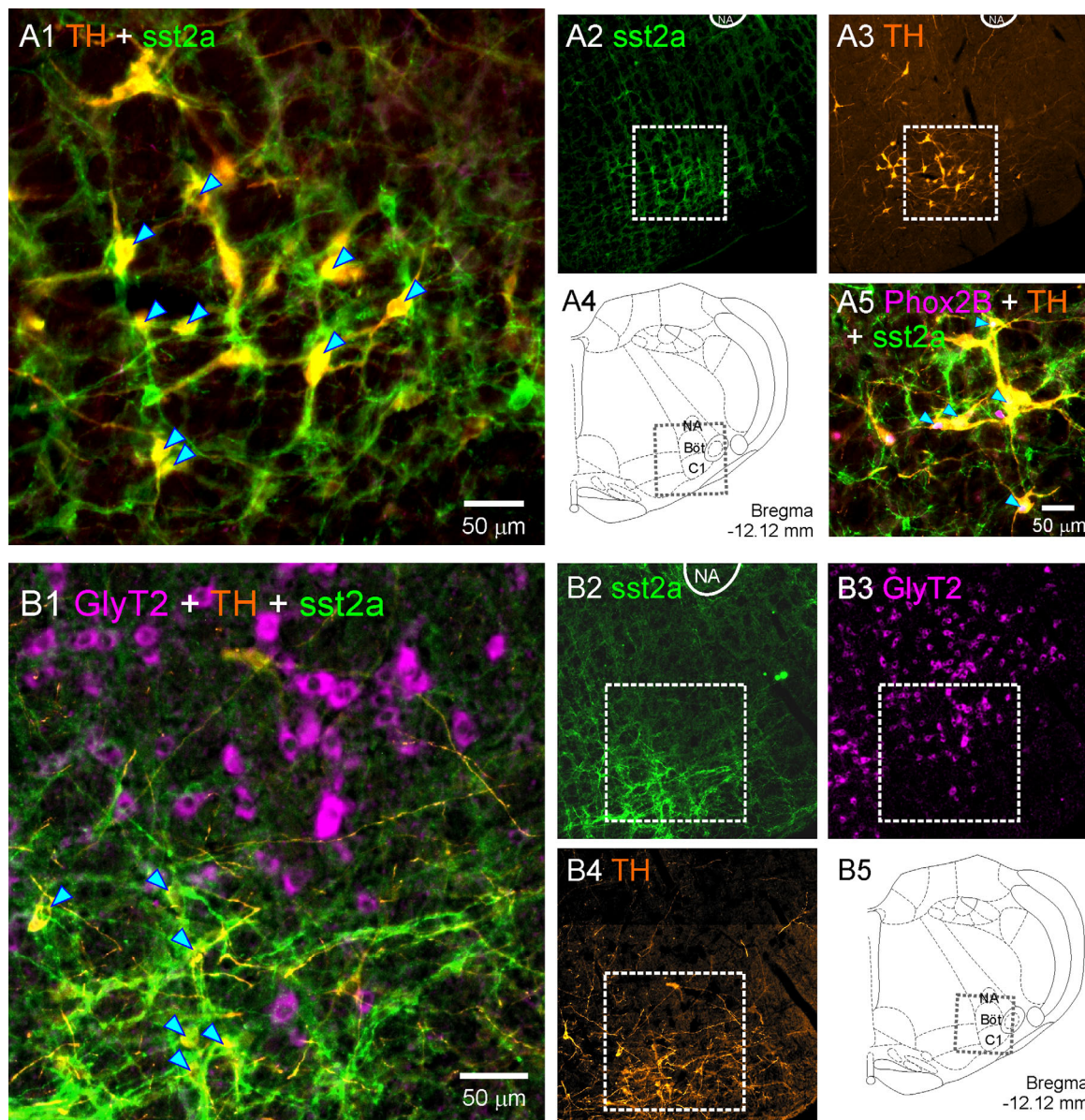


Figure 3. *sst*_{2a} expression is colocalized with markers of cardiovascular but not respiratory function in the RVLM/BötC. **A:** Epifluorescent photomicrographs show colocalization of *sst*_{2a} with TH immunoreactivity (A1, arrowheads). Region shown in A1 indicated by hatched boxes in individual channel images (A2,A3). Similarly, region illustrated in A2 + A3 indicated by hatched box in stereotaxic reference image (A4). A5 shows colocalization of *sst*_{2a} with Phox2B and TH (arrowheads) in another experiment. **B:** *sst*_{2a} immunoreactivity does not colocalize with GlyT2 ISH product in the BötC. No GlyT2-positive *sst*_{2a}-positive neurons were ever identified. Format as in (A); (B1) shows pseudocolored inverted ISH signal overlaid with TH and *sst*_{2a} immunoreactivity. Arrowheads indicate double-labeled TH/*sst*_{2a}-positive neurons.

immunoreactivity observed in the RVLM C1 region, *sst*_{2a} immunofluorescence was absent in the BötC. Expression of GlyT2 mRNA and *sst*_{2a} was quantified in one representative BötC section from three rats using the same segregation into dorsal and ventral regions illustrated in Figure 2A. The dorsal compartment contained 115 ± 9 GlyT2-positive neurons per section and 4 ± 1 *sst*_{2a}-immunoreactive neurons, none of which colocalized with GlyT2 (Fig. 3B). The ventral compartment contained 46

± 9 GlyT2-positive neurons and 36 ± 4 *sst*_{2a} neurons; one double-labeled neuron was encountered.

*sst*_{2a}-immunoreactive neurons in the preBötC are either NK1R- or TH-immunoreactive

The difference in dorsoventral distribution of *sst*_{2a} immunoreactivity seen in the rC1/BötC was not observed

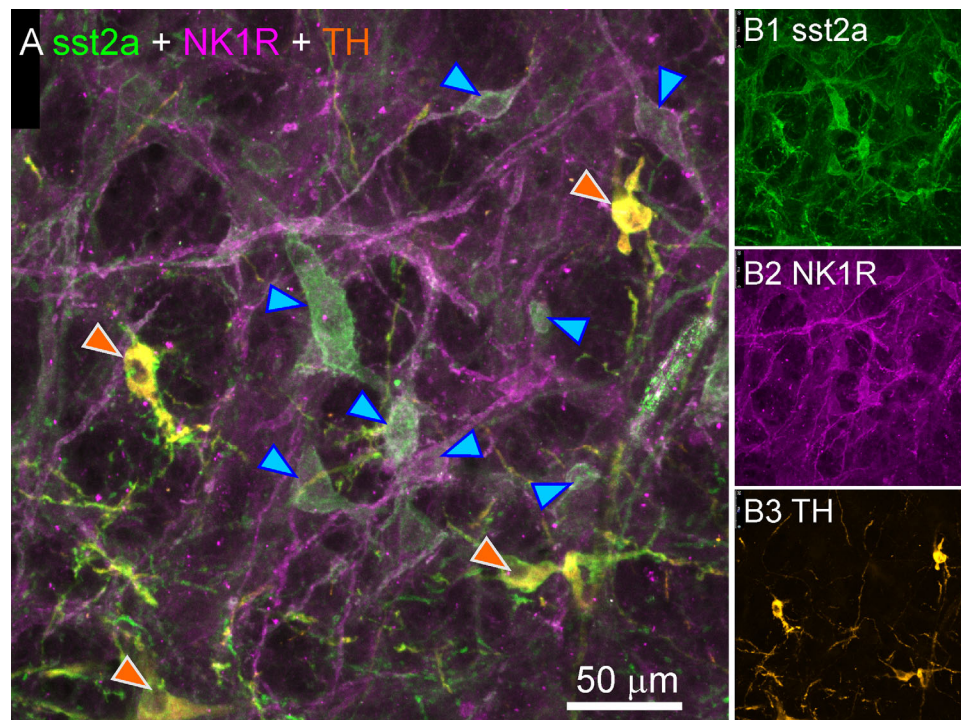


Figure 4. sst_{2a} immunoreactivity in the preBötC is partially colocalized with NK1R and TH. **A:** Merged confocal stack showing colocalization of sst_{2a} with NK1R (blue arrowheads) and TH (orange arrowheads). Individual channel images are shown in **B1–3**.

in confocal images containing the preBötC (13 ± 2 [dorsal] vs. 14 ± 1 [ventral] neurons per image, $P = 0.4$, $t = 1.03$, $df = 3$, $n = 13$ images from four rats, paired t -test). The distribution of sst_{2a} -immunoreactive neurons partially overlapped with the expression of NK1R immunoreactivity in both compartments (Fig. 4), with a significantly greater proportion of sst_{2a} -positive neurons expressing NK1R in the dorsal region (corresponding to preBötC) compared to the ventral region, corresponding to the caudal C1 (cC1) / CVLM region (54 ± 5 vs. $20 \pm 2\%$ respectively, $P = 0.003$, $t = 8.5$, $df = 3$, $n = 4$, paired t -test). Difficulties in accurately quantifying the total number of NK1R-positive neurons precluded reliable estimates of the total fraction of NK1R-immunoreactive cells that were also sst_{2a} -positive, but many NK1R-immunoreactive neurons were sst_{2a} -negative.

Catecholaminergic neurons continued to account for a significant portion of sst_{2a} -positive neurons in the preBötC and cC1/CVLM regions (27 ± 1 and $33 \pm 2\%$, respectively), with sst_{2a} immunoreactivity identified in 57 ± 4 of dorsal compartment and $46 \pm 4\%$ of ventral compartment TH-immunoreactive neurons. No coexpression of NK1R with TH was detected (although we have previously reported a marginal coexpression of NK1R with TH in the RVLM: Makeham et al., 2001): preBötC and cC1/CVLM sst_{2a} -positive neurons that coexpress NK1R or TH therefore accounted for $81 \pm 4\%$ of the total sst_{2a} -positive pop-

ulation. In the rVRG, sst_{2a} -immunoreactive cells formed a dense cluster that colocalized with TH neurons (data not shown).

sst_{2a} immunoreactivity on functionally identified respiratory neurons

Fifty-two respiratory neurons (electroporated: 45, juxtacellularly labeled: 7) were evenly filled with neurobiotin ($n = 42$) or dextran ($n = 10$), with dendritic/axonal filling also visible. A further four recovered respiratory neurons were positive for ChAT immunoreactivity (and sst_{2a} -negative), identifying them as respiratory motoneurons, and were excluded from the current dataset. ChAT-negative cells were considered respiratory interneurons or premotor neurons. In nine cases two neurons were recovered in close proximity to each other when a single labeling attempt had been made. In all cases in which multiple neurons were labeled, both were negative for sst_{2a} immunoreactivity, so the data were included and counted as a single cell but excluded from morphometric analysis.

Cycle-triggered averages of unit firing with respect to diaphragmatic/phrenic nerve activity were used to classify neurons according to the functional criteria described by Smith et al. (2007) (Fig. 5): expiratory decrementing neurons (E-dec: $n = 10$), expiratory augmenting neurons (E-aug: $n = 4$), expiratory tonic

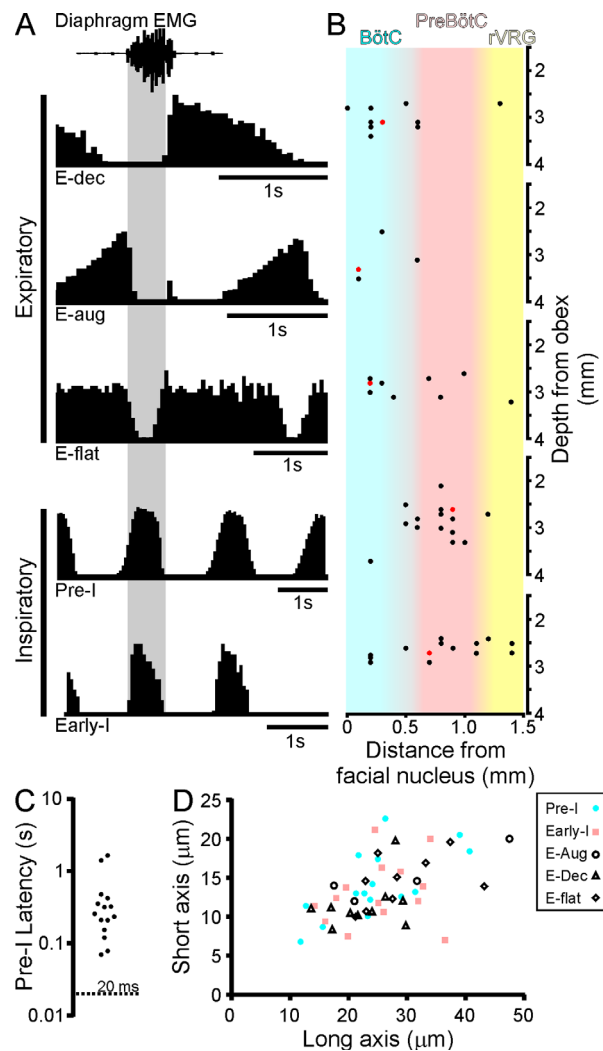


Figure 5. Functional classifications and anatomical locations of recovered respiratory neurons. **A:** Cycle-triggered histograms illustrating different functional classes of respiratory neuron and **(B)** stereotaxic coordinates at which neurons of each class were recorded and recovered. X-axes of each histogram was adjusted such that inspiratory period in each recording is equivalent to the width of the gray band. Red dots in B indicate cells illustrated in Fig. 6. **C:** Latencies between the onset of neuronal firing and the onset of the phrenic/diaphragmatic burst in neurons classified as preinspiratory. Dashed line indicates threshold for classification. The two neurons with pre-I latencies of >1 s were recorded in one experiment, in which the respiratory period was unusually long. Each data point represents the average value recorded in 6–10 consecutive respiratory cycles. **D:** Dimensions of recovered neurons, classified by functional properties.

discharge neurons (E-flat: $n = 9$), preinspiratory neurons (pre-I: $n = 15$), and early inspiratory neurons (early-I: $n = 14$). Most E-dec and E-aug neurons (10/14) were located within 500 μm of the caudal pole of the facial nucleus, with an average depth of 3.04 ± 0.08 mm from the level of obex, anatomically consist-

ent with being within the confines of the BötC (Sun et al., 1998). The distribution of E-flat neurons was more spread out through the VRC. According to the criteria described by Guyenet and Wang (2001), neurons were considered pre-I when the first action potential recorded in each respiratory cycle consistently preceded the phrenic/diaphragmatic inspiratory burst by >20 ms and discharge continued to the peak of phrenic/diaphragmatic discharge. The “pre-I latencies” of neurons classified as preinspiratory are presented in Figure 5C. A total of 17/29 pre-I and early-I neurons were recorded between 600–1,100 μm caudal to the facial nucleus, anatomically consistent with the preBötC.

Size estimates of recovered biotin- or dextran-labeled respiratory neurons are presented in Figure 5D. Excluding data in which multiple neurons were labeled in a single attempt, diameters of E-dec, E-aug, E-flat, pre-I, and early-I neurons were 17.1 ± 1.3 ($n = 10$), 22.5 ± 3.5 ($n = 4$), 21.5 ± 1.4 ($n = 9$), 19.3 ± 1.4 ($n = 15$), and 19.4 ± 1.1 ($n = 14$) μm , respectively. No recovered neurons were sst_{2a} -immunoreactive. In some cases, dye-labeled neurons were recovered in close proximity to sst_{2a} -immunoreactive cell bodies or fibers, and in all cases sst_{2a} -positive labeling was apparent on the same sections, but clear evidence of sst_{2a} expression was absent (Fig. 6).

DISCUSSION

The current study provides a detailed description of the distribution of sst_{2a} -expressing neurons in the VLM with reference to functionally and neurochemically distinct respiratory compartments. We report that sst_{2a} is distributed across a contiguous region of the ventral brainstem that encompasses the RTN, RVLM C1 group, preBötC, and rVRG, but that colocalization of sst_{2a} with markers of respiratory function, as defined by anatomical location and neurochemical phenotype, is sparse or absent in all but the preBötC, where substantial colocalization of sst_{2a} with NK1R was identified. These findings were supported by electrophysiological experiments in which neurons were selected by anatomical and functional criteria and recovered for sst_{2a} immunohistochemistry: no sst_{2a} -positive neurons were identified. Taken together, the findings suggest that somatic expression of sst_{2a} is rare on classically defined respiratory neurons, and challenges the mechanisms previously proposed to account for the effects of SST administration on respiratory rhythm generation and pattern formation.

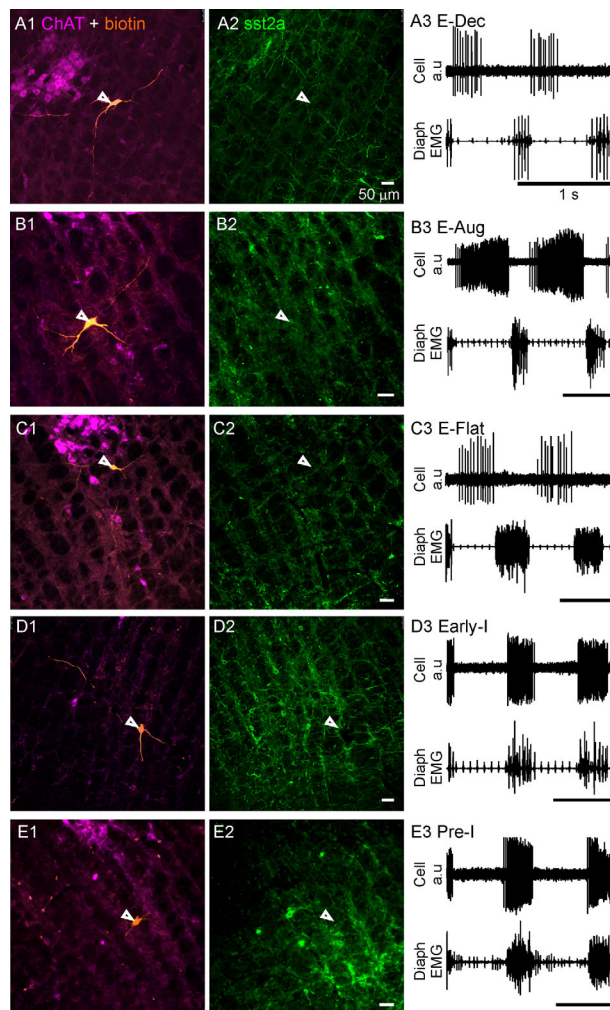


Figure 6. Medullary respiratory neurons do not express sst_{2a} . **A–E:** Examples of neurobiotin-labeled respiratory neurons that were processed for sst_{2a} immunoreactivity. Panel 1 shows neurobiotin labeling (orange) and ChAT (magenta) immunoreactivity; none of the neurons shown are ChAT-positive, and are therefore considered respiratory interneurons. In each case sst_{2a} -positive fibers or somata were visible in the region of the recovered neuron (Panel 2), but no neurobiotin-labeled cells ($n = 52$) were sst_{2a} -positive. Panel 3 shows corresponding electrophysiological recordings from each neuron. Photomicrographs are taken in the coronal plane with the ventral surface towards the bottom of the field of view; nucleus ambiguus is visible as a cluster of cholinergic neurons in A,B,C,E. Scale bars in electrophysiological recordings = 1 second. Electrical noise in EMG trace shown in E3 has been edited to aid clarity. Scale bars in photomicrographs = 50 μ m.

Somatic expression of sst_{2a} receptor is absent in BötC

One of the specific aims of the current study was to examine the hypothesis that sst_{2a} is marker for BötC E-Dec neurons. This population is, along with other subsets of BötC expiratory neurons, largely glycinergic (Schreihofer et al., 1999; Ezure et al., 2003), and is proposed to play a

role in inspiratory-to-expiratory phase transition and generation of postinspiratory activity (Ezure and Manabe, 1988; Smith et al., 2013; Dutschmann et al., 2014). Our hypothesis was based on the observation that microinjection of SST into the BötC evokes apneusis and loss of postinspiratory activity in vagal (and sympathetic) nerve activities (Burke et al., 2010), suggestive of a specific inhibitory effect on E-Dec neurons. We found that sst_{2a} immunoreactivity was closely associated with the C1 cell group, which lies immediately ventral to the BötC, but sparse in the BötC, with no colocalization with GlyT2 mRNA, the distribution of which was similar to that described in previous investigations (Schreihofer et al., 1999; Ezure et al., 2003; Tanaka et al., 2003). No sst_{2a} immunoreactivity was detected in 15 expiratory-locked BötC neurons, of which seven had a decrementing firing pattern. We conclude that somatic expression of sst_{2a} is absent from the BötC, and therefore not a marker BötC E-Dec neurons.

sst_{2a} is associated with preBötzinger Complex NK1R neurons but not widely expressed on functionally identified neurons

In contrast to the BötC, high levels of sst_{2a} expression were consistently observed in the preBötC. Most sst_{2a} -positive neurons in this region were also immunoreactive for either NK1R (54%) or TH (27%), leaving the neurochemical phenotype of only 19% of sst_{2a} -positive neurons unaccounted for. The association between sst_{2a} and NK1R expression in the preBötC has not previously been quantified, but our findings are consistent with qualitative studies of neonatal mice (Gray et al., 2010; Gray, 2013), which propose that glutamatergic neurons that express NK1R, sst_{2a} , and/or SST are an anatomical marker for the “core” of the preBötC.

We observed no expression of sst_{2a} on 18 neurons recorded within the strict anatomical boundaries of the preBötC, of which 11 exhibited the preinspiratory discharge that is a signature for putative pacemaker neurons. We therefore conclude that, despite a relatively high expression of sst_{2a} within the preBötC, the expression of sst_{2a} on inspiratory-locked neurons, or at least those neurons amenable to extracellular recording *in vivo*, is unexpectedly low.

Technical considerations

There are two caveats to our conclusion that sst_{2a} is rarely expressed on preBötC inspiratory neurons. First, it may be that sst_{2a} is present on some, but expressed at levels too low to detect using immunohistochemistry. Second, it may be that sst_{2a} -expressing respiratory neurons are abundant, but difficult to record and/or label.

The monoclonal anti-*sst*_{2a} antibody used in the current study resulted in robust labeling of neuronal cell bodies in regions in which *sst*_{2a} immunoreactivity has previously been observed using other well-validated anti-*sst*_{2a} antibodies (Burke et al., 2008; Spary et al., 2008; Gray et al., 2010), and resulted in labeling of fibers in brainstem regions in which little or no somatic labeling was visible, suggesting a reasonable level of sensitivity. The specificity of this antibody has previously been verified to a high standard, including artificial expression and knockout animals (Fischer et al., 2008), and the antibody has been recommended as a gold standard tool for the clinical detection of *sst*_{2a}-expressing tumors (Korner et al., 2012). We have recently shown that binding of the rabbit monoclonal anti-*sst*_{2a} antibody correlates well with SST sensitivity in RVLM bulbospinal neurons recorded *in vitro* (Bou Farah et al., 2015), and therefore interpret *sst*_{2a} labeling as reliable evidence of *sst*_{2a} protein expression, although it is possible that low levels of *sst*_{2a} expression remained undetected.

Alternatively, it may be that *sst*_{2a}-expressing neurons contribute to the generation of respiratory drive, but that their activity profile does not conform to the expected phasic bursting pattern used to select putative respiratory neurons for labeling, or that their morphologies or size make them unamenable to stable recording (Humphrey and Schmidt, 1990). Although we observed no obvious influence of cell size on labeling efficiency when developing our single-cell electroporation technique *in vitro* (Dempsey et al., 2015), the size range of respiratory neurons labeled in the current study indicates a bias towards larger neurons, probably reflecting a limitation of the extracellular recording technique rather than a deficiency in the approach used to label them. This may be problematic when considering putative preinspiratory neurons in the preBötC, as SST is largely restricted to smaller neurons (typically $10 \times 18 \mu\text{m}$; Stornetta et al., 2003a; Wei et al., 2012). Indeed, the same argument has been proposed to explain the absence of SST in functionally identified preBötC neurons (Stornetta et al., 2003a). Although some of the labeled preBötC neurons fell within that range, most were larger, with average dimensions of $14.1 \pm 1.1 \times 23.7 \pm 1.9 \mu\text{m}$ ($n = 17$). Another possibility is that *sst*_{2a} is expressed on a small minority of respiratory neurons, and that our sample size was insufficient to detect the *sst*_{2a}-positive population. The Monte Carlo model presented by Del Negro et al. (2002b) is useful for calculating the statistical power of strings of binary observations, such sequences of coin-tosses. Applied to our observation that *sst*_{2a} was undetectable in all 17 preBötC neurons, their model indi-

cates a 96% probability that *sst*_{2a} is expressed on less than 20% of preBötC neurons (assuming that *sst*_{2a}-positive and *sst*_{2a}-negative neurons are equally likely to be labeled) and, extended to include all 52 neurons recovered in the current study, <5.5% of VRC respiratory neurons overall (95% confidence).

Functional implications

Based on our previous findings (Burke et al., 2010) we hypothesized that the expression of SST receptors on BötC E-Dec neurons likely mediates the apneusis evoked by BötC SST microinjection at doses above 6 pmol. The results of the current study unambiguously indicate that *sst*_{2a} expression is not associated with glycinergic or expiratory-locked BötC neurons. We therefore conclude that the effects evoked by SST microinjection in the BötC are probably not mediated by somatic expression of *sst*_{2a} on respiratory neurons, and may instead indicate expression of other SST receptor isoforms or effects on neurons presynaptic to BötC neurons. Given that RVLM sympathetic premotor neurons lie immediately adjacent to BötC neurons (Kanjhan et al., 1995), are inhibited by exogenous SST application (Burke et al., 2008; Bou Farah et al., 2015), and have been recently shown to accelerate respiration frequency when optogenetically activated (Abbott et al., 2013, 2014; Burke et al., 2014), it is conceivable that withdrawal of excitatory drive from RVLM C1 neurons contributes to the apneustic breathing previously observed following microinjection of SST in the BötC.

We focused on the *sst*_{2a} receptor isoform following numerous surveys of SST receptor protein and mRNA expression that consistently identified high levels of *sst*_{2a} in the VLM. However, of the five other SST receptor isoforms, only *sst*₃ and *sst*₅ have been reported as completely absent, with *sst*₁, *sst*_{2b}, and *sst*₄ expressed at variable levels (Burke et al., 2008; Spary et al., 2008; Ramírez-Jarquín et al., 2012). Functional studies support a key role for *sst*₂ in driving responses to exogenous SST in the C1 region and preBötC, as they are abolished by *sst*₂ blockade and mimicked by the *sst*₂-selective agonist BIM23014c (Burke et al., 2008; Ramírez-Jarquín et al., 2012). However, to date no agents with selectivity for the *sst*_{2a} or *sst*_{2b} splice variants have been used to define SST-sensitive populations of respiratory neurons, and no subtype-specific agents have been used to assess SST sensitivity in respiratory compartments other than preBötC, leaving potential roles for other SST receptor isoforms in mediating responses to exogenous SST.

The intersection of the *sst*_{2a}-, NK1R-, and somatostatin-positive populations is widely believed to represent the core rhythm-generating kernel of the

preBötC (Stornetta et al., 2003a; Gray et al., 2010; Feldman et al., 2013; Smith et al., 2013). This hypothesis is based on the restricted distribution of this group and observations that selective silencing of SSTergic, SST-, or substance P-sensitive preBötC neurons profoundly inhibits respiratory rhythmogenesis (Gray et al., 2001; McKay et al., 2005; McKay and Feldman, 2008; Tan et al., 2008; Burke et al., 2010). However, a logical prediction of this hypothesis is that neurons with a pre-inspiratory activity profile should express NK1R, SST, or *sst_{2a}*, and this does not seem to be the case. NK1R is only expressed on a minority of electrophysiologically characterized preBötC preinspiratory neurons (~34%; Guyenet and Wang, 2001). The same investigators were unable to detect evidence of SST expression in 36 respiratory neurons labeled in the same region (Stornetta et al., 2003a), and we report here that *sst_{2a}* was not detected on inspiratory preBötC neurons. Taken together, these findings suggest that modification of the existing hypotheses regarding the neurochemical phenotype of the rhythm-generating core may be necessary.

Given the low prevalence of NK1/SST/*sst_{2a}* expression in phasic preBötC neurons, we support the proposal that NK1/SST/*sst_{2a}*-positive neurons may possess an electrophysiological signature that is tonic, not phasic, as previously postulated (Gray et al., 1999; Stornetta et al., 2003a). This would allow them to contribute to the rhythm-generating circuit while eluding electrophysiological characterization as “respiratory” neurons. Such properties would explain the discord between predicted neurochemical and functional phenotype, and is consistent with some older models of respiratory rhythm generation, in which tonic excitatory drive regulates the excitability of the rhythmogenic kernel (Smith et al., 2000). Alternatively, it may be that input from this group is not required by rhythm generating core of the preBötC, but instead represents a peripheral component of the rhythm generating network. This view is supported by recent work by Tupal et al. (2014), who found that elimination of glutamate release from SSTergic preBötC neurons is not associated with any respiratory phenotype, as would be predicted if this population contained the pacemaking kernel.

In the current study we describe widespread expression of *sst_{2a}* immunoreactivity that spans regions of the VLM associated with respiratory function. However, the association between *sst_{2a}* and neurochemical markers of respiratory function is poor, and we were unable to find any evidence of *sst_{2a}* expression in neurons with phasic respiratory discharge. We therefore conclude that somatic *sst_{2a}* expression is a poor marker of respiratory function in this region.

CONFLICT OF INTEREST

The authors report no conflicts of interest

AUTHOR ROLES

PGB, NNK, SM, and AKG conceived the study; SL conducted the immunohistochemistry and imaging; SL, SM and AJT conducted single cell labeling experiments; LMP synthesized the GlyT2 ISH probe; SL and SM analyzed the data. All authors wrote the article.

LITERATURE CITED

- Abbott SB, DePuy SD, Nguyen T, Coates MB, Stornetta RL, Guyenet PG. 2013. Selective optogenetic activation of rostral ventrolateral medullary catecholaminergic neurons produces cardiorespiratory stimulation in conscious mice. *J Neurosci* 33:3164–3177.
- Abbott SB, Holloway BB, Viar KE, Guyenet PG. 2014. Vesicular glutamate transporter 2 is required for the respiratory and parasympathetic activation produced by optogenetic stimulation of catecholaminergic neurons in the rostral ventrolateral medulla of mice in vivo. *Eur J Neurosci* 39: 98–106.
- Al-Khater KM, Kerr R, Todd AJ. 2008. A quantitative study of spinothalamic neurons in laminae I, III, and IV in lumbar and cervical segments of the rat spinal cord. *J Comp Neurol* 511:1–18.
- Allen JP, Hathway GJ, Clarke NJ, Jowett MI, Topps S, Kendrick KM, Humphrey PP, Wilkinson LS, Emson PC. 2003. Somatostatin receptor 2 knockout/lacZ knockin mice show impaired motor coordination and reveal sites of somatostatin action within the striatum. *Eur J Neurosci* 17:1881–1895.
- Berube-Carriere N, Riad M, Dal Bo G, Levesque D, Trudeau LE, Descarries L. 2009. The dual dopamine-glutamate phenotype of growing mesencephalic neurons regresses in mature rat brain. *J Comp Neurol* 517:873–891.
- Bochorishvili G, Stornetta RL, Coates MB, Guyenet PG. 2012. Pre-Bötzinger complex receives glutamatergic innervation from galaninergic and other retrotrapezoid nucleus neurons. *J Comp Neurol* 520:1047–1061.
- Bou Farah L, Bowman BR, Bokinić P, Karim S, Le S, Goodchild AK, McMullan S. 2015. Somatostatin in the rat rostral ventrolateral medulla: Origins and mechanism of action. *J Comp Neurol* [Epub ahead of print].
- Burke PG, Li Q, Costin ML, McMullan S, Pilowsky PM, Goodchild AK. 2008. Somatostatin 2A receptor-expressing presympathetic neurons in the rostral ventrolateral medulla maintain blood pressure. *Hypertension* 52:1127–1133.
- Burke PGR, Abbott SBG, McMullan S, Goodchild AK, Pilowsky PM. 2010. Somatostatin selectively ablates post-inspiratory activity after injection into the Bötzing complex. *Neuroscience* 167:528–539.
- Burke PG, Abbott SB, Coates MB, Viar KE, Stornetta RL, Guyenet PG. 2014. Optogenetic stimulation of adrenergic C1 neurons causes sleep state-dependent cardiorespiratory stimulation and arousal with sighs in rats. *Am J Respir Crit Care Med* 190:1301–1310.
- Chen ZB, Hedner T, Hedner J. 1990. Local application of somatostatin in the rat ventrolateral brain medulla induces apnea. *J Appl Physiol* (1985) 69:2233–2238.
- Del Negro CA, Koshiya N, Butera RJ Jr, Smith JC. 2002a. Persistent sodium current, membrane properties and

- bursting behavior of pre-Botzinger complex inspiratory neurons in vitro. *J Neurophysiol* 88:2242–2250.
- Del Negro CA, Morgado-Valle C, Feldman JL. 2002b. Respiratory rhythm: an emergent network property? *Neuron* 34:821–830.
- Dempsey B, Turner AJ, Le S, Sun Q-J, Bou Farah L, Allen AM, Goodchild AK, McMullan S. 2015. Recording, labeling, and transfection of single neurons in deep brain structures. *Physiol Rep* 3:e12246.
- Dobbins EG, Feldman JL. 1994. Brainstem network controlling descending drive to phrenic motoneurons in rat. *J Comp Neurol* 347:64–86.
- Dutschmann M, Jones SE, Subramanian HH, Stanic D, Bautista TG. 2014. The physiological significance of post-inspiration in respiratory control. *Prog Brain Res* 212:113–130.
- Ezure K, Manabe M. 1988. Decrementing expiratory neurons of the Botzinger complex. II. Direct inhibitory synaptic linkage with ventral respiratory group neurons. *Exp Brain Res* 72:159–166.
- Ezure K, Tanaka I, Kondo M. 2003. Glycine is used as a transmitter by decrementing expiratory neurons of the ventrolateral medulla in the rat. *J Neurosci* 23:8941–8948.
- Feldman JL, Del Negro CA, Gray PA. 2013. Understanding the rhythm of breathing: So near, yet so far. *Annu Rev Physiol* 75:423–452.
- Fischer T, Doll C, Jacobs S, Kolodziej A, Stumm R, Schulz S. 2008. Reassessment of sst2 somatostatin receptor expression in human normal and neoplastic tissues using the novel rabbit monoclonal antibody UMB-1. *J Clin Endocrinol Metab* 93:4519–4524.
- Forlano PM, Woolley CS. 2010. Quantitative analysis of pre- and postsynaptic sex differences in the nucleus accumbens. *J Comp Neurol* 518:1330–1348.
- Gray PA. 2013. Transcription factors define the neuroanatomical organization of the medullary reticular formation. *Front Neuroanat* 7:7.
- Gray PA, Reikling JC, Bocchiaro CM, Feldman JL. 1999. Modulation of respiratory frequency by peptidergic input to rhythmogenic neurons in the preBotzinger complex. *Science* 286:1566–1568.
- Gray PA, Janczewski WA, Mellen N, McCrimmon DR, Feldman JL. 2001. Normal breathing requires preBotzinger complex neurokinin-1 receptor-expressing neurons. *Nat Neurosci* 4:927–930.
- Gray PA, Hayes JA, Ling GY, Llona I, Tupal S, Picardo MC, Ross SE, Hirata T, Corbin JG, Eugenin J, Del Negro CA. 2010. Developmental origin of preBotzinger complex respiratory neurons. *J Neurosci* 30:14883–14895.
- Guyenet PG, Wang H. 2001. Pre-Botzinger neurons with pre-inspiratory discharges “in vivo” express NK1 receptors in the rat. *J Neurophysiol* 86:438–446.
- Guyenet PG, Sevigny CP, Weston MC, Stornetta RL. 2002. Neurokinin-1 receptor-expressing cells of the ventral respiratory group are functionally heterogeneous and predominantly glutamatergic. *J Neurosci* 22:3806–3816.
- Hayashi F, Coles SK, McCrimmon DR. 1996. Respiratory neurons mediating the Breuer-Hering reflex prolongation of expiration in rat. *J Neurosci* 16:6526–6536.
- Humphrey DR, Schmidt EM. 1990. Extracellular single-unit recording methods. In: Boulton AA, Baker GB, Vanderwolf CH, editors. *Neuromethods: neurophysiological techniques applications to neural systems*. Clifton, New Jersey: The Humana Press inc., Vol 15. p 1–64.
- Kanjhan R, Lipski J, Kruszevska B, Rong W. 1995. A comparative study of pre-sympathetic and Botzinger neurons in the rostral ventrolateral medulla (RVLM) of the rat. *Brain Res* 699:19–32.
- Koizumi H, Koshiya N, Chia JX, Cao F, Nugent J, Zhang R, Smith JC. 2013. Structural-functional properties of identified excitatory and inhibitory interneurons within pre-Botzinger complex respiratory microcircuits. *J Neurosci* 33:2994–3009.
- Korner M, Eltschinger V, Waser B, Schonbrunn A, Reubi JC. 2005. Value of immunohistochemistry for somatostatin receptor subtype sst2A in cancer tissues: lessons from the comparison of anti-sst2A antibodies with somatostatin receptor autoradiography. *Am J Surg Pathol* 29:1642–1651.
- Korner M, Waser B, Schonbrunn A, Perren A, Reubi JC. 2012. Somatostatin receptor subtype 2A immunohistochemistry using a new monoclonal antibody selects tumors suitable for in vivo somatostatin receptor targeting. *Am J Surg Pathol* 36:242–252.
- Koshiya N, Smith JC. 1999. Neuronal pacemaker for breathing visualized in vitro. *Nature* 400:360–363.
- Lazarenko RM, Milner TA, Depuy SD, Stornetta RL, West GH, Kievits JA, Bayliss DA, Guyenet PG. 2009. Acid sensitivity and ultrastructure of the retrotrapezoid nucleus in Phox2b-EGFP transgenic mice. *J Comp Neurol* 517:69–86.
- Lindemann C, Alam M, Krauss JK, Schwabe K. 2013. Neuronal activity in the medial associative-limbic and lateral motor part of the rat subthalamic nucleus and the effect of 6-hydroxydopamine-induced lesions of the dorsolateral striatum. *J Comp Neurol* 521:3226–3240.
- Llona I, Ampuero E, Eugenin JL. 2004. Somatostatin inhibition of fictive respiration is modulated by pH. *Brain Res* 1026:136–142.
- Low MJ, Otero-Corchon V, Parlow AF, Ramirez JL, Kumar U, Patel YC, Rubinstein M. 2001. Somatostatin is required for masculinization of growth hormone-regulated hepatic gene expression but not of somatic growth. *J Clin Invest* 107:1571–1580.
- Makeham JM, Goodchild AK, Pilowsky PM. 2001. NK1 receptor and the ventral medulla of the rat: Bulbospinal and catecholaminergic neurons. *NeuroReport* 12:3663–3667.
- McKay LC, Feldman JL. 2008. Unilateral ablation of pre-Botzinger complex disrupts breathing during sleep but not wakefulness. *Am J Respir Crit Care Med* 178:89–95.
- McKay LC, Janczewski WA, Feldman JL. 2005. Sleep-disordered breathing after targeted ablation of preBotzinger complex neurons. *Nat Neurosci* 8:1142–1144.
- McMullan S, Dick TE, Farnham MM, Pilowsky PM. 2009. Effects of baroreceptor activation on respiratory variability in rat. *Respir Physiol Neurobiol* 166:80–86.
- Pantaleo T, Mutolo D, Cinelli E, Bongianini F. 2011. Respiratory responses to somatostatin microinjections into the Bötzing complex and the pre-Bötzing complex of the rabbit. *Neuroscience Letters* 498:26–30.
- Pattyn A, Morin X, Cremer H, Goriadis C, Brunet JF. 1997. Expression and interactions of the two closely related homeobox genes Phox2a and Phox2b during neurogenesis. *Development* 124:4065–4075.
- Paxinos G, Watson C. 2006. *The rat brain in stereotaxic coordinates*. New York: Academic Press.
- Ptak K, Burnet H, Blanchi B, Sieweke M, De Felipe C, Hunt SP, Monteau R, Hilaire G. 2002. The murine neurokinin NK1 receptor gene contributes to the adult hypoxic facilitation of ventilation. *Eur J Neurosci* 16:2245–2252.
- Qiu C, Zeyda T, Johnson B, Hochgeschwender U, de Lecea L, Tallent MK. 2008. Somatostatin receptor subtype 4 couples to the M-current to regulate seizures. *J Neurosci* 28:3567–3576.
- Rajput PS, Kharmate G, Norman M, Liu SH, Sastry BR, Brunicardi CF, Kumar U. 2011. Somatostatin receptor 1

- and 5 double knockout mice mimic neurochemical changes of Huntington's disease transgenic mice. *PLoS One* 6:e24467.
- Ramírez-Jarquín JO, Lara-Hernández S, López-Guerrero JJ, Aguilera MA, Rivera-Angulo AJ, Sampieri A, Vaca L, Ordaz B, Peña-Ortega F. 2012. Somatostatin modulates generation of inspiratory rhythms and determines asphyxia survival. *Peptides* 34:360–372.
- Schreihöfer AM, Stornetta RL, Guyenet PG. 1999. Evidence for glycinergic respiratory neurons: Botzinger neurons express mRNA for glycinergic transporter 2. *J Comp Neurol* 407:583–597.
- Schulz S, Schreff M, Schmidt H, Händel M, Przewlocki R, Höllt V. 1998a. Immunocytochemical localization of somatostatin receptor sst2A in the rat spinal cord and dorsal root ganglia. *Eur J Neurosci* 10:3700–3708.
- Schulz S, Schulz S, Schmitt J, Wiborny D, Schmidt H, Olbricht S, Weise W, Roessner A, Gramsch C, Höllt V. 1998b. Immunocytochemical detection of somatostatin receptors sst1 sst(2A), sst(2B), and sst3 in paraffin-embedded breast cancer tissue using subtype-specific antibodies. *Clin Cancer Res* 4:2047–2052.
- Smith JC, Ellenberger HH, Ballanyi K, Richter DW, Feldman JL. 1991. Pre-Botzinger complex: A brainstem region that may generate respiratory rhythm in mammals. *Science* 254:726–729.
- Smith JC, Butera RJ, Koshiya N, Del Negro C, Wilson CG, Johnson SM. 2000. Respiratory rhythm generation in neonatal and adult mammals: the hybrid pacemaker-network model. *Respir Physiol* 122:131–147.
- Smith JC, Abdala AP, Koizumi H, Rybak IA, Paton JF. 2007. Spatial and functional architecture of the mammalian brain stem respiratory network: a hierarchy of three oscillatory mechanisms. *J Neurophysiol* 98:3370–3387.
- Smith JC, Abdala AP, Borgmann A, Rybak IA, Paton JF. 2013. Brainstem respiratory networks: building blocks and microcircuits. *Trends Neurosci* 36:152–162.
- Spary EJ, Maqbool A, Batten TF. 2008. Expression and localisation of somatostatin receptor subtypes sst1-sst5 in areas of the rat medulla oblongata involved in autonomic regulation. *J Chem Neuroanat* 35:49–66.
- Spirovski D, Li Q, Pilowsky PM. 2012. Brainstem galanin synthesising neurons are differentially activated by chemoreceptor stimuli and represent a subpopulation of respiratory neurons. *J Comp Neurol* 520:154–173.
- Stornetta RL, Rosin DL, Wang H, Sevigny CP, Weston MC, Guyenet PG. 2003a. A group of glutamatergic interneurons expressing high levels of both neurokinin-1 receptors and somatostatin identifies the region of the pre-Botzinger complex. *J Comp Neurol* 455:499–512.
- Stornetta RL, Sevigny CP, Guyenet PG. 2003b. Inspiratory augmenting bulbospinal neurons express both glutamatergic and enkephalinergic phenotypes. *J Comp Neurol* 455:113–124.
- Sun QJ, Goodchild AK, Chalmers JP, Pilowsky PM. 1998. The pre-Botzinger complex and phase-spanning neurons in the adult rat. *Brain Res* 809:204–213.
- Tan W, Janczewski WA, Yang P, Shao XM, Callaway EM, Feldman JL. 2008. Silencing preBotzinger complex somatostatin-expressing neurons induces persistent apnea in awake rat. *Nat Neurosci* 11:538–540.
- Tanaka I, Ezure K, Kondo M. 2003. Distribution of glycine transporter 2 mRNA-containing neurons in relation to glutamic acid decarboxylase mRNA-containing neurons in rat medulla. *Neurosci Res* 47:139–151.
- Upal S, Rieger MA, Ling GY, Park TJ, Dougherty JD, Goodchild AK, Gray PA. 2014. Testing the role of preBotzinger complex somatostatin neurons in respiratory and vocal behaviors. *Eur J Neurosci* 40:3067–3077.
- Wallen-Mackenzie A, Gezelius H, Thoby-Brisson M, Nygard A, Enjin A, Fujiyama F, Fortin G, Kullander K. 2006. Vesicular glutamate transporter 2 is required for central respiratory rhythm generation but not for locomotor central pattern generation. *J Neurosci* 26:12294–12307.
- Wang H, Stornetta RL, Rosin DL, Guyenet PG. 2001. Neurokinin-1 receptor-immunoreactive neurons of the ventral respiratory group in the rat. *J Comp Neurol* 434:128–146.
- Wei XY, Zhao Y, Wong-Riley MT, Ju G, Liu YY. 2012. Synaptic relationship between somatostatin- and neurokinin-1 receptor-immunoreactive neurons in the pre-Botzinger complex of rats. *J Neurochem* 122:923–933.
- Yamamoto Y, Runold M, Prabhakar N, Pantaleo T, Lagercrantz H. 1988. Somatostatin in the control of respiration. *Acta Physiol Scand* 134:529–533.
- Yu YJ, Arttamangkul S, Evans CJ, Williams JT, von Zastrow M. 2009. Neurokinin 1 receptors regulate morphine-induced endocytosis and desensitization of mu-opioid receptors in CNS neurons. *J Neurosci* 29:222–233.

Somatostatin in the Rat Rostral Ventrolateral Medulla: Origins and Mechanism of Action

Lama Bou Farah, Belinda R. Bowman, Phil Bokinić, Shafinaz Karim, Sheng Le, Ann K. Goodchild, and Simon McMullan*

Australian School of Advanced Medicine, Macquarie University, 2109, NSW Australia

ABSTRACT

Somatostatin (SST) or agonists of the SST-2 receptor (ss_{t2}) in the rostral ventrolateral medulla (RVLM) lower sympathetic nerve activity, arterial pressure, and heart rate, or when administered within the Böttinger region, evoke apneusis. Our aims were to describe the mechanisms responsible for the sympathoinhibitory effects of SST on bulbospinal neurons and to identify likely sources of RVLM SST release. Patch clamp recordings were made from bulbospinal RVLM neurons ($n = 31$) in brainstem slices prepared from juvenile rat pups. Overall, 58% of neurons responded to SST, displaying an increase in conductance that reversed at -93 mV, indicative of an inwardly rectifying potassium channel (GIRK) mechanism. Blockade of ss_{t2} abolished this effect, but application of tetrodotoxin did not, indicating that the SST effect is independent of presynaptic activity. Fourteen bulbospinal

RVLM neurons were recovered for immunohistochemistry; nine were SST-insensitive and did not express ss_{t2a} . Three out of five responsive neurons were ss_{t2a} -immunoreactive. Neurons that contained preprosomatostatin mRNA and cholera-toxin-B retrogradely transported from the RVLM were detected in: paratrigeminal nucleus, lateral parabrachial nucleus, Kölliker-Fuse nucleus, ventrolateral periaqueductal gray area, central nucleus of the amygdala, subnucleus extended amygdala, interstitial nucleus of the posterior limb of the anterior commissure nucleus, and bed nucleus of the stria terminalis. Thus, those brain regions are putative sources of endogenous SST release that, when activated, may evoke sympathoinhibitory effects via interactions with subsets of sympathetic premotor neurons that express ss_{t2} . *J. Comp. Neurol.* 524:323–342, 2016.

© 2015 Wiley Periodicals, Inc.

INDEXING TERMS: retrograde tracing; patch clamp; GIRK; ss_{t2a} ; somatostatin; RVLM

The inhibitory peptide somatostatin (SST) is expressed widely throughout the brain; its two isoforms, SST-14 and SST-28, act on six receptors, ss_{t1-5} , with ss_{t2} receptors present in two subtypes, ss_{t2a} and ss_{t2b} (Bruno et al., 1992; O'Carroll et al., 1992; Vanetti et al., 1992, 1994; Yasuda et al., 1992).

The expression of SST and its receptors within the rostral ventrolateral medulla (RVLM), and the functional consequences of SST transmission in this region, has emerged as a topic of considerable interest in both the fields of central respiratory and central cardiovascular control. The medullary distribution of SST partially overlaps with putative markers of respiratory rhythm-generating neurons in the pre-Böttinger complex (Stornetta et al., 2003; Gray et al., 2010; Tupal et al., 2014), and pharmacogenetic silencing of SSTergic neurons in and around the pre-Böttinger complex causes apnea in vivo (Tan et al., 2008), leading to the proposal that SST may be a marker of pre-Böttinger complex pacemaker neurons (Stornetta et al., 2003; Gray et al.,

2010). Furthermore, microinjection of SST into the Böttinger region, one target of pre-Böttinger complex SSTergic neurons (Tan et al., 2010), evokes apneusis, a gasping breathing pattern characterized by a lengthened inspiratory phase and a shortened expiratory period (Burke et al., 2010).

The first two authors contributed equally to this work.

The last two authors are joint authors.

Grant sponsor: National Health and Medical Research Council of Australia; Grant numbers: NHMRC 457068, APP1028183, APP1030301; Grant sponsor: National Heart Foundation of Australia; Grant number: NHF G09S4340; Grant sponsor: Australian Research Council; Grant number: DP120100920; Grant sponsor: Macquarie University and Hillcrest Foundation (Perpetual).

*CORRESPONDENCE TO: Simon McMullan, Australian School of Advanced Medicine, 2 Technology Place, Macquarie University, 2109, NSW Australia. E-mail: simon.mcmullan@mq.edu.au

Received February 22, 2015; Revised June 22, 2015;

Accepted June 23, 2015.

DOI 10.1002/cne.23846

Published online July 21, 2015 in Wiley Online Library (wileyonlinelibrary.com)

© 2015 Wiley Periodicals, Inc.

SST also causes dose-dependent sympathoinhibition, hypotension, and bradycardia, as well as attenuation of chemo- and somatosympathetic reflexes, when microinjected into the pressor region of the RVLM (Burke et al., 2008). A direct effect of SST agonists on RVLM sympathetic premotor neurons is presumed to underlie this effect, as *sst_{2a}* receptors are the predominant receptor subtype expressed in the region and are widely expressed on RVLM C1 and non-C1 neurons (Burke et al., 2008; Spary et al., 2008), including those with bulbospinal projections (Burke et al., 2008). Involvement of other receptor subtypes is unlikely, as *sst₅* mRNA is absent from the VLM, and isoforms 1, 2b, and 4 are expressed at low levels (Spary et al., 2008; Ramírez-Jarquín et al., 2012). Similarly, we and others have reported pronounced VLM expression of *sst_{2a}* immunoreactivity, weak expression of *sst₄*, and no consistent neuronal expression of any other subtype (Burke et al., 2008; Spary et al., 2008). Finally, pretreatment with the *sst₂*-selective antagonist BIM-23627 abolishes cardiovascular responses evoked by both SST and the *sst₂* agonist lanreotide (Burke et al., 2008).

The cellular mechanisms that underlie the inhibitory effects of RVLM SST receptor activation, the sources of RVLM SST release, and the circumstances under which SST is released in the RVLM are unknown. In general, the cellular responses evoked by SST receptor activation are wide-ranging, modulating multiple second messenger systems. These include G-protein modulation of adenylate cyclase, Ca^{2+} and K^{+} channels, phospholipases, MAP kinase, and phosphotyrosine protein phosphatases (Patel, 1999). When *sst₂₋₅* receptors were coexpressed with a GIRK subunit in oocytes, *sst₂* receptors were the most efficient in activating a GIRK-mediated current (Kreienkamp et al., 1997). Similarly, whole-cell patch clamp recordings of neurons in the periaqueductal gray (Connor et al., 2004) or the substantia gelatinosa of the spinal cord (Nakatsuka et al., 2008) show that SST application evokes a large outward current mediated by K^{+} channels, consistent with GIRK characteristics, although calcium currents may also be activated (Connor et al., 2004).

Regions innervating the RVLM are well described and widely distributed (Hopkins and Holstege, 1978; Ross et al., 1985; Dampney et al., 1987; Carrive et al., 1988; M'Hamed et al., 1993; Padley et al., 2007; Bowman et al., 2013), as is the brain-wide distribution of neurons expressing SST-immunoreactivity or preprosomatostatin (PPS) mRNA (De León et al., 1992; Gray and Magnuson, 1992; Smith et al., 1994). However, whether or not RVLM-projecting neurons synthesize SST is largely unknown.

Therefore, the aims of this study were, first, to determine the cellular mechanisms responsible for the inhibition of RVLM sympathetic premotor neurons by SST, using whole-cell patch clamp in acute brainstem slices and, second, to define likely sources of SST by identifying RVLM-projecting neurons that contain PPS mRNA using a combination of retrograde tracing and in situ hybridization.

MATERIALS AND METHODS

All experiments were approved by the Macquarie University Animal Ethics Committee and performed in accordance with the Australian Code of Practice for the Care and Use of Animals for Scientific Purposes.

In vitro electrophysiology

Labeling of bulbospinal RVLM neurons

Sprague Dawley rat pups (postnatal day (P5–P25) were anesthetized with 2–5% isoflurane (Veterinary Companies of Australia) in oxygen and moved onto a heated pad. A dorsal laminectomy was performed and the T2 spinal cord exposed. Fluorescently conjugated cholera toxin β subunit (CTB-Alexa 555 or 488, 0.5–1%, Invitrogen, La Jolla, CA) was injected bilaterally at coordinates corresponding to the interomediolateral cell column (1–3 100 nl injections each side). After completion of microinjections the wound was closed with cyanoacrylate glue and anesthesia discontinued. Pups were allowed to recover on a warm pad until ambulatory and were then placed back in the cage with their mother and littermates. Postoperative rats were carefully monitored for the duration of experiments and treated with additional analgesia when indicated (Carprofen, 2 mg/kg s.c. Norbrook Pharmaceuticals, Australia).

Electrophysiology solutions (all values in mM): cutting solution: 125 NaCl, 25 NaHCO_3 , 3 KCl, 1.25 $\text{NaH}_2\text{PO}_4 \cdot \text{H}_2\text{O}$, 10 D-glucose, 1 CaCl_2 , 6 MgCl_2 ; equilibrated with 95% O_2 / 5% CO_2 . Artificial cerebrospinal fluid (aCSF): 125 NaCl, 25 NaHCO_3 , 3 KCl, 1.25 $\text{NaH}_2\text{PO}_4 \cdot \text{H}_2\text{O}$, 25 D-glucose, 2 CaCl_2 , 1 MgCl_2 ; equilibrated with 95% O_2 / 5% CO_2 (pH = 7.35). Potassium gluconate internal solution: 125 K-gluconate, 10 Hepes, 11 EGTA, 15 NaCl, 1 MgCl_2 , 2 MgATP, 0.25 NaGTP, 0.05% biocytin (pH = 7.3, Osmolarity 280–285 mOsm).

Whole-cell recordings

Two to five days following tracer injection, pups (P8–P28) were anesthetized with isoflurane and decapitated. The brain was rapidly removed and placed in ice-cold oxygenated cutting solution. The brainstem was isolated, mounted in a vibratome, and immersed in ice-cold aCSF solution. Coronal sections of 300 μm

thickness were taken from the region immediately caudal to the caudal pole of the facial nucleus and transferred to continuously oxygenated aCSF at 36°C and left for at least 1 hour before recordings in an oxygenated aCSF-filled chamber maintained at room temperature. Tracer-labeled neurons were viewed under epifluorescence: CTB-labeled neurons ventral to nucleus ambiguus and lateral to the inferior olive were identified as putative RVLM premotor neurons and targeted.

Whole-cell recordings were obtained from RVLM neurons in voltage clamp mode using borosilicate pipettes with 1.5–2 μm tip diameters (pipette resistance: 3–6 M Ω when filled with internal solution). After formation of a gigaseal, voltage clamp recordings were obtained using a Multiclamp 700B (Molecular Devices, Palo Alto, CA). Once the holding current and input resistance stabilized, baseline recordings were made for at least 5 minutes prior to commencement of the experimental protocol. Series resistance was compensated by 70–80%. All recorded parameters were digitized using Spike 2 v. 6.11 (RRID: nlx_156886) with a Power 1401 mark II digitizer (Cambridge Electronic Design, UK). In some experiments two neurons were simultaneously recorded from the same slice.

Recorded neurons were labeled using 0.05% biocytin contained in the internal solution. At the conclusion of experiments slices were briefly fixed in 4% paraformaldehyde and cryoprotected until immunohistochemical processing.

Experimental protocol

The effect of SST on bulbospinal RVLM neurons was determined by superfusing slices with 50–300 nM SST (Auspep, Australia) in carbogen-equilibrated aCSF for up to 100 seconds, which was then washed out until recovery to baseline was achieved. 300 nM SST has been reported to evoke $\sim 75\%$ maximal inhibitory effect on spontaneously firing locus coeruleus neurons recorded in acute brain slices (Chessell et al., 1996) and 95% inhibition of calcium currents in dissociated periaqueductal gray neurons (Connor et al., 2004). Membrane currents were evoked by voltage command steps from -60 to -130 mV in 10 mV increments and 250 ms duration before, at peak response to SST, and after return to baseline (see Figs. 4, 5). Voltage steps in SST-insensitive neurons were performed at equivalent times. In initial experiments the sensitivity of neurons to 10 μM baclofen (Sigma Aldrich, St. Louis, MO), an agonist of the metabotropic GABA B receptor that exerts its effects via activation of GIRK channels (Kerr and Ong, 1995; Lüscher et al., 1997), was used to ensure that the diminished responsiveness to repeated SST exposure was specific to SST receptor activation,

rather than, for example, dialysis of intracellular GIRK effectors.

In order to assess whether the inhibition seen following SST application was mediated by SST₂ receptor activation, the effects of repeated SST application were compared before and after the addition of the sst₂ receptor antagonist cyanamid to the perfusate (CYN-154806, 300 nM, Tocris, UK). Baseline responses to 300 or 50 nM SST were assessed as described above; once a response to SST was detected sections were washed in aCSF for 1,000 seconds, then CYN-154806 was perfused for 500 seconds before the second application of SST.

To determine whether responses to SST were dependent on activity in putative presynaptic neurons, we compared responses to 100 nM SST before and after addition of 10 μM tetrodotoxin (TTX, Jomar Bioscience, Australia) to the perfusion. This concentration blocked electrically evoked synaptic currents in pilot experiments (data not shown) and exceeds that generally used elsewhere (Kawai et al., 1999; Kawashima et al., 2013). Baseline responses to SST were recorded and allowed to recover for 1,000 seconds before incubation with TTX for 5 minutes and reexposure to SST.

Data analysis

Responses to SST were quantified by measuring the peak change in holding current recorded immediately following SST application. The current–voltage relationship was calculated by plotting membrane current against holding potential (Connor et al., 2004). In some experiments hyperpolarization-activated currents were observed; these were quantified by subtracting initial from steady-state currents evoked by hyperpolarizing steps from a holding potential of -60 mV to -130 mV in 10 mV increments (Gao et al., 2012; see Fig. 7). Repeated responses of bulbospinal neurons to SST following application of TTX or cyanamid to the perfusate were compared using Student's paired *t*-test for comparison of raw data within groups or unpaired *t*-test for comparison of normalized responses between groups. Grouped data are expressed as mean \pm SEM for parametric series or median (range) for nonparametric series. Differences were judged significant at $P < 0.05$. Statistical analyses were performed using GraphPad Prism 6.0 (RRID: rid_000081) or GraphPad Quickcalcs (<http://www.graphpad.com/quickcalcs/>) for categorical data.

Immunohistochemical processing and analysis of recorded neurons

All slices were fixed overnight in 4% paraformaldehyde in phosphate buffer (0.1 M, pH 7.4) then frozen in cryoprotectant (30% sucrose plus glycerol). Slices were then processed for sst_{2a} receptor immunoreactivity using a

TABLE 1.
Antibody Details

Antibody name	Immunogen	Manufacturer details	Concentration
<i>Primary Antibodies</i>			
Guinea pig anti-SST _{2a}	C-terminus amino acid sequence 355–369 (ETQRTLLNGDLQTSI) of synthetic sst2a peptide	Gramscs Laboratories, Schwabhausen Germany-Cat# SS-870RRID: AB_2491104Polyclonal	1:1,000
Rabbit anti-SST _{2a}	C-terminus amino acid sequence 355–369 (ETQRTLLNGDLQTSI) of synthetic sst2a peptide	Bio-trendCat# ss-8000-rmcLot# a080826RRID: AB_2491103Monoclonal	1:100
Guinea pig anti-neurokinin 1 receptor (NK1R)	C-terminus synthetic rat NK1R	MilliporeCat# AB15810Lot# LV1587443RRID: AB_992894Polyclonal	1:1,000
Mouse anti-tyrosine hydroxylase (TH)	Rat tyrosine hydroxylase N-terminal region (approx. aa 9–16)	Sigma-AldrichCat# T1299RRID: AB_477560Monoclonal	1:8,000
Rabbit anti-CTB	B subunit of cholera toxin	ViroStat, USACat# 7927RRID: AB_2313635Polyclonal	1:5,000
Sheep anti-digoxigenin	Digoxigenin, whole	Roche Applied ScienceCat# 110932749 10RRID: AB_514497Polyclonal	1:1,000
<i>Secondary Antibodies</i>			
ExtrAvidin-FITC	n/a	Sigma-AldrichCat# E2761RRID: AB_2492295	1:500
Alexa Fluor 647-AffiniPure donkey antirabbit IgG (H+L)	Whole molecule rabbit IgG	Jackson ImmunoResearch Laboratories, INCCat# 711-605-152Lot# 105115RRID: AB_2492288Polyclonal	1:250
Cy3- AffiniPure donkey antigoat IgG (H+L)	Whole molecule goat IgG	Jackson ImmunoResearch Laboratories, INCCat# 705-165-147Lot# 68839RRID: AB_2307351Polyclonal	1:250
Alexa Fluor 488-AffiniPure donkey anti-guinea pig IgG (H+L)	Whole molecule guinea pig IgG	Jackson ImmunoResearch Laboratories, INCCat# 706-545-148Lot# 161406RRID: AB_2340472Polyclonal	1:250
Dylight 488-conjugated donkey antirabbit IgG (H+L)	Whole molecule rabbit IgG	Jackson ImmunoResearch Laboratories, RRID: AB_2492289)Polyclonal	1:500
Alexa Fluor 488 donkey antimouse IgG (H+L)	Mouse, IgG heavy & light chains	Life TechnologiesCat# A21202RRID: AB_10049285Polyclonal	1:250

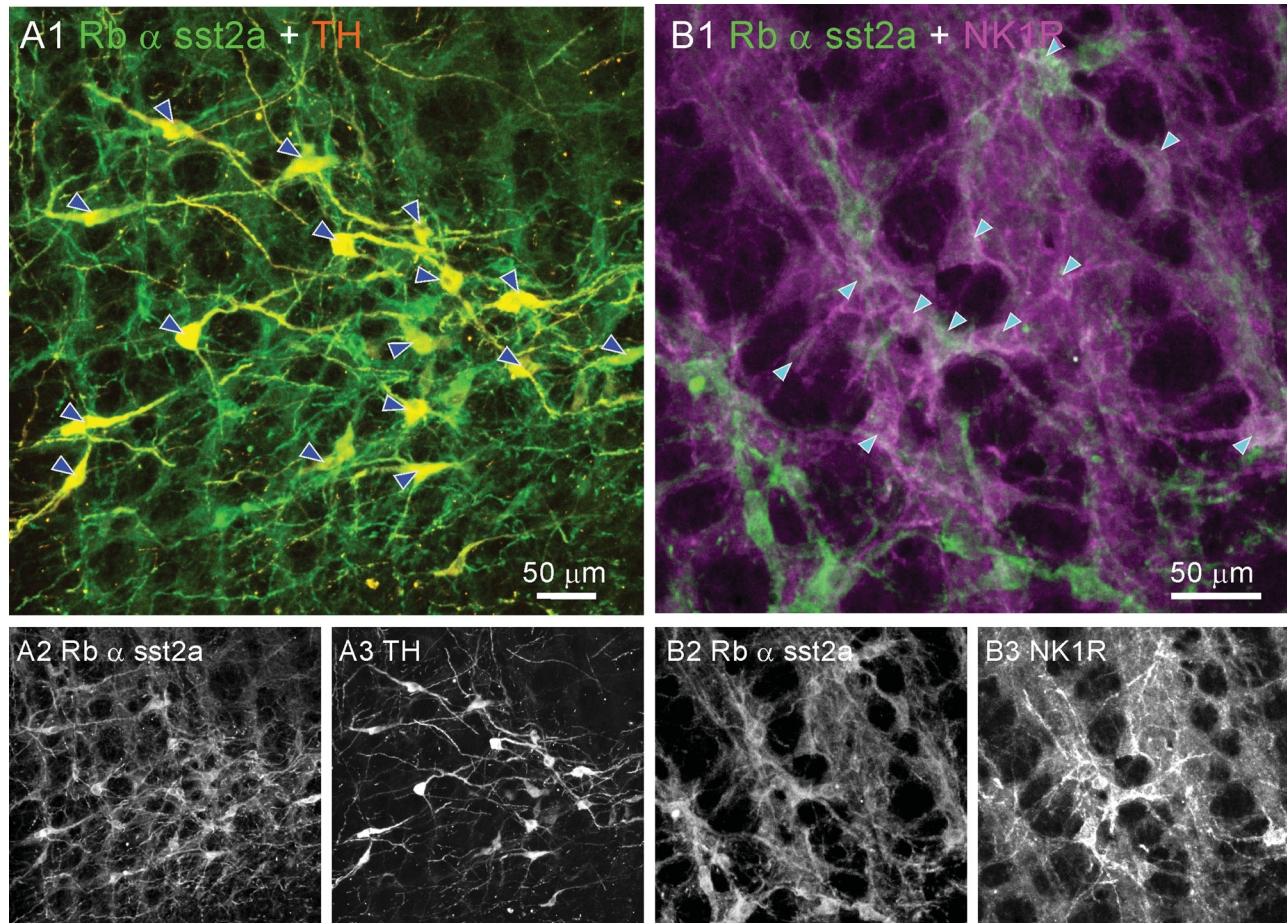


Figure 1. Distribution of rabbit anti- sst_{2a} antibody binding in the ventrolateral medulla. Confocal stack images demonstrate colocalization of rabbit anti- sst_{2a} immunoreactivity with TH in the RVLM, 200 μm caudal to the facial nucleus (A) and with neurokinin-1 receptor (NK1R) in the pre-Bötzinger complex, 800 μm caudal to the facial nucleus (B). Individual channel images shown in panels 2, 3. Arrowheads indicate double-labeled neurons.

protocol based on that described by Gogolla et al. (2006).

Free-floating slices were washed in 20 ml pots for 10 minutes in 0.01 M phosphate-buffered saline (PBS) and incubated overnight at 4°C in 0.5% Triton X-100 in 0.01 M PBS. Then slices underwent a blocking step in 5% bovine serum albumin (BSA) in 0.01 M PBS for 4 hours at room temperature. Primary antibodies (see Table 1) were added to 5% BSA / 0.01 M PBS for a 4 hour incubation at room temperature, then washed off with 30 minutes TPBS. Sections were then incubated at 4°C overnight in 5% BSA / 0.01 M PBS containing secondary antibody for detection of sst_{2a} receptor expression and ExtrAvidin-FITC for detection of biocytin-filled cells. Antibodies were washed off with TPBS for 30 minutes. Slices were wet-mounted on glass slides, coverslipped, and viewed under epifluorescence to confirm labeling before mounting with DAKO fluorescent mounting medium. Fourteen slices contained intact recovered

neurons and were imaged using an AxioImager Z2 microscope with ZEN software (Carl Zeiss, RRID: SCR_013672). In some cases neurons were also imaged using a Leica SP5 TCS confocal microscope and processed using Leica LAS AF software (RRID: SCR_013673). All figures were prepared using Corel-Draw and Corel Photopaint X4 (RRID: SCR_013674).

Antibody characterization

The rabbit anti- sst_{2a} antibody used in the current study (Biotrend UMB-1) has previously been characterized by western blot and immunoprecipitation experiments in wildtype and sst_2 knockout mice, and is reported to specifically label HEK cells transfected with sst_{2a} , but not other SST receptor isoforms (Fischer et al., 2008). In initial experiments we directly compared the binding of the rabbit monoclonal sst_{2a} antiserum to that obtained using a guinea pig antiserum raised against the same antigen sequence. Binding of the guinea pig

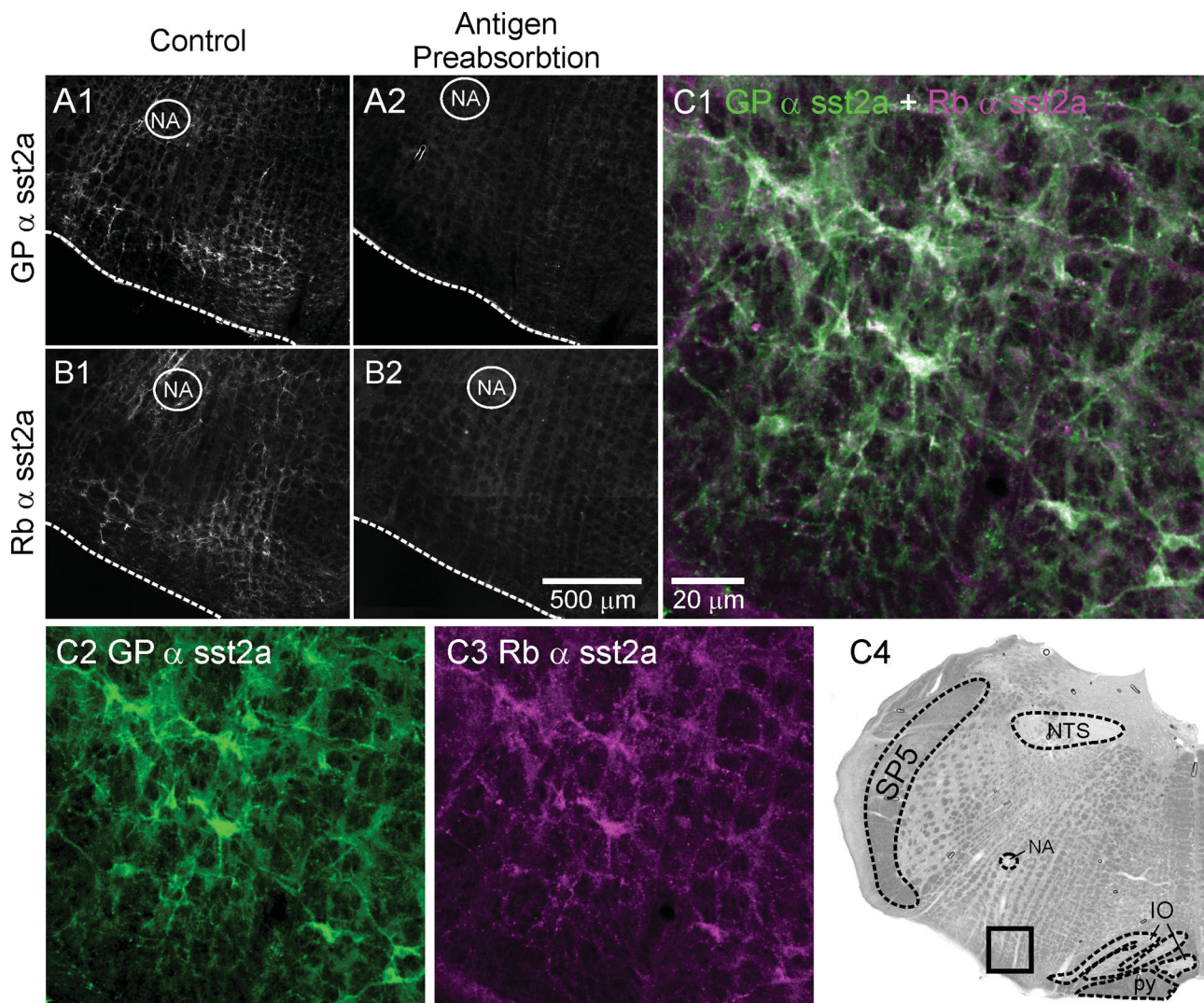


Figure 2. Comparison of rabbit and guinea pig anti- sst_{2a} antibody binding. Epifluorescent images demonstrate binding of anti- sst_{2a} primary antibodies raised in guinea pig (**A1**) and rabbit (**B1**), which was blocked by incubating alternate sections from the same animals with the antigen (**A2,B2**), and resulted in overlapping patterns of expression when incubated together (**C1**). **C2** and **C3** depict individual channels from merged image shown in **C1**. Box in **C4** shows region in which high-powered images shown in **C** were taken. NA = nucleus ambiguus; NTS = nucleus of the solitary tract. IO = inferior olive; PY = pyramidal tract; SP5 = Spinal trigeminal nucleus.

antiserum has previously been verified by dot blot and western blot assay and screening in sst_2 knockout animals (Schulz et al., 1998a,b; Allen et al., 2003; Korner et al., 2005; Spary et al., 2008), and its distribution in the RVLM has been used to define sst_{2a} expression in regions of the medulla associated with cardiovascular (Burke et al., 2008) and respiratory function (Gray et al., 2010), where it is colocalized with tyrosine hydroxylase (TH) and neurokinin-1 receptor (NK1R), respectively.

In pilot studies using 50- μm -thick sections processed as described below, the binding distribution of the rabbit antiserum was consistent with that reported for the guinea pig antiserum: binding was colocalized with TH throughout the VLM and with NK1R between 600 and

1,200 μm caudal to the facial nucleus, corresponding to the pre-Bötzinger complex (Fig. 1).

No immunoreactivity was observed when either antibody was preincubated for 8 hours at 4°C with the sst_{2a} antigen (Biotrend SS-801, 1:5 by weight, RRID: SCR_013675, Fig. 2A,B). Binding of rabbit and guinea pig antisera overlapped completely in tissue incubated with both primary antibodies and visualized with different fluorescent secondary antibodies (Fig. 2C).

Retrograde tracing of SSTergic neurons

Animal surgery

Experiments were performed on male Sprague Dawley rats ($n = 10$), 14–15 weeks old (400–550 g) from the

Animal Resources Centre, Perth, Western Australia. The retrograde tracing and combined in situ hybridization and immunohistochemistry methods used here have been previously published (Kumar et al., 2009). In brief, rats were anesthetized with ketamine (Parnell Laboratories, Australia) mixed with medetomidine hydrochloride (Pfizer Animal Health, 75 and 0.5 mg/kg respectively, i.p.) and treated with preoperative analgesia (carprofen, 5 mg/kg s.c.) and prophylactic antibiotics (cephazolin, 20 mg/kg i.m., Mayne Pharma, Australia). A flat skull approach was used to microinject the retrograde tracer cholera toxin subunit B (CTB, 1% in 200 nl saline; List Biological, Campbell, CA) unilaterally into the RVLM. After conducting a small craniotomy through the occipital bone and incision through the dura, antidromic facial field potentials were evoked by stimulation of the facial nerve. CTB microinjections were made 0.3 mm caudal to the facial nucleus, 1.7–2.1 mm lateral to midline and 0.3 mm deep to the ventral margin of the facial field (that is, 8.8–9.2 mm from the dorsal surface of the brain). After withdrawal of the pipette, the wound was closed and 5 ml of physiological saline was administered i.p. Rats were then administered the sedative reversal agent atipamezole hydrochloride (Pfizer Animal Health, Australia, 0.75 mg, 0.15 ml s.c.) and allowed to recover for 2–3 days under close monitoring.

Tissue preparation

Animals were deeply anesthetized with sodium pentobarbitone (>100 mg/kg i.p.) and perfused transcardially with 250 ml heparinized 0.9% sodium chloride followed by 250 ml 4% paraformaldehyde in phosphate buffer (0.1 M, pH 7.4). The brain was removed, the medulla dissected and fixed overnight at 4°C. Brains were sectioned coronally at 40 µm into four series using a vibrating microtome (VT1200S; Leica, Germany). Sections in each series were thus separated by 160 µm. Fluorescent immunohistochemical detection of CTB was conducted using a rabbit anti-CTB primary antibody and a 488-conjugated donkey antirabbit alongside detection of mRNA using digoxigenin (DIG)-labeled riboprobes targeting PPS mRNA as described previously (Burke et al., 2008). Both antisense and sense probes were synthesized with RNA polymerase T7 and SP6 promoters attached to the 5' end of the reverse and forward oligonucleotide primers, respectively (primers listed below in lowercase with promoter attached in uppercase). Polymerase chain reaction (PCR)-amplified cDNA template was then in vitro transcribed using T7 (AmpliScribe T7-Flash Transcription Kit, #ASF 3257, Epicentre Biotechnologies, Madison, WI) or SP6 (RiboMAX large scale RNA production system, #P1280, Promega, Madison, WI) in vitro transcription kits. Digoxigenin-11-

UTP (Roche Applied Sciences, Mannheim, Germany) was incorporated into the riboprobes during in vitro transcription. PPS Forward: GGATCCATTAGGTGACAC TATAGAAGctcaagctcggctgtctgag. PPS Reverse: GAATTC TAATACGACTCACTATAGGGAGAggaggagagggatcagaggt.

Free-floating brain sections were processed using the protocol described by Li et al. (2005). No labeling in any brain region was seen when the sense probe was substituted for the antisense probe.

Cell counts and analysis

Tissue sections were mounted on glass slides, coverslipped (Vectashield Hardset, Vector Laboratories, Burlingame, CA), and viewed and imaged using a Zeiss AxioImager Z1 microscope under epifluorescence. Images were acquired with Zeiss Axiovision software (v. 4.8, RRID: SciRes_000111). In each whole brain, sections separated by 160 µm were analyzed from the bregma level 5.16 mm to –15.24 mm. Six of the ten brains injected with CTB were selected for quantitative analysis, with every region quantified in at least three brains and confirmation assessed qualitatively in all other cases. Brains were selected due to their small CTB injection sites centered in the RVLM with little impingement on surrounding regions.

Each brain region containing CTB-labeled neurons was assessed for expression of PPS mRNA. CTB immunoreactivity (-ir) was determined using the criteria described by Bowman et al. (2013), in which neurons were considered CTB-ir if distinct Dylight-488 labeling was apparent within the cytoplasm, organelles, and/or in the proximal dendrites. Where intense ISH signal obfuscated cytoplasmic CTB-ir, neurons were considered double-labeled where CTB-ir proximal dendrites or organelles were clearly visible. When a region was found to contain double-labeled neurons, the section that contained the most CTB labeling was selected for counting, and, dependent on the rostrocaudal extent of the region, a second and third section was also assessed for double labeling (>300 µm apart). Regions of interest were imaged at multiple focal planes ("z-stack") so that CTB-positive proximal dendrites could be clearly discriminated in neurons in which intense ISH signal quenched the cytoplasmic CTB signal (Bowman et al., 2013).

Using these counts, the percentage of CTB-ir neurons that colocalized with PPS in that brain region, combining all sampled rostrocaudal levels, was determined for 3–4 animals and the mean ± SEM was calculated.

In addition, in order to describe those regions that provided the greatest number of retrogradely traced neurons containing PPS mRNA, the number of double-labeled neurons in each region (combining the selected rostrocaudal levels) was determined as a proportion of

all double-labeled neurons and the results expressed as the mean percentage.

RESULTS

In vitro electrophysiology

Superfusion of 300 nM SST produced an outward current (I_{SST}) in 18/31 (58%) bulbo-spinal neurons tested. The mean value of I_{SST} was 40.7 ± 4.8 pA (Fig. 3). Subsequent application of the GABA_B agonist baclo-

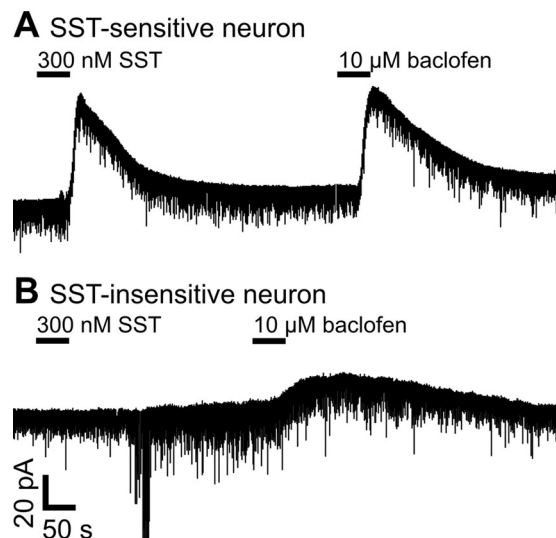


Figure 3. Electrophysiological characterization of outward currents evoked by SST. **(A)** Voltage-clamp recordings from CTB-labeled RVLM neurons: bulbo-spinal RVLM neurons in which SST and baclofen perfusion (black horizontal bars indicate time of application) evoked outward currents were categorized as SST-sensitive. **(B)** Bulbo-spinal RVLM neurons in which baclofen but not SST evoked outward currents were considered SST-insensitive.

fen (10 μ M) produced an outward current in SST-responsive (49.3 ± 5.9 pA, $n = 4$, Fig. 3A) and SST-insensitive neurons (42.6 ± 4.3 pA, $n = 5$, Fig. 3B).

SST-sensitive neurons displayed desensitization to repeated application of 50 ($n = 2$), 100 ($n = 2$), or 300 nM ($n = 1$) SST. Responses to 50, 100, or 300 nM SST were reduced by 20.0%, 32.4%, or 43.8%, respectively: pooled responses were 36.6 ± 5.5 vs. 24.8 ± 2.4 pA, paired t -test $t = 3.4$, $df = 4$, 2-tailed $P = 0.027$ (Fig. 4A). A similar reduction of response amplitude following repeated 100 nM SST application was observed following addition of TTX to the perfusate between SST trials (39.7 ± 4.9 vs. 25.9 ± 4.6 pA, paired t -test $t = 15.4$, $df = 4$, 2-tailed $P = 0.0001$, $n = 5$, Fig. 4B).

In order to assess whether sst_2 -receptor activation underlies responses of bulbo-spinal neurons to SST, we reapplied SST to neurons previously shown to be SST-sensitive in the presence of the sst_2 antagonist cyanamid (300 nM). Baseline responses to 300 nM ($n = 2$) or 50 nM ($n = 3$) SST were 40.15 ± 3.5 pA (300 nM) or 25.12 ± 2.9 pA (50 nM), respectively. Cyanamid reduced the amplitude of SST-evoked responses from 31.1 ± 4.1 pA to 2.8 ± 0.6 pA (paired t -test $t = 6.7$, $df = 4$, 2-tailed $P = 0.0025$, $n = 5$, Fig. 5). When normalized with respect to control responses, responses to second applications of SST were more attenuated in the presence of cyanamid ($9.9 \pm 2.7\%$) compared to repeated SST applications conducted in normal aCSF ($70.3 \pm 4.6\%$, unpaired t -test vs. cyanamid: $t = 11.3$, $df = 8$, $P < 0.0001$, $n = 5$) or in the presence of TTX ($63.4 \pm 4.6\%$, unpaired t -test vs. cyanamid: $t = 10$, $df = 8$, $P < 0.0001$, $n = 5$).

In 17 bulbo-spinal neurons in which SST induced an outward current at a holding potential of -60 mV, baseline slope conductances of 3 ± 0.4 nS and

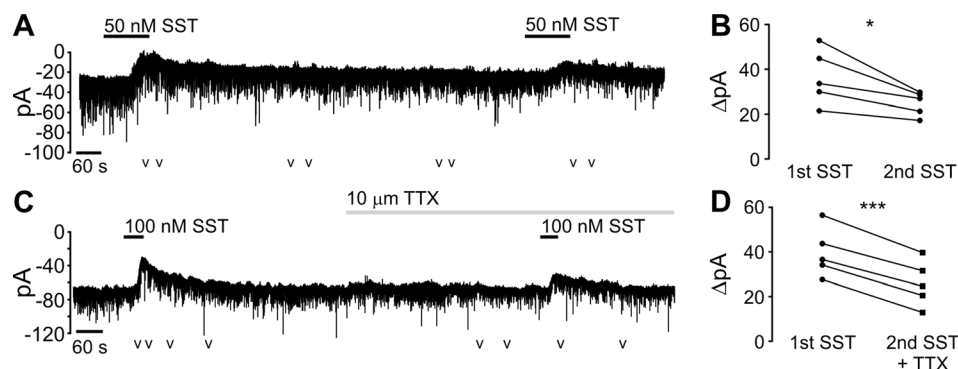


Figure 4. Responses of bulbo-spinal RVLM neurons to repeated SST application exhibited desensitization. **(A)** Voltage-clamp recordings illustrate desensitization of responses to repeated application of 50 nM SST ("v" denotes timing of voltage steps; steps have been removed from traces to aid clarity). **(B)** Pooled data; responses to 50, 100, and 300 nM SST have been combined. **(C)** Experimental recording demonstrating that responses to repeated SST were unaffected by tetrodotoxin (TTX). **(D)** Pooled data of responses to 100 nM SST before and after addition of TTX to the perfusate. * $P < 0.05$, *** $P < 0.001$.

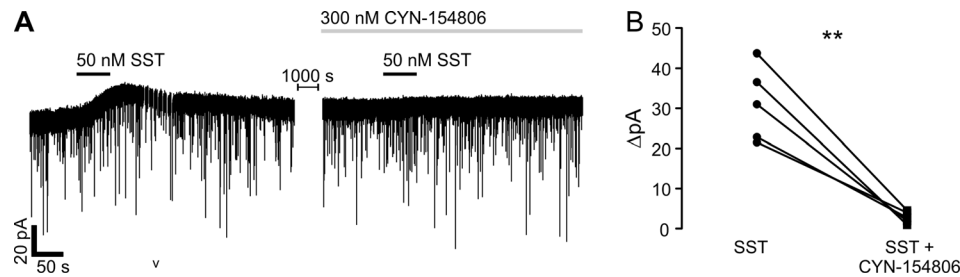
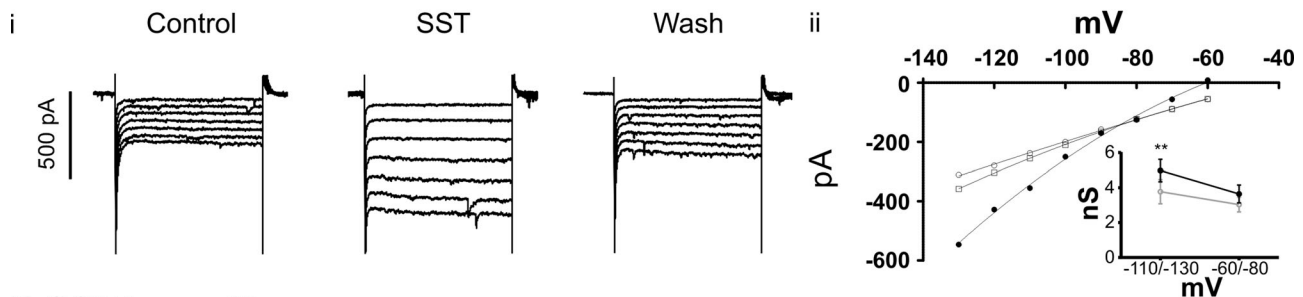


Figure 5. sst_2 blockade abolished SST-induced outward currents. **(A)** Voltage-clamp recordings of responses to SST application before and after superfusion with the sst_2 blocker CYN-154806 ("v" denotes timing of voltage steps). **(B)** pooled data showing effects of SST₂ blockade on five SST-sensitive spinally projecting RVLM neurons. ** $P < 0.01$.

A SST sensitive



B SST insensitive

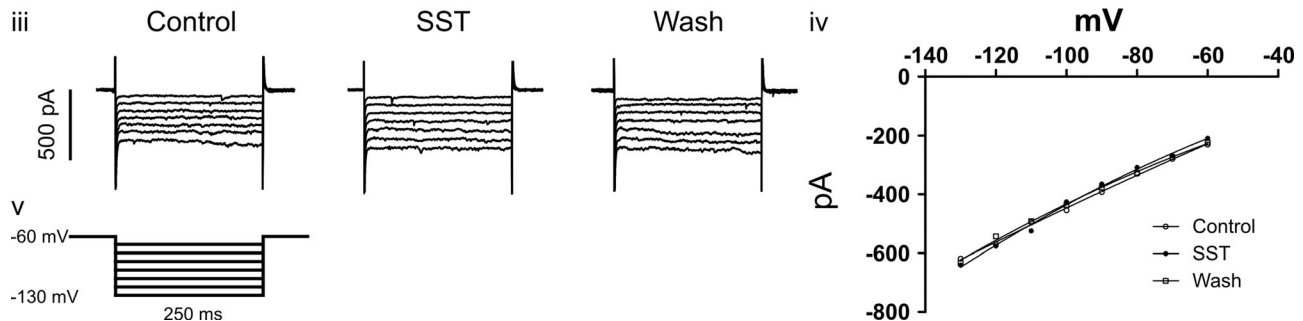


Figure 6. Current-voltage relationship of SST-sensitive **(A)** and SST-insensitive **(B)** bulbospinal RVLM neurons. Examples of membrane currents evoked by voltage steps before, during, and after 300 nM SST superfusion; experimental recordings are shown in i and iii, I-V plots are shown in ii and iv. 250 ms command voltages were stepped from -60 to -130 mV in 10 mV increments (v). Inset in A(ii) denotes pooled slope conductances from 17 SST-sensitive bulbospinal neurons. ** $P < 0.01$, Bonferroni post-test.

3.7 ± 0.6 nS were measured between $-60/-80$ and $-110/-130$ mV, respectively. Following 300 nM SST, slope conductances increased to 3.6 ± 0.5 nS and 4.9 ± 0.6 nS over the same potentials, indicating inward rectification (2-way ANOVA: $F_{1, 32} = 10.57$, $P = 0.002$, pooled data inset in Fig. 6A(ii)). The SST-evoked current was greater at more negative currents, had a reversal potential of -93 ± 6 mV, and was not detected in SST-insensitive neurons.

Hyperpolarizing steps beyond -70 mV were also associated with slowly activating inward currents in 10/26 neurons tested (Fig. 7), which were consistent in time-course and profile with activation of the

hyperpolarization-activated cation channel, I_h . The amplitudes of hyperpolarization-activated currents were highly variable between neurons, with a median value of -55 pA at -130 mV (range: 10–291 pA). The proportion of SST-sensitive neurons was not significantly different in neurons that expressed I_h compared to those that did not ($P = 1$, Fisher's Exact Test).

sst_{2a} receptor expression on electrophysiologically characterized bulbospinal neurons

Fourteen biocytin-labeled bulbospinal neurons were recovered for histological processing. No sst_{2a}

immunoreactivity was ever identified on SST-insensitive neurons ($n = 9$, Fig. 8A). SST evoked responses of 42.3 ± 7.9 pA in the remaining 5 neurons: 3/5 were subsequently identified as *sst*_{2a}-positive (Fig. 8B).

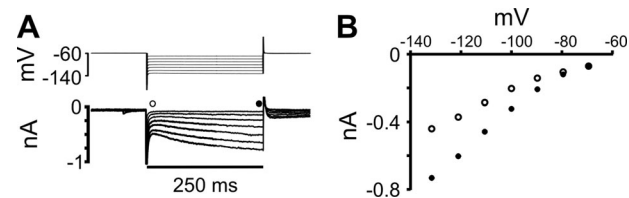


Figure 7. Example of hyperpolarization-activated inward current recorded in a bulbospinal RVLM neuron. **(A)** Hyperpolarizing membrane steps from -70 to -130 mV evoked a slowly activating inward current. The amplitude of the hyperpolarization-activated current was estimated by measuring the difference between the instantaneous (open circle) and steady-state currents (closed circles) evoked by each step **(B)**.

Retrograde tracing of SSTergic neurons

CTB injection sites were located in the RVLM and extended 0.7 – 1.1 mm caudal to the facial nucleus (bregma -11.64 mm) with the core of the injection sites centered between bregma -11.8 and -12.3 mm (Fig. 9).

The majority of brain regions that contained CTB-labeled neurons also contained neurons expressing PPS mRNA. Table 2 presents the distribution and relative density of cells containing CTB and/or PPS mRNA in all brain regions that contained CTB labeled neurons.

Colocalization of PPS mRNA with CTB immunoreactivity was restricted to eight brain regions: the paratrigeminal nucleus (Pa5), lateral parabrachial nucleus (LPB), Kölliker-Fuse nucleus (KF), ventrolateral periaqueductal gray area (VLPAG), central nucleus of the amygdala (CeA), subnucleus extended amygdala (SLEA), interstitial nucleus of the posterior limb of the anterior

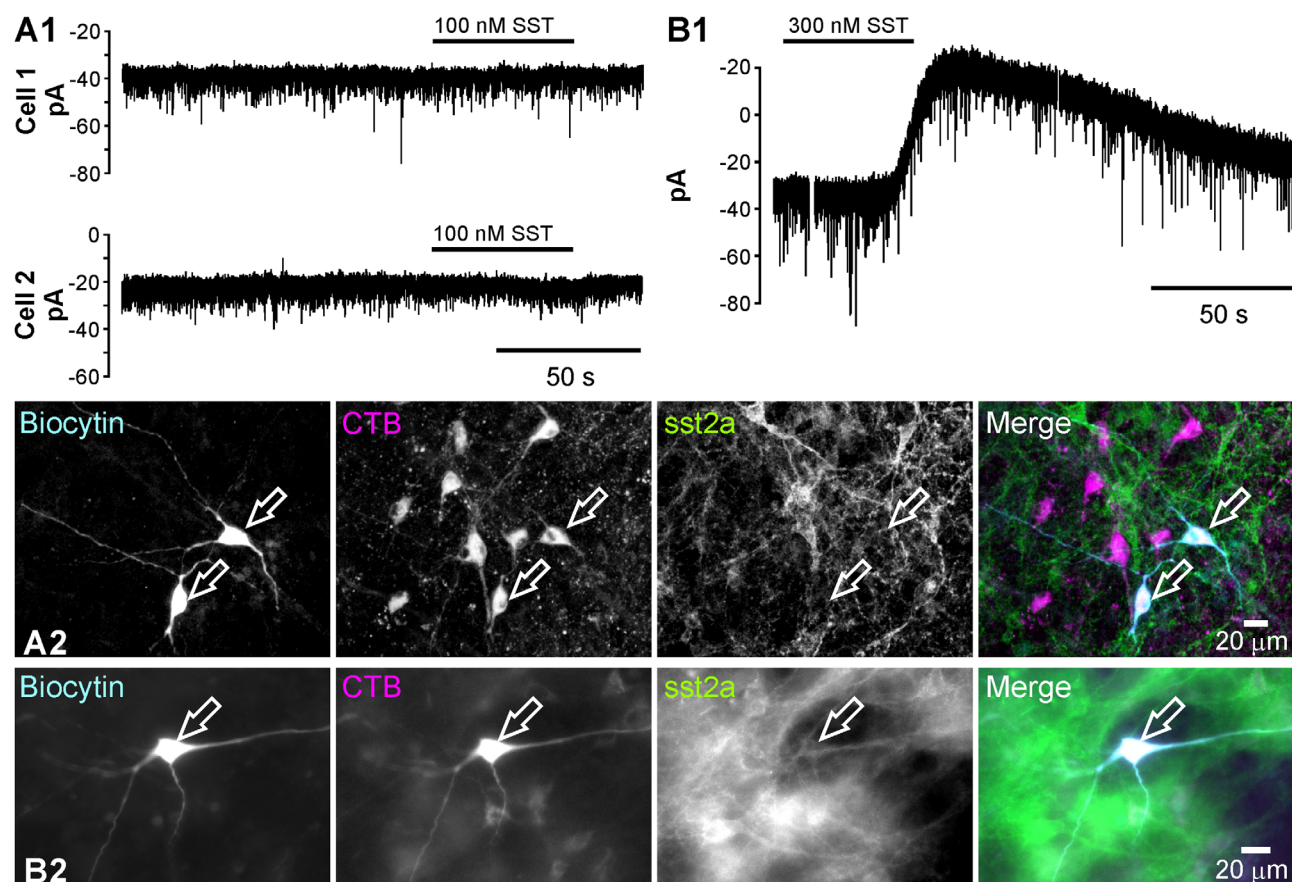


Figure 8. Immunohistochemical recovery of electrophysiologically characterized RVLM bulbospinal neurons. **(A1)** Simultaneous voltage-clamp recordings from two bulbospinal RVLM neurons recorded with biocytin-filled pipettes; neither responded to 100 nM SST application. **(A2)** $22\text{-}\mu\text{m}$ -thick confocal projection image of the same neurons; both biocytin-filled neurons were confirmed as CTB-positive and *sst*_{2a}-negative. **(B1)** Example of an SST-sensitive neuron recorded in a different experiment; the neuron was subsequently shown to be weakly *sst*_{2a}-immunoreactive under epifluorescence **(B2)**. Breaks in recording B1 indicate switches in recording mode at which seal resistance was assessed.

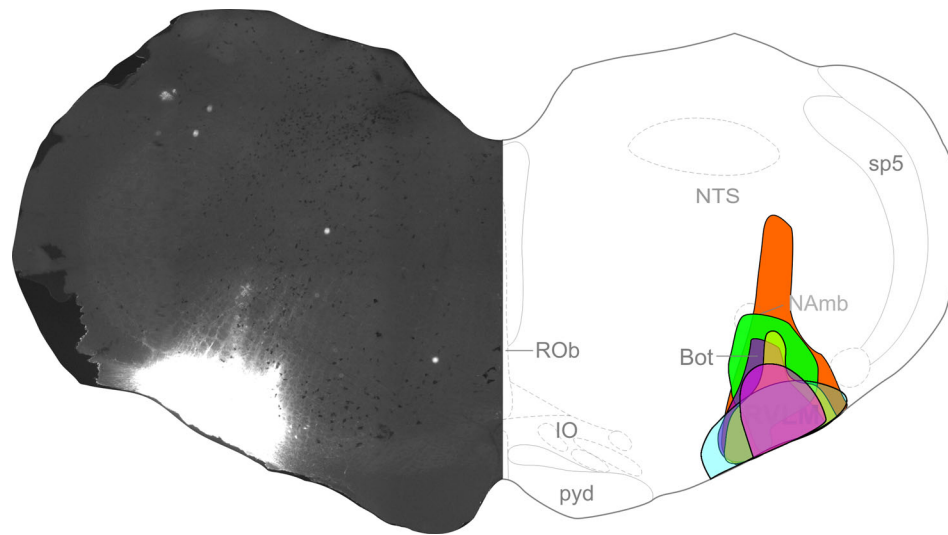


Figure 9. CTB injection sites targeting the RVLM. The left coronal hemisection shows the CTB injection site from one animal. The right hemisection shows schematically the extents of six injection sites in animals used for quantitative analysis.

commissure nucleus (IPAC), and bed nucleus of the stria terminalis (BNST). Figure 10 shows examples of double labeling in the Pa5, VLPAG, CeA and BNST.

The proportion of CTB-labeled neurons that contain PPS mRNA within each region is shown in Figure 11. Of the eight brain regions, CTB-labeled cells in Pa5 contained the highest PPS expression ($40 \pm 3\%$, 73/173 CTB-ir cells, $n = 4$), followed closely by the SLEA ($34 \pm 6\%$, 65/180, $n = 3$). The IPAC possessed a small, variable population of double-labeled cells across animals ($26 \pm 10\%$, 20/68 CTB-ir cells, $n = 3$). The VLPAG contained PPS mRNA expression in approximately one-fifth of its RVLM-projecting cell population ($22 \pm 3\%$); however, this region also exhibited the highest number of double-labeled cells of all regions analyzed (158/791, $n = 4$). Retrogradely traced populations of the LPB and BNST contained similar proportions of PPS ($13 \pm 1\%$, 47/369, $n = 4$ and $12 \pm 2\%$, 48/406, $n = 3$ respectively), followed by the KF ($10 \pm 0.5\%$, $n = 4$), which furthermore contained the lowest number of double-labeled cells of all RVLM-projecting populations. Despite the CeA possessing the lowest percentage of double-labeled neurons ($10 \pm 1\%$), it contained a relatively large number of PPS-expressing CTB labeled cells (110/713 cells, $n = 3$), which was only overshadowed by the size of the VLPAG projection.

DISCUSSION

The main findings are: first, that SST evoked an outward current suggestive of activation of an inwardly rectifying potassium channel in approximately half of RVLM bulbospinal neurons. Second, this effect is most

likely due to activation of sst_2 receptors, as SST-activated currents were blocked by cyanamid and sst_{2a} receptor expression was identified on SST-sensitive neurons. Third, putative sources of SSTergic drive to the RVLM were identified in eight distinct brain regions: the Pa5, KF, LPB, VLPAG, CeA, SLEA, IPAC, and BNST.

SST hyperpolarizes spinally projecting RVLM neurons via GIRK channels

SST hyperpolarized about 60% of bulbospinal neurons in acute brain slices from young rats. The response amplitudes obtained and dose range used were similar to those reported in SST-sensitive neurons in the periaqueductal gray (Connor et al., 2004). The SST-evoked responses were effectively blocked by cyanamid, a selective antagonist of sst_2 receptors (Nunn et al., 2003), suggesting specific involvement of sst_2 receptors in mediating the response in bulbospinal neurons. Addition of TTX to the perfusate did not alter outward currents evoked by SST, indicating that the evoked currents were mediated by postsynaptic rather than presynaptic mechanisms. The proportion of SST-sensitive neurons in the current study is consistent with the proportion of bulbospinal (35%) and C1 neurons (50%) that were previously identified as sst_{2a} -immunoreactive in adult animals (Burke et al., 2008), although higher than the overall proportion of biotin-labeled bulbospinal neurons identified as sst_{2a} -immunoreactive in the current study (21%). Of the five recovered neurons that responded to SST, only three clearly expressed sst_{2a} immunoreactivity, whereas all nine nonresponsive neurons were sst_{2a} -negative. In neurons that expressed

TABLE 2.

Relative Abundance of Neurons Containing CTB-ir and/or PPS mRNA in Each Brain Region Projecting to the RVLM

Location	Subregion	Laterality of CTB	CTB	PPS
Cortical	Motor Cortex (MC)	Bi	++	+++
	Sensory Cortex (SC)	Bi	++	++
	Infralimbic Cortex (IL)	Bi	+++	+++
	Prelimbic Cortex (PrL)	Bi	++	+++
	Insular Cortex (IC)	Bi	++	++
Subcortical	Vascular Organ, Lamina Terminalis	-	++	+
	Medial Preoptic Area (MPA)	bi	++	+
	Bed Nucleus, Stria Terminalis (BNST)	bi	+++	++++
	Interstitial Nucleus of Posterior Limb, Anterior Commissure (IPAC)	ipsi	++	+++
	Sublenticular Extended Amygdala (SLEA)	ipsi	+++	+++
	Paraventricular Nucleus, Hypothalamus (PVN)	bi	++++	++
	Ventromedial Hypothalamus (VMH)	Bi	+	+++
	Central Nucleus of the Amygdala (CeA)	ipsi	++++	+++
	Dorsomedial Hypothalamus (DMH)	bi	++	++
	Zona Incerta (ZI)	bi	++	++
	Lateral Hypothalamic Area (LHA)	Bi	+++	++
	Lateral PAG (LPAG)	bi	+	++
	Ventrolateral PAG (VLPAG)	bi	+++	+++
	Dorsomedial PAG (DMPAG)	bi	+++	++
	Oculomotor Nucleus, Parvocellular (3PC)	contra	+	++++
Midbrain	Intermediate White Layer, Superior Colliculus (InWh)	contra	+	+++
	Inferior Colliculus (InC)	bi	++	+++
	Dorsal Raphe, Caudal Part (DRC)	-	++	-
	Retrorubral Field (RRF)	Bi	++	+
	Pedunculo-pontine Tegmental Area (PPTg)	Bi	++	+
	Lateral Parabrachial Nucleus (LPB)	Bi	+++	+++
	Medial Parabrachial Nucleus (MPB)	Bi	++	++
	Kölliker Fuse (KF)	Bi	+++	++++
	Locus Coeruleus (LC)	ipsi	++	+
	Subcoeruleus (SubC)	ipsi	++	-
Pons	A5 region	Bi	++	+
	Midline Raphe	-	+++	++
	Vestibular Nucleus	bi	++	+++
	Gigantocellular Reticular Nucleus (Gi)	bi	+	+
Medulla	Caudal Ventrolateral Medulla (CVLM)	bi	+++	++
	Intermediate Reticular Nucleus	bi	+	+
	Nucleus of the Solitary Tract (NTS)	bi	++++	++
	Area Postrema (AP)	-	++++	-
	Paratrigeminal Nucleus (Pa5)	bi	+	+++
	A1 region/ Retro Ambiguus	bi	++	+

Scattered (+) labeling refers to sparsely distributed cells (<5 per region) Light (++) labeling indicates coverage of less than one third of the defined region. Moderate (+++) labeling indicates a range of labeling from approximately one to two thirds coverage of the cell group while dense (++++) labeling describes an area containing a high number of labeled cells which cover more than two-thirds of the anatomically defined region.

sst_{2a} it seems likely that the SST-evoked response was mediated via this receptor. In neurons that responded to SST in which sst_{2a} immunoreactivity was undetectable, it is possible that other SST receptor isotypes mediated electrophysiological responses. This lower than expected expression of sst_{2a} on SST-sensitive neurons could also be an artifact that reflects the limited sensitivity of immunofluorescence for discriminating lightly immunoreactive neurons in thick slices, or could even be due to dialysis of SST receptors, which become internalized and migrate away from the cell membrane after agonist binding (Cescato et al., 2006).

The outward current evoked by SST resulted from an increase in inwardly rectifying potassium conductance, since at more negative potentials SST activated a greater conductance and had a reversal potential approaching the Nernst potential calculated for potassium (-93 mV). This is in keeping with data indicating that sst_2 couples efficiently to GIRK1, examined by comparing dose-response curves and the maximum currents obtained by the five different rat SST receptor subtypes (sst_1 - sst_5) that were coexpressed with GIRK1 (Kreienkamp et al., 1997). Our results are consistent with the effects of SST on inwardly rectifying potassium

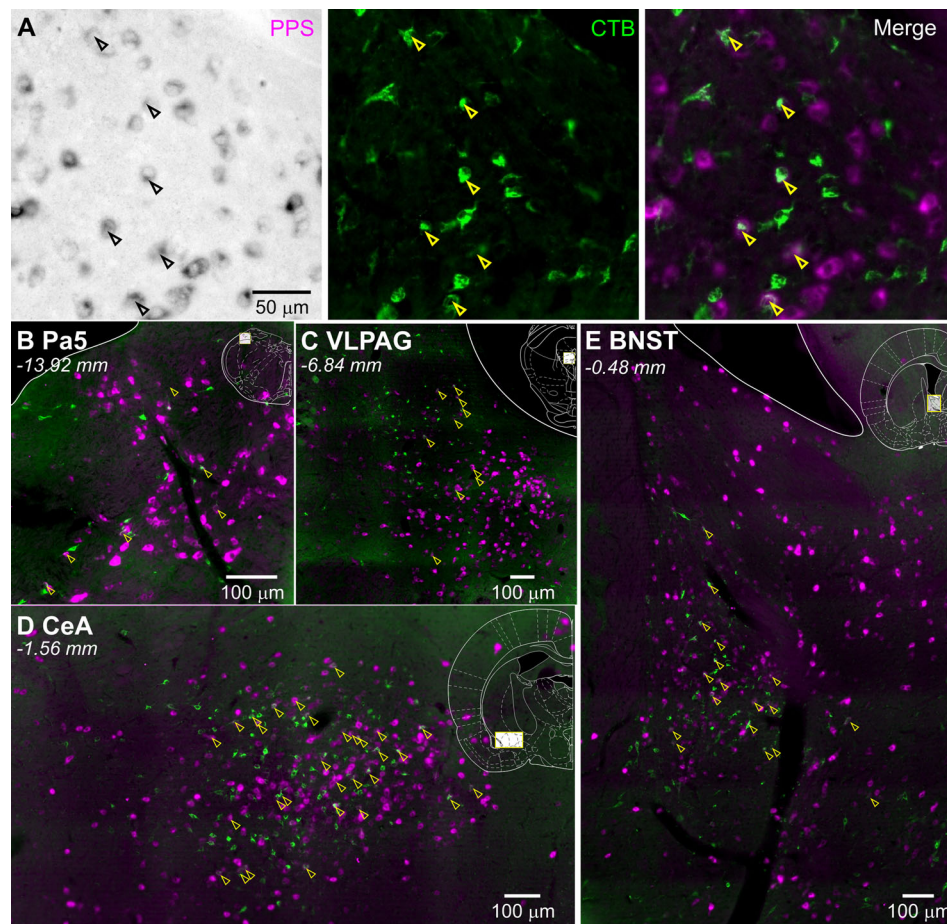


Figure 10. Combined PPS in situ hybridization and retrograde tracing reveals putative RVLM-projecting somatostatinergic neurons. **(A)** High-power photomicrograph showing neurons labeled for PPS mRNA (brightfield) and CTB immunofluorescence (green channel). Double-labeled neurons are indicated by arrowheads; PPS mRNA is magenta in merged pseudocolored images. Merged epifluorescence images in **B–E** illustrate the distribution of double-labeled neurons in the paratrigeminal nucleus (Pa5, B), ventrolateral periaqueductal gray (VLPAG, C), central nucleus of the amygdala (CeA, D), and bed nucleus of the stria terminalis (BNST, E). A schematic diagram indicating the region shown (yellow box) and the rostrocaudal coordinate with respect to bregma is superimposed onto each photomicrograph; schematic diagrams adapted from Paxinos and Watson (2006).

conductance in neurons in other brainstem regions including the locus coeruleus (Inoue et al., 1988) and PAG (Connor et al., 2004). In addition, in different brain regions such as the superior cervical ganglion (Shapiro and Hille, 1993), amygdala (Viana and Hille, 1996), and PAG (Connor et al., 2004), SST directly activates potassium conductance and inhibits GABA release via a pre-synaptic calcium-dependent mechanism and may contribute to the effects of SST on RVLM sympathetic premotor neurons. In the current study, repeated application of SST evoked hyperpolarizing responses that showed considerable desensitization. Following long exposure to agonists, G-protein-coupled receptors mediate a signal that triggers receptor dephosphorylation (Premont et al., 1995; Böhm et al., 1997; Lefkowitz, 1998; Horie and Insel, 2000). Desensitization of SST receptors has been reported in rat hippocampal and

neocortical neurons (Wang et al., 1990; Priestley, 1992; Young Shim et al., 2006; Yin et al., 2009), and, of particular relevance to the current study, Liu et al. (2008) found that SST₂ receptors internalize and desensitize following agonist stimulation within minutes.

An incidental finding of the current study is the presence of a hyperpolarization-activated channel in some bulbospinal RVLM neurons. Although not studied in detail, the time-course and activation threshold of the identified current is consistent with the distinctive profile of hyperpolarization and cyclic nucleotide channel-mediated current, I_h (reviewed by Robinson and Siegelbaum, 2003). This finding supports observations of I_h in bulbospinal RVLM neurons recorded in neonatal rats by previous investigators (Kangrga and Loewy, 1995; Li et al., 1995). Although I_h has been implicated in the generation of spontaneous pacemaker activity in other

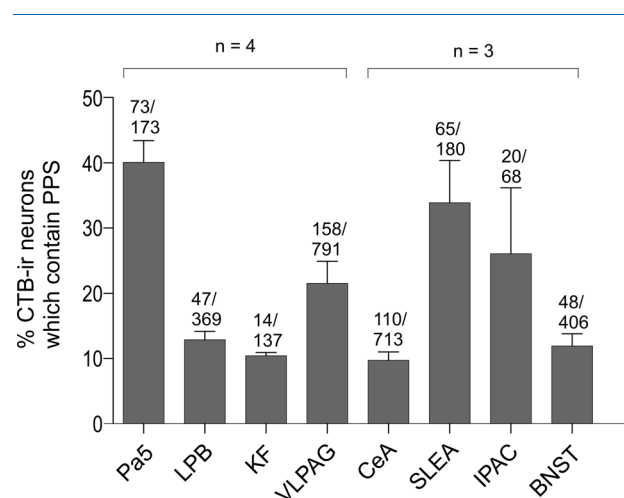


Figure 11. Brain regions containing RVLM projecting (CTB-ir) neurons that express PPS mRNA.

cell types (recently reviewed by He et al., 2014), it is not thought to play a critical role in driving autodepolarization in RVLM, as its blockade by ZD7288 evokes no significant effect on sympathetic nerve activity or blood pressure (Miyawaki et al., 2003).

Technical limitations

Electrophysiological recordings were confined to bulbospinal neurons encountered lateral to the pyramidal tract, ventral to nucleus ambiguus, and medial to the spinal trigeminal nucleus. Bulbospinal neurons in this region contain the highest density of TH expression and have been interpreted as putative sympathetic premotor neurons in similar studies (Kangrga and Loewy, 1995; Li et al., 1995; Li and Guyenet, 1996). Due to the technical difficulties associated with examining more than three fluorescent labels at a time, we did not survey biocytin-labeled neurons for TH immunoreactivity in the current study. However, RVLM bulbospinal neurons selected using the same criteria were intermingled with and included TH-positive neurons in a recent study by our group (Korim et al., 2014).

Brain slices for recordings were made from 8–28-day-old rats. As global SST binding and brain-wide SST receptor expression undergo some lability in the neonatal period in rats (Gonzalez et al., 1989; Thoss et al., 1995), it is possible that changes in the relative expression of SST receptor isoforms in the brainstem could complicate interpretation of the current data. No developmental study has yet described the relative expression of SST receptor isoforms in the brainstem over the neonatal period. However, the expression of *sst_{2a}* in putative TH-positive neurons containing the *Lmx1b* and *Phox2b* transcription factors is already established by

birth (Gray, 2013). Furthermore, the gross pattern of *sst* expression, including *sst_{2a}*, in P5 rats is similar to that observed in adults (Thoss et al., 1995). Although the quality of *sst_{2a}* labeling in thick brain slices reported here is inferior to that observed in conventional thin sections (Burke et al., 2008), *sst_{2a}*-like immunoreactivity was detected on all slices tested and the general pattern of expression was similar to that seen in adult rats, suggesting that *sst_{2a}* expression in juveniles is likely to be representative of older animals.

In common with many other studies using conventional retrograde tracers, interpretation of our anatomical study should be tempered with three caveats. First, CTB may be taken up by fibers that pass through the site of tracer deposition, an effect that is particularly prevalent following pressure-ejection (Luppi et al., 1990; Chen and Aston-Jones, 1995). We cannot therefore determine whether retrogradely labeled neurons form synaptic terminals within the RVLM or simply represent fibers of passage, and therefore urge conservative interpretation of our data. Second, assuming some CTB-labeled neurons do actually form terminals within the RVLM, we cannot determine the function or phenotype of their postsynaptic targets. Finally, significant numbers of neurons in the ventrolateral medulla express somatostatin and project to the ipsi- and contralateral RVLM (Tan et al., 2010). However, discrimination of local SSTergic neurons was confounded by the tracer injection site; we therefore cannot exclude local interneurons as a potential source of SST release.

Finally, we and others (Kiyama and Emson, 1990; Giehl and Mestres, 1995; Stornetta et al., 2003) have interpreted the presence of PPS mRNA as indicative of SST synthesis and release. As discussed by Giehl and Mestres (1995), the correspondence between brain-wide SST mRNA and protein expression is generally robust, but PPS can be cleaved into a number of peptides other than SST-14 and SST-28 (Patel and O'Neil, 1988; Rabbani and Patel, 1990), including a recently discovered neuropeptide, neuronostatin (Samson et al., 2008). Therefore, although PPS mRNA expression is a sensitive assay of PPS production, PPS expression per se does not necessarily correspond with translation of SST peptide or its release. Interestingly, intracerebroventricular neuronostatin has been reported to drive a sympathetically mediated rise in arterial blood pressure (Samson et al., 2008; Yosten et al., 2011) via a proposed (Samson et al., 2008) but currently unproven action at the paraventricular nucleus of the hypothalamus. Preliminary experiments in our laboratory have revealed no effect of neuronostatin when microinjected into the RVLM pressor region in urethane-anaesthetized rats (Burke et al., unpublished data).

PPS mRNA is found in select groups of neurons projecting to the RVLM

Paratrigeminal nucleus

Distinct clusters of PPS mRNA-expressing neurons were found in the Pa5 in the current study, as previously noted (Kiyama and Emson, 1990). Both anterograde and retrograde studies have revealed projections from the Pa5 to the RVLM (Caous et al., 2001; de Sousa Buck et al., 2001); however, this is the first study to describe a somatostatinergic phenotype in just under half the RVLM-projecting neurons in the region. Enkephalin, calbindin, and neuronal nitric oxide synthetase (nNOS) have been detected in Pa5 neurons that project to the dorsal motor nucleus of the vagus (Armstrong and Hopkins, 1998); these groups may also overlap with the PPS-containing population described here. Pa5 microinjection of bradykinin evokes pressor effects (Lindsey et al., 1997) via direct activation of barosensitive RVLM neurons (Caous et al., 2004). Many (60–80%) Pa5 neurons are themselves barosensitive, increasing their firing rate in response to phenylephrine administration (Balan et al., 2004; Sousa and Lindsey, 2009b), while bilateral Pa5 ablation reduces cardiac barosensitivity (Sousa and Lindsey, 2009a). Whether SST participates in mediating such reflex modulation in the RVLM is unknown.

Kölliker-Fuse and lateral parabrachial nuclei

Together, the KF and LPB form the pontine respiratory group, and while PPS expression has been explicitly demonstrated in the LPB (Kiyama and Emson, 1990), reporting of its localization in the KF has been overlooked prior to the current study (Kiyama and Emson, 1990; Giehl and Mestres, 1995). Projections from both KF and LPB to the RVLM region have been described (Smith et al., 1989). Although cardiovascular responses to chemical stimulation of parabrachial nuclei have been examined, they are inconsistent, brief, and/or small (Ward, 1988; Chamberlin and Saper, 1994; Lara et al., 1994), and the region's function in respiratory control is certainly better understood (Smith et al., 1989; Morschel and Dutschmann, 2009). At LPB/KF sites corresponding to the location of PPS-expressing RVLM projecting neurons detected in the current study, glutamate microinjection has been reported to drive inspiratory facilitation (Chamberlin and Saper, 1994) or brief apnea (Chamberlin and Saper, 1994; Dutschmann and Herbert, 2006), whereas inhibition of the same sites drives apneustic prolongation of inspiratory phase duration (Dutschmann and Herbert, 2006), similar to that evoked by microinjection of SST into the Böttinger complex (Burke et al., 2010).

Ventrolateral periaqueductal gray (VLPAG)

PPS mRNA expression was observed in the VLPAG, as previously described (Smith et al., 1994), and in neurons projecting to the raphe magnus (Beitz et al., 1983). Although projections from the VLPAG to the RVLM have been described (Carrive and Bandler, 1991), this is the first study to attribute a somatostatinergic phenotype to some elements of the pathway. Depressor responses associated with reductions in renal vascular resistance are evoked chiefly by stimulation of the caudal VLPAG (Carrive and Bandler, 1991), which overlaps anatomically with the PPS-expressing RVLM projecting neurons identified in the current study. On the other hand, stimulation of the VLPAG also evokes vasodilation in the hindlimb (Lovick, 1992) and this has been attributed to a raphe-mediated pathway (Wang and Lovick, 1993). It is possible that raphe and RVLM projections arise from discrete regions of the VLPAG, as changes in iliac or renal blood flow are associated with different rostrocaudal levels of the VLPAG and corresponding RVLM termination sites (Carrive and Bandler, 1991). The caudal VLPAG has also been implicated in hemorrhage as the activity of neurons in the region increase during the decompensatory or hypotensive phase (Cavun and Millington, 2001).

Central nucleus of the amygdala (CeA) and the extended amygdala

Somatostatinergic neurons have been described in the CeA (Vincent et al., 1985) and these project to the PAG (Gray and Magnuson, 1992) and/or dorsal vagal complex, in particular the NTS (Veening et al., 1984; Gray and Magnuson, 1987; Saha et al., 2002). The present study, however, is the first to demonstrate a dense PPS-expressing projection to the RVLM. Both coronal transection caudal to, or sagittal transection medial to, the CeA reduce the amount of SST-ir fibers in the ventrolateral medulla (Kawai et al., 1982), supporting our findings. Furthermore, the CeA also contains a glutamatergic population which projects to the RVLM (Takayama and Miura, 1991), and terminals arising from cells in the CeA appose barosensitive C1 neurons and non-C1 neurons (Cassell and Gray, 1989; Saha et al., 2005). Therefore, it is possible that the PPS-expressing neurons in the CeA described in the present study also contain glutamate.

The functional role of these neurons is more difficult to ascribe. Low-frequency stimulation of CeA in the awake animal promotes inspiration, even respiratory entrainment (Harper et al., 1984). At higher frequencies (>10 Hz), phrenic nerve frequency is increased (Cox et al., 1987) and a prolonged period of inspiration

occurs (Harper et al., 1984), while mostly pressor and some depressor effects have been reported (Stock et al., 1978; Harper et al., 1984; Frysinger et al., 1984; Gelsema et al., 1987; Iwata et al., 1987). It also appears that the responses evoked are state-dependent, with sleep and anesthesia either dampening or reversing cardiorespiratory effects (Stock et al., 1978; Cox et al., 1987; Harper et al., 1984; Frysinger et al., 1984; Gelsema et al., 1987; Iwata et al., 1987). As the CeA forms a crucial link in the coordination of autonomic and behavioral responses to stress such as conditioned fear (LeDoux et al., 1988; Paré et al., 2004; Wilensky et al., 2006), it is possible that the somatostatinergic pathway identified in the current study may be involved in recovery responses such as the return of mean arterial pressure to baseline levels following freezing responses to conditioned fear (Carrié, 2000; Dielenberg et al., 2001) or the suppression of sympathetic responses during passive versus active coping (Sherwood et al., 1990; Roozendaal et al., 1991).

Extending dorsomedially from rostral parts of the CeA, the SLEA also contained a population of PPS-expressing RVLM-projecting neurons, which has otherwise only been referred to briefly in studies of the developing and adult rodent brain (Real et al., 2009; deCampo and Fudge, 2013). Prior to this study, knowledge of the SLEA's descending projections was restricted to the NTS/dorsal motor nucleus of the vagus nerve and parabrachial complex (Grove, 1988; Sun et al., 1994; Waraczynski, 2006). Chemical stimulation of the SLEA elicits depressor responses (Gelsema et al., 1993). Although a respiratory relationship is associated with the SLEA, it is somewhat complex, as SLEA activity is normally synchronized with the onset of spontaneous breathing but suppressed during the cognitive tasks that drive respiration (Evans et al., 2009). Activation of the SLEA is evident in subjects experiencing dyspnea, and is associated with the unpleasant emotional processing that occurs during a dyspneic episode (von Leupoldt et al., 2008). It is possible that the PPS-expressing pathway to the RVLM from the SLEA may be part of a complex circuit linking emotional state to cardiovascular and respiratory outflows.

The interstitial nucleus of the posterior limb of the anterior commissure (IPAC) expresses PPS mRNA in neurons projecting to the RVLM; however, very little is known about its function except for its role in reward and motivational processes (Waraczynski, 2003). Perhaps, as with other components of the extended amygdala, the IPAC is involved in the integration of emotional processing and autonomic outflows.

We have identified PPS-expressing neurons in the BNST that project to the RVLM despite the fact that such neurons have been found previously to project to the LPB, the PAG, and dorsal vagal complex (Gray and Magnuson, 1987, 1992; Moga et al., 1989), and furthermore, neurochemically undefined neurons are known to project to the lateral tegmental field (Holstege et al., 1985). Although ablation of the region does not affect baseline arterial pressure or heart rate (Crestani et al., 2006), both chemical and electrical stimulation of the lateral subdivisions of BNST (where many PPS neurons in the present study were located) evoke a depressor response (Dunn and Williams, 1995). As PPS neurons projecting to the LPB and NTS are involved in feeding-related responses (Smith et al., 2005; Li and Cho, 2006; Saggu and Lundy, 2008; Panguluri et al., 2009), it is possible that the projection identified here has a corresponding role. Alternatively, the BNST modulates MAP and HR during exercise (Alves et al., 2011), so whether the bradycardic and depressor responses evoked by SST microinjection in the RVLM (Burke et al., 2008) are simulating this function remains to be determined.

CONCLUSION

This study reveals that a discrete subset of brain regions provides somatostatinergic projections to the RVLM: the Pa5, KF, LPB, VLPAG, CeA, SLEA, IPAC, and BNST, and we have provided evidence-based speculation as to the roles of these projections. The projection from the KF and LPB most likely has a respiratory function; however, the role of the other pathways suggested remains to be tested. Nevertheless, it is clear that SST released from these projection neurons activates G-protein-coupled sst_2 (most likely sst_{2a}) receptors whereby GIRK channels are activated that serve to hyperpolarize neurons in the RVLM.

CONFLICT OF INTEREST

The authors report no conflicts of interest

AUTHOR ROLES

SM and AKG conceived and designed the study; LBF, PB, and SK conducted in vitro electrophysiology; SM and BB conducted tracing studies. SL conducted antibody characterization. All authors analyzed data and prepared the article.

LITERATURE CITED

Allen JP, Hathway GJ, Clarke NJ, Jowett MI, Topps S, Kendrick KM, Humphrey PPA, Wilkinson LS, Emson PC. 2003. Somatostatin receptor 2 knockout/lacZ knockin mice show impaired motor coordination and reveal sites of

- somatostatin action within the striatum. *Eur J Neurosci* 17:1881–1895.
- Alves F, Resstel L, Correa F, Crestani C. 2011. Bed nucleus of the stria terminalis $\alpha 1$ and 2-adrenoceptors differentially modulate the cardiovascular responses to exercise in rats. *Neuroscience* 177:74–83.
- Armstrong CL, Hopkins DA. 1998. Neurochemical organization of paratrigeminal nucleus projections to the dorsal vagal complex in the rat. *Brain Res* 785:49–57.
- Balan A Jr, Caous CA, Yu YG, Lindsey CJ. 2004. Barosensitive neurons in the rat tractus solitarius and paratrigeminal nucleus: A new model for medullary, cardiovascular reflex regulation. *Can J Physiol Pharmacol* 82:474–484.
- Beitz AJ, Shepard RD, Wells WE. 1983. The periaqueductal gray-raphe magnus projection contains somatostatin, neurotensin and serotonin but not cholecystokinin. *Brain Res* 261:132–137.
- Bohm SK, Grady EF, Bunnett NW. 1997. Regulatory mechanisms that modulate signalling by G-protein-coupled receptors. *Biochem J* 322(Pt 1):1–18.
- Bowman BR, Kumar NN, Hassan SF, McMullan S, Goodchild AK. 2013. Brain sources of inhibitory input to the rat rostral ventrolateral medulla. *J Comp Neurol* 521:213–232.
- Bruno JF, Xu Y, Song J, Berelowitz M. 1992. Molecular cloning and functional expression of a brain-specific somatostatin receptor. *Proc Natl Acad Sci U S A* 89:11151–11155.
- Burke PG, Li Q, Costin ML, McMullan S, Pilowsky PM, Goodchild AK. 2008. Somatostatin 2A receptor-expressing presympathetic neurons in the rostral ventrolateral medulla maintain blood pressure. *Hypertension* 52:1127–1133.
- Burke PG, Abbott SB, McMullan S, Goodchild AK, Pilowsky PM. 2010. Somatostatin selectively ablates post-inspiratory activity after injection into the Botzinger complex. *Neuroscience* 167:528–539.
- Caous CA, de Sousa Buck H, Lindsey CJ. 2001. Neuronal connections of the paratrigeminal nucleus: a topographic analysis of neurons projecting to bulbar, pontine and thalamic nuclei related to cardiovascular, respiratory and sensory functions. *Auton Neurosci* 94:14–24.
- Caous CA, Balan A, Lindsey CJ. 2004. Bradykinin microinjection in the paratrigeminal nucleus triggers neuronal discharge in the rat rostroventrolateral reticular nucleus. *Can J Physiol Pharmacol* 82:485–492.
- Carrive P. 2000. Conditioned fear to environmental context: cardiovascular and behavioral components in the rat. *Brain Res* 858:440–445.
- Carrive P, Bandler R. 1991. Viscerotopic organization of neurons subserving hypotensive reactions within the midbrain periaqueductal gray: a correlative functional and anatomical study. *Brain Res* 541:206–215.
- Carrive P, Bandler R, Dampney RA. 1988. Anatomical evidence that hypertension associated with the defence reaction in the cat is mediated by a direct projection from a restricted portion of the midbrain periaqueductal gray to the subretrofacial nucleus of the medulla. *Brain Res* 460:339–345.
- Cassell MD, Gray TS. 1989. The amygdala directly innervates adrenergic (C1) neurons in the ventrolateral medulla in the rat. *Neurosci Lett* 97:163–168.
- Cavun S, Millington WR. 2001. Evidence that hemorrhagic hypotension is mediated by the ventrolateral periaqueductal gray region. *Am J Physiol Regul Integr Comp Physiol* 281:R747–R752.
- Cescato R, Schulz S, Waser B, Eltschinger V, Rivier JE, Wester HJ, Culler M, Ginj M, Liu Q, Schonbrunn A, Reubi JC. 2006. Internalization of sst2, sst3, and sst5 receptors: effects of somatostatin agonists and antagonists. *J Nucl Med* 47:502–511.
- Chamberlin N, Saper C. 1994. Topographic organization of respiratory responses to glutamate microstimulation of the parabrachial nucleus in the rat. *J Neurosci* 14:6500–6510.
- Chen S, Aston-Jones G. 1995. Evidence that cholera toxin B subunit (CTb) can be avidly taken up and transported by fibers of passage. *Brain Res* 674:107–111.
- Chessell IP, Black MD, Feniuk W, Humphrey PP. 1996. Operational characteristics of somatostatin receptors mediating inhibitory actions on rat locus coeruleus neurones. *Br J Pharmacol* 117:1673–1678.
- Connor M, Bagley EE, Mitchell VA, Ingram SL, Christie MJ, Humphrey PP, Vaughan CW. 2004. Cellular actions of somatostatin on rat periaqueductal gray neurons in vitro. *Br J Pharmacol* 142:1273–1280.
- Cox GE, Jordan D, Paton JF, Spyer KM, Wood LM. 1987. Cardiovascular and phrenic nerve responses to stimulation of the amygdala central nucleus in the anaesthetized rabbit. *J Physiol* 389:541–556.
- Crestani CC, Alves FHF, Resstel LBM, Correa FM. 2006. The bed nucleus of the stria terminalis modulates baroreflex in rats. *NeuroReport* 17:1531–1535.
- Dampney RAL, Czachurski J, Dembowski K, Goodchild AK, Seller H. 1987. Afferent connections and spinal projections of the pressor region in the rostral ventrolateral medulla of the cat. *J Auton Nerv Syst* 20:73–86.
- De León M, Coveñas R, Narváez JA, Tramu G, Aguirre JA, González-Barón S. 1992. Distribution of somatostatin-28 (1–12) in the cat brainstem: an immunocytochemical study. *Neuropeptides* 21:1–11.
- de Sousa Buck H, Caous CA, Lindsey CJ. 2001. Projections of the paratrigeminal nucleus to the ambiguous, rostroventrolateral and lateral reticular nuclei, and the solitary tract. *Auton Neurosci* 87:187–200.
- deCampo DM, Fudge JL. 2013. Amygdala projections to the lateral bed nucleus of the stria terminalis in the macaque: comparison with ventral striatal afferents. *J Comp Neurol* 521:3191–3216.
- Dielenberg RA, Carrive P, McGregor IS. 2001. The cardiovascular and behavioral response to cat odor in rats: unconditioned and conditioned effects. *Brain Res* 897:228–237.
- Dunn JD, Williams TJ. 1995. Cardiovascular responses to electrical stimulation of the bed nucleus of the stria terminalis. *J Comp Neurol* 352:227–234.
- Dutschmann M, Herbert H. 2006. The Kolliker-Fuse nucleus gates the postinspiratory phase of the respiratory cycle to control inspiratory off-switch and upper airway resistance in rat. *Eur J Neurosci* 24:1071–1084.
- Evans KC, Dougherty DD, Schmid AM, Scannell E, McCallister A, Benson H, Dusek JA, Lazar SW. 2009. Modulation of spontaneous breathing via limbic/paralimbic-bulbar circuitry: an event-related fMRI study. *NeuroImage* 47:961–971.
- Fischer T, Doll C, Jacobs S, Kolodziej A, Stumm R, Schulz S. 2008. Reassessment of sst2 somatostatin receptor expression in human normal and neoplastic tissues using the novel rabbit monoclonal antibody UMB-1. *J Clin Endocrinol Metab* 93:4519–4524.
- Fryssinger RC, Marks JD, Trelease RB, Schechtman VL, Harper RM. 1984. Sleep states attenuate the pressor response to central amygdala stimulation. *Exp Neurol* 83:604–617.
- Gao LL, McMullan S, Djouhri L, Acosta C, Harper AA, Lawson SN. 2012. Expression and properties of hyperpolarization-activated current in rat dorsal root

- ganglion neurons with known sensory function. *J Physiol* 590(Pt 19):4691–4705.
- Gelsema AJ, McKittrick DJ, Calaresu FR. 1987. Cardiovascular responses to chemical and electrical stimulation of amygdala in rats. *Am J Physiol* 253(5 Pt 2):R712–718.
- Gelsema AJ, Copeland NE, Drolet G, Bachelard H. 1993. Cardiovascular effects of neuronal activation of the extended amygdala in rats. *Brain Res* 626:156–166.
- Giehl K, Mestres P. 1995. Somatostatin-mRNA expression in brainstem projections into the medial preoptic nucleus. *Exp Brain Res* 103:344–354.
- Gogolla N, Galimberti I, DePaola V, Caroni P. 2006. Staining protocol for organotypic hippocampal slice cultures. *Nat Protoc* 1:2452–2456.
- Gonzalez BJ, Leroux P, Bodenant C, Laquerriere A, Coy DH, Vaudry H. 1989. Ontogeny of somatostatin receptors in the rat brain: biochemical and autoradiographic study. *Neuroscience* 29:629–644.
- Gray PA. 2013. Transcription factors define the neuroanatomical organization of the medullary reticular formation. *Front Neuroanat* 7:7.
- Gray TS, Magnuson DJ. 1987. Neuropeptide neuronal efferents from the bed nucleus of the stria terminalis and central amygdaloid nucleus to the dorsal vagal complex in the rat. *J Comp Neurol* 262:365–374.
- Gray TS, Magnuson DJ. 1992. Peptide immunoreactive neurons in the amygdala and the bed nucleus of the stria terminalis project to the midbrain central gray in the rat. *Peptides* 13:451–460.
- Gray PA, Hayes JA, Ling GY, Llona I, Tupal S, Picardo MC, Ross SE, Hirata T, Corbin JG, Eugenin J, Del Negro CA. 2010. Developmental origin of preBotzinger complex respiratory neurons. *J Neurosci* 30:14883–14895.
- Harper RM, Frysinger RC, Trelease RB, Marks JD. 1984. State-dependent alteration of respiratory cycle timing by stimulation of the central nucleus of the amygdala. *Brain Res* 306:1–8.
- He C, Chen F, Li B, Hu Z. 2014. Neurophysiology of HCN channels: from cellular functions to multiple regulations. *Prog Neurobiol* 112:1–23.
- Holstege G, Meiners L, Tan K. 1985. Projections of the bed nucleus of the stria terminalis to the mesencephalon, pons, and medulla oblongata in the cat. *Exp Brain Res* 58:379–391.
- Hopkins DA, Holstege G. 1978. Amygdaloid projections to the mesencephalon, pons and medulla oblongata in the cat. *Exp Brain Res* 32:529–547.
- Horie K, Insel PA. 2000. Retrovirally mediated transfer of a G protein-coupled receptor kinase (GRK) dominant-negative mutant enhances endogenous calcitonin receptor signaling in Chinese hamster ovary cells. GRK inhibition enhances expression of receptors and receptor mRNA. *J Biol Chem* 275:29433–29440.
- Inoue M, Nakajima S, Nakajima Y. 1988. Somatostatin induces an inward rectification in rat locus coeruleus neurons through a pertussis toxin-sensitive mechanism. *J Physiol* 407:177–198.
- Iwata J, Chida K, LeDoux JE. 1987. Cardiovascular responses elicited by stimulation of neurons in the central amygdaloid nucleus in awake but not anesthetized rats resemble conditioned emotional responses. *Brain Res* 418:183–188.
- Kangrga IM, Loewy AD. 1995. Whole-cell recordings from visualized C1 adrenergic bulbospinal neurons: ionic mechanisms underlying vasomotor tone. *Brain Res* 670:215–232.
- Kawai Y, Inagaki S, Shiosaka S, Senba E, Hara Y, Sakanaka M, Takatsuki K, Tohyama M. 1982. Long descending projections from amygdaloid somatostatin-containing cells to the lower brain stem. *Brain Res* 239:603–607.
- Kawai Y, Qi J, Comer AM, Gibbons H, Win J, Lipski J. 1999. Effects of cyanide and hypoxia on membrane currents in neurones acutely dissociated from the rostral ventrolateral medulla of the rat. *Brain Res* 830:246–257.
- Kawashima T, Kitamura K, Suzuki K, Nonaka M, Kamijo S, Takemoto-Kimura S, Kano M, Okuno H, Ohki K, Bito H. 2013. Functional labeling of neurons and their projections using the synthetic activity-dependent promoter E-SARE. *Nat Methods* 10:889–895.
- Kerr DIB, Ong J. 1995. GABAB receptors. *Pharmacol Ther* 67:187–246.
- Kiyama H, Emson PC. 1990. Distribution of somatostatin mRNA in the rat nervous system as visualized by a novel non-radioactive in situ hybridization histochemistry procedure. *Neuroscience* 38:223–244.
- Korim WS, Bou Farah L, McMullan S, Verberne AJ. 2014. Orexinergic activation of medullary premotor neurons modulates the adrenal sympathoexcitation to hypothalamic glucoprivation. *Diabetes* 63:1895–1906.
- Korner M, Eltschinger V, Waser B, Schonbrunn A, Reubi JC. 2005. Value of immunohistochemistry for somatostatin receptor subtype sst2A in cancer tissues: lessons from the comparison of anti-sst2A antibodies with somatostatin receptor autoradiography. *Am J Surg Pathol* 29:1642–1651.
- Kreienkamp H-J, Hönck H-H, Richter D. 1997. Coupling of rat somatostatin receptor subtypes to a G-protein gated inwardly rectifying potassium channel (GIRK1). *FEBS Lett* 419:92–94.
- Kumar NN, Ferguson J, Padley JR, Pilowsky PM, Goodchild AK. 2009. Differential muscarinic receptor gene expression levels in the ventral medulla of spontaneously hypertensive and Wistar-Kyoto rats: role in sympathetic baroreflex function. *J Hypertens* 27:1001–1008.
- Lara JP, Parkes MJ, Silva-Carvalho L, Izzo P, Dawid-Milner MS, Spyer KM. 1994. Cardiovascular and respiratory effects of stimulation of cell bodies of the parabrachial nuclei in the anaesthetized rat. *J Physiol* 477(Pt 2):321–329.
- LeDoux J, Iwata J, Cicchetti P, Reis D. 1988. Different projections of the central amygdaloid nucleus mediate autonomic and behavioral correlates of conditioned fear. *J Neurosci* 8:2517–2529.
- Lefkowitz RJ. 1998. G protein-coupled receptors. III. New roles for receptor kinases and beta-arrestins in receptor signaling and desensitization. *J Biol Chem* 273:18677–18680.
- Li C-S, Cho YK. 2006. Efferent projection from the bed nucleus of the stria terminalis suppresses activity of taste-responsive neurons in the hamster parabrachial nuclei. *Am J Physiol Regul Integr Comp Physiol* 291:R914–R926.
- Li YW, Guyenet PG. 1996. Activation of GABA(B) receptors increases a potassium conductance in rat bulbospinal neurons of the C1 area. *Am J Physiol Regul Integr Comp Physiol* 271:R1304–R1310.
- Li YW, Bayliss DA, Guyenet PG. 1995. C1 neurons of neonatal rats: intrinsic beating properties and alpha 2-adrenergic receptors. *Am J Physiol* 269(6 Pt 2):R1356–1369.
- Li Q, Goodchild AK, Seyedabadi M, Pilowsky PM. 2005. Preprothymokinin A mRNA is colocalized with tyrosine hydroxylase-immunoreactivity in bulbospinal neurons. *Neuroscience* 136:205–216.
- Lindsey CJ, Buck HS, Fior-Chadi DR, Lapa RC. 1997. Pressor effect mediated by bradykinin in the paratrigebral nucleus of the rat. *J Physiol* 502(Pt 1):119–129.
- Liu Q, Dewi DA, Liu W, Bee MS, Schonbrunn A. 2008. Distinct phosphorylation sites in the SST2A somatostatin

- receptor control internalization, desensitization, and arrestin binding. *Mol Pharmacol* 73:292–304.
- Lovick TA. 1992. Inhibitory modulation of the cardiovascular defence response by the ventrolateral periaqueductal gray matter in rats. *Exp Brain Res* 89:133–139.
- Luppi PH, Fort P, Jouvett M. 1990. Ionophoretic application of unconjugated cholera toxin B subunit (CTb) combined with immunohistochemistry of neurochemical substances: a method for transmitter identification of retrogradely labeled neurons. *Brain Res* 534:209–224.
- Lüscher C, Jan LY, Stoffel M, Malenka RC, Nicoll RA. 1997. G protein-coupled inwardly rectifying K⁺ channels (GIRKs) mediate postsynaptic but not presynaptic transmitter actions in hippocampal neurons. *Neuron* 19:687–695.
- M'Hamed S. B., Sequeira H, Poulain P, Bennis M, Roy JC. 1993. Sensorimotor cortex projections to the ventrolateral and the dorsomedial medulla oblongata in the rat. *Neurosci Lett* 164:195–198.
- Miyawaki T, Goodchild AK, Pilowsky PM. 2003. Maintenance of sympathetic tone by a nickel chloride-sensitive mechanism in the rostral ventrolateral medulla of the adult rat. *Neuroscience* 116:455–464.
- Moga MM, Saper CB, Gray TS. 1989. Bed nucleus of the stria terminalis: cytoarchitecture, immunohistochemistry, and projection to the parabrachial nucleus in the rat. *J Comp Neurol* 283:315–332.
- Morschel M, Dutschmann M. 2009. Pontine respiratory activity involved in inspiratory/expiratory phase transition. *Philos Trans R Soc Lond B Biol Sci* 364:2517–2526.
- Nakatsuka T, Fujita T, Inoue K, Kumamoto E. 2008. Activation of GIRK channels in substantia gelatinosa neurones of the adult rat spinal cord: a possible involvement of somatostatin. *J Physiol* 586:2511–2522.
- Nunn C, Schoeffter P, Langenegger D, Hoyer D. 2003. Functional characterisation of the putative somatostatin sst2 receptor antagonist CYN 154806. *Naunyn Schmiedeberg Arch Pharmacol* 367:1–9.
- O'Carroll AM, Lolait SJ, König M, Mahan LC. 1992. Molecular cloning and expression of a pituitary somatostatin receptor with preferential affinity for somatostatin-28. *Mol Pharmacol* 42:939–946.
- Padley JR, Kumar NN, Li Q, Nguyen TB, Pilowsky PM, Goodchild AK. 2007. Central command regulation of circulatory function mediated by descending pontine cholinergic inputs to sympathoexcitatory rostral ventrolateral medulla neurons. *Circ Res* 100:284–291.
- Panguluri S, Saggu S, Lundy R. 2009. Comparison of somatostatin and corticotrophin-releasing hormone immunoreactivity in forebrain neurons projecting to taste-responsive and non-responsive regions of the parabrachial nucleus in rat. *Brain Res* 1298:57–69.
- Paré D, Quirk GJ, Ledoux JE. 2004. New Vistas on Amygdala Networks in Conditioned Fear. *J Neurophysiol* 92:1–9.
- Patel YC. 1999. Somatostatin and Its Receptor Family. *Front Neuroendocrinol* 20:157–198.
- Patel YC, O'Neil W. 1988. Peptides derived from cleavage of prosomatostatin at carboxyl- and amino-terminal segments. Characterization of tissue and secreted forms in the rat. *J Biol Chem* 263:745–751.
- Paxinos G, Watson C. 2006. The rat brain in stereotaxic coordinates. New York: Academic Press.
- Premont RT, Inglese J, Lefkowitz RJ. 1995. Protein kinases that phosphorylate activated G protein-coupled receptors. *FASEB J* 9:175–182.
- Priestley T. 1992. The effect of baclofen and somatostatin on neuronal activity in the rat ventromedial hypothalamic nucleus in vitro. *Neuropharmacology* 31:103–109.
- Rabbani SN, Patel YC. 1990. Peptides derived by processing of rat prosomatostatin near the amino-terminus: characterization, tissue distribution, and release. *Endocrinology* 126:2054–2061.
- Ramírez-Jarquín JO, Lara-Hernández S, López-Guerrero JJ, Aguilera MA, Rivera-Angulo AJ, Sampieri A, Vaca L, Ordaz B, Peña-Ortega F. 2012. Somatostatin modulates generation of inspiratory rhythms and determines asphyxia survival. *Peptides* 34:360–372.
- Real MA, Heredia R, del Carmen Labrador M, Dávila JC, Guirado S. 2009. Expression of somatostatin and neuropeptide Y in the embryonic, postnatal, and adult mouse amygdalar complex. *J Comp Neurol* 513:335–348.
- Robinson RB, Siegelbaum SA. 2003. Hyperpolarization-activated cation currents: from molecules to physiological function. *Annu Rev Physiol* 65:453.
- Roosendaal B, Koolhaas JM, Bohus B. 1991. Central amygdala lesions affect behavioral and autonomic balance during stress in rats. *Physiol Behav* 50:777–781.
- Ross CA, Ruggiero DA, Reis DJ. 1985. Projections from the nucleus tractus solitarius to the rostral ventrolateral medulla. *J Comp Neurol* 242:511–534.
- Saggu S, Lundy RF. 2008. Forebrain neurons that project to the gustatory parabrachial nucleus in rat lack glutamic acid decarboxylase. *Am J Physiol Regul Integr Comp Physiol* 294:R52–R57.
- Saha S, Henderson Z, Batten TFC. 2002. Somatostatin immunoreactivity in axon terminals in rat nucleus tractus solitarius arising from central nucleus of amygdala: coexistence with GABA and postsynaptic expression of sst2A receptor. *J Chem Neuroanat* 24:1–13.
- Saha S, Drinkhill MJ, Moore JP, Batten TF. 2005. Central nucleus of amygdala projections to rostral ventrolateral medulla neurones activated by decreased blood pressure. *Eur J Neurosci* 21:1921–1930.
- Samson WK, Zhang JV, Avsian-Kretschmer O, Cui K, Yosten GLC, Klein C, Lyu R-M, Wang YX, Chen XQ, Yang J, Price CJ, Hoyda TD, Ferguson AV, Yuan X-b, Chang JK, Hsueh AJW. 2008. Neuronostatin encoded by the somatostatin gene regulates neuronal, cardiovascular, and metabolic functions. *J Biol Chem* 283:31949–31959.
- Schulz S, Schreff M, Schmidt H, Händel M, Przewlocki R, Höllt V. 1998a. Immunocytochemical localization of somatostatin receptor sst2A in the rat spinal cord and dorsal root ganglia. *Eur J Neurosci* 10:3700–3708.
- Schulz S, Schulz S, Schmitt J, Wiborny D, Schmidt H, Olbricht S, Weise W, Roessner A, Gramsch C, Höllt V. 1998b. Immunocytochemical detection of somatostatin receptors sst1 sst(2A), sst(2B), and sst3 in paraffin-embedded breast cancer tissue using subtype-specific antibodies. *Clin Cancer Res* 4:2047–2052.
- Shapiro MS, Hille B. 1993. Substance P and somatostatin inhibit calcium channels in rat sympathetic neurons via different G protein pathways. *Neuron* 10:11–20.
- Sherwood A, Dolan CA, Light KC. 1990. Hemodynamics of blood pressure responses during active and passive coping. *Psychophysiology* 27:656–668.
- Smith JC, Morrison DE, Ellenberger HH, Otto MR, Feldman JL. 1989. Brainstem projections to the major respiratory neuron populations in the medulla of the cat. *J Comp Neurol* 281:69–96.
- Smith GST, Savary D, Marden C, Costa JLL, Averill S, Priestley JV, Rattray M. 1994. Distribution of messenger RNAs encoding enkephalin, substance P, somatostatin, galanin, vasoactive intestinal polypeptide, neuropeptide Y, and calcitonin gene-related peptide in the midbrain periaqueductal gray in the rat. *J Comp Neurol* 350:23–40.

- Smith DV, Ye M-K, Li C-S. 2005. Medullary taste responses are modulated by the bed nucleus of the stria terminalis. *Chem Senses* 30:421–434.
- Sousa LO, Lindsey CJ. 2009a. Cardiovascular and baroreceptor functions of the paratrigeminal nucleus for pressor effects in non-anaesthetized rats. *Auton Neurosci* 147:27–32.
- Sousa LO, Lindsey CJ. 2009b. Discharge rate profiles of paratrigeminal nucleus neurons throughout a pressor event in non-anaesthetized rats. *Auton Neurosci* 147:20–26.
- Spary EJ, Maqbool A, Batten TF. 2008. Expression and localisation of somatostatin receptor subtypes sst1-sst5 in areas of the rat medulla oblongata involved in autonomic regulation. *J Chem Neuroanat* 35:49–66.
- Stock G, Schlör KH, Heidt H, Buss J. 1978. Psychomotor behaviour and cardiovascular patterns during stimulation of the amygdala. *Pflügers Arch* 376:177–184.
- Stornetta RL, Rosin DL, Wang H, Sevigny CP, Weston MC, Guyenet PG. 2003. A group of glutamatergic interneurons expressing high levels of both neurokinin-1 receptors and somatostatin identifies the region of the pre-Botzinger complex. *J Comp Neurol* 455:499–512.
- Takayama K, Miura M. 1991. Glutamate-immunoreactive neurons of the central amygdaloid nucleus projecting to the subretrofacial nucleus of SHR and WKY rats: a double-labeling study. *Neurosci Lett* 134:62–66.
- Tan W, Janczewski WA, Yang P, Shao XM, Callaway EM, Feldman JL. 2008. Silencing preBotzinger complex somatostatin-expressing neurons induces persistent apnea in awake rat. *Nat Neurosci* 11:538–540.
- Tan W, Pagliardini S, Yang P, Janczewski WA, Feldman JL. 2010. Projections of preBotzinger complex neurons in adult rats. *J Comp Neurol* 518:1862–1878.
- Thoss VS, Ferez J, Duc D, Hoyer D. 1995. Embryonic and postnatal mRNA distribution of five somatostatin receptor subtypes in the rat brain. *Neuropharmacology* 34:1673–1688.
- Tupal S, Rieger MA, Ling GY, Park TJ, Dougherty JD, Goodchild AK, Gray PA. 2014. Testing the role of preBotzinger complex somatostatin neurons in respiratory and vocal behaviors. *Eur J Neurosci* 40:3067–3077.
- Vanetti M, Kouba M, Wang X, Vogt G, Höllt V. 1992. Cloning and expression of a novel mouse somatostatin receptor (SSTR2B). *FEBS Lett* 311:290–294.
- Vanetti M, Ziolkowska B, Wang X, Horn G, Höllt V. 1994. mRNA distribution of two isoforms of somatostatin receptor 2 (mSSTR2A and mSSTR2B) in mouse brain. *Brain Res Mol Brain Res* 27:45–50.
- Veening JG, Swanson LW, Sawchenko PE. 1984. The organization of projections from the central nucleus of the amygdala to brainstem sites involved in central autonomic regulation: a combined retrograde transport-immunohistochemical study. *Brain Res* 303:337–357.
- Viana F, Hille B. 1996. Modulation of high voltage-activated calcium channels by somatostatin in acutely isolated rat amygdaloid neurons. *J Neurosci* 16:6000–6011.
- Vincent SR, McIntosh CHS, Buchan AMJ, Brown JC. 1985. Central somatostatin systems revealed with monoclonal antibodies. *J Comp Neurol* 238:169–186.
- von Leupoldt A, Sommer T, Kegat S, Baumann H Jr, Klose H, Dahme B, Bachel C. 2008. The unpleasantness of perceived dyspnea is processed in the anterior insula and amygdala. *Am J Respir Crit Care Med* 177:1026–1032.
- Wang WH, Lovick TA. 1993. The inhibitory effect of the ventrolateral periaqueductal gray matter on neurones in the rostral ventrolateral medulla involves a relay in the medullary raphe nuclei. *Exp Brain Res* 94:295–300.
- Wang HL, Dichter M, Reisine T. 1990. Lack of cross-desensitization of somatostatin-14 and somatostatin-28 receptors coupled to potassium channels in rat neocortical neurons. *Mol Pharmacol* 38:357–361.
- Waraczynski M. 2003. Lidocaine inactivation demonstrates a stronger role for central versus medial extended amygdala in medial forebrain bundle self-stimulation. *Brain Res* 962:180–198.
- Ward DG. 1988. Stimulation of the parabrachial nuclei with monosodium glutamate increases arterial pressure. *Brain Res* 462:383–390.
- Wilensky AE, Schafe GE, Kristensen MP, LeDoux JE. 2006. Rethinking the fear circuit: the central nucleus of the amygdala is required for the acquisition, consolidation, and expression of Pavlovian fear conditioning. *J Neurosci* 26:12387–12396.
- Yasuda K, Rens-Domiano S, Breder CD, Law SF, Saper CB, Reisine T, Bell GI. 1992. Cloning of a novel somatostatin receptor, SSTR3, coupled to adenyllylcyclase. *J Biol Chem* 267:20422–20428.
- Yin H, Lee KE, Park SA, Bhattarai JP, Suh BJ, Jeon JG, Kim BG, Park SJ, Han SK. 2009. Inhibitory effects of somatostatin on the substantia gelatinosa neurons of trigeminal sub-nucleus caudalis via somatostatin type 2 receptors in juvenile mice. *Brain Res* 1304:49–56.
- Yosten GLC, Pate AT, Samson WK. 2011. Neuronostatin acts in brain to biphasically increase mean arterial pressure through sympatho-activation followed by vasopressin secretion: the role of melanocortin receptors. *Am J Physiol Regul Integr Comp Physiol* 300:R1194–R1199.
- Young Shim E, Jung Kim H, Kim MJ, Rhie DJ, Jo YH, Kim MS, June Hahn S, Lee MY, Yoon SH. 2006. Desensitization of somatostatin-induced inhibition of low extracellular magnesium concentration-induced calcium spikes in cultured rat hippocampal neurons. *Brain Res* 1111:61–71.

ORIGINAL RESEARCH

Recording, labeling, and transfection of single neurons in deep brain structures

Bowen Dempsey¹, Anita J. Turner¹, Sheng Le¹, Qi-Jian Sun¹, Lama Bou Farah¹, Andrew M. Allen², Ann K. Goodchild¹ & Simon McMullan¹

¹ Australian School of Advanced Medicine, Macquarie University, Sydney, NSW, 2109, Australia

² Department of Physiology, The University of Melbourne, Parkville, VIC, 3010, Australia

Keywords

Electroporation, gene delivery, juxtacellular, labeling.

Correspondence

Simon McMullan, Australian School of Advanced Medicine, F10A Macquarie University, NSW 2109, Australia.
Tel: +61 2 9850 2710
Fax: +61 2 9850 2701
E-mail: Simon.mcmullan@mq.edu.au

Funding Information

This work was funded by Macquarie University, the Australian Research Council (DP120100920) and National Health & Medical Research Council of Australia (604002).

Received: 17 November 2014; Revised: 19 November 2014; Accepted: 24 November 2014

doi: 10.14814/phy2.12246

Physiol Rep, 3 (1), 2015, e12246,
doi: 10.14814/phy2.12246

Abstract

Genetic tools that permit functional or connectomic analysis of neuronal circuits are rapidly transforming neuroscience. The key to deployment of such tools is selective transfection of target neurons, but to date this has largely been achieved using transgenic animals or viral vectors that transduce subpopulations of cells chosen according to anatomical rather than functional criteria. Here, we combine single-cell transfection with conventional electrophysiological recording techniques, resulting in three novel protocols that can be used for reliable delivery of conventional dyes or genetic material in vitro and in vivo. We report that techniques based on single cell electroporation yield reproducible transfection in vitro, and offer a simple, rapid and reliable alternative to established dye-labeling techniques in vivo, but are incompatible with targeted transfection in deep brain structures. In contrast, we show that intracellular electrophoresis of plasmid DNA transfects brainstem neurons recorded up to 9 mm deep in the anesthetized rat. The protocols presented here require minimal, if any, modification to recording hardware, take seconds to deploy, and yield high recovery rates in vitro (dye labeling: 89%, plasmid transfection: 49%) and in vivo (dye labeling: 66%, plasmid transfection: 27%). They offer improved simplicity compared to the juxtacellular labeling technique and for the first time offer genetic manipulation of functionally characterized neurons in previously inaccessible brain regions.

Introduction

Techniques that combine electrophysiological recording of neuronal activity with dye labeling have been used to address fundamental questions about the relationship between neurochemistry, morphology, and cell behavior (Schreihofer and Guyenet 1997; Bevan 1998; Mileykovskiy et al. 2005; Nosedá et al. 2010; Jiang et al. 2013). Historically, investigators have used three main strategies to introduce dye from a recording pipette to the cell interior. In the first, intracellular access is obtained by impalement of the neuron with a sharp electrode

and fluorescent dyes or biotin conjugates are deposited by intracellular electrophoresis (Stretton and Kravitz 1968; Horikawa and Armstrong 1988). In the second, whole cell access is obtained using a low-resistance patch pipette and dye is passively dialyzed into the cell (Edwards et al. 1989; Pickering et al. 1991). In the third approach, an extracellular recording electrode is positioned in close contact with the cell membrane (a “juxtacellular” position) and a train of 200 ms long positive current pulses up to 10 nA in amplitude is used to initiate and maintain membrane electroporation and simultaneously eject positively charged dyes, typically

over a period of 2–30 min (Pinault 1996; for review, see Pinault 2011).

All three approaches are technically difficult and require experience and skill for efficient use, particularly *in vivo*. The quality of labeling obtained using the juxtacellular approach is generally inferior to that obtained using intracellular dye deposition; however, the technical difficulty associated with maintaining stable sharp recordings or obtaining whole cell access in deep brain regions *in vivo* has led to the ascendancy of Pinault's juxtacellular technique as the gold-standard approach for labeling functionally identified neurons.

Recent advances in molecular biology have provided incentives for the development of single-cell labeling techniques that are compatible with intracellular nucleotide delivery. The major challenge associated with delivery of genetic material is the large molecular weight of gene constructs and the high copy number required for efficient transfection. For example, the molecular weight of the plasmid that encodes yellow fluorescent protein, pCAG-YFP (MW 1.8 MDa) is approximately 6000 times greater than that of neurobiotin (MW 286 Da). This obstacle has been overcome using two approaches. First, as with traditional dyes, plasmids can be dialyzed into neurons during low-resistance whole cell recordings (Rancz et al. 2011). Although the transfection rate associated with this approach is high (56%; Rancz et al. 2011) and the use of whole-cell patch recordings *in vivo* is becoming more commonplace, this approach is still restricted to more superficial brain regions as whole-cell recordings become difficult to obtain beyond about 2 mm deep (Margrie et al. 2002; Schramm et al. 2014).

An alternative approach combines conventional electrophysiological recording methods with single cell electroporation (SCE) (Haas et al. 2001; Rae and Levis 2002; Rathenberg et al. 2003; Bestman et al. 2006; Steinmeyer and Yanik 2012). In common with the juxtacellular technique, SCE uses voltage trains to induce localized dielectric breakdown of the cell membrane and drive charged molecules from the pipette into the cell, but differs in terms of the duration (~1 ms), frequency (50–1000 Hz), and amplitude of pulses (~10 V, equivalent to ~500 nA assuming a series resistance of 20 M Ω). SCE is an efficient and quick transfection method, but suffers some limitations: first, it is critically dependent on gentle contact between the pipette and target cell, meaning its use is largely restricted to preparations in which direct visualization of the cell is possible (Rathenberg et al. 2003; Kitamura et al. 2008; Judkewitz et al. 2009). Furthermore, the voltages required for efficient SCE are beyond the limits of commercially available voltage-clamp amplifiers, meaning SCE cannot readily be combined with electrophysiological characterization of target neurons.

Three recent reports detail amplifier modifications and protocols that combine traditional electrophysiological recordings with SCE, allowing transfection of recorded neurons *in vitro* (Daniel et al. 2013) or, within superficial layers of the cortex, *in vivo* (Cohen et al. 2013; Oyama et al. 2013). These achievements represent an important technical landmark that, in common with the whole-cell transfection technique (Rancz et al. 2011), may prove valuable to investigators studying neurons in easily accessible brain regions. However, their applicability to neurons in deep or fibrous regions of the adult brain remains unproven.

Our group has a long-standing interest in the anatomy, behavior, and network dynamics of autonomic and respiratory nuclei deep in the ventrolateral medulla of the rat (McMullan et al. 2008; Seigny et al. 2008; Burke et al. 2011). These neurons are located up to 9 mm deep to the cerebellar surface, lie intermingled with large fiber tracts, and are not amenable to whole-cell recordings in recovery experiments. The objective of the current study was to develop a technique that can be used for the targeted transfection of electrophysiologically profiled neurons in deep brain regions. We first independently developed an approach that combines extracellular recording of unit activity with SCE. We then validated its efficacy *in vitro* and extensively tested its suitability for transfection of neurons recorded >2 mm deep in the brainstem. We report that SCE-based approaches provide good transfection efficiency *in vitro* and can be used *in vivo* for dye-labeling as a simple and reliable alternative to the juxtacellular technique. However, in our hands SCE did not result in reliable transfection *in vivo*. To circumvent this limitation we describe a protocol for intracellular electrophoresis of DNA and show that this is a more useful approach.

Methods

Ethical Approval: All experiments were approved by Macquarie University Animal Ethics Committee and conformed to the Australian Code of Practice for the Care and Use of Animals for Scientific Purposes.

General preparation

Preparation of brain slices for *in vitro* electroporation

P2–8 Sprague–Dawley rat pups of either sex were anesthetized with isoflurane and decapitated when areflexic. The head was submerged in ice-cold carbogen-bubbled artificial cerebrospinal fluid (ACSF, in mM: 125 NaCl, 25 NaHCO₃, 3 KCl, 1.25 NaH₂PO₄·H₂O, 10 glucose, 2

CaCl₂, 1 MgCl₂). The brain was dissected and 250 μ m slices of hippocampus, cortex, or brainstem were cut using a vibratome in ice-cold ACSF. Slices were maintained and recorded at 34°C in ACSF. In some cases spontaneous activity was enhanced by superfusing slices in 5–12 mM [K⁺] ACSF (Onimaru and Homma 2007).

Organotypic slice cultures of hippocampus, cortex, brainstem, and cerebellum were prepared as previously described (De Simoni and Yu 2006). Cultures were maintained on organotypic culture mesh inserts (Millipore, Billerica, MA; PICM03050) in six well dishes, submerged in 1 mL of culture media. Slices were kept in a CO₂ incubator at 37°C, 5% CO₂ for at least 2 days prior to use.

Animal preparation: acute experiments

Adult Sprague–Dawley rats of either sex (250–650 g) were anesthetized with 10% urethane (1.3 g/kg i.p.) and prepared for single unit recording as previously described (Turner *et al.* 2013). In brief, vascular access was obtained and rats were intubated and instrumented to record blood pressure, core temperature, and end-tidal CO₂. Rats were positioned in a stereotaxic frame in the skull flat or nose-down (~30°) position. Bone overlying the brainstem was removed and the dura reflected. In experiments targeting respiratory neurons the caudal pole of the facial nucleus, an anatomical landmark for the respiratory cell column, was mapped by antidromic field potentials as previously described (Brown and Guyenet 1985). Diaphragmatic EMG was recorded as an index of respiratory phase via fine steel wire hook electrodes inserted through the thoracic wall into the diaphragm using a 26 gauge needle. When indicated by respiratory movements that interfered with recording stability, rats were artificially ventilated at parameters that maintained end-tidal CO₂ at 3.5–4.5% and movements suppressed by careful titration with pancuronium bromide (0.2–2 mg/kg i.v., AstraZeneca, North Ryde, NSW, Australia) such that diaphragmatic EMG was still observable. In long experiments, hydration and electrolyte balance was maintained by intravenous infusion of 0.9% NaCl or 5% glucose (5 mL/kg/h). Anesthetic depth was carefully monitored by examining autonomic, respiratory, and/or motor responses to firm pinch of the hindpaw; supplementary anesthesia (10% initial dose) was provided as required.

Animal preparation: recovery experiments

Adult Sprague–Dawley rats of either sex (85–605 g) were anesthetized with intraperitoneal ketamine (75 mg/kg; Parnell Laboratories, Alexandria, NSW, Australia) mixed with medetomidine (0.5 mg/kg; Pfizer Animal Health, West Ryde, NSW, Australia). Prophylactic antibiotics

(20 mg/kg Cephazolin sodium, i.m.; Mayne Pharma, Salisbury South, SA, Australia) and analgesia (2.5 mg/kg Carprofen, s.c.; Norbrook Pharmaceuticals, Tullamarine, VIC, Australia) were administered and the left femoral artery and vein were cannulated under aseptic conditions. The brain was exposed as described above under minimally invasive conditions, medetomidine was reversed (atipamazole 1 mg; Pfizer Animal Health, Australia, s.c.), and anesthesia switched to 1–3% isoflurane (Veterinary Companies of Australia Pty Ltd, Artarmon, NSW, Australia) in 100% oxygen and monitored as described above for the remainder of the procedure. In some experiments rats were artificially ventilated following endotracheal intubation with a 14 gauge cannula.

After conclusion of recordings, wounds were irrigated and the exposed brain covered with oxidized cellulose hemostat. Neck muscles were sutured and skin closed with stainless steel suture clips. Femoral catheters were removed, vessels tied off, and incisions closed. Anesthesia was discontinued, rats were removed from the stereotaxic frame and, where applicable, extubated. Rats were treated with postoperative carprofen, (2.5 mg/kg s.c.; Norbrook Pharmaceuticals, Australia) and monitored closely for up to 36 h with additional analgesia as required.

Histology

At the conclusion of *in vivo* experiments rats were euthanized with pentobarbitone (>100 mg/kg i.v. (acute experiments) or i.p.(recovery)), transcardially perfused with heparinised saline followed by 4% PFA, and the brain removed and postfixed in 4% PFA solution overnight. At the conclusion of *in vitro* experiments brain slices were briefly immersed in 4% PFA and transferred into TBPS until imaging.

Brainstems from *in vivo* experiments in which dextran or plasmids encoding fluorescent reporters were used were cut into 50 μ m coronal sections with a vibrating microtome, wet-mounted, and immediately visualized under epi-fluorescence. As part of a separate study, neurobiotin-labeled neurons were processed for ChAT and somatostatin 2A receptor immunoreactivity before visualization. Sections were washed in 0.01 M phosphate buffered saline containing 0.2% Triton-100 for 3 \times 15 min, and incubated in 0.01 M phosphate buffered saline containing 2% bovine serum albumin and 0.2% Triton-100 for 1 h at room temperature. Primary antibodies (Goat-anti-choline acetyltransferase, 1:800 (Chemicon, Millipore, Cat#AB144P), Rabbit anti-SST 2a receptor 1:100 (Bio-trend, Köln, Germany; ss-8000-rmc, Lot# a080826)), were added to the blocking buffer and sections were incubated for 48 h at 4°C. Sections were washed in TPBS 3 \times 30 min and incubated in secondary antibodies

(ExtrAvidin[®]-FITC 1:500 (Sigma-Aldrich, Sydney, NSW, Australia; Cat#E2760), Cy3[®]-conjugated AffiniPure Donkey anti-Goat IgG (H+L) 1:250 (Jackson ImmunoResearch Laboratories, INC, West Grove, PA; Code#705-165-147, Lot#68839), Alexa Fluor[®] 647-AffiniPure Donkey Anti-Rabbit IgG (H+L) 1:250 (Jackson ImmunoResearch Laboratories, INC, Code#711-605-152, Lot#105115)) for 12 h at 4°C. Processed sections were washed again in TPBS 3 × 30 min before being mounted in serial order on glass slides and coverslipped for imaging with Zeiss Z1 (Carl Zeiss Pty Ltd, North Ryde, Australia) epifluorescent or Leica TCS SP5X (Leica Microsystems Pty Ltd, North Ryde, NSW, Australia) confocal microscopes. In two cases, CFP and EGFP immunoreactivity were enhanced using Rabbit-anti-GFP (1:1000, Life Technologies, Mulgrave, VIC, Australia; Cat# A-6455).

Recording parameters

Recordings were made using an Axoclamp 900A amplifier with HS-9AX1 headstage (Molecular Devices, Sunnyvale, CA) in current clamp mode. This model has several features that make it suitable: its high maximum current output (1000 nA) is convenient for constant-current electroporation, and the headstage is tolerant of externally generated voltages of up to 10 V.

Extracellular activity was simultaneously measured on two channels, one using conventional extracellular configuration (AC channel: Gain: 20–50, Band pass: 100–3000 Hz) and one configured for intracellular recordings (DC channel: Gain: 1, Band pass: DC–3000 Hz). Data were sampled at 10 (AC) or 5 (DC) ksamples/s using a 1401plus or power1401 running Spike 2 version 7 (Cambridge Electronic Design, Cambridge, UK). AC recordings were played back as an audio signal during experiments.

Pipettes were pulled from filamented borosilicate glass (external diameter 1 mm, internal diameter 0.5 mm) using a P-2000 pipette puller (Sutter Instruments, Novato, CA). Pipettes with a long taper and tip diameter of approximately 1 μm (Resistance 10–20 MΩ when filled with 0.9% NaCl) were considered ideal for extracellular recordings. All pipettes were inspected using a microscope with a calibrated graticule.

Intracellular recordings were made using similar pipettes pulled to <1 μm tip diameters and filled with either Tris EDTA buffer or water containing freshly filtered plasmid DNA diluted to a concentration of 250–350 ng/μL in 1M KCl.

Constant voltage switching circuit

A constant voltage generator (DS2A-mkII, Digitimer Ltd., Welwyn Garden City, Hertfordshire, UK) was connected

in parallel to the recording pipette by connecting one pole of the stimulator to the pipette and the other to the experimental preparation. A high-impedance recording circuit was maintained by isolating the stimulator from the pipette assembly with an electromagnet-controlled reed switch. The increased capacitance (~7 pF) of the assembly was offset by the amplifier capacitance compensation. For electroporation the electromagnet was engaged with a 5 V TTL pulse and the stimulator triggered to produce the desired voltage train.

In vitro electroporation

Experiments were performed on a patch electrophysiology rig under an Olympus microscope with differential interference contrast optics and immersion lenses. Pipettes were back loaded with plasmid DNA, fluorescent dextran (tetramethylrhodamine- or fluorescein-conjugated dextran (3000 MW, Invitrogen # D3307 and D3305, respectively, 1–3% in 0.9% NaCl), or neurobiotin (1–2% in 0.9% NaCl) and mounted on the recording headstage. Brain slices were placed in the recording chamber and perfused at 1–2 mL per minute. The pipette tip was guided onto the surface of the target cell until a dimple was formed. Pipette patency was maintained with positive pressure as required. Following electroporation the pipette was carefully retracted from the cell and reused until clogging occurred.

The same approach was used for transfection of neurons in organotypic culture, except pipettes were filled with freshly filtered plasmid DNA in 0.9% NaCl (0.3–3 μg/μL). SCE of organotypic cultures was typically completed within 15 min. Transfected neurons were washed in fresh media and restored to the incubator for 24–48 h before fixation and imaging of reporter-expressing neurons.

In vivo electroporation

Pipettes were prepared as above, mounted on the recording headstage and slowly (~10 μm/s) lowered into the brainstem using a piezo microstepper. For extracellular recordings, pipette pressure was maintained at >200 mmHg until a the tip reached a depth of 2 mm at which point the pressure was reduced to 0–50 mmHg. The pipette was advanced in 3 μm steps until a spontaneously active neuron was isolated and pressure was released. In many cases no pressure was applied beyond 2 mm deep, without any apparent effect on dye labeling efficiency or quality. Positive pressure was always used in attempted extracellular transfection.

Correct pipette position was verified by induction of an open-cell response to single cell microstimulation. Once a recording from a single cell was isolated the pipette was withdrawn until spike amplitude was 0.2–0.5 mV and

microstimulation was attempted. If no response was obtained the pipette was advanced and retested in 3 μm steps until a response was observed (interpreted as establishment of contact) or the spike height receded (interpreted as passage of the pipette past the cell without making contact).

Electroporation was generally only attempted in neurons in which normal neuronal activity resumed after responses to microstimulation, although electroporation before recovery was still associated with robust labeling (see Fig. 5C). After electroporation the pipette was slowly withdrawn. Fresh pipettes were used for each track.

For the majority of intracellular recordings no pressure was applied during positioning of the pipette: it was lowered to a depth of 1.5 mm and then advanced in 1–5 μm steps until an extracellular recording of a spontaneously active neuron was isolated. A capacitive buzz was applied to gain intracellular access and the pipette was further maneuvered until a stable membrane potential was obtained. After electrophoresis the pipette was slowly withdrawn in until the membrane potential returned to zero and was then withdrawn completely. New pipettes were used for each track.

Plasmid preparation

Plasmids encoding fluorescent reporter proteins were used to validate electroporation: pCAG-DsRed (Addgene: 11151), pCAG-YFP (Addgene: 11180), pCAG-EGFP (Addgene: 11150), pCAG-CFP (Addgene: 11179), pCBA-TdTomato (Addgene: 28017). Plasmids were amplified and purified according to the suppliers' recommendations, filtered, and stored at -20°C until use.

Avoidance of inadvertent neuronal labeling

Partial blockage of recording pipettes is commonly resolved by passing a high-amplitude 'clearing' current through the pipette. In early experiments, we occasionally observed false-positive dextran-labeled neurons at locations at which anionic 'clearing' currents had been used; this can be avoided using clearing currents opposite in polarity to that of the dye. As was the case with *in vitro* experiments, *in vivo* electroporation sometimes labeled more than one neuron. This rarely happened with TMR-dextran (2/79 recovered neurons, 2.5%), but occurred significantly more frequently with neurobiotin (7/51 neurons, 14%, $P = 0.03$, Fisher's exact test). Inadvertent labeling of neurons due to positive pressure ejection of dextran/neurobiotin was almost never seen; unintentionally labeled neurons were easily identified by their position dorsal to the end of the recording track.

Results

Dye-labeling *in vitro*

In pilot experiments performed on acute brain slices we first established that SCE was compatible with the micropipettes and recording amplifier used for extracellular recordings. Recording pipettes with a 1 μm tip diameter were filled with 0.9% NaCl containing 1–3% fluorescein- or tetramethylrhodamine-dextran (TMR-dextran: MW 3000, resistance = 8–20 M Ω) and electroporation currents were delivered by the amplifier current ejection system. The pipette was positioned in gentle contact with the target cell under optical guidance and series resistance (R_s) was measured using the amplifier bridge-balance function. The electroporation current (I_e) required to generate the target electroporation voltage

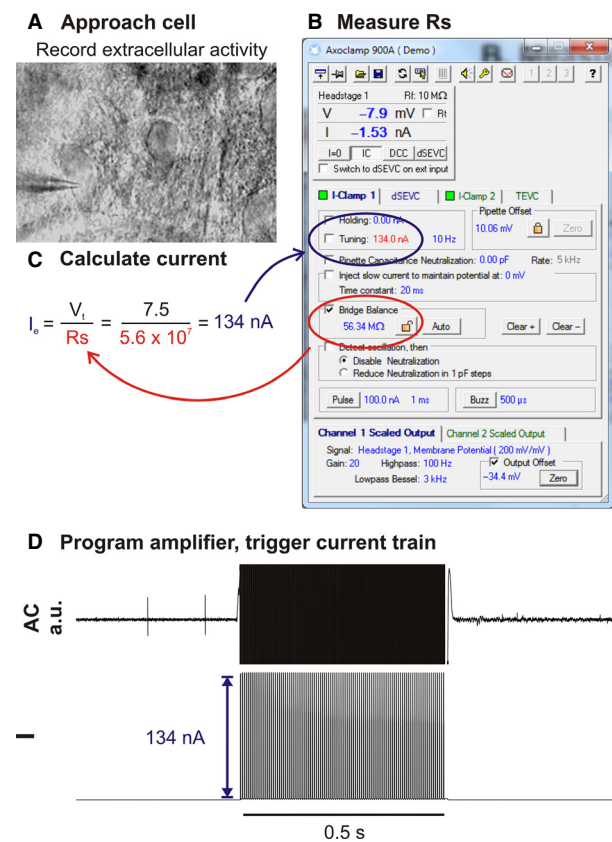


Figure 1. Illustration of workflow used for constant-current electroporation *in vitro*. (A) Recording pipette is moved into gentle contact with the target cell under optical guidance. (B) Immediately prior to electroporation R_s is measured using the amplifier bridge-balance function and (C) used to calculate the electroporation current (I_e) required to generate the target voltage (V_t ; in this example 7.5 V). (D) The amplifier is programmed to deliver a train of current pulses at I_e .

(V_t) was calculated by Ohm's Law and programmed into the amplifier current-injection dialogue (Fig. 1). As the amplitude of currents injected using this approach remain constant over the course of the electroporation train, we term this approach *constant-current electroporation*.

Constant-current electroporation was compatible with high-quality recording of extracellular action potentials and resulted in labeling of the soma and dendritic tree using a wide range of train parameters: reproducible single-cell labeling was obtained with trains of 1 ms pulses delivered at 200 Hz for 0.5 s ($V_t = 7.5$ V: 36/48 cells labeled on the first attempt, Fig. 2, Video S1). Electroporation with even relatively low (<1%) concentrations of fluorescent dextrans resulted in extensive filling of fine axons and fibers, allowing resolution of fine morphological details (e.g. dendritic spines) that were clearly observable under epifluorescent illumination in the live slice. Resolution was enhanced by increasing the concentration

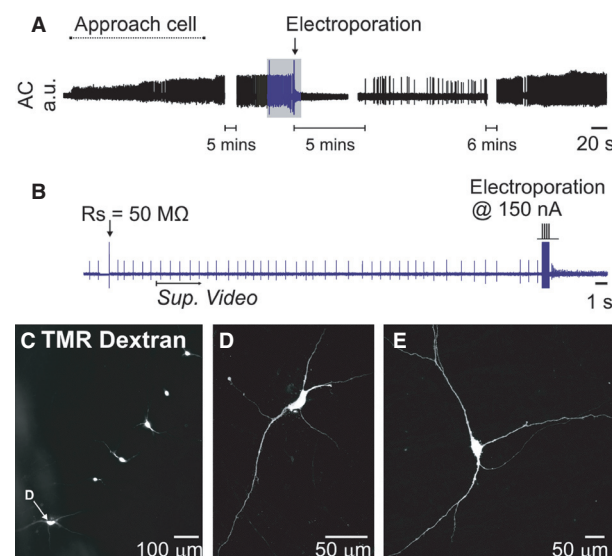


Figure 2. Extracellular recording and constant-current electroporation of a spontaneously active neuron in an acute brain slice (same recording as Video S1). (A) Overview of entire recording. (B) Detailed view of portion indicated in blue in A. To electroporate R_s was first measured using the amplifier bridge-balance function and used to calculate the appropriate electroporation current (see Fig. 1). A 200 Hz train of 100×150 nA, 1 ms pulses immediately filled the cell with 1% tetramethylrhodamine (TMR)-dextran and abruptly halted its spontaneous discharge. Spontaneous activity returned after five minutes and was maintained for the remainder of the experiment. *Sup. Video* indicates starting point of Supplementary Video 1. (C) Low-power fluorescence image of six dextran-filled neurons recorded and electroporated in a single slice (D) Confocal image of the neuron indicated in C. (E) Example of a neuron from a different experiment.

of dextran used. In the vast majority of cases electroporation (successful or unsuccessful) caused an immediate cessation of spontaneous firing that rarely recovered within 10 min (although resumption of firing was not systematically investigated).

Electroporation occasionally labeled more than one cell (3/129 cells, 2.4%). In such cases the intended target was always labeled too, and processes extending from the unintentionally filled cell were always observed in close proximity to the recording pipette, and were therefore presumably labeled *en passant*.

Single-cell transfection in vitro

Using the same approach we attempted to transfect neurons in organotypic cultures with plasmids that encode fluorescent proteins ($V_t = -10$ to -12 V, 100×0.5 –1 ms pulses, 100 Hz, 1 s train). Although occasionally effective, this approach did not reliably result in protein transcription. As discussed in detail below, we postulated that low transfection efficiency may have resulted from voltage drop-off during pore formation, so we modified our pipette assembly to incorporate a constant-voltage source connected in parallel to the recording pipette by an electronic switch (*“constant-voltage electroporation”*, Fig. 3A).

This modification allows delivery of constant-voltage across the recording electrode (and headstage) when the switch is engaged, irrespective of R_s , but electrically isolates the voltage generator during when disengaged, preserving recording quality. This refinement improved the transfection efficiency achieved in organotypic cultures

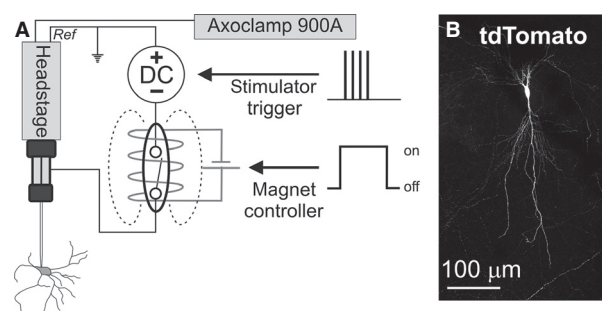


Figure 3. (A) Circuit configuration used for recording and constant-voltage electroporation. A DC generator is connected in parallel to the recording and reference terminals of the amplifier headstage and is isolated from the recording electrode by a reed switch placed inside a cylindrical electromagnet. When the electromagnet is engaged the circuit is closed, allowing delivery of electroporation voltages. (B) TdTomato fluorescence 24 h after transfection of a hippocampal neuron in organotypic culture with pCBA-TdTomato.

(reporter expression confirmed in 25/51 cells within 24 h of electroporation, Fig. 3B), making it equivalent to a commercial standalone SCE device (16/30 cells, AxoporaTM, Fisher's Exact Test: $P = 0.82$) using the same electroporation parameters (-10 V, 100 Hz, 1 ms pulses, 1 s train). This modification also simplified the electroporation process, as it eliminated the requirement for measurement of R_s and calculation of I_e prior to electroporation. As described elsewhere, transfection of single neurons with plasmids that encode fluorescent reporters resulted in bright and complete filling of proximal and distal neuronal compartments, in most cases sufficient to clearly visualize fine branching of axons and dendrites, axonal varicosities and terminals, and dendritic spines (Haas et al. 2001).

Establishing cell contact in blind recordings

SCE is critically dependent on gentle contact between the pipette and target neuron. In fields of view with a high cell density or recordings made deep in the slice it was often difficult to unambiguously determine when the recorded neuron had been correctly identified and

contacted. Furthermore, in initial experiments *in vivo*, we were unable to achieve reliable electroporation when using changes in R_s to indicate cell contact (TMR-dextran: 2/29 cells recovered, $n = 4$ rats), although other investigators have recently reported success using this strategy (Oyama et al. 2013).

To resolve this problem we developed a protocol that uses stereotypical responses to a single 50–100 nA, 1 ms pulse (“single-cell microstimulation”) to definitively identify contact between the recording pipette and soma. In acutely prepared brain slices this stimulus evoked electrophysiological responses characterized by four distinct elements (Fig. 4): (1) Increased discharge rate and altered spike morphology that included (2) an increase in spike height and (3) adoption of an asymmetrical spike shape with a conspicuous after-hyperpolarization (4) a 1–20 mV reduction in potential recorded in DC mode. All four components were *always* apparent in spontaneously active cells, but sometimes transient changes in pipette potential (with or without a short burst of action potentials) were the only features apparent in silent cells. Electrophysiological changes evoked by microstimulation typically recovered within 10 s and

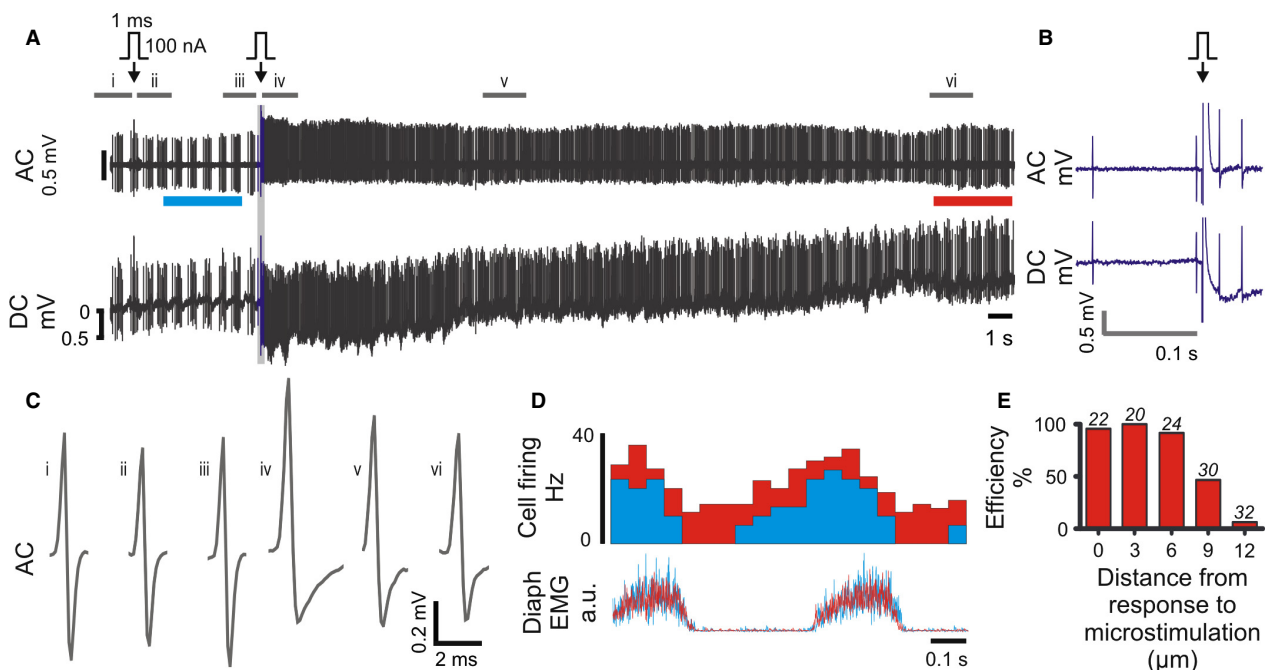


Figure 4. Single-cell microstimulation of a medullary respiratory neuron in vivo. (A) 100 nA microstimulation (arrow) initially evoked no effect on neuronal firing. The pipette was advanced 3 μ m and stimulation repeated. This time the stimulus evoked transient stereotypical changes in firing frequency, spike amplitude and spike shape, apparent in the AC trace, and a small hyperpolarization of the pipette, visible as a 1 mV shift in the DC trace. (B) Expanded view of region drawn in blue in A. (C) Average spike waveforms; source data indicated in A. (D) Diaphragm-triggered histograms of neuronal firing before (cyan, bar indicated in A) and after (red, bar indicated in A) microstimulation: the firing pattern is maintained over the recording. (E) Response to single-cell microstimulation (0 μ m) is correlated with high labeling efficiency (TMR-dextran, *in vitro*), which decreases as the pipette is withdrawn from the cell membrane. Number of replicates shown over each series.

were never observed in the absence of physical contact between pipette and cell, confirmed as a dimpling of the cell membrane.

Although single-cell microstimulation was apparently innocuous in vitro (where gentle contact between pipette and cell were closely monitored), microstimulation of spontaneously active neurons in vivo was initially associated with loss of recordings and presumed cell rupture and death. This was mitigated by withdrawal of the pipette from the cell once stable recordings were established such that spikes were <0.5 mV in amplitude prior to microstimulation. Where no response to microstimulation was observed the pipette was advanced in 1–3 μm increments and stimulation repeated until a response was obtained. Using this approach transient responses, in which normal neuronal activity resumed within ~ 10 s, were achieved in approximately 50% of neurons (see Figs 4 and 5).

Responses to single-cell microstimulation were a reliable indicator of contact between the pipette and cell and were predictive of successful electroporation. Under blind conditions in vitro, the probability of achieving dextran labeling on the first attempt was 89% (55/62 cells) following a positive response to single-cell microstimulation, and rapidly declined as the pipette was withdrawn from the cell membrane (Fig. 4E). Positive responses to microstimulation were also correlated with successful constant-current electroporation in randomly sampled spontaneously active neurons encountered 0.3–9.7 mm deep in vivo (dextran electroporation in 82/137 neurons, 60%, $n = 26$ rats, $V_t = 5$ –10 V, 200 Hz, 1 ms pulses, 0.5 s train). A similar proportion (49/74, 66%, $P = 0.37$, Fisher's exact test) were labeled using dextran or neurobiotin in a second cohort of experiments ($n = 21$ rats) in which neurons in the ventrolateral medulla with respiratory-related activity were preferentially targeted with constant-voltage electroporation (7.5–10 V, 200 Hz, 1 ms pulses, 0.5 s train: Fig. 5).

Single-cell transfection in vivo

Having verified that constant-voltage electroporation is capable of reliable single-cell transfection in vitro and established a protocol that results in reproducible dye-labeling in vivo, we then examined its suitability for single-cell transfection in vivo.

Brainstem neurons were recorded 1.6–9.8 mm deep in either nonrecovery experiments, in which urethane anesthesia was maintained for 12–18 h after electroporation ($n = 5$ rats), or recovery experiments ($n = 7$ rats), in which anesthesia was reversed at the conclusion of recording and rats were recovered for 1–2 days. Contact between the pipette and target neuron was first verified

by observing a positive response to single-cell microstimulation, and neurons that recovered were electroporated at negative polarity (–10 V, 50–100 Hz, 0.5–1 ms pulses, 1 s). Regardless of surgical preparation, electroporation parameters, or plasmid construct used, this approach rarely resulted in reporter expression (6/87 neurons, 7%).

We initially hypothesized that the low success rate may have reflected an incorrect assumption regarding the predictive value of our microstimulation technique. We adopted an approach similar to that used for electroporation of superficial cortical neurons (Judkewitz et al. 2009; Oyama et al. 2013), in which the pipette is maneuvered such that R_s is increased by 30%, and attempted SCE in 31 neurons in five recovery experiments; no transfected cells were subsequently identified.

Review of recordings from successfully transfected neurons revealed that microstimulation had in some cases resulted in full intracellular access prior to electroporation (5/6 neurons), suggesting that transfection could be achieved by direct intracellular plasmid electrophoresis. This hypothesis was examined in experiments in which brainstem neurons were targeted for intracellular recordings using semisharp pipettes (tip diameter: <1 μm , resistance 18 ± 3 M Ω). This configuration was compatible with stable recording of unit activity in extracellular mode prior to brief (typically <10 s) intracellular access and plasmid ejection (–10 V, 50 Hz, 1 ms pulses, 1 s train or –10 V, 1000 Hz, 0.1 ms pulses, 0.1 s train: Steinmeyer and Yanik (2012)). Transfection was achieved in 13/48 (27%) neurons in which intracellular access (membrane potential –30 to –70 mV) was obtained prior to electrophoresis (Fig. 6). Transfected neurons were recorded 1.6–8.3 mm deep to the brain surface using pipettes between 8 and 37 M Ω in resistance. 3/13 neurons were silent; the remainder showed spontaneous activity between 1 and 20 Hz. Cross-sectional areas of transfected neurons were 141 – 1178 μm^2 , equivalent to 13–39 μm in diameter.

Discussion

The current study provides researchers with three novel protocols that can be used for reliable dye-labeling or transfection of functionally identified neurons in deep brain regions in vivo. Constant-current electroporation can be performed without any customization of the recording amplifier and yields rapid and high quality dye labeling in vitro and in vivo. Constant-voltage electroporation requires minimal modification of hardware and yields in vitro transfection at efficiency equivalent to a widely used proprietary device, but in our hands this approach was incompatible with high transfection efficiency in vivo. In contrast, we found that intracellular

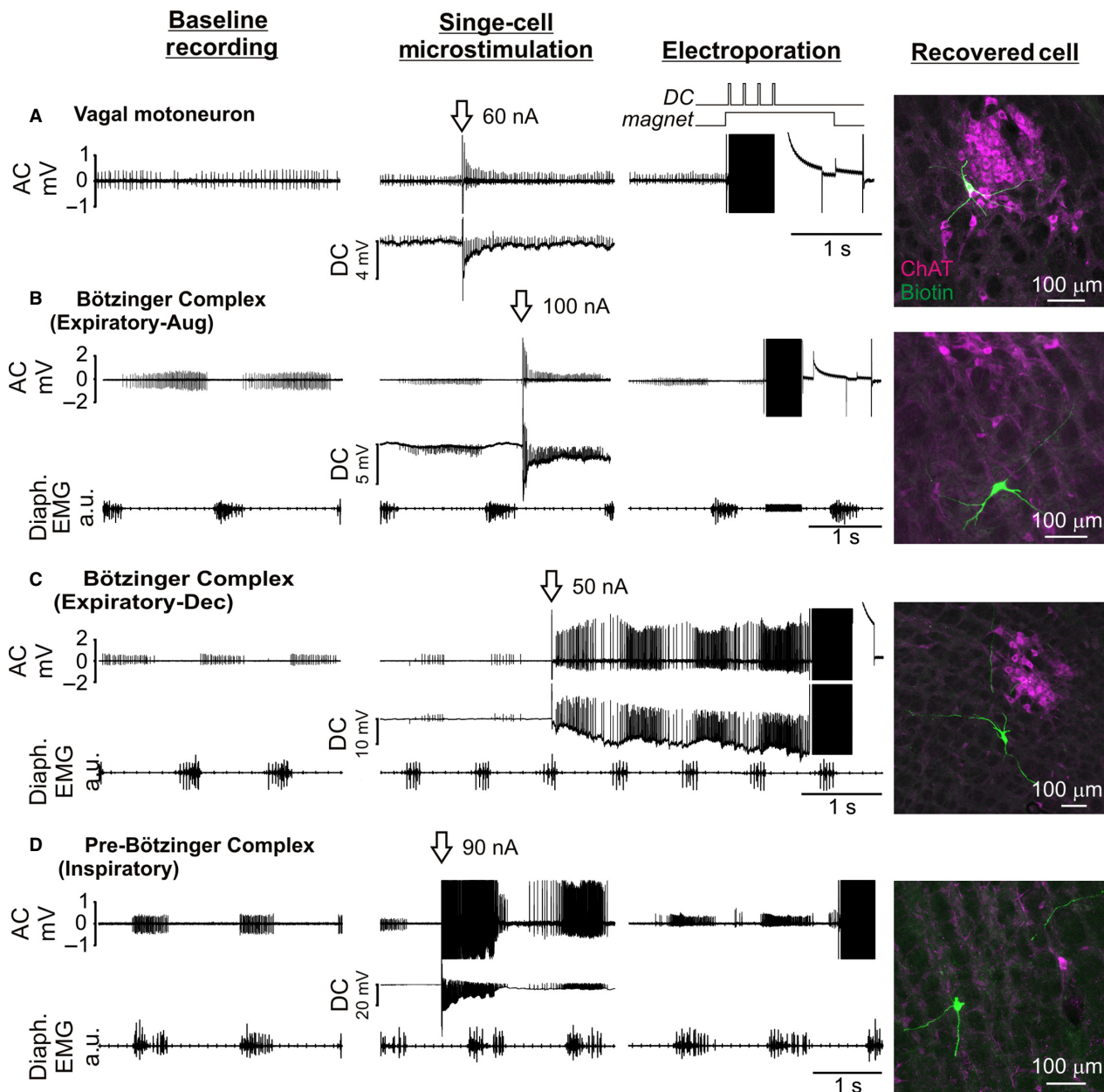


Figure 5. Examples of nonrespiratory (A) and respiratory (B–D) neurons recorded in extracellular mode in the ventrolateral medulla and labeled with neurobiotin by constant-voltage electroporation *in vivo*. After establishment of baseline recordings and repositioning of the recording pipette such that spike height was <0.5 mV, single-cell microstimulation (arrow) was used to verify cell contact. In most cases neurons were allowed to recover from microstimulation prior to electroporation (100×1 ms pulses, 200 Hz, +7.5 to +10 V). Photomicrographs show neurobiotin-filled neurons (green) recovered at the appropriate stereotaxic co-ordinates; magenta channel shows immunoreactivity for choline acetyl transferase (ChAT). Diaphragmatic EMG activity indicates inspiration, permitting functional identification of respiratory neurons. (A) Tonicly active ChAT-immunoreactive neuron in the nucleus ambiguus; (B) Augmenting expiratory neuron recorded ventral to nucleus ambiguus; (C) Decrementing expiratory neuron recorded ventral to nucleus ambiguus; (D) inspiratory-locked neuron.

electrophoresis of genetic material may instead offer a more reliable method for transfection of functional identified neurons in inaccessible brain regions.

In establishing our transfection methodology we developed dye-labeling techniques that offer some advantages

to the juxtacellular method in terms of simplicity and speed. Successful juxtacellular labeling is indicated by 'entrainment' of neuronal firing to regular anodal pulsing of the recording pipette, which must be maintained for several minutes for reasonable labeling to occur. Longer

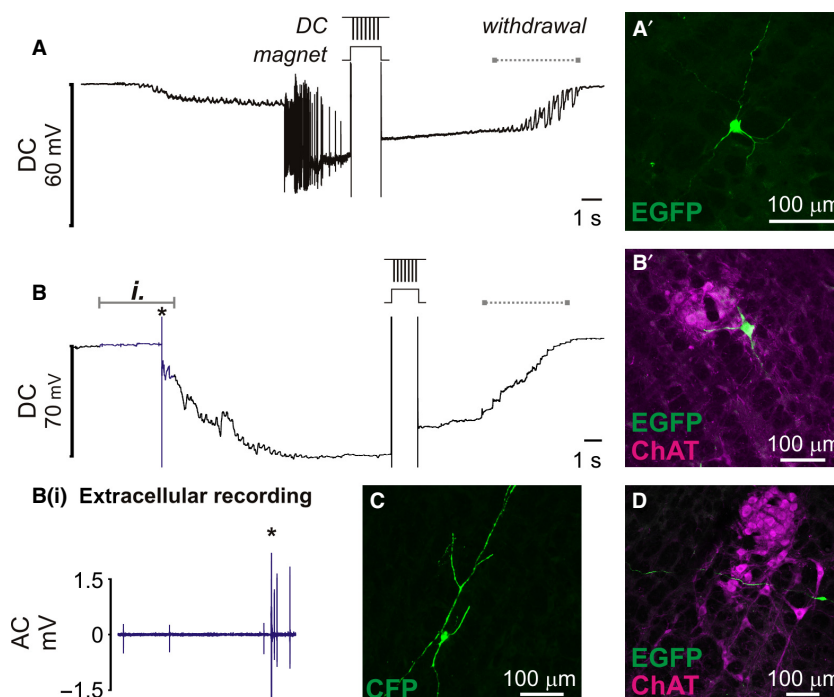


Figure 6. Transfection of ventrolateral brainstem neurons following intracellular penetration in vivo. Once membrane potential had stabilized plasmid DNA encoding fluorescent protein was electrophoretically injected by -10 V pulses (50×1 ms pulses, 1 s). Membrane potential was retained after electrophoresis until withdrawal of the pipette (indicated by dashed lines). (A) Electrophysiological recording from a silent neuron that started firing after penetration. A' shows EGFP-labeled neuron recovered at the corresponding stereotaxic coordinates. (B) Slowly firing spontaneously active neuron: extracellular spikes (blue data, detailed in Bi.) were resolved prior to cell penetration (*). (B') Colocalization of EGFP with ChAT immunoreactivity indicates that this example is a cholinergic motor neuron in nucleus ambiguus. (C + D) show examples of other neurons transfected using the same approach.

periods of entrainment are associated with more complete labeling (up to 60 min: Nosedá et al. 2010). Although the juxtacellular approach can yield efficient labeling in the hands of the technically elite (100/115 cells: Pinault 1996; 45/50 cells: Guyenet and Wang 2001), establishing and maintaining entrainment requires considerable finesse, and recordings are often lost before or during entrainment. It is notable that the number of neurons lost during attempted labeling is often omitted from reports that use this approach, perhaps boosting the apparent efficiency of the technique: in unpublished pilot experiments we found that recordings were lost before or during entrainment in 145/248 (58%) attempts.

In contrast with the imprecise cues used to guide entrainment over minutes of juxtacellular labeling, single-cell microstimulation provides an instant binary output; a cell either responds with an unambiguous electrophysiological signature, in which case it may be immediately electroporated with a high probability of recovery, or does not, in which case the pipette is maneuvered and stimulation repeated (in cases where there is no response) or another cell is sought (in cases where the recording is

lost). This makes the protocol quick to perform and easy to learn: most of the experiments targeting respiratory neurons were performed by a graduate student (SL) who learned the technique in a week and recovered two labeled neurons in his first experiment.

The increase in neuronal excitability and effects on spike shape and amplitude seen in response to microstimulation are consistent with induction of an “open-cell” state by the stimulus, a transient permeabilization of the neuronal membrane evoked by its partial electroporation (Braeken et al. 2012; Spira and Hai 2013). Our observation that such responses only occur when the pipette is in contact with the neuron are supported by similar reports by Santos et al. (2007, 2009), who found that 30–100 nA, 1 ms pulses could be used to effectively stimulate spinal cord neurons in loose-seal mode, but not in the absence of physical contact between the pipette and cell. We conclude that single-cell microstimulation provides a reliable and objective indicator of contact between the pipette and neuron. The major shortcoming associated with using single-cell microstimulation to guide electroporation is its high attrition rate in vivo; this is most likely due to excessive

contact between the pipette and target cell, as it does not seem to occur *in vitro* (where contact can be closely monitored), although factors such as cell size and pipette geometry may also contribute to the effect.

Constant-current and constant-voltage electroporation offer dye-labeling with similar efficiencies *in vitro* and *in vivo*; both resulting in labeling that is at least equivalent in quality to that offered by the juxtacellular technique *in vivo* and comparable to standard SCE *in vitro*, where fine morphological features such as dendritic spines and terminals are consistently revealed (Haas et al. 2001; Umeda et al. 2005). The quality of labeling obtained using the juxtacellular technique varies according to the brain region targeted and tissue processing, hampering direct comparison with the protocols described here. However, extensive filling of brainstem neurons juxtacellularly labeled with neurobiotin and visualized with fluorescent avidin conjugates is rare in the literature (Sartor and Verberne 2003; Abbott et al. 2009; Kanbar et al. 2011; Boucetta et al. 2014; Iceman and Harris 2014) and in our own experience (unpublished data). In contrast, although variability in labeling quality was observed using the approaches described here, we often saw extensively filled neurons that projected across dozens of histological sections in which fine morphological details were visible. We did not extensively investigate the quality of labeling possible using diaminobenzidine visualization, but details such as terminals and dendritic spines were visible in one of three neurons processed that way. Constant-current electroporation may be conducted without modification to hardware provided the recording amplifier is capable of generating sufficiently high currents (400–800 nA), making it fast and cheap to adopt. However, we found it more convenient to use the constant-voltage approach, as it eliminates measurement of R_s and current calculation from the workflow, speeding up the protocol, and is compatible with single-cell transfection *in vitro*.

Why does not constant-current electroporation result in transfection? In constant-current mode the measured value of R_s has a critical influence on voltage output. Constant-current pulses may initially succeed in generating V_t for a given R_s ; however, pores are formed in the membrane within microseconds of voltage application (see DeBruin and Krassowska 1999; Wang et al. 2010), lowering membrane resistance and consequently R_s , resulting in a proportionate reduction in trans-membrane voltage. As a consequence of this voltage drop-off, constant-current electroporation may fail to sustain the voltages required for large and stable pore formation, which are crucial for efficient plasmid delivery (Rae and Levis 2002).

In vitro transfection efficiency was restored by integration of a constant-voltage generator to the recording

circuit. This modification allowed the delivery of up to ± 10 V without risk to the recording headstage (following advice from the manufacturer), and made transfection efficiency equivalent to that obtained with a commercial single-cell electroporator and comparable to that reported elsewhere (Rae and Levis 2002; Rathenberg et al. 2003; Steinmeyer and Yanik 2012). However, exhaustive attempts to translate it for single-cell gene delivery *in vivo* were fruitless. This is surprising, given the similarities between our approach and protocols recently described by other investigators, in which some level of transfection was observed under all parameters tested (Cohen et al. 2013; Oyama et al. 2013). Differences in the brain regions and, perhaps crucially, the depths at which neurons were targeted, may underlie this disparity, as Cohen et al. (2013) and Oyama et al. (2013) restricted their attempts to neurons within 450 μm or 1.5 mm of the brain surface, respectively, where pipette patency is easier to manage.

We conclude that techniques based on SCE are unlikely to yield reliable transfection of neurons in deep brain structures, and speculate that blockage of pipettes is most likely responsible for the poor transfection efficiency seen *in vivo*. Despite applying high positive pressure to the internal solution during brain penetration and cell hunting, we rarely saw any evidence of dye leakage or hydraulic injury along pipette tracks, both of which indicate pipette patency *in vivo* (Rancz et al. 2011), and the quality and efficiency of dye-labeling and reporter expression were consistently higher *in vitro* than *in vivo*. Although we were able to use SCE for efficient dye-labeling nearly 10 mm deep to the brain surface, this does not necessarily mean that recording pipettes were patent: in our experience electrophoretic ejection of fluorescent dextran is consistently possible from clogged pipettes in which no dextran may be pressure-ejected, and we were able to produce robust labeling with such pipettes *in vitro*. However, we and others have found that blocked pipettes absolutely preclude transfection by SCE (Haas et al. 2001; Rae and Levis 2002; Rathenberg et al. 2003; Bestman et al. 2006; Kitamura et al. 2008; Judkewitz et al. 2009).

If patency is the main issue affecting the efficiency of SCE in deep brain regions, pipette clogging probably reduces rather than completely obstructing plasmid ejection, as intracellular plasmid electrophoresis reproducibly transfected neurons up to 8.3 mm deep. Stable intracellular access is difficult to achieve even in acute preparations, where extensive craniotomy or pneumothoraces are commonly used to reduce movement. However, we found that brief access, sufficient for transfection, could be gained in minimally invasive preparations (although we found tracheal intubation with neuromuscular block and artificial ventilation useful) and that large neurons could be impaled and transfected using low-resistance pipettes.

The current data provide a proof-of-principle that intracellular recording may be used to transfect neurons in deep brain regions, but the efficiency of the approach will ultimately depend on factors including operator experience, animal age, brain region targeted, and the size of targeted neurons.

The current data provide relatively simple protocols that can be used for reliable and robust labeling of recorded neurons and a novel approach for transfection of neurons in deep brain regions. The clear-cut criteria used to guide electroporation and the rapidity at which labeling can be performed may prove particularly attractive to novice investigators, whereas the potential to select neurons for genetic modification based on their functional properties may prove useful to investigators interested in applying advanced connectome-tracing technologies at single-cell resolution (Wickersham et al. 2007; Marshel et al. 2010; Rancz et al. 2011).

Conflict of Interest

None declared.

References

- Abbott, S. B., R. L. Stornetta, C. S. Socolovsky, G. H. West, and P. G. Guyenet. 2009. Photostimulation of channelrhodopsin-2 expressing ventrolateral medullary neurons increases sympathetic nerve activity and blood pressure in rats. *J. Physiol.* 587:5613–5631.
- Bestman, J. E., R. C. Ewald, S.-L. Chiu, and H. T. Cline. 2006. In vivo single-cell electroporation for transfer of DNA and macromolecules. *Nat. Protoc.* 1:1267–1272.
- Bevan, M. D. 1998. Selective innervation of neostriatal interneurons by a subclass of neuron in the globus pallidus of the rat. *J. Neurosci.* 18:9438–9452.
- Boucetta, S., Y. Cisse, L. Mainville, M. Morales, and B. E. Jones. 2014. Discharge profiles across the sleep-waking cycle of identified cholinergic, GABAergic, and glutamatergic neurons in the pontomesencephalic tegmentum of the rat. *J. Neurosci.* 34:4708–4727.
- Braeken, D., D. Jans, R. Huys, A. Stassen, N. Collaert, L. Hoffman, et al. 2012. Open-cell recording of action potentials using active electrode arrays. *Lab Chip* 12:4397–4402.
- Brown, D. L., and P. G. Guyenet. 1985. Electrophysiological study of cardiovascular neurons in the rostral ventrolateral medulla in rats. *Circ. Res.* 56:359–369.
- Burke, P. G., J. Neale, W. S. Korim, S. McMullan, and A. K. Goodchild. 2011. Patterning of somatosympathetic reflexes reveals nonuniform organization of presympathetic drive from C1 and non-C1 RVLM neurons. *Am. J. Physiol. Regul. Integr. Comp. Physiol.* 301:R1112–R1122.
- Cohen, L., N. Koffman, H. Meiri, Y. Yarom, I. Lampl, and A. Mizrahi. 2013. Time-lapse electrical recordings of single neurons from the mouse neocortex. *Proc. Natl Acad. Sci. USA* 110:5665–5670.
- Daniel, J., H. R. Polder, V. Lessmann, and T. Brigadski. 2013. Single-cell juxtacellular transfection and recording technique. *Pflügers Arch.* 465:1637–1649.
- De Simoni, A., and L. M. Yu. 2006. Preparation of organotypic hippocampal slice cultures: interface method. *Nat. Protoc.* 1:1439–1445.
- DeBruin, K. A., and W. Krassowska. 1999. Modeling electroporation in a single cell. I. Effects of field strength and rest potential. *Biophys. J.* 77:1213–1224.
- Edwards, F. A., A. Konnerth, B. Sakmann, and T. Takahashi. 1989. A thin slice preparation for patch clamp recordings from neurones of the mammalian central nervous system. *Pflügers Arch.* 414:600–612.
- Guyenet, P. G., and H. Wang. 2001. Pre-Botzinger neurons with preinspiratory discharges “in vivo” express NK1 receptors in the rat. *J. Neurophysiol.* 86:438–446.
- Haas, K., W. C. Sin, A. Javaherian, Z. Li, and H. T. Cline. 2001. Single-cell electroporation for gene transfer in vivo. *Neuron* 29:583–591.
- Horikawa, K., and W. E. Armstrong. 1988. A versatile means of intracellular labeling: injection of biocytin and its detection with avidin conjugates. *J. Neurosci. Methods* 25:1–11.
- Iceman, K. E., and M. B. Harris. 2014. A group of non-serotonergic cells is CO₂-stimulated in the medullary raphe. *Neuroscience* 259:203–213.
- Jiang, X., G. Wang, A. J. Lee, R. L. Stornetta, and J. J. Zhu. 2013. The organization of two new cortical interneuronal circuits. *Nat. Neurosci.* 16:210–218.
- Judkewitz, B., M. Rizzi, K. Kitamura, and M. Häusser. 2009. Targeted single-cell electroporation of mammalian neurons in vivo. *Nat. Protoc.* 4:862–869.
- Kanbar, R., S. D. Depuy, G. H. West, R. L. Stornetta, and P. G. Guyenet. 2011. Regulation of visceral sympathetic tone by A5 noradrenergic neurons in rodents. *J. Physiol.* 589:903–917.
- Kitamura, K., B. Judkewitz, M. Kano, W. Denk, and M. Häusser. 2008. Targeted patch-clamp recordings and single-cell electroporation of unlabeled neurons in vivo. *Nat. Methods* 5:61–67.
- Margrie, T. W., M. Brecht, and B. Sakmann. 2002. In vivo, low-resistance, whole-cell recordings from neurons in the anaesthetized and awake mammalian brain. *Pflügers Arch.* 444:491–498.
- Marshel, J. H., T. Mori, K. J. Nielsen, and E. M. Callaway. 2010. Targeting single neuronal networks for gene expression and cell labeling in vivo. *Neuron* 67:562–574.
- McMullan, S., K. Pathmanandavel, P. M. Pilowsky, and A. K. Goodchild. 2008. Somatic nerve stimulation evokes qualitatively different somatosympathetic responses in the cervical and splanchnic sympathetic nerves in the rat. *Brain Res.* 1217:139–147.

- Mileykovskiy, B. Y., L. I. Kiyashchenko, and J. M. Siegel. 2005. Behavioral correlates of activity in identified hypocretin/orexin neurons. *Neuron* 46:787–798.
- Nosedá, R., V. Kainz, M. Jakubowski, J. J. Gooley, C. B. Saper, K. Digre, et al. 2010. A neural mechanism for exacerbation of headache by light. *Nat. Neurosci.* 13:239–245.
- Onimaru, H., and I. Homma. 2007. Spontaneous oscillatory burst activity in the piriform-amygdala region and its relation to in vitro respiratory activity in newborn rats. *Neuroscience* 144:387–394.
- Oyama, K., S. Ohara, S. Sato, F. Karube, F. Fujiyama, Y. Isomura, et al. 2013. Long-lasting single-neuron labeling by in vivo electroporation without microscopic guidance. *J. Neurosci. Methods* 218:139–147.
- Pickering, A. E., D. Spanswick, and S. D. Logan. 1991. Whole-cell recordings from sympathetic preganglionic neurons in rat spinal cord slices. *Neurosci. Lett.* 130:237–242.
- Pinault, D. 1996. A novel single-cell staining procedure performed in vivo under electrophysiological control: morpho-functional features of juxtacellularly labeled thalamic cells and other central neurons with biocytin or Neurobiotin. *J. Neurosci. Methods* 65:113–136.
- Pinault, D. 2011. The juxtacellular recording-labeling technique. Pp. 41–75 in R. P. Vertes, R. W. Stackman, eds. *Electrophysiological recording techniques*. Springer Science+Business Media, LLC, Humana Press. Available at http://link.springer.com/protocol/10.1007%2F978-1-60327-202-5_3# (accessed 3 December 2014).
- Rae, J. L., and R. A. Levis. 2002. Single-cell electroporation. *Pflugers Arch.* 443:664–670.
- Rancz, E. A., K. M. Franks, M. K. Schwarz, B. Pichler, A. T. Schaefer, and T. W. Margrie. 2011. Transfection via whole-cell recording in vivo: bridging single-cell physiology, genetics and connectomics. *Nat. Neurosci.* 14:527–532.
- Rathenberg, J., T. Nevian, and V. Witzemann. 2003. High-efficiency transfection of individual neurons using modified electrophysiology techniques. *J. Neurosci. Methods* 126:91–98.
- Santos, S. F., S. Rebelo, V. A. Derkach, and B. V. Safronov. 2007. Excitatory interneurons dominate sensory processing in the spinal substantia gelatinosa of rat. *J. Physiol.* 581:241–254.
- Santos, S. F., L. L. Luz, P. Szucs, D. Lima, V. A. Derkach, and B. V. Safronov. 2009. Transmission efficacy and plasticity in glutamatergic synapses formed by excitatory interneurons of the substantia gelatinosa in the rat spinal cord. *PLoS ONE* 4:e8047.
- Sartor, D. M., and A. J. M. Verberne. 2003. Phenotypic identification of rat rostromedullary presympathetic vasomotor neurons inhibited by exogenous cholecystokinin. *J. Comp. Neurol.* 465:467–479.
- Schramm, A. E., D. Marinazzo, T. Gener, and L. J. Graham. 2014. The touch and zap method for in vivo whole-cell patch recording of intrinsic and visual responses of cortical neurons and glial cells. *PLoS ONE* 9:e97310.
- Schreihofer, A. M., and P. G. Guyenet. 1997. Identification of C1 presympathetic neurons in rat rostral ventrolateral medulla by juxtacellular labeling in vivo. *J. Comp. Neurol.* 387:524–536.
- Sevigny, C. P., J. Bassi, A. G. Teschemacher, K. S. Kim, D. A. Williams, C. R. Anderson, et al. 2008. C1 neurons in the rat rostral ventrolateral medulla differentially express vesicular monoamine transporter 2 in soma and axonal compartments. *Eur. J. Neurosci.* 28:1536–1544.
- Spira, M. E., and A. Hai. 2013. Multi-electrode array technologies for neuroscience and cardiology. *Nat. Nanotechnol.* 8:83–94.
- Steinmeyer, J. D., and M. F. Yanik. 2012. High-throughput single-cell manipulation in brain tissue. *PLoS ONE* 7: e35603.
- Stretton, A. O., and E. A. Kravitz. 1968. Neuronal geometry: determination with a technique of intracellular dye injection. *Science* 162:132–134.
- Turner, A., N. Kumar, M. Farnham, M. Lung, P. Pilowsky, and S. McMullan. 2013. Rostromedullary neurons with commissural projections provide input to sympathetic premotor neurons: anatomical and functional evidence. *Eur. J. Neurosci.* 38:2504–2515.
- Umeda, T., T. Ebihara, and S. Okabe. 2005. Simultaneous observation of stably associated presynaptic varicosities and postsynaptic spines: morphological alterations of CA3-CA1 synapses in hippocampal slice cultures. *Mol. Cell Neurosci.* 28:264–274.
- Wang, M., O. Orwar, J. Olofsson, and S. G. Weber. 2010. Single-cell electroporation. *Anal. Bioanal. Chem.* 397:3235–3248.
- Wickersham, I. R., D. C. Lyon, R. J. Barnard, T. Mori, S. Finke, K. K. Conzelmann, et al. 2007. Monosynaptic restriction of transsynaptic tracing from single, genetically targeted neurons. *Neuron* 53:639–647.

Supporting Information

Additional Supporting Information may be found in the online version of this article:

Video S1. Extracellular recording and constant-current electroporation in vitro. The electrophysiological recording (same recording shown in Fig. 2) has been converted into audio and embedded into the video file; action potentials are audible as clicks.